

DISS. ETH NO. 27220

**Developing stoichiometrically well-defined antibody-drug
conjugates by enzymatic conjugation of native antibodies**

A thesis submitted to attain the degree of
DOCTOR OF SCIENCES of ETH ZURICH
(Dr. sc. ETH Zurich)

presented by

JÖRI ELIAS WEHRMÜLLER

MSc in Biology, ETH Zurich

Born on 14.11.1988

citizen of Neuenkirch LU and Malters LU, Switzerland

Accepted on the recommendation of

Prof. Dr. Roger Schibli, examiner

Prof. Dr. Stefanie Krämer, co-examiner

Dr. Martin P. Béhé, co-examiner

2021

“So what? Nothing. Exactly.”

WŁODZIMIERZ BOROWSKI, 1981

Acknowledgments

I would like to express my sincere thanks to Prof. Roger Schibli and Dr. Martin Béhé for the trust they have placed in me by giving me the opportunity to work on this exciting antibody project in their research group. I had many interesting and fruitful conversations with them, and I could learn a lot from their experience and supervision.

My special thanks go to Dr. Philipp Spycher for his supervision in the first year of my thesis. We had many good moments, and I wish him good luck with the Startup Araris he founded based on our patent. Furthermore, I would like to thank all the Master's students that have been involved in projects with the amazing enzyme MTG: Christian Amann, Daniel Herrmann, and Claudia Graf. Special thanks go to Dr. Alexander Meisel, who kindly provided us with many of the antibodies that we tested in the project.

My gratitude goes to all former and current members of the Schibli group at CRS. They made the last four years special and I am thankful that I could spend so many good moments with them in- and outside the lab: Dr. Nathalie Grob, Dr. Claudia Adriana Castro Jaramillo, Dr. Christoph Umbricht, Dr. Julia Frei, Dr. Marco Taddio, Giulia Valpreda, Gregory Holtzhauer, Belinda Trachsel, Patrycja Guzik, Chiara Favaretto, Sara Jordi, Dr. Nadezda Gracheva, Dr. Silvan Boss, Dr. Ahmed Haider, Dr. Andreas Ritler, Dr. Hazem Ahmed, Dr. Francesca Borgna, Dr. Aleksandra Pekosak, Yingfang He, Caitlin Jie, Yun Qin, Viviane Tschan, and Tihomir Todorov. Thank you Gregy, to read through and correcting my thesis. Special thanks go to Julia Gallino and Dailenys Espinosa Martinez, who joined me from South America for two amazing months.

I would like to thank all the technicians that supported me in the lab, especially Christine de Pasquale and Stefan Imobersteg. Stefan was in the last three years of my work indispensable for all the support for the animal experiments, but much more, an invaluable support for my mental health. Furthermore, I also would like to point out Alain Blanc. He taught me all I had to know about MS measurements, and was always around for all kind of questions or technical issues. Danke, Stefan. Merci, Alain. It would not have worked out without you! My sincere thanks also go to Dr. Jürgen Grünberg and Dr. Michal Grzmil, who supported me through my whole thesis with their knowledge. They always took time when I approached them with questions, what I appreciated a lot.

Special thanks I would like to give to Dr. Julia Frei, from which I could profit a lot about knowledge on antibodies, and which not only became a companion in the lab, but also a friend outside working hours.

My sincere gratitude goes to the whole family at ETH, especially group leaders Prof. Stefanie Krämer and Dr. Linjing Mu, which always welcomed me for my sub-projects that were performed at ETH. Special thanks go to Dr. Nathalie Grob, who introduced me to the amazing world of peptide synthesis,

and to Giulia Valpreda, Gregory Holtzhauer, Stefan Gruber, and Vera Gomez, who were involved in linker synthesis and many other valuable tasks at ETH.

Furthermore, my gratitude goes to the Paul Scherrer Institute and ETH Zurich, their technical and scientific staff members, and especially to Sandha Keller and Cordula Küderli for their administrative support.

Finally, I would like to say thank you to all my friends and family. Over the years, I had such amazing support from all the wonderful people I have met, and especially as well from my beloved WG Hunzreal and from the people I have met in my undergraduate studies. I cannot thank enough for the invaluable support I had from my old loves. I am happy that they shared some part of that journey with me.

I am sincerely thankful to my parents, Othmar and Brigitta, and my brothers Fadri and Men-Andrea, for their love, encouragement, and patience they have given me over the years. I could not have made this journey without their support.

Table of Contents

List of Abbreviations, Acronyms, and Symbols.....	viii
Summary	xi
Zusammenfassung	xiv
1. General Introduction.....	1
1.1. Therapeutic antibodies.....	1
1.2. Glycosylation of antibodies	2
1.3. Antibody-Drug Conjugates	3
1.4. Strategies to attach toxins to antibodies	7
1.5. Microbial Transglutaminase	12
1.6. MTG mediated conjugation of antibodies/antibody-fragments.....	13
2. Prelude	15
3. Aims of this thesis.....	18
4. MTG mediated conjugation of lysine containing peptides to Q295 of native antibodies	20
4.1. Introduction.....	21
4.2. Results	21
4.3. Discussion	32
5. Computational screening for suitable MTG-substrates.....	36
5.1. Introduction.....	37
5.2. Results	37
5.3. Discussion	40
6. Chemo-enzymatic functionalization of native antibodies with mono- and bifunctional peptide linkers and toxins	44
6.1. Introduction.....	45
6.2. Results	46
6.3. Discussion	51

7. Trastuzumab biodistribution with linker NH₂-K(N₃)-CRAK-OH and comparative biodistributions of NODAGA-K(N₃)-RAK-NH₂ with and without toxin	54
7.1. Introduction.....	55
7.2. Results	55
7.3. Discussion	62
8. Site-specific MTG mediated conjugation and SPECT of an EGFR-Nanobody with and without albumin binder	65
8.1. Introduction.....	66
8.2. Results	66
8.3. Discussion	69
9. Discussion and conclusion	72
10. Outlook	74
11. Material and Methods	77
11.1. Chapter 4: MTG mediated Conjugation of primary amine containing peptides to Q295 of antibodies.....	77
Method 1 (for peptide screening and condition testing):.....	79
Method 2 (for the isotype/species screening):	79
Method 3 (for azide-functionalized peptides):	79
11.2. Chapter 5: Computational screening for suitable MTG substrates.....	81
11.3. Chapter 6: Chemo-enzymatic functionalization of native antibodies with mono- and bifunctional peptide linkers and toxins.....	82
11.4. Chapter 7: Trastuzumab biodistribution with linker NH ₂ -K(N ₃)-CRAK-OH and comparative biodistributions of NODAGA-K(N ₃)-RAK-NH ₂ with and without toxin.....	86
11.5. Chapter 8: Site-specific MTG mediated conjugation and SPECT of an EGFR-Nanobody with and without albumin binder.....	87
12. References	90
13. Annex.....	100
13.1. Chapter 4: MTG mediated Conjugation of primary amine containing peptides to Q295100	
13.2. Chapter 5: Computational screening for suitable MTG-substrates	122

13.3.	Chapter 6: Chemo-enzymatic functionalization of native antibodies with mono- and bifunctional peptide linkers and toxins.....	133
13.4.	Chapter 7: Trastuzumab biodistribution with linker NH ₂ -K(N ₃)-CRAK-OH and comparative biodistributions of NODAGA-K(N ₃)-RAK-NH ₂ with and without toxin.....	137
13.5.	Chapter 8: Site-specific MTG mediated conjugation and SPECT of an EGFR-Nanobody	141
14.	CURRICULUM VITAE	144

List of Abbreviations, Acronyms, and Symbols

aa	any amino acid
Ac	acylated (or acetylated)
ADC	antibody-drug conjugate
ADCC	antibody-dependent cellular cytotoxicity
biAbs	bispecific antibodies
BPA	benzoylphenylalanine
BSA	bovine serum albumine
CDC	complement-dependent cytotoxicity
CH2/CH3	constant heavy region 2/3
DBCO	dibenzocyclooctyne
dhaa	dehydroascorbic acid
DIPEA	N,N-diisopropylethylamine
DMEM	Dulbecco's modified eagle medium
DMSO	dimethyl sulfoxide
DMF	N,N-dimethylformamide
DM1	mertansine
EDTA	ethylenediaminetetraacetic acid
EGFR	epidermal growth factor receptor
FAM	carboxyfluorescein
Fc	fragment crystallizable (region)
Fc γ RI	immunoglobulin gamma Fc receptor I
FCS	fetal calf serum
Fmoc	fluorenylmethyloxycarbonyl protecting group
GalT	β -1,4-galactosyltransferase
HATU	1-[Bis(dimethylamino)methylene]-1H-1,2,3-triazolo[4,5-b]pyridinium 3-oxide hexafluorophosphate

HER2/neu	human epidermal growth factor receptor 2
IgG (IgG1/-4)	immunoglobulin G (1-4)
LC-MS	liquid chromatography–mass spectrometry
mAb	monoclonal antibody
MMAE	Monomethyl auristatin E
MTG	microbial transglutaminase
MS	mass spectrometry
Nle	norleucine (non-natural amino acid)
NODAGA	1,4,7-triazacyclononane,1-glutaric acid-4,7-acetic acid
PBS	phosphate-buffered saline
PET	positron-emission tomography
p.i.	post injection
RPMI-1640	Gibco Roswell Park Memorial Institute - 1640
rt	room temperature
SialT	α -2,6-sialyltransferase
SOM	self-organizing map
SPECT	single-photon emission computed tomography
TG	transglutaminase
UAA	unnatural amino acid
VHH	camelid single-domain antibody / Nanobody
Å	Ångström, $1 \cdot 10^{-10}$ m

Three-/one-letter code of amino acids

Ala / A	alanine
Arg / R	arginine
Asp / D	aspartate
Asn / N	asparagine

Cys / C	cysteine
Gln / Q	glutamine
Glu / E	glutamate
Gly / G	glycine
His / H	histidine
Ile / I	isoleucine
Leu / L	leucine
Lys / K	lysine
Met / M	methionine
Phe / F	phenylalanine
Pro / P	proline
Ser / S	serine
Thr / T	threonine
Trp / W	tryptophan
Tyr / Y	tyrosine
Val / V	valine

Summary

Cancer is responsible for 17% of death and is the second leading cause for unnatural deaths in the world according to WHO 2020. Systemic therapies made a lot of progress in the recent years, but one of the main drawbacks is still the toxicity in healthy tissue. One way to address this issue is the use of targeted antibodies carrying cytotoxic payloads, so called antibody drug conjugates (ADC). Already nine ADCs have been approved by the United States Federal Drug Administration (FDA). However, clinical and preclinical studies showed that the number of attached toxins, the position of the attachment and the linker are decisive for therapeutic efficacy. Recently, biodistribution studies showed that site-specific attachment of a toxin to the antibody leads to ADCs with better pharmacokinetic behavior, compared to ADCs where the toxin is heterogeneously attached. Our group pioneered the site-specific modification of antibodies with the use of the enzyme Microbial Transglutaminase (MTG). We discovered that MTG forms an isopeptidic bond between glutamine 295 (Q295) of the mAb's heavy chain and a primary amine. However, until the present thesis, the site-directed, homogeneous modification of Q295 was only feasible with aglycosylated, or deglycosylated antibodies. Glycosylated, native variants did not or only to a minor extent show modification at the position Q295. It was reasoned at that time that the branched oligosaccharides at asparagine 297 (N297) presumably sterically hinder Q295 functionalization of antibodies with MTG. Glycans are partially responsible for the antibody-dependent cellular cytotoxicity (ADCC), complement-dependent cytotoxicity (CDC), and for the interaction with the high affinity immunoglobulin gamma Fc receptor I (Fc γ RI). At the same time, glycosylation stabilizes the quaternary and tertiary structure of the mAb.

In the course of our studies, we have found accidentally that certain peptides containing lysine (K) can be conjugated to Q295 of native, fully glycosylated antibodies by MTG. Because this was contradictory to our previous observations, we systematically investigated this phenomenon. In **chapter 4**, a peptide library consisting of 42 sequences with 3-8 amino acids including at least one K has been tested for conjugation ability to Trastuzumab, a human epidermal growth factor receptor 2 (HER2/neu) targeting mAb, that is often used as benchmark for various immunoconjugates. Conjugation efficiencies to Q295 vary between 0-94% for the various peptides at standardized reaction conditions (Trizma pH 7.6 Buffer, incubation time of 20 h at 37 °C, with 80 eq. peptide, 1 mg/mL mAb, and 6 U MTG/ mg mAb). We observed that peptides with high conjugation efficiency, like peptides RAK (94 \pm 0.4% conjugation yield) and RAAK (94 \pm 0.7% conjugation yield), possess a positive overall charge, whereas rather negatively charged peptides such as KADDD and FKETAA showed low or no conjugation. In order to optimize the enzymatic coupling yield, we varied parameters such as temperature, pH, buffer systems, inorganic salts and the antibody concentration. Optimal results were obtained at temperatures such as 42 °C, in

the buffer media Trizma, HEPES, or MOPS at pH 7.6. Furthermore, higher antibody concentrations (tested until 5 mg/mL) lead to higher yields of the conjugate.

To equip the antibodies with functionalities such as toxins or chelators for radiolabeling, we added a biorthogonal, chemical handle to the peptides. We extended the best peptide sequences RAK, KHR, RSK and RAKAR with an ϵ -azido-lysine for subsequent click reactions with alkyne and alkyne derivatives. To explore the scope of the enzymatic method and the peptide substrates towards various isotopes of antibodies, we used the substrate Ac-RAK-K(N₃)-NH₂. It was coupled to human IgG1, IgG2, IgG4, murine and rat antibodies as well as the commercial ADCs Kadcyła[®] and Adcetris[®]. All human IgG1's and ADCs Kadcyła[®] and Adcetris[®] were conjugated quantitatively (>95%) with the peptide Ac-RAK-K(N₃)-NH₂. Nivolumab, an IgG4 isotype antibody, showed a second coupling site at Q311, though the modification at Q311 was not quantitative (<20 %). Some rodent antibodies showed additionally conjugation at the light chain. Mice antibodies IgG2a and IgG2b showed no or low attachment in the heavy chain due to the missing Q295, but efficient conjugation of the light chain of IgG2b (>95%), but not for IgG2a.

In **chapter 5**, we describe how we rationally identified further suitable peptide substrates by applying an *in silico* method, developed by the Schneider group at the ETHZ. We created a self-organizing map (SOM) based on the initial 42 experimentally screened peptide using a randomly selected threshold of >60% coupling yield to be considered as a *good* substrate. More than 500 peptide sequences including at least one lysine were subjected to a virtual screening and attributed to our SOM. Out of these screened peptides, 17 were experimentally tested to verify the validity of the SOM. We observed that all sequences predicted to be good substrates were correctly assigned (>60% labeling yield) whereas 3 out of 6 peptides predicted to be bad substrates in fact conjugated >60%.

In **chapter 6**, we verified *in vitro* the features of MTG mediated immunoconjugates with Ac-RAKAR-K(N₃)-NH₂ and NH₂-K(N₃)-CRAK-OH. The two peptide derivatives were quantitatively attached to Trastuzumab, and in a second step functionalized with the fluorescent dye DBCO-PEG₄-5/6-FAM (Ac-RAKAR-K(N₃)-NH₂). NH₂-K(N₃)-CRAK-OH, comprising next to the azide an additional cysteine as a second coupling site, allows chemical modification by a maleimide group. The immunoconjugate showed a retained binding towards antigen HER2/neu on Skov3-ip ovarian cancer cells. After attaching the linker to Trastuzumab, chelator maleimide-NODAGA was conjugated towards the sulfhydryl group on the cysteine, and in a third step the toxin DBCO-PEG₄-Ahx-maytansine via the azide functionality. Mass spectrometry (MS) analysis showed the formation of >95% homogenous Trastuzumab-NH₂-K(maytansine)-C(NODAGA)RAK-OH. To reduce conjugation steps, the chelator NODAGA was covalently attached to a third linker construct, NODAGA-K(N₃)-RAK-NH₂. After quantitative conjugation to

Trastuzumab, maytansine was attached to the azide. MS analysis showed full conversion to Trastuzumab-NODAGA-K(maytansine)-RAK-NH₂. The Trastuzumab-conjugates with chelator NODAGA attached were radiolabeled with ¹¹¹In with >95% purity. Lindmo analysis for Trastuzumab-NH₂-K(maytansine)-C(NODAGA)RAK-OH, Trastuzumab-NODAGA-K(N₃)-RAK-NH₂, and Trastuzumab-NODAGA-K(maytansine)-RAK-NH₂ showed immunoreactive fractions of 102%, 111.1%, and 110.9%, respectively.

In **chapter 7**, we present the results of a comparative biodistribution study with ¹¹¹In labeled Trastuzumab-NODAGA-K(N₃)-RAK-NH₂, and Trastuzumab-NODAGA-K(maytansine)-RAK-NH₂ and as well as with a deglycosylated variant of the latter, Trastuzumab_{deglyc.}-NODAGA-K(maytansine)-RAK-NH₂ in a s.c. Skov3-ip mouse model. We wanted to see if the hydrophobic toxin changes tumor-, and off-target uptake. Furthermore, we were interested to see if the glycosylation has an impact on organ uptake, especially since our older enzymatically produced ADCs were dependent on the deglycosylation step. The conjugates showed efficient tumor uptake, already in the range of 20% of the injected dose per gram organ (%iD/g) after 24 h, and up to 40%iD/g or higher for the other time points of 48 h, 72 h, and 96 h. The other organs had low uptake, with the blood containing approx. 10%iD/g. We observed for all the time points no significant difference in tumor uptake in-between the three radiolabeled ADCs, showing that the hydrophobic toxin is not affecting the biodistribution within our tested setting.

Zusammenfassung

Krebs ist verantwortlich für 17% der Todesfälle und somit die zweithäufigste unnatürliche Todesursache, gemäss der Weltgesundheitsorganisation (2020). Systemische Therapie hat viele Fortschritte erzielt in den letzten Jahren, aber einer der grossen Nachteile ist immer noch die Toxizität im gesunden Gewebe. Ein Weg dieses Problem zu beheben ist der Gebrauch von Antikörpern die ein zelltoxisches Gift tragen, so genannte Antikörper-Wirkstoff Konjugate (ADC), und gezielt den Krebs angreifen. Bereits neun ADCs wurden genehmigt von der United States Federal Drug Administration (FDA). Jedoch zeigten klinische und präklinische Studien, dass die Anzahl von festgemachten Toxinen, ihre Position, sowie der verbindende Linker entscheidend sind für einen therapeutischen Effekt. Kürzlich zeigten Biodistributionsstudien, dass das ortsspezifische Festmachen vom Toxin zu besserem pharmakokinetischen Verhalten führte, verglichen mit nicht-ortsspezifischem, heterogenem Befestigen. Unsere Gruppe war Pionier für den Gebrauch vom Enzym mikrobielle Transglutaminase (MTG) für das ortsspezifische Befestigen von Toxinen. Wir konnten zeigen, dass MTG eine isopeptidische Bindung zwischen dem Glutamin 295 (Q295) vom mAb und einem primären Amin formt. Jedoch, bis hin zu dieser Thesis, war das ortsspezifische, homogene Befestigen beim Q295 nur möglich mit aglykosilierten, oder deglykosilierten Antikörper. Glykosilierte native Antikörper zeigten nur wenig oder gar keine Modifikation an der Position Q295. Dies wurde dazumal damit begründet, dass das verzweigte Oligosaccharid beim Asparagin 297 (N297) vermutlich sterisch die Funktionalisierung des mAb mit MTG hindert. Die Zuckermoleküle sind teilweise verantwortlich für die Antikörper abhängige zelluläre Toxizität (ADCC), der komplementierenden abhängigen Zelltoxizität (CDC), oder für die Interaktion mit dem stark affinen Immunoglobulin Gamma Fc Rezeptor I (Fc γ RI). Gleichzeitig stabilisiert die Glykosylation die quaternäre und tertiäre Struktur vom mAb.

Während unseren Studien haben wir zufällig herausgefunden, dass bestimmte Peptide mit einem Lysin ans Q295 von komplett nativen, voll glykolisierten mAb konjugieren können mit MTG. Da dies widersprüchlich zu unseren vorherigen Observationen war, haben wir dieses Phänomen systematisch weiter untersucht. Im **Kapitel 4** haben wir eine Peptidserie von 42 Sequenzen mit 3-8 Aminosäuren und mindestens einem Lysin mit MTG an Trastuzumab konjugiert, einem menschlichen Epidermis Wachstumsfaktor Rezeptor 2 (HER2/neu) bindenden mAb. Die Effizienz der Konjugation an das Q295 variierte zwischen 0-94% bei standardisierten Bedingungen (Trizma pH 7.6 Puffer, Inkubationszeit von 20 h bei 37 °C, mit 80 Eq. Peptiden, 1 mg/mL mAb, und 6 U MTG/ mg mAb). Wir stellten fest, dass Peptide mit hoher Konjugationseffizienz, wie Peptide RAK (94 \pm 0.4%) oder RAAK (94 \pm 0.7%), eine allgemeine positive Ladung besitzen, während hauptsächlich negativ geladene Peptide wie KADDD und FKETAA keine oder nur sehr wenig Konjugation zeigten. Um die Ausbeute dieser enzymatischen

Reaktion zu steigern, haben wir verschiedene Parameter wie die Temperatur, den pH, die Puffersysteme, anorganische Salze, sowie Antikörper Konzentrationen variiert. Ideale Resultate erreichten wir bei einer Temperatur von 42 °C, in den Puffern Trizma, HEPES, oder MOPS bei einem pH von 7.6. Zudem brachten höhere Antikörperkonzentrationen (bis zu 5 mg/mL getestet) bessere Ausbeute vom Konjugat.

Um dem Antikörper Funktionalitäten wie Toxine oder Chelatoren für die Radiomarkierung zu befestigen, haben wir einen bioorthogonalen chemischen Halter befestigt. Wir erweiterten die besten Peptidsequenzen RAK, KHR, RSK, und RAKAR mit einem ϵ -azido-Lysin für eine anschließende click Chemie Reaktion mit Alkinen und Alkin-Derivaten. Um herauszufinden wie breit die enzymatische Methode anwendbar ist auch für verschiedene Isotypen von Antikörpern, haben wir das Substrat Ac-RAK-K(N₃)-NH₂ benutzt. Es wurde an menschliche IgG1, IgG2, IgG4, Mäuse, Ratten-Antikörper sowie auch an kommerzielle ADCs Kadcyla[®] und Adcetris[®] gekoppelt. Alle menschlichen IgG1's sowie die ADCs Kadcyla[®] und Adcetris[®] konjugierten quantitativ (>95%) mit dem Peptid Ac-RAK-K(N₃)-NH₂. Nivolumab, ein IgG4, hatte eine zweite Konjugationsstelle beim Q311, aber diese Modifikation war nicht quantitativ (<20%). Einige Nagetier-Antikörper zeigten zudem Konjugation in der leichten Antikörper-Kette. Mausantikörper IgG2a und IgG2b zeigten keine oder wenig Konjugation in der schweren Kette, da sie kein Q295 besitzen, jedoch gute Konjugation an der leichten Kette für IgG2b (>95%).

Im **Kapitel 5** beschreiben wir, wie wir rational neue brauchbare Peptidsubstrate identifiziert haben, in dem wir eine *in silico* Methode angewendet haben, die von der Schneider Gruppe an der ETHZ entwickelt wurde. Wir kreierten eine selbst-organisierte Karte (self-organizing map, SOM) basierend auf den initialen 42 experimentell getesteten Peptiden indem wir einen Grenzwert von >60% Konjugationseffizienz festlegten, der die Substrate darüber als gut bezeichnete. Mehr als 500 Peptidsequenzen mit je einem Lysin wurden in eine virtuelle Durchleuchtung gegeben, die die Sequenzen der SOM zuordnete. Von diesen Sequenzen haben wir 17 experimentell getestet um die SOM zu validieren. Wir stellten fest, dass alle als gut vorhergesagten Sequenzen korrekt zugeordnet wurden (>60% Konjugationseffizienz), während 3 von 6 als schlecht vorhergesagten Substraten auch über 60% konjugierten.

Im **Kapitel 6** verifizierten wir die *in vitro* Eigenschaften von unseren MTG behandelten Immunokonjugaten mit Ac-RAKAR-K(N₃)-NH₂ und NH₂-K(N₃)-CRAK-OH. Die beiden Peptidderivate wurden quantitativ an Trastuzumab befestigt und in einem zweiten Schritt mit dem fluoreszierenden Farbstoff DBCO-PEG_{4-5/6}-FAM funktionalisiert (Ac-RAKAR-K(N₃)-NH₂). NH₂-K(N₃)-CRAK-OH hat neben dem Azid zusätzlich noch ein Cystein als zusätzliche Kopplungsseite, was chemische Modifikation

mittels einer Maleimid-Gruppe ermöglicht. Das Immunokonjugat behielt die Bindung an HER2/neu Antigene an Skov3-ip Eierstockkrebszellen bei. Nach dem Befestigen vom Linker an Trastuzumab, wurde der Chelator Maleimide-NODAGA an die Sulfhydryl Gruppe vom Cystein konjugiert und in einem dritten Schritt das Toxin DBCO-PEG₄-Ahx-Maytansin via die Azid Funktionalität. Eine Massenspektrometrieanalyse (MS) zeigte >95% von unserem generierten ADC Trastuzumab-NH₂-K(maytansine)-C(NODAGA)RAK-OH. Um Kopplungsschritte zu reduzieren, haben wir Chelator NODAGA kovalent an ein drittes Linkerkonstrukt gebunden, NODAGA-K(N₃)-RAK-NH₂. Nach quantitativer Befestigung an Trastuzumab wurde Maytansine ans Azid gebunden. MS Analyse zeigte vollständige Konversion zu Trastuzumab-NODAGA-K(maytansine)-RAK-NH₂. Alle Trastuzumab-Konjugate mit Chelator NODAGA daran wurden radiomarkiert mit ¹¹¹In mit einer Effizienz von >95%. Lindmo Analysen für Trastuzumab-NH₂-K(maytansine)-C(NODAGA)RAK-OH, Trastuzumab-NODAGA-K(N₃)-RAK-NH₂, und Trastuzumab-NODAGA-K(maytansine)-RAK-NH₂ zeigten immunoreaktive Fraktionen von 102%, 111.1%, und 110.9%.

Im **Kapitel 7** präsentieren wir die Resultate einer vergleichenden Biodistributionsstudie mit ¹¹¹In radiomarkiertem Trastuzumab-NODAGA-K(N₃)-RAK-NH₂, Trastuzumab-NODAGA-K(maytansine)-RAK-NH₂ und sowie einer deglykosylierten Variante des vorherigen, Trastuzumab_{deglyc.}-NODAGA-K(maytansine)-RAK-NH₂ in einem s.c. Skov3-ip Mausmodell. Wir wollten sehen ob die Hydrophobizität vom Toxin die Tumoraufnahme und die ungezielte Aufnahme beeinflusst. Zusätzlich waren wir interessiert zu sehen ob die Glykosylierung einen Einfluss hat auf die Organaufnahme, da unsere alten enzymatisch produzierten ADCs von einem Deglykosylierung-Schritt abhängig waren. Die Konjugate zeigten effiziente Tumoraufnahme, schon im Bereich um 20% nach 24 h, und bis zu 40% oder höher für die anderen Zeitpunkte 48 h, 72 h, und 96 h. Die Aufnahme in andere Organe war tief, während das Blut etwa 10% der injizierten Dosis beinhaltete. Wir observierten für alle Zeitpunkte keine signifikante Veränderung der Tumoraufnahme zwischen den drei radiomarkierten ADCs, was aufzeigt, dass das hydrophobe Toxin keinen Einfluss auf die Biodistribution hat in unserem getesteten Rahmen.

1. General Introduction

1.1. Therapeutic antibodies

With 1 out of 6 deaths, cancer is the second leading cause of death in the world according to the World Health Organization (2020). For men prostate cancer is the most prevalent form, whereas for women it is breast cancer. The most lethal cancer in numbers is still lung cancer for both sex, with 23% in men, and 21% in woman (estimates for 2020)^[1]. Common therapies include surgical removal of tumors, radiation-, or systemic therapy. Especially in systemic therapy, the field made a lot of progress in the recent years. It promises less toxicity and greater efficacy for cancer treatment by targeted therapy^[2]. This principle is not new, as Paul Ehrlich mentioned a century ago the concept of a “magic bullet” that seeks their target for their own accord^[3]. In the field of targeted medicine, especially in oncology, monoclonal antibodies (mAbs) have become very important. They show highly specific antigen binding and induce immune system mediated toxicity^[4,5]. Alone at the end of November 2019, 79 new mAbs were in late-stage clinical studies, with 40 of them being developed for cancer treatment. This number has tripled since 2010. As of the end of 2019, 6 novel mAbs were approved either in the US or EU, and around 13 are expected to get approval in 2020^[6]. Human mAbs are classified into four immunoglobulin (IgG) subclasses, IgG1, IgG2, IgG3, and IgG4 (Figure 1). Their main structural difference is the number of disulfide bonds, whereas the classification identifies their targets (e.g. membrane-, and bacterial antigens for IgG1 and IgG2)^[7]. Therapeutic immunoconjugates mainly are made with subclasses IgG1 and IgG4^[8].

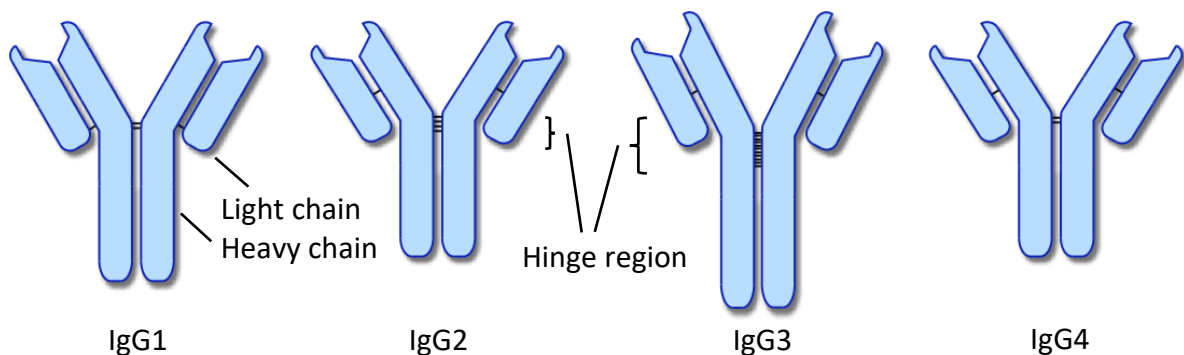


Figure 1: Scheme of the four IgG subclasses, which share 90% amino acid sequence homology. They differ in numbers and positions of disulfide bridges, as well as on the length of the hinge region^[7]. Black lines between heavy and light chains indicate disulfide bridges. Compared to IgG1, IgG2 and IgG4 have shortened hinge regions, whereas the hinge of IgG3 is prolonged.

Other than just receptor blocking, there are two main working principles of mAbs leading to the toxic impact on the bound cell. One is the antibody-dependent cellular cytotoxicity, ADCC. After binding of the human IgG1 to the antigen on the cancer cell, the Fc receptors on immune effector cells (macrophages, natural killer cells, neutrophils) will interact with the crystallizable fragment (Fc) region of the IgG1 (CH2+CH3). This induces tumor cell elimination by lysis or phagocytosis^[9-11]. The second

toxic working principle is the complement-dependent cytotoxicity, CDC, whereas recruitment of the complement component C1q is inducing a membrane attack complex that subsequently kills the tumor cell by lysis. However, these effector functions can be mild. While mAb engineering helped to improve the therapeutic effect of mAbs^[12,13], nowadays there is a big trend in creating either armed mAbs, so called antibody-drug-conjugates (ADC), or bispecific mAbs (biAbs). Since the end of 2017, over 500 manuscripts were published involving biAbs^[14]. By cross-engineering light, and/or heavy chains of two distinct mAbs, two different cancer antigens can be targeted, thus enhancing the specificity. This technology shows successful results especially in cancer immunotherapy, whereas one mAb arm is engineered to recruit T-cells. BiAbs show reduced adverse effects and drug resistance^[14–16]. The other big promising class used for mAb therapy are ADCs, discussed below.

1.2. Glycosylation of antibodies

At the position Asn297, IgGs have a glycan attached, most often a biantennary structure consisting of different oligosaccharides (mainly sialic acid, mannose, N-acetylglucosamine, fucose, galactose, and N-acetylneuraminic acid, Figure 2)^[17]. Depending on the glycan composition, the mAb efficacy can vary^[18]. When core-fucose levels are decreased, ADCC can be increased up to 50x by making IgG1 more affine to Fc γ RIIIa on immune cells^{[19,20][21]}. On the other hand, the role of glycans in FcRn binding is believed to be marginal^[17]. Some studies show no change of pharmacokinetics depending on different glycosylation^[22,23], whereas other studies showed an impact^[24,25]. Recently, Vivier *et al.* compared the Fc γ RI interactions more closely. They compared deglycosylated immunoconjugates with immunoconjugates with different glycosylation states. Interestingly, they saw a strong correlation that immunoconjugates with impaired Fc γ RI interaction (due to the missing glycan) lead to higher tumor uptake and significantly less off-target uptake (up to 3.5 fold less uptake in liver in NSG mice) compared to glycosylated versions^[26]. However, deglycosylated mAbs are also more prone to unfolding when induced with guanidine HCl, and lose thermal stability in the CH2 region^[27]. Molecular dynamic simulations show increased quaternary and tertiary structure deformation with deglycosylated IgGs^[28]. Furthermore, they aggregate faster, which is a very critical point for ADCs with the anyway hydrophobic toxins attached^[29].

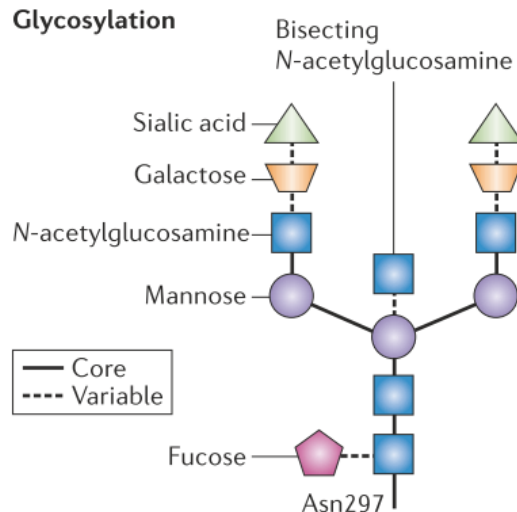


Figure 2: Schematic display of the classical glycans attached to Asn297 on human IgGs. The structure is biantennary, with variable glycans at both ends. Figure from Carter et al.^[30].

1.3. Antibody-Drug Conjugates

Conventional anticancer drugs for chemotherapy often show high systemic toxicity for healthy tissue and with it severe side effects^[31]. Selective delivery of toxins with mAbs as targeting devices is circumventing this problem. These so-called ADCs consist of three important parts, the mAb, the toxin, and the linker as connecting device (Figure 3). The high specificity of mAbs allows attaching highly potent toxins, thereby increasing the therapeutic index of cytotoxic agents^[32]. The working principle is very simple. Upon binding of the receptor, the ADC is internalized, whereas the toxins are cleaved with or without lysosomal activation (Figure 4)^[33]. Dependent on the toxin class, the cell is accordingly put under stress, which leads eventually to cell death.

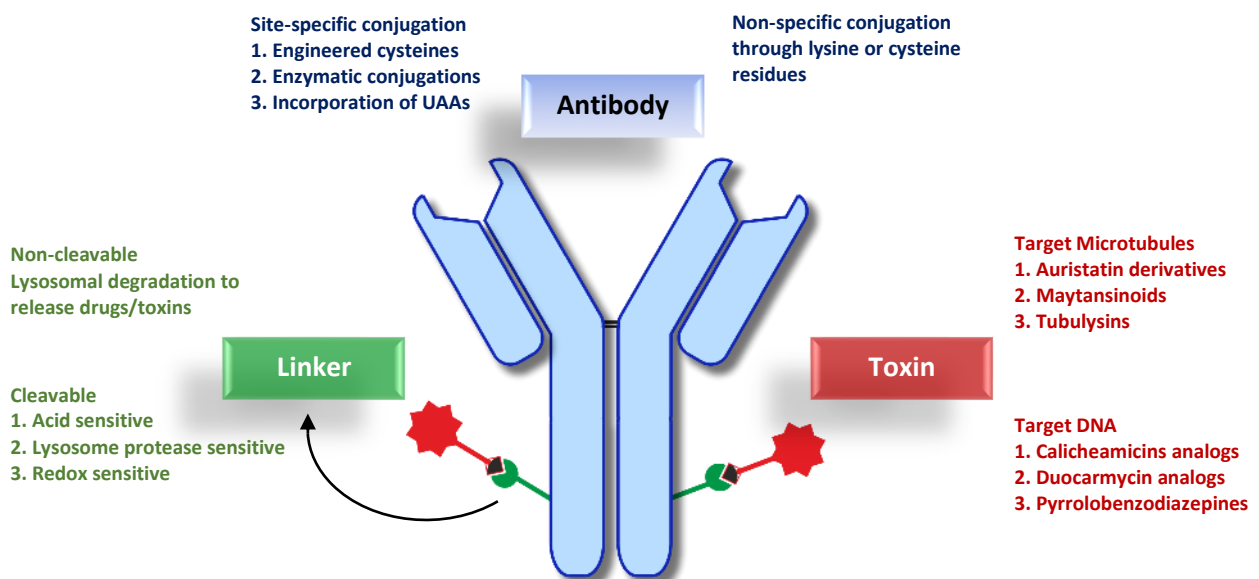


Figure 3: Schematic view of the three important hallmarks of an effective ADC: mAb, linker, and the drug/toxin. Figure adapted from Zhao et al.^[34]

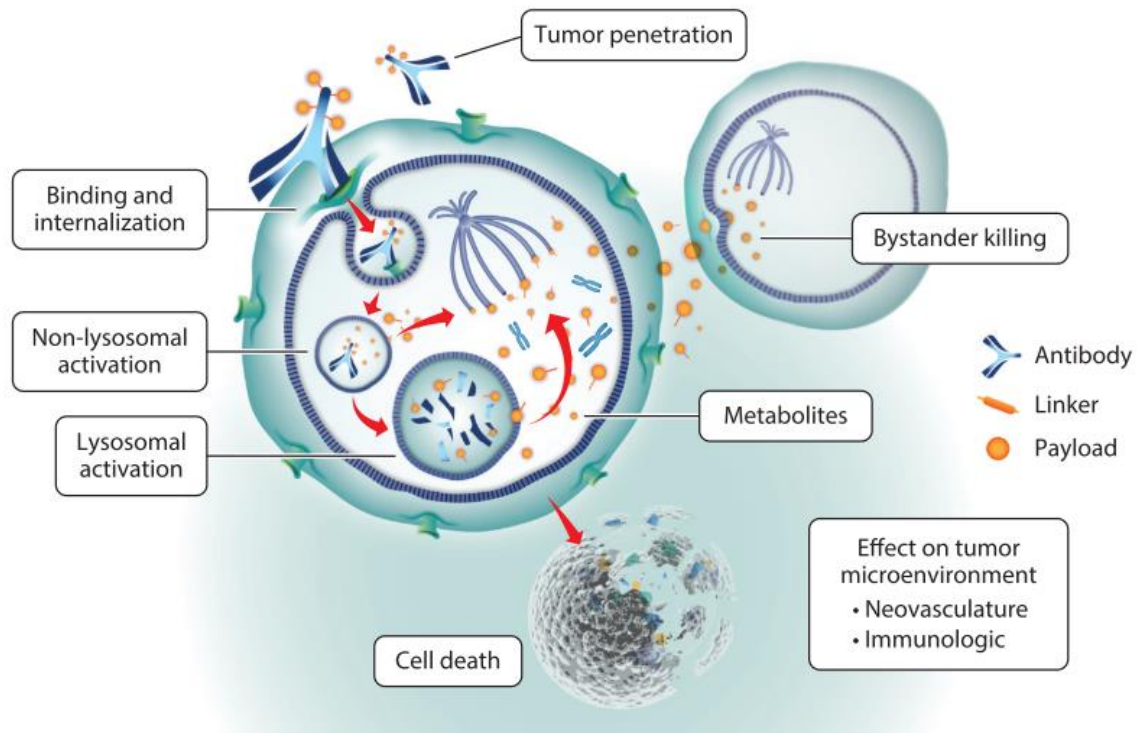


Figure 4: Simplified working principle of ADCs. The ADC binds to the target receptor, gets internalized, whereas the toxin is released. In the shown figure, the toxin disrupts microtubule dynamics (toxins: maytansine, auristatine). The toxin can diffuse to neighboring cells after cleavage from the mAb, leading to the bystander effect. Figure from Walko et al.^[33]

Membrane permeable drugs can kill neighboring cells as well, a term called bystander killing. Interestingly, there has been a lot of success as well with ADCs that are non-internalizing^[35]. A thorough study of Genentech compared different ADCs targeting internalizing and non-internalizing antigens for the Non-Hodgkin's Lymphoma. Surprisingly, non-internalizing ADCs expressed comparable tumor toxicity vs. the internalizing variant^[36]. They carry a mAb-toxin linker that is cleavable and have toxins attached that are membrane permeable. The advantage of such ADCs is that extracellular toxin delivery is not dependent on the tumor biology. Since the toxin is diffusing into several cells, also neighboring cancer cells without overexpressed antigen are targeted. This is called the bystander effect. A similar effect was seen by G bleux and coworkers who found that FDA approved Adcetris[ ] (brentuximab vedotin; targeting CD30) could work extracellularly^[37]. However, Adcetris[ ] was designed to work as internalizing ADC. It is after Mylotarg[ ] (gemtuzumab ozogamicin) the second FDA approved ADC and received marketing approval in 2011^[38]. It has mono methyl auristatin attached and showed overall response rates of 86% (for systemic anaplastic large cell lymphoma, ALCL)^[39] and 75% (for relapsed Hodgkin's lymphoma)^[40]. Adcetris[ ], Mylotarg[ ], and other ADCs were mainly developed for hematologic malignancies, since it has been shown that solid tumors are less amenable for mAbs^[41]. Nevertheless, more and more studies have been conducted targeting solid tumors^[33]. Kadcyla[ ] (Ado-trastuzumab emtansine, T-DM1; FDA approved in 2013) is the first ADC targeting metastatic breast cancer overexpressing human epidermal growth factor receptor 2 (HER2/neu)^[42]. It carries the

maytansinoid DM1 which is attached to Trastuzumab with a non-cleavable linker^[43]. As of 2020, approximately 600 clinical trials have been conducted with ADCs^[34], whereas nine (Mylotarg[®], Adcetris[®], Kadcyca[®], Besponsa[®], Polivy[®], Padcev[®], Enhertu[®], Trodelvy[®], Blenrep[®]) reached FDA approval with around 65 still in clinical trials (www.fda.gov press releases).

1.3.1. Radioimmunoconjugates

While the next generation ADCs improve on all the three hallmarks toxin, linker, and mAb, another way to tackle poor accessibility of heterogeneous tumors are radioimmunoconjugates (RIC). A radionuclide is chemically or via chelator linked to a mAb, enabling therapy or imaging^[2,44,45]. While applying RIC for solid tumors is still limited, excellent results have been reported applying radioimmunoconjugates for advanced haematologic malignancies^[46]. Today, two RICs have been approved, Bexxar[®] (tositumomab) and Zevalin[®] (ibritumomab tiuxetan)^[47]. Bexxar is radiolabeled with ¹³¹I and Zevalin with ⁹⁰Y, both β^- emitters. Since the cellular diameter is smaller than the decay sphere of the radionuclide, RICs may benefit from the bystander effect, but in return can attack healthy tissue at the target site as well. Recently, an interesting study was published by Lakes et al., comparing ²²⁵Ac (α emitter) and ¹⁷⁷Lu (β^-) RICs against an ADC (bearing a pyrrolobenzodiazepine, PDB, toxin) for Small-Cell Lung Cancer^[48]. Both of the radiolabeled mAbs controlled growth in xenografted NOD-SCID mice, with ²²⁵Ac showing lengthened survival. However, the ADC showed full tumor suppression in 9/10 mice. Another interesting short lived radionuclide to mention is ¹¹¹In, which can be used in RIC for therapy or SPECT/PET imaging^[49-51]. One of the big challenges is still to find the balance between the dose exposure of healthy tissue and the dose delivered to the tumor^[52].

1.3.2. Toxins employed in antibody-drug conjugates

Over the past 30 years, more than 50 different toxins have been tested on ADCs. The ones currently in clinical trials either target microtubules or DNA. DNA drugs have an additional advantage as they are cytotoxic as well for non-proliferating cells^[53]. Delivery of toxins to the cancer cell is limited by the overexpression of the antigens as well as by the amount of toxins an ADC can carry. Most of the ADCs in clinical trials have a drug-to-antibody ratio (DAR) of 2-4^[8]. This is why an adequate toxin has to be very potent (picomolar range). Furthermore, their potential for aggregation should be checked, as these toxins are often very hydrophobic, which can lead to fast serum clearance of the ADC^[53,54]. Compounds from the following classes have been and still are tested within the last years: auristatins, maytansinoids, indolino-benzodiazepines, pyrrolobenzodiazepines (PBD), calicheamicins, duocarmycins, amanitins, irinotecan derivatives, doxorubicin and tubulysins^[32,53]. Auristatins, such as

monomethyl auristatin E (MMAE), is the biggest group and are vastly tested by many companies. FDA approved Adcetris® bears MMAE. After release of the mAb, they inhibit tubulin dependent GTP binding, which inactivates the microtubule dynamics^[32]. The other big group of tubulin inhibitors are the maytansinoids, such as DM1/mertansine. Kadcyra® is carrying maytansine as payload. Maytansine binds close to the vinca alkaloid site, suppressing microtubule dynamics, which leads the cell to stop the cell cycle and progresses into apoptosis^[55]. Another interesting working principle of cytotoxins are benzodiazepines and calicheamicins. They are highly potent cytotoxic compounds that bind to the minor groove of DNA, inducing crosslinking or cleaving double stranded DNA, respectively^[56,57]. A third mechanism to highlight is the one from amanitines. The main component α -amanitin, mushroom derived, is structured as bicyclic octapeptide and can inhibit RNA polymerase II^[58]. Similar to the DNA targeting drugs, amanitin is also toxic for non-proliferating cancer cells.

1.3.3. Adverse effects and shortcomings of antibody-drug conjugates

Clinical studies with ADCs conducted in the last years have unveiled limitations and challenges, leading to termination of approx. 55 clinical trials mainly due to toxicity^[59]. ADCs accumulate only to approx. 0.1% of the given dose per gram at the tumor^[60]. Responsible for the limited accumulation are the binding site barriers, shedding of antigens, and hindering of intratumoral ADC movement by interstitial fluid pressure^[44,61–63]. The binding site barrier is a phenomenon that mAbs show differential binding of antigens in the periphery of a tumor, due to high affinity binding of antigens. Expression of the antigen on normal tissue can lead to toxicity, as seen e.g. for a BR96-doxorubicin ADC (gastric mucosal cells are expressing Lewis Y antigens)^[64]. However, it is hard to predict this kind of target-dependent toxicity, as Kadcyra® (vs. HER2/neu) does not show toxicity in heart and kidney, even though they express HER2/neu^[65,66]. Other factors than target-antigen expression are influencing ADC toxicity: antigen trafficking/recycling kinetics, ADC *in vivo* biodistribution to healthy tissue, internalization rate, or the sensitivity of the attached drug^[67]. The distribution and exposure of ADCs in healthy tissue with relatively leaky vasculature and high perfusion is problematic due to non-targeted uptake. Examples are spleen, liver, or bone marrow^[68,69]. Thus, ADC toxicity often is target independent, with the attached drug being the main cause for the toxic impact^[70–72]. A good example is Adcetris®, which has peripheral neuropathy and neutropenia as dose limiting factors^[71]. Recently it was shown, that premature release of the Adcetris® toxin MMAE (attached by cleavable vc-PAB linker) is the main cause for neutropenia^{[73][74]}. For the toxin DM1, attached in Kadcyra®, thrombocytopenia and gastrointestinal effects have been reported^[75,76]. These data is one of the reason why for the next generation mAbs the stability of the linker plays an important role. Mahalingaiah *et al.* made an extensive review with

examples of ADCs currently in clinical trials for the mentioned shortcomings^[66]. A short overview over different uptake mechanisms of payload and ADCs is given in Figure 5.

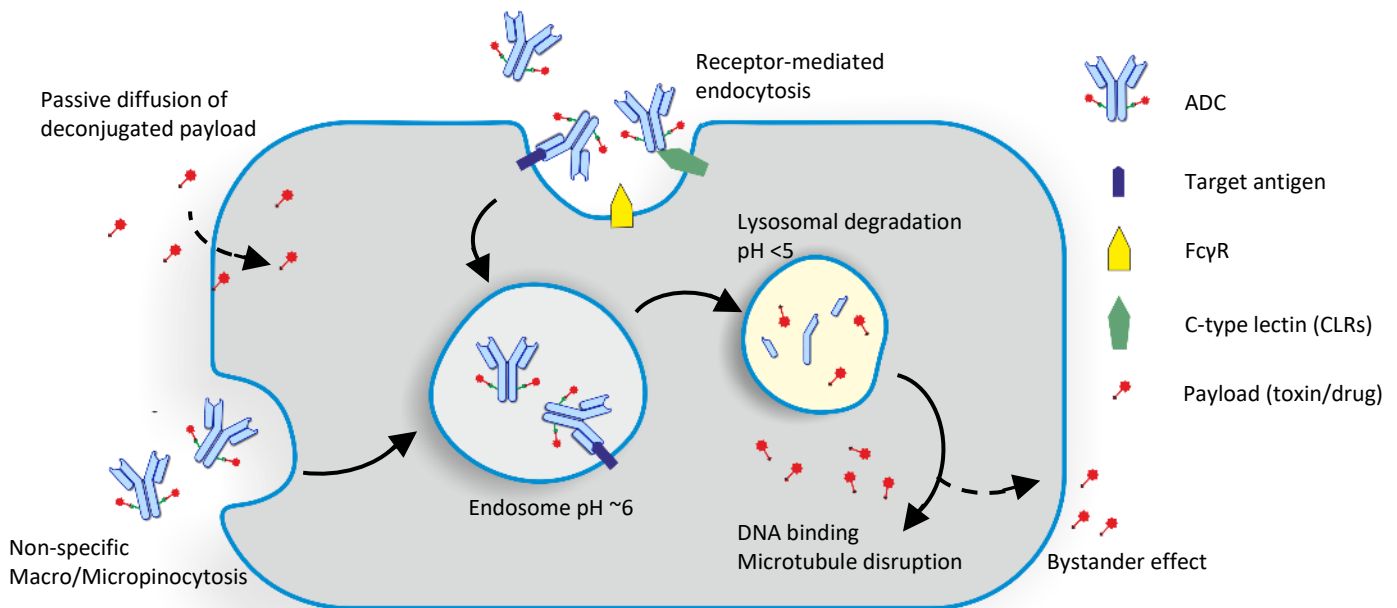


Figure 5: Simplified scheme of possible payload/ADC uptake mechanisms into healthy cells. Figure adapted from Mahalingaiah *et al.*^[66]

1.4. Strategies to attach toxins to antibodies

The next generation of ADCs put a lot of work in optimizing the linkage between toxin or another payload and the mAb. The drug needs to be released at the target site, but should be stable in blood to limit off-target toxicity. A lot of recent studies show that this is a limiting factor^[53,77]. One example are the enzymatically cleavable valine-citrulline linkers (vc), as a mechanistic study from Zhao *et al.* showed. Neutrophils in the bone marrow secrete serine proteases, which can cleave vc-linkers^[73], that leads to off-target toxicity. Though, better performing cleavable linkers have been reported recently, mainly making use of enzymes at the tumor site for cleavage, but also using pH- or reactive oxygen species- sensitivity^[78]. Furthermore, site-specific attachment and position on the mAb are important. Strop *et al.* found that depending on the position, the pharmacokinetics (PK) of the ADC and stability of the linker was significantly changed^[79]. Several studies show that site-specific attachment of linkers, leading to homogeneous ADCs, have a superior PK profile compared to ADCs with heterogeneous toxin attachment^[8,80–82]. Linkers often are designed hydrophilic, to compensate for the most often hydrophobic toxins^[83]. Over the years several methods have been developed to attach linkers in either a site-specific or heterogeneous level (Figure 6). The most prevalent technique right now is the

attachment of toxins to engineered cysteines (No. 3 in Figure 6). In the next two chapters, we show the most used methods separated into chemical and enzymatic attachment.

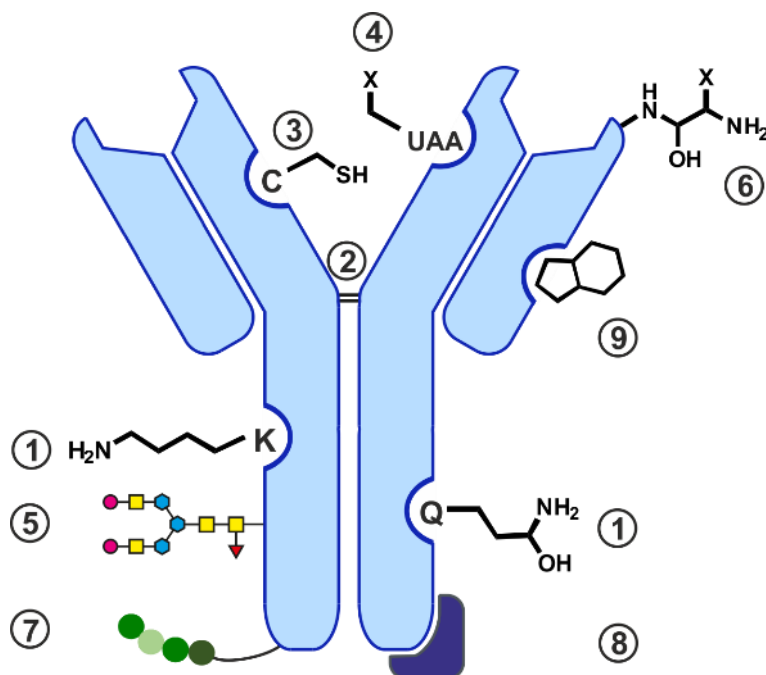


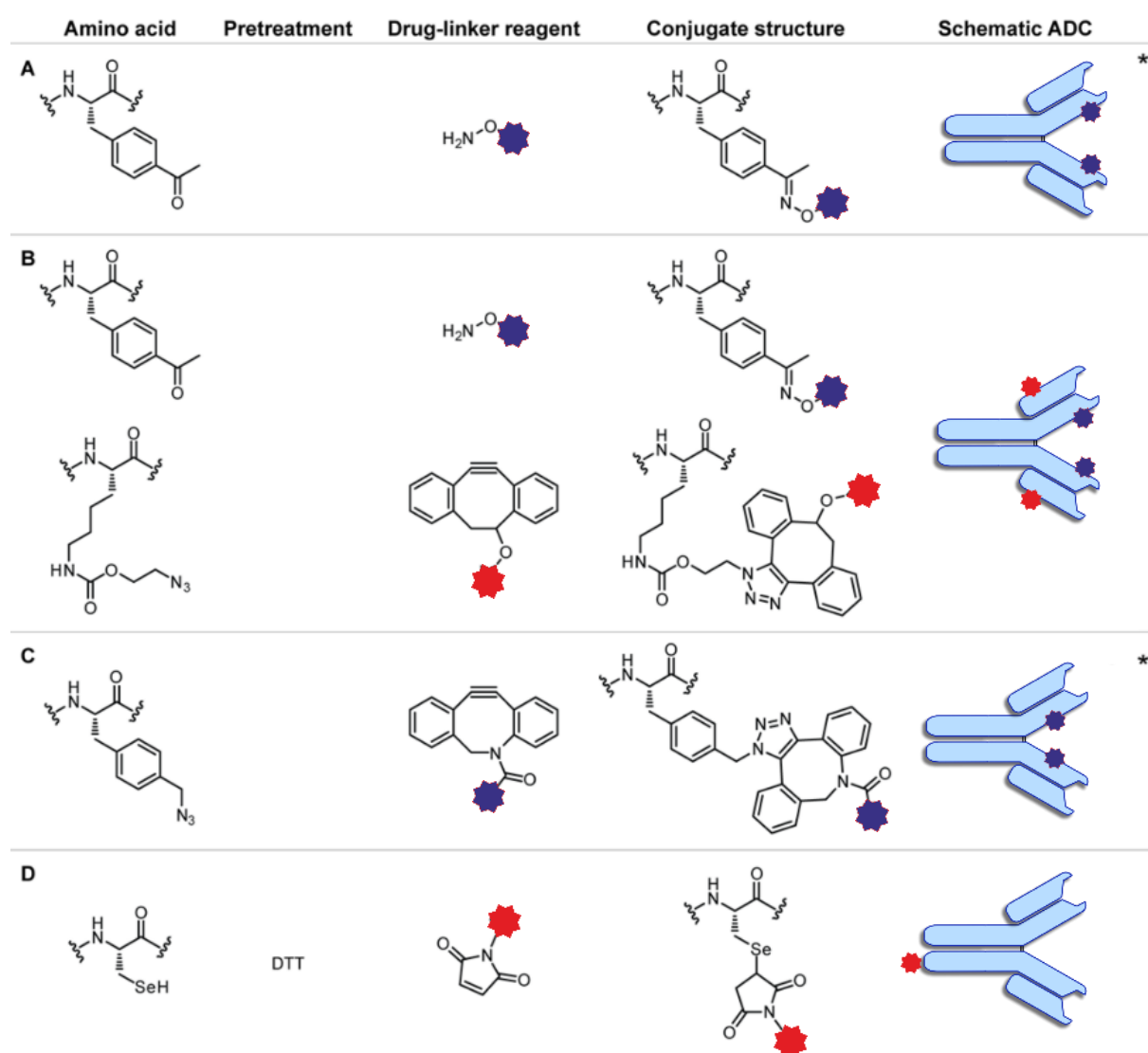
Figure 6: “Antibody conjugates can be generated by targeting natural amino acids (1) including interchain disulfides (2), engineered cysteines (3), non-natural amino acids (4), the carbohydrate moiety (5), the N-terminus of heavy and light chain (6) or engineered tags (7). Strong protein-protein interaction, i.e., Fc-binding domains (FcBD) can be used to form non-covalent antibody conjugates (8). Additionally, the nucleotide binding site (NBS) is a valuable antibody modification site for photoaffinity labeling (9) and mAbs with catalytic activity (10) can be exploited to form bioconjugates where the coupled pharmacophore, e.g., a peptide assumes the targeting function and the antibody acts as a cargo molecule.” Adapted figure and citation from Dennler et al.^[84]

1.4.1. Chemical conjugation

There are two main approaches of chemical conjugation of mAbs that have been used the last years. One is the attachment of payloads that are activated with an N-hydroxysuccinimide (NHS) ester towards native lysines of the mAb. Peptide mapping showed that approx. 40 Lys are recognized at both, the light and the heavy chains of mAbs, leading to more than a million variants^[42,85]. This non-specific approach is used for Kadcyla[®], resulting in a DAR of 3.5^[42]. The second vastly used technology is the conjugation of toxins via native cysteines of the mAb’s disulfide bonds using a maleimide functionality. A reduction step is required (e.g. DTT), to cleave the disulfide bonds in-between the heavy-heavy, heavy-light, and light-light chains before attachment of maleimide is feasible. 8 possible positions are available, leading to theoretically around 100 possible ADC variants^[86]. Furthermore, the maleimide-cysteine bond (succinimides) can undergo retro-Michael reactions, and it has been shown that the payload can transfer to circulating glutathione or albumin in serum. Replacing the maleimide

with a acetamide moiety or other modifications seems to have solved the stability problem^[87,88]. This technology found use in Adcetris[®], which has approx. four MMAE toxins attached^[38]. From the lessons-learned of this first generation ADCs (instable linkers, varying pharmacokinetics of heterogeneous ADCs), the field needed more homogeneous and site-specific approaches for a better defined DAR.

THIOMAB is one of the most used approaches with a defined DAR, licensed from Genetech^[82]. Two cysteines are engineered into the mAb backbone ready for conjugation. However, this approach needs engineering and extensive pretreatment. Other groups are engineering unnatural amino acids (UAAs) into the backbone as an elegant site-selective solution. In Figure 7 is shown a short overview of the most commonly used UAAs. In short: one approach is using *p*-acetylphenylalanine, whereas the ketone is reactive for oxim-moieties^[89,90]. A similar approach was used by Sato *et al.*, by incorporating *p*-



*Several different ADCs were produced by varying the conjugation site, but only one representative structure is shown.

Figure 7: "Conjugation methods based on UAA incorporation. (A) Incorporation of *p*-acetylphenylalanine followed by oxime condensation. (B) Simultaneous incorporation of *p*-acetylphenylalanine and an azido-lysine derivative followed by oxime condensation and Cu-free click chemistry to attach a fluorophore (green star). (C) Cell-free incorporation of *p*-azidomethylphenylalanine followed by Cu-free click chemistry. (D) Incorporation of selenocysteine followed by mild reduction and alkylation." Figure and citation from Agarwal *et al.*^[80]

azidomethylphenylalanine^[91]. The azide group can be targeted subsequently reacted with an alkyne or alkyne derivative (e.g. dibenzo-cyclooctyne, DBCO). Engineering selenocysteines into mAbs is interesting, as remains nucleophilic for conjugation with maleimides at lower pH (5.5), whereas competing aa's such as lysine or cysteine are unreactive^[92,93]. Another chemical method is the chemical conjugation towards the glycan at Asn297. Several techniques have been developed to attach payloads to different (engineered) glycans, whereas most of them need extensive pretreatment. Chemical groups such as thiols for subsequent maleimide chemistry, and azides for subsequent click chemistry are installed on the glycan^[80]. A last site-selective chemical method is the use of affinity peptides. Affinity peptides are selected and engineered (e.g. Z domain of Protein A) to bind towards a specific position on the mAb. Additionally, they have benzoylphenylalanine (BPA) incorporated. BPA can form covalent bonds with amino acids on the mAb upon UV exposure^[94-96]. In conclusion, chemical methods either are non-selective, or they require engineering/pretreatment of mAbs to reach a defined DAR.

1.4.2. Enzymatic conjugation

Over the last years a few enzymatic methods have been developed to generate ADCs or RICs. Their big advantage is the exquisite specificity for amino acids (sequence) on the mAb, resulting in homogeneous and site-specific ADCs with tightly controlled DAR. This specificity itself is their drawback at the same time, as not all linkers are accepted as substrates. Figure 8 shows an overview of the recently developed strategies. Sortase A, from *Staphylococcus aureus*, can recognize the LPXTG motif, with X being any amino acid^[97,98]. Engineered into the backbone of the mAb, the payload is getting conjugated over an oligoglycine linker towards the threonine on the tag, having one glycine as leaving group. Beerli *et al.* showed the ADC potential of this technology, by engineering LPETG motifs towards the C-termini of light and heavy chains of an mAb. By subsequent incubation with sortase A and a MMAE coupled to the oligoglycine, a DAR of approx. 3.2 was reached^[99]. A second conjugation method is making use of the enzymes α -2,6-sialyltransferase (SialT) and β -1,4-galactosyltransferase (GalT). Both conjugate a sialic acid towards both ends of the glycan at Asn297^[100]. In a secondary step, with NaIO₄ sialic acid can be turned into an aldehyde, which then can react with an oxime. It is a versatile technology since Asn97 is conserved all over IgGs. Recently, the technology was developed that directly non-natural saccharides with biorthogonal reaction handles can get attached, licensed as GlycoConnect^[101]. The formylglycine generating enzyme is combining non-natural amino acids from the chemical methods with a peptide tag, which is often used in enzymatic methodologies. The enzyme is coexpressed together with the mAb, whereas the mAb has a CXPXR tag inserted into the sequence.

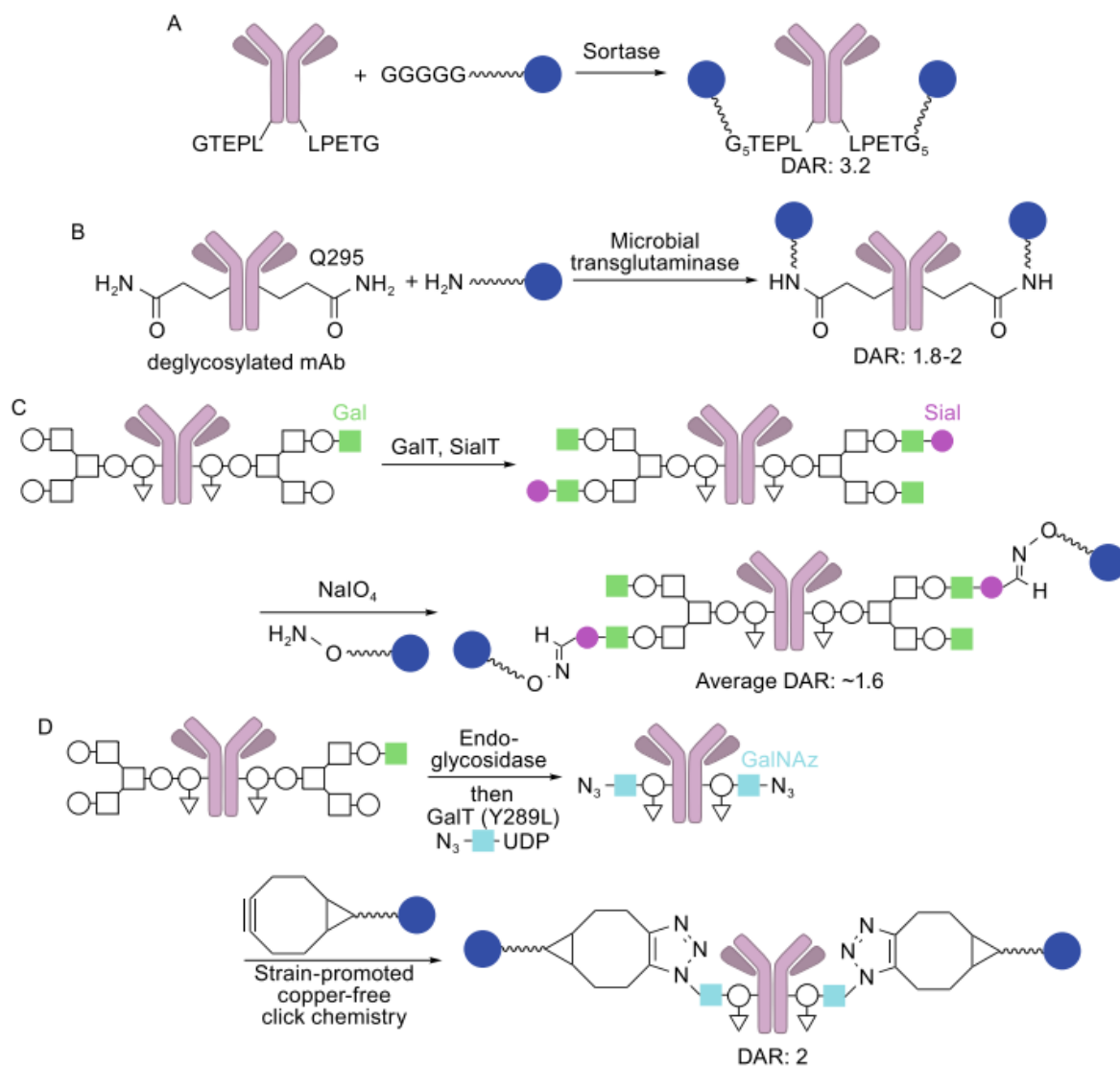


Figure 8: “Site-specific (chemo)enzymatic conjugation. (A) Sortase-mediated conjugation. Sortase attaches oligoglycine-functionalized linkers to LPETG tags on the mAb. (B) Microbial transglutaminase-mediated conjugation. The enzyme attaches an ADC linker possessing a primary amine to Q295 of the heavy chain (DAR: 1.8–2, high homogeneity). (C) Conjugation using β -1,4-galactosyltransferase (GalT) and α -2,6-sialyltransferase (SialT) (light green square: β -1,4-galactose, magenta circle: sialic acid). The aldehyde groups installed react with alkoxyamine-functionalized linkers (average DAR: \sim 1.6). (D) GlycoConnect technology using endoglycosidase, galactosyltransferase, and *N*-azidoacetylgalactosamine (GalNAz, light blue square). The azide groups installed react with strained cyclooctyne-functionalized linkers (DAR: 2, high homogeneity).” Figure and citation from Tsuchikama et al.^[83]

The cysteine within the tag, is enzymatically converted to a formylglycine^[102]. ADCs were produced with a cysteine-to-formylglycine yield of 86-98%, with a subsequent maytansine attachment yielding in 90%^[103]. Not shown in Figure 8 is the enzymatic approach using SpyLigase. The Kolmar group is using this enzyme that can make spontaneous, but specific isopeptide bonds between two sequences, called SpyTag and KTag. They have produced ADCs with toxicity in the subnanomolar range, by engineering the SpyTag into the mAb backbone, whereas the payload was attached to the KTag^[104]. The use of microbial Transglutaminase in the ADC field is introduced in the next chapters.

1.5. Microbial Transglutaminase

Microbial Transglutaminase from *Streptomyces mobaraensis* (MTG, EC 2.3.2.13) has the first time been isolated in 1989^[105,106]. It catalyzes the crosslinking of proteins, forming an isopeptidic bond between a lysine and a glutamine. It is 37.8 kDa in size, and in comparison with mammalian transglutaminases (TGs), shows broader substrate specificity and is calcium-independent. This made it an interesting enzyme for the industry, especially as it has a decreased deamidation rate compared to other TGs as well, with a high reaction rate^[107–109]. It is widely used in the food industry (especially meat processing), textile industry, and more and more in biomedical applications. Despite the widespread use in industry, MTG is still poorly understood in its native function and catalytic mechanism^[110,111]. The 3D structure is disc-like shaped with the active site in a deep cleft. The hypothetical catalytic cycle (Figure 9) uses a triad of amino acids, namely C64, H274, and D255. The substrate specificity for the acyl donor (Gln) has been tested by several groups. A GGGQGGG test peptide was taken and the glycines exchanged with different amino acids, then enzymatically conjugated towards monodansylcadaverin. All the

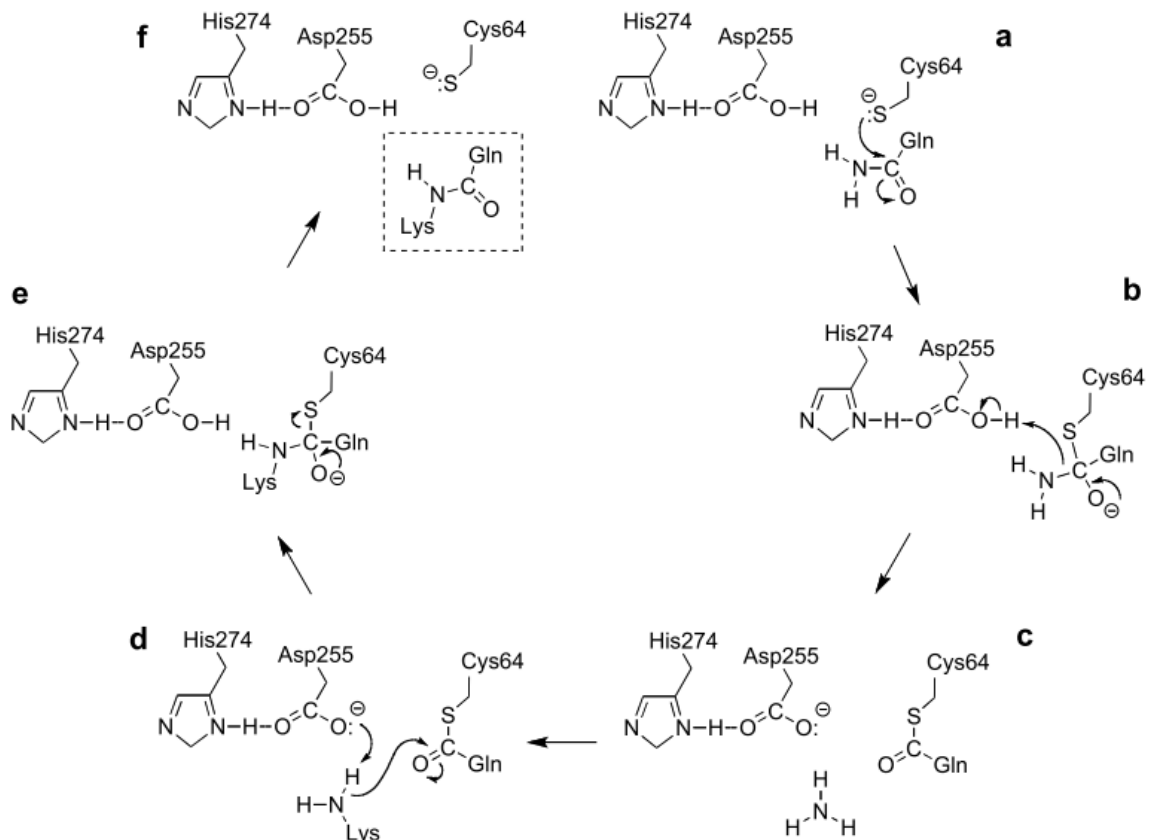


Figure 9: "Hypothetical catalytic mechanism of BTG. (a) His274, Asp255 and Cys64 form the catalytic triad. The nucleophilic thiolate ion of Cys64 attacks the acyl donor (glutamine side chain of a protein). (b) Asp255 donates a proton to the resultant acyl-enzyme intermediate. (c) Ammonium is released. (d) The acyl acceptor (lysine side chain of another protein) approaches the active site, and the side chain of the now negatively charged Asp255 removes a proton from the acyl acceptor. (e) and (f) The product (two proteins crosslinked by a $N\epsilon$ (γ -glutamyl)lysine isopeptide bridge) is released and the active centre of the enzyme is re-established¹⁹⁶." Citation and Figure from the thesis of S. Jeger^[112], proposed mechanism from Kashiwagi et al.^[108]

tested substrates showed activity, yet highest for hydrophobic residues close to the Gln^[113]. Phage-display analysis with tripeptides revealed that basic and hydrophobic amino acids, especially tyrosine, arginine, and leucine, are advantageous close to the Gln (tested with monodansylcadaverin as acyl acceptor)^[114,115]. Furthermore, it has been postulated that the secondary structure influences if a Gln can act as substrate for MTG^[116]. Peptide chain flexibility and local unfolding can improve the reactivity^[117]. Furthermore, Zhao *et al.* showed that MTG can be engineered to gain specificity for specific Glns^[118]. On the acyl-donor side, MTG is not specific for lysines only. A myriad of non-natural substrates containing primary (and some secondary/tertiary) amines has been tested in conjugations towards Z-Gln-Gly^[119]. Even glycine, short-chain alkyl based amino acids, and esterified α -amino acids (Cys, Thr, Ser, Trp) formed the covalent bond with Z-Gln-Gly. A phage display analysis by Malesevic *et al.* was made using tripeptides containing lysine (vs. acyl donor LQR)^[114]. Aromatic amino acids were well accepted +1 or -1 aa from the Lys, whereas anionic residues were making the reaction less effective. In conclusion, MTG reactions are dependent on the acyl donors, whereas the high tolerability for acyl acceptor widens up the scope even for non-natural amine containing compounds^[111,114].

1.6. MTG mediated conjugation of antibodies/antibody-fragments

Our group has pioneered the use of microbial transglutaminase (MTG) for the chemo-enzymatic modification of tumor targeting mAbs with different (radio)metal chelators, fluorescent dyes and toxins via glutamine 295 (Q295) of the Fc (See Figure 8B)^{[84,120],[121]}. However, quantitative modification of Q295 with substrates containing a primary amine was observed only for aglycosylated or deglycosylated IgGs. This either requires the use of PNGase for deglycosylation of N297 or genetic engineering to abolish glycosylation via N297A, which in return reduces antibody-dependent cell-mediated cytotoxicity (ADCC) and can decrease the stability of an mAb due to enhanced proteolytic digestion and aggregation^[27]. However, a homogeneous and site-specific ADC with toxin MMAE was produced with this chemo-enzymatic methodology using aglycosylated Brentuximab[®] yielding in a DAR of 4. A comparison with Adcetris[®] (Brentuximab, with chemically conjugated MMAE towards Cysteines) showed significant higher tumor uptake vs. less liver and spleen uptake for the chemo-enzymatically produced ADC^[122]. The drawback of reduced ADCC because of the truncated/abolished glycans could be circumvented by installing a highly active Gln containing peptide-tag to mAbs. The myc-tag is one of it. Dennler *et al.* showed the strength of the myc-tag (Sequence: EQKLISEEDL), by c-terminally engineering it towards Fab, Nano-, and Affibody segments. Different functionalities (amine containing chelators/dyes/biotin) were attached subsequently with MTG^[123]. Recently, the Kolmar group genetically introduced glutamine tags that are recognized by MTG at various positions in a

mAb^[124], while Spidel *et al.* reported on the conjugation of IgGs via engineered Lys using MTGase^[125]. Dieckgiesser *et al.* used an engineered MTG variant to modify native IgG1 with primary amine substrates^[126]. The last three methods allowed the retention of the glycans but required either substantial genetic engineering of the enzyme/mAb, or the conjugation of the mAbs was not quantitative.

2. Prelude

One of the ongoing ideas in the ADC field is to create a mAb with several chemical entities for orthogonal modification. It would enable to employ two different toxins to tackle the problem of a possible drug resistance, or, when combined with a fluorescent dye or chelator for subsequent radiometal labeling, the ability to use the mAb for interoperative imaging or a theranostic approach. While installing a single multifunctional linker with a convenient method can be straight forward, several biorthogonal and site-selective approaches have been developed for peptides and proteins that enable dual functionalization^[127]. They include functionalization of N- and C-termini of proteins^[128], the use of specific enzymes^[129], unnatural amino acids^[129–131], or combinations thereof^[132]. Useful are also differences in reactivity or accessibility of specific amino acids (aa) within the biomolecule^[133–135]. Lee *et al.* recently combined the use of sortase A and π -clamp conjugation to generate dual functionalized mAb fragments^[136]. Xiuling *et al.* made another successful approach by dual functionalizing an mAb by engineered selenocysteines and cysteines^[137]. Within our group, we wanted to take advantage of the selectivity of MTG. On one side, MTG can target Q295 on the deglycosylated IgG1 heavy chain, but potentially also on N- or C-terminally engineered lysines or glutamines on the heavy and light chain. Our initial strategy using the in house available L1-CAM targeting mAb chCE7 is depicted in Figure 11. Since Dennler *et al.* have shown that the glutamine of a

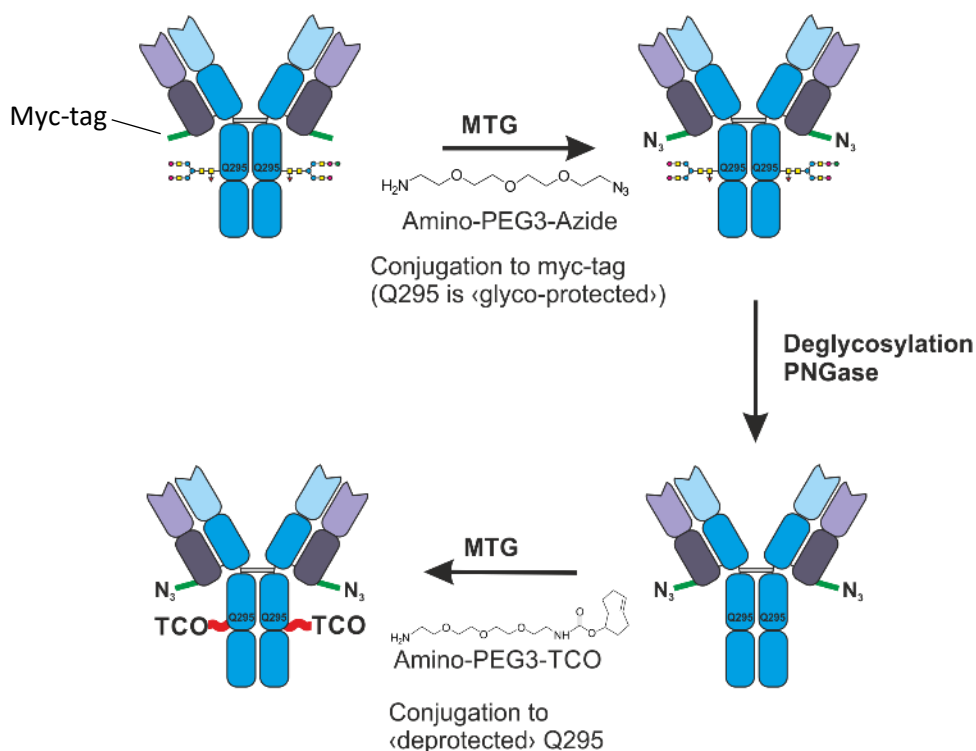


Figure 10: Schematic view of the mAb chCE7 (top left) and its conversion into its dual functionalized version (bottom left) with a TCO and an azide handle. In a first step, amino-PEG₃-azide is conjugated to a myc-tag on the light chain by MTG. Then, the glycan is detached by PNGase, releasing Q295 for conjugation. In a last step, Amino-PEG₃-TCO is conjugated towards the Q295. This approach did not work site-specifically. Figure is adapted from Philipp Spycher.

myc-tag (Glu-Gln-Lys-Leu-Ile-Ser-Glu-Glu-Asp-Leu) is readily recognized by MTG, we engineered a myc-tag to the N-terminus of the light chain. In a first step, amino-PEG₃-azide is conjugated towards the Gln on the tag. The glycans at position Asp297 of native chCE7 are protecting Q295 from any MTG-mediated conjugation. In a secondary step, the glycans should be detached with PNGase, releasing Q295 and making it accessible for the second moiety to be attached, e.g. an amino-PEG₃-TCO. Now, the mAb would be armed with two orthogonal functional groups that can react by click chemistry with substrates, such as chelators or toxins. LC-MS analysis of the light chain showed quantitative conversion between the substrate amino-PEG₃-azide and the myc-tag glutamine. However, we were surprised by an unexpected mass shift detected on the heavy chain (Figure 11). Native chCE7 displays three different heavy chain masses within an LC-MS spectra, all corresponding to different glycosylations (-> HC + glycan 1, HC + glycan 2, HC + glycan 3)^[112]. Since we consider these glycans to block, we were surprised to observe an increased mass of one specific (glycosylated) peak, which corresponds exactly to the mass of attached amino-PEG₃-azide. A glycan analysis identified it as the heavy chain with a Mannose-5 glycan^[112]. This surprising finding let us shift our focus of a dual functionalization via the glyco-protected Q295 to a more thorough investigation of substrates that enable a direct functionalization of Q295 on fully glycosylated, native mAbs vis MTG, leading to the new aims of this thesis.

MS spectra of Heavy chain
before conjugation



MS spectra of Heavy chain
after conjugation

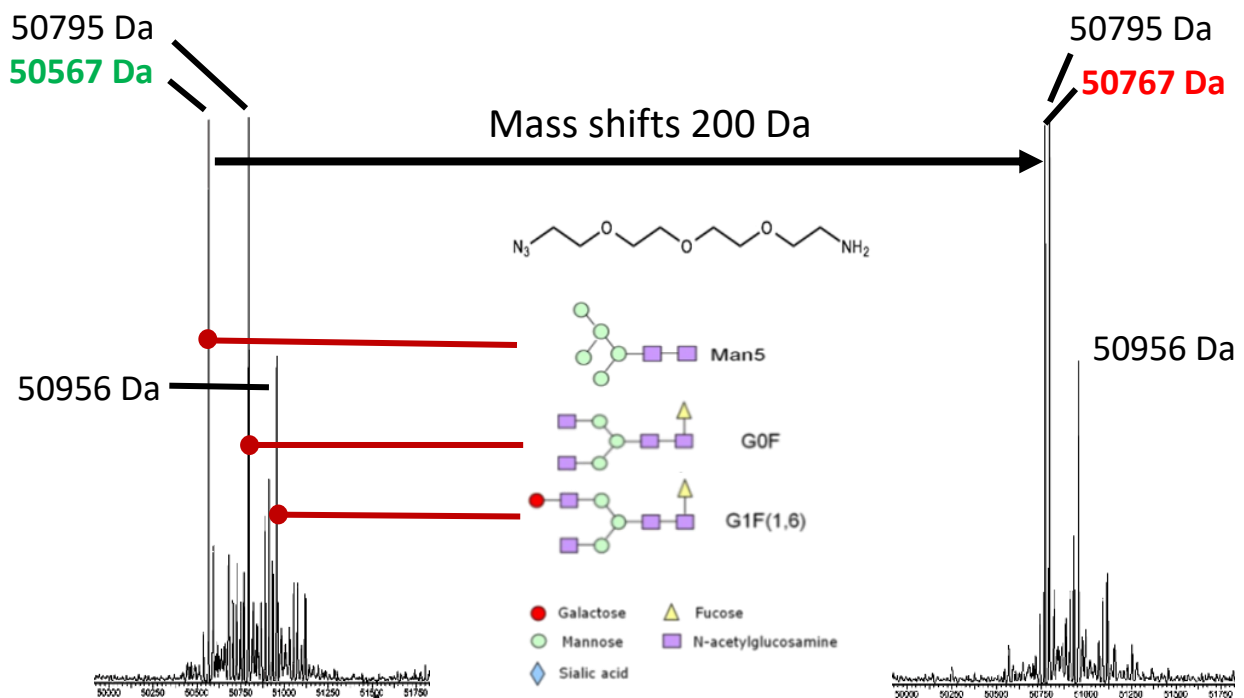


Figure 11: LC-MS spectra of the heavy chain before (left) and after (right) an enzymatic MTG conjugation of amino-PEG₃-azide towards mAb chCE7. The x-axis shows the mass [Da], whereas the y-axis shows intensity [%]. The substrate gets fully attached to the heavy chain bearing the glycan Man5, whereas the HC's bearing G0F and G1F glycans do not show any sign of conjugated amino-PEG₃-azide.

3. Aims of this thesis

There is still a lack of site-specific and efficient methods to functionalize fully glycosylated mAbs with chelators or toxins. Approaches with enzymatic couplings have been proven to overcome the issue of random attachment of payloads that come along with chemical conjugations. Our group was pioneering the field of using MTG for creating immunoconjugates. Previous work shows conjugation of primary amines towards Q295 of de- and aglycosylated IgG's. Recent surprising experiments revealed that this enzymatic conjugation works as well on fully glycosylated and native mAbs with small and specific lysine containing peptides.

Our aim is to screen for short peptide sequences that conjugate to Q295 on native Trastuzumab in a highly efficient manner. We investigate in parameters such as pH, temperature, buffer media, and varying concentrations of reactants to improve the conjugation efficiency. For promising sequences, we attach N- or C-terminally azido-lysine for subsequent click chemistry. Furthermore, we investigate on the diversity of the technology, by conjugating promising substrates to a variety of human IgG isotypes and as well to IgG's of rodent species.

To enable a quick screening of novel substrates, we subject the experimentally tested peptides to an algorithm that generates a self-organizing map. We want to use this tool, to predict promising sequences for MTG conjugation computationally without laborious experimental screening. We synthesize some of the predicted sequences to test conjugation efficiency on Trastuzumab, validating the computational approach.

Furthermore, we want to get a step ahead by attaching linkers that wear functional moieties such as azides, cysteines, and chelators. Subsequently, these linkers are conjugated with toxin DBCO-PEG₄-Ahx-maytansine to achieve ADC's with a DAR of 2, with and without having the chelator NODAGA covalently attached. Labeling with ¹¹¹In allows for further *in vitro* and *in vivo* testing, namely Lindmo assays and biodistributions in Skov3-ip xenografted mice. We hope to see similar or better tumor uptake as reported in other publications^[81,138,139].

Finally, we evaluate the transfer of our developed knowledge of site-specifically MTG coupling to smaller proteins like Nanobodies, equipped with a myc-tag. Two amine-containing linkers are tested for conjugation to the Gln within the tag. Both have equipped chelator NODAGA, whereas one has additionally an albumin binder attached, to test if it prolongs serum half-life with that variant.

4. MTG mediated conjugation of lysine containing peptides to Q295 of native antibodies

Scientific Contributors:

Claudia Graf was performing the buffer media-, salt-, and linker excess conjugation reactions, supervised by Dr. Philipp Spycher and Jöri Wehrmüller. Dr. Philipp Spycher was supervising the project and was involved together with Jöri Wehrmüller in planning, designing, and analysis of the data. Parts of the 1 mg/mL conjugation reactions to different isotypes were performed and analyzed by Dr. Julia C. Frei. The rest of the work was planned, performed, and analyzed by Jöri Wehrmüller.

4.1. Introduction

Based on the observation made in Chapter 2, we started the project with test conjugations with primary amine linkers, mainly lysine-containing peptides. We worked with native MTG and chose Trastuzumab as model mAb, since the glycans are more comparable to other “off-the-shelf” IgGs’s and less complex than the ones from the in-house mAb chCE7.

4.2. Results

4.2.1. Peptide library screening

For the peptide screening (comprising of 3-8 amino acids per peptide) we used standardized reaction conditions, which included: 1 mg/mL mAb, 80 eq. peptide, 6 U MTG/mg mAb, 20 h at 37 °C in Trizma pH 7.6 buffer. The screening revealed differences in conjugation efficiency ranging from 0%-94% (Figure 12 and Table A 1). The analysis was monitored by LC-MS after reduction with dithiothreitol (DTT) of the heavy and the light chain (HC and LC, respectively, Figure A 1-Figure A 34).

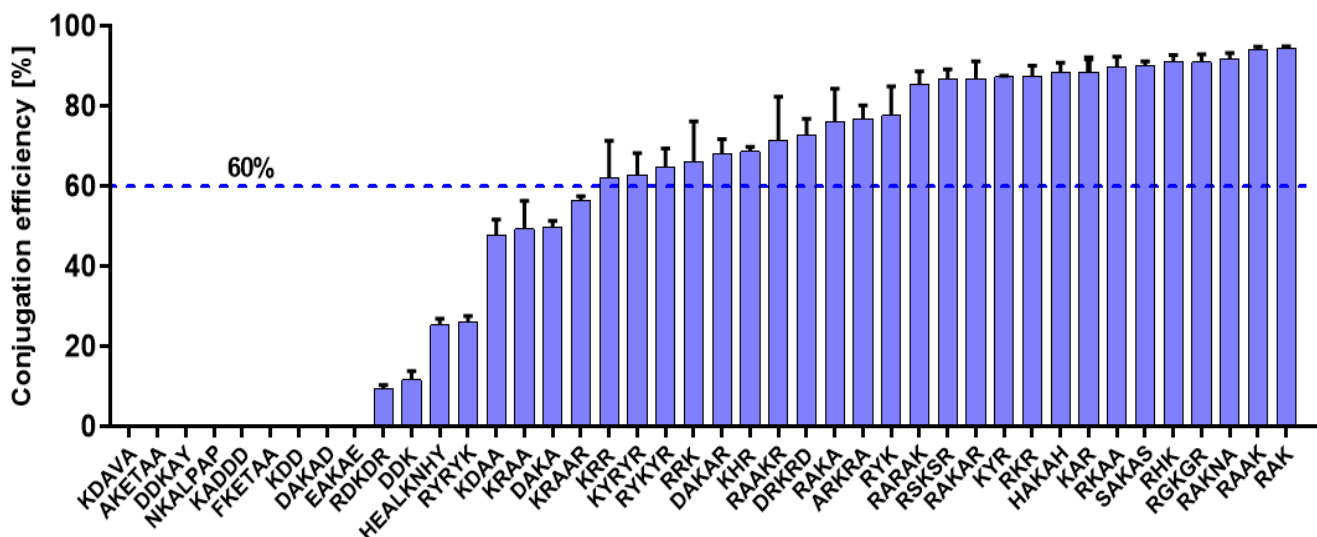


Figure 12: Conjugation efficiencies [%] of different K-containing peptides with mAb Trastuzumab, using standard conditions. A wide range of efficiencies has resulted, from 0% attachment from mainly negatively charged amino acids towards approx. 90% for positively charged peptides such as RAK, RAAK, or RAKNA. All the peptides are N-terminally acylated and C-terminally amidated but KDAVA, AKETAA, DDKAY, NKALPAP, KADDD, and FKETAA. $N_{\text{RAKAR,ARKRA,RGKGR}}=6$, $N_{\text{KDAVA,AKETAA,DDKAY,NKALPAP,HEALKNHY,KADDD,FKETAA}}=2$.

Peptides KDAVA, AKETAA, DDKAY, NKALPAP, HEALKNHY, KADDD, and FKETAA are not N- and C-terminally acylated and amidated, respectively. In Figure 13, the LC-MS spectra of such an experiment are shown before and after the reaction. To have a better insight on the lysine positioning within the peptide linkers we have made an alignment, which is shown in Figure 14. From the best peptides (RAK 94±0.4% and RAAK 94±0.7%) to the worst conjugating peptides (9 peptides with 0%) we have listed the overall net charge at pH 7 and put a focus on acidic and basic residues, which are color coded in orange and green, respectively. Overall positively charged linkers conjugate better to Trastuzumab.

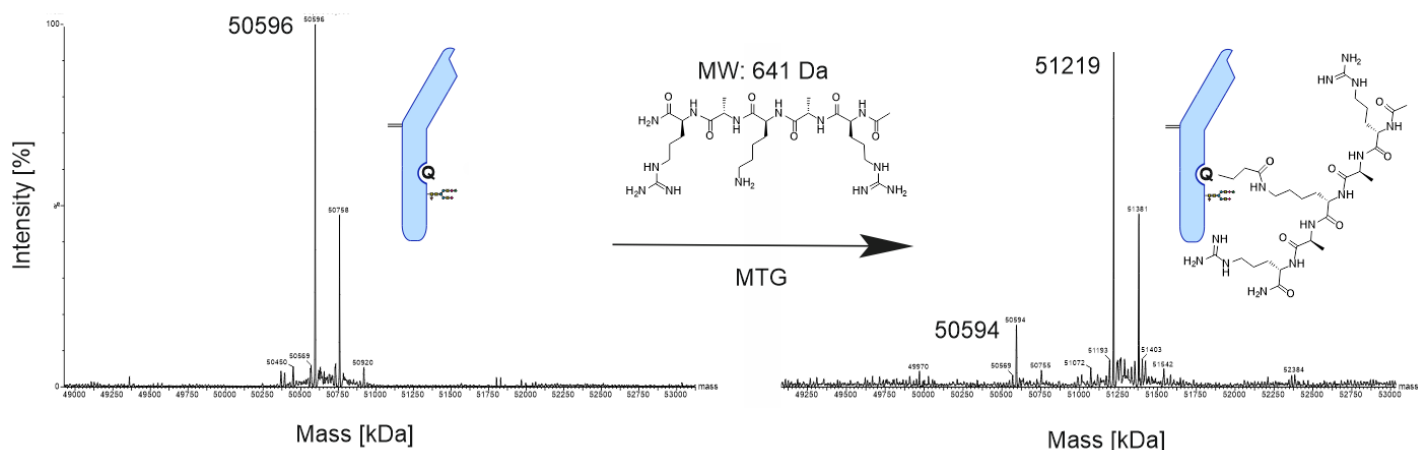


Figure 13: LC-MS spectra of the Trastuzumab heavy chain before (native, left) and after the conjugation (right) of peptide Ac-RAKAR-NH₂ towards Q295 of Trastuzumab. Standard conditions were used (1 mg/mL mAb, 80 eq. peptide, 6 U MTG/mg mAb, 20 h at 37 °C in Trizma pH 7.6). The two peaks on the left at 50596 Da and 50758 Da correspond to two different glycosylations of native Trastuzumab. On the right side, conjugated and non-conjugated material can be detected. Calculated conjugated HC's: 51220 Da and 51382 Da; Detected conjugated HC's: 51219 Da and 51381 Da. The conjugation efficiency, calculated from the intensity, is 85%.

There is no clear trend visible if an N- or C-terminal position of K is in favor for the enzymatic reaction (Figure 14, right side). Due to the possible charge-sensitivity of the substrates, we tested NH₂-RAKAR-OH, the variant of Ac-RAKAR-NH₂ without N- and C-terminal acylation and amidation. Compared with the acylated and amidated variant with 87±4% conjugation efficiency, the non-protected variant conjugated to 89±2% (N=3). Further substrates have been tested as non-protected variant for this thesis. The results are summarized in Table A 2.

Sequence	Con. Eff [%]	Std. error	Net charge at pH 7	Basic aa: R H K Acidic aa: D E	Sequence	Con. Eff [%]	Std. error	Net charge at pH 7	Basic aa: R H K Acidic aa: D E
RAK	94 ±0.4	2		R A K	RAK	94 ±0.4	2		R A K
RAAK	94 ±0.7	2		R A A K	RAAK	94 ±0.7	2		R A A K
RAKNA	92 ±1	2		R A A K N A	RKAA	90 ±2	2		R K A A
RGKGR	91 ±2	3		R G K G R	KAR	88 ±3	2		K A R
RHK	91 ±1	2		R H K	RKR	88 ±2	3		R K R
SAKAS	90 ±0.8	1		S A K A S	RAKAR	87 ±4	3		R A K A R
RKAA	90 ±2	2		R K A A	RARAK	85 ±3	3		R A R A K
KAR	88 ±3	2		K A R	RAKA	76 ±7	2		R A K A
HAKAH	88 ±2	1		H A K A H	RAAKR	71 ±9	3		R A A K R
RKR	88 ±2	3		R K R	RRK	66 ±8	3		R R K
KYR	87 ±0.3	2		K Y R	KRR	62 ±8	3		K R R
RAKAR	87 ±4	3		R A K A R	KRAAR	56 ±0.9	3		K R A A R
RSKSR	87 ±2	3		R S K S R	KRAA	49 ±6	2		K R A A
RARAK	85 ±3	3		R A R A K					
RYK	78 ±6	2		R Y K					
ARKRA	77 ±3	3		A R K R A					
RAKA	76 ±7	2		R A K A					
DRKRD	73 ±3	1		D R K R D	RHK	91 ±1	2		R H K
RAAKR	71 ±9	3		R A A K R	HAKAH	88 ±2	1		H A K A H
KHR	69 ±1	2		K H R	KHR	69 ±1	2		K H R
DAKAR	68 ±3	1		D A K A R					
RRK	66 ±8	3		R R K					
RYKYR	65 ±4	3		R Y K Y R					
KYRYR	63 ±4	2		K Y R Y R					
KRR	62 ±8	3		K R R					
KRAAR	56 ±0.9	3		K R A A R	KYR	87 ±0.3	2		K Y R
DAKA	50 ±1	0		D A K A	RYK	78 ±6	2		R Y K
KRAA	49 ±6	2		K R A A	RYKYR	65 ±4	3		R Y K Y R
KDAA	48 ±3	0		K D A A	KYRYR	63 ±4	2		K Y R Y R
RYRYK	26 ±1	3		R Y R Y K	RYRYK	26 ±1	3		R Y R Y K
HEALKNHY	25 ±1	0		H E A L K N H Y					
DDK	12 ±2	-1		D D K					
RDKDR	9 ±0.8	1		R D K D R					
EAKAE	0 ±0	-1		E A K A E	DRKRD	73 ±3	1		D R K R D
DAKAD	0 ±0	-1		D A K A D	DAKAR	68 ±3	1		D A K A R
KDD	0 ±0	-1		K D D	DAKA	50 ±1	0		D A K A
FKETAA	0 ±0	0		F K E T A A	KDAA	48 ±3	0		K D A A
KADDD	0 ±0	-2		K A D D D	DDK	12 ±2	-1		D D K
NKALPAP	0 ±0	1		N K A L P A P	RDKDR	9 ±0.8	1		R D K D R
DDKAY	0 ±0	-1		D D K A Y	DAKAD	0 ±0	-1		D A K A D
AKETAA	0 ±0	0		A K E T A A	KDD	0 ±0	-1		K D D
KDAVA	0 ±0	0		K D A V A	KADDD	0 ±0	-2		K A D D D

Figure 14: Sequences of the peptide linkers and conjugation efficiencies with Trastuzumab. It is the same data as shown in Figure 12 but with a focus on the lysine position and acidic and basic residues, which are color coded in orange and green, respectively. Left: All sequences are shown, with the most efficient one on top, and the least efficient on the bottom. Right: A selection of peptides from the left that share the same amino acids. Additionally, the net charge at pH 7 is listed for all the peptides. Peptides KDAVA, AKETAA, DDKAY, NKALPAP, HEALKNHY, KADDD, and FKETAA are not N- and C-terminally acylated or amidated, respectively.

4.2.2. Analysis of parameters influencing the MTG-mediated conjugation

We went on with Ac-RAKAR-NH₂ for a thorough screening of other reaction parameters that could influence the enzymatic conjugation reaction. Our aim was to find conditions that lead to quantitative attachment, by ideally using less substrates.

First, we tested the influence of the temperature. At 42 °C, the reaction reached 90% conjugation after 24 h (Figure 15). A similar efficiency was reached with the conjugation at 37 °C, our standard

conditions. Room temperature drastically slowed down the reaction, whereas at 8 °C no attached linker to the HC could be detected by LC-MS analysis.

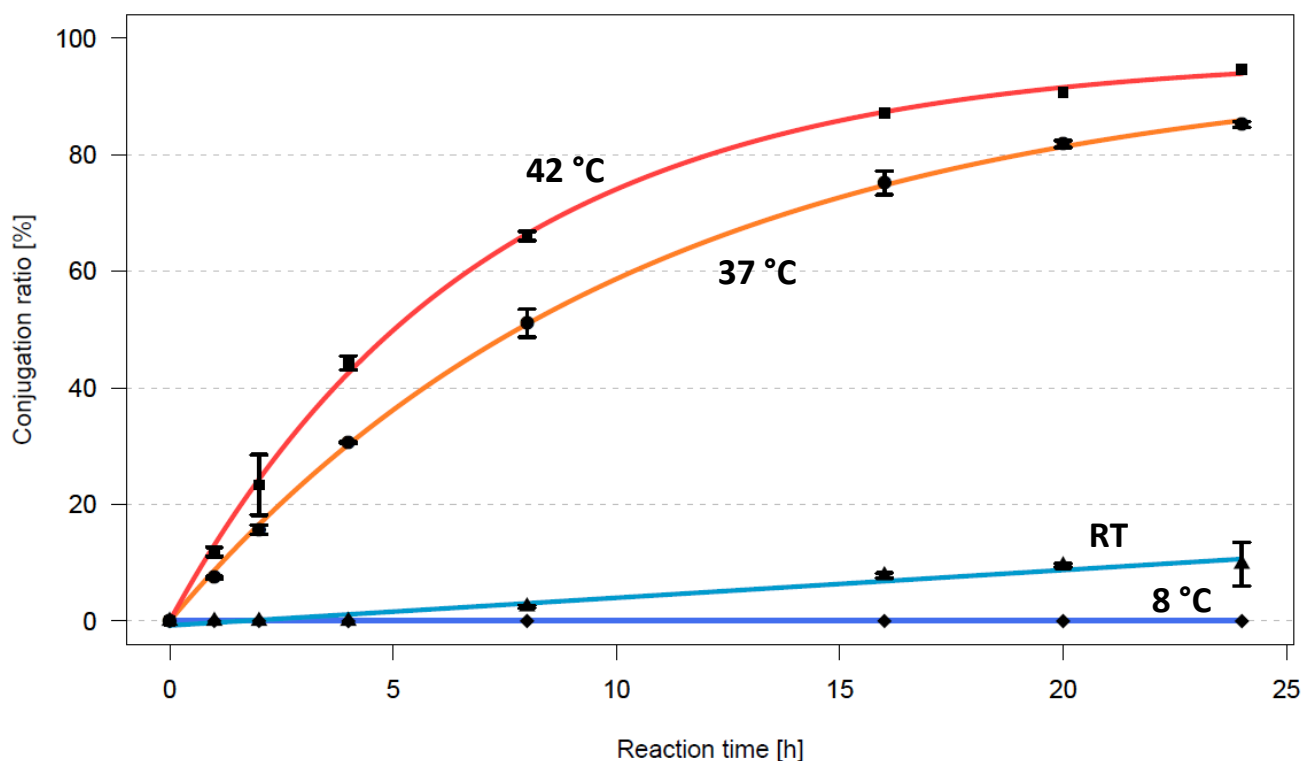


Figure 15: Conjugation efficiencies of reactions using standard conditions with Ac-RAKAR-NH₂ and Trastuzumab. The reactions were made at 8 °C (dark blue), room temperature (RT, bright blue), 37 °C (orange) and 42 °C (dark red). The efficiency is the best at 42 °C while at 8 °C there is no reaction at all. The colored lines at 37 °C and 42 °C correspond to non-linear regressions calculated and plotted with $R(\text{Conj.}(t)) = \text{Conj.}(\text{Max}) * 100 * (1 - e^{-(\ln(2)/t_{1/2} * t)})$. Following parameters were calculated: $\text{Conj.}(\text{Max})_{42\text{ }^\circ\text{C}} = 96.9\%$, $t_{1/2_{42\text{ }^\circ\text{C}}} = 4.8\text{ h}$, $\text{Conj.}(\text{Max})_{37\text{ }^\circ\text{C}} = 95.6\%$, $t_{1/2_{37\text{ }^\circ\text{C}}} = 7.3\text{ h}$. At RT a linear regression is displayed, whereas at 8 °C is shown a line at 0% conj. efficiency.

Second, we tested the influence of the buffer media. Four different buffers Trizma, HEPES, MOPS, PBS, and phosphate buffer were tested (all 50 mM and 1x for PBS [137 mM NaCl, 2.7 mM KCl, 8 mM Na₂HPO₄, and 2 mM KH₂PO₄], whereas the final reaction mix reached concentrations of approx. 40 mM, and 0.8x for PBS). All other, initial parameters were kept constant. The results are summarized in Figure 16. For Trizma, HEPES, and MOPS, no difference could be detected, whereas in PBS and phosphate buffer the reaction showed significantly lower labeling efficiencies (approx. 25% and 60%, respectively). The same trend was observed using two other mAbs, namely Daratumumab (IgG1) and Nivolumab (IgG4). Decreasing the concentration of Trizma pH 7.6 from 50 mM to 25 mM resulted in $94 \pm 1\%$ conjugation efficiency compared to $87 \pm 4\%$. An increase to 150 mM resulted in $51 \pm 10\%$ efficiency (same for HEPES).

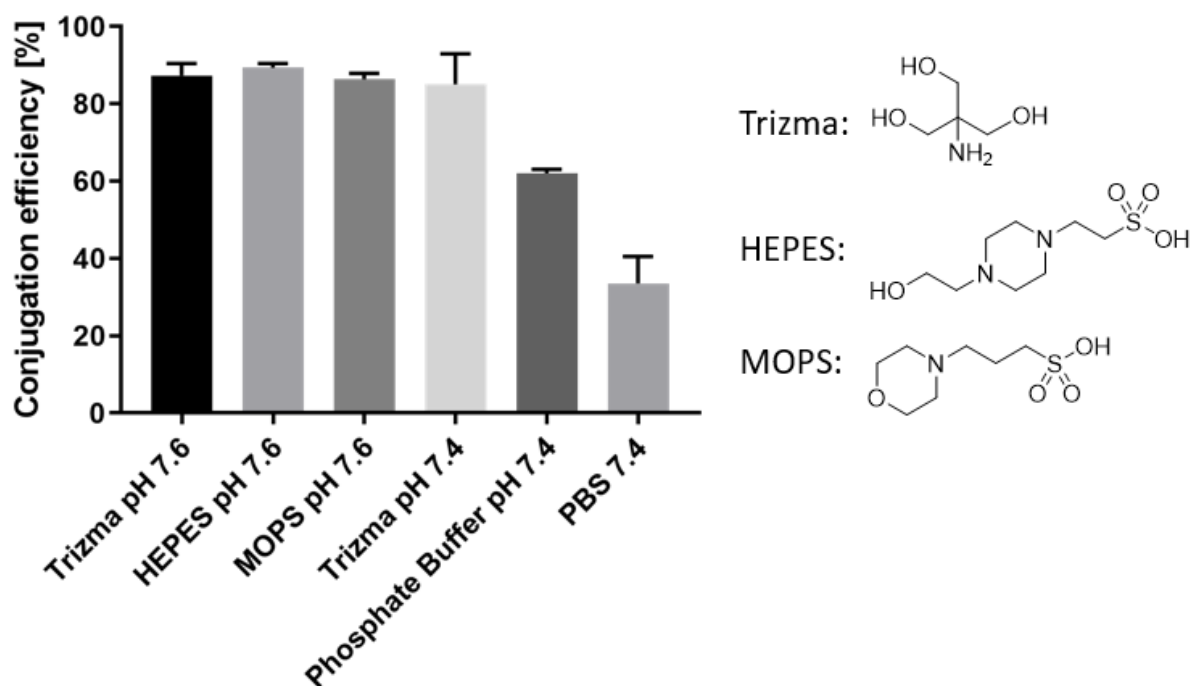
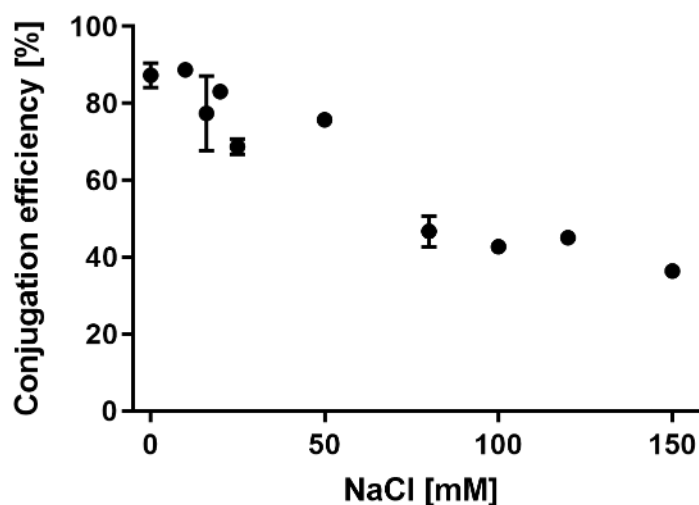


Figure 16: Conjugation efficiency of Ac-RAKAR-NH₂ to Trastuzumab using standard conjugation conditions. Different buffers were used at a concentration of 50 mM (or PBS). In the phosphate containing buffers Ac-RAKAR-NH₂ conjugates less efficiently. On the right, the chemical structures of the carbon based buffers are shown. N=3.

Third, we wanted to evaluate if NaCl within PBS is reducing the conjugation efficiency. All the other parameters were kept constant (20 h, 37 °C). In Triplicates, the conjugation efficiency of RAKAR towards Trastuzumab was tested within the varying salt exposed buffers. NaCl concentrations below ≤20 mM had no influence on the reaction compared to our standard buffer (Trizma). With increasing concentration, the conjugation efficiency decreased. At 80 mM NaCl the conjugation efficiency decreased to 50% (Figure 17).

Figure 17: Conjugation efficiency of linker Ac-RAKAR-NH₂ to Trastuzumab using standard conjugation conditions. Shown on



the x-axis are the increasing NaCl concentrations from 0-150 mM in Trizma pH 7.6 buffer. On the y-axis is the conjugation efficiency in %. With increasing NaCl concentration, the efficiency decreases. N=3.

Having seen the influence of NaCl, we investigated the influence of different ions on the reaction, especially those abundant in physiological processes. Trizma pH 7.6 buffer was prepared with low and high amount of different salts. The results of 1 mM CaCl₂, MgCl₂, FeCl₃, NH₄Cl, NH₄HCO₃, and (NH₄)₂SO₄ in Trizma pH 7.6 are summarized in Figure 18. While CaCl₂, MgCl₂, FeCl₃ did not show significant differences to Trizma pH 7.6 without any salts, all the three ammonia containing buffers showed a decrease by almost 50% compared to the control. This decrease was even more prominent when increasing the concentration to 5 mM with 16 ± 2%, 12 ± 2%, and 3 ± 2%, for NH₄Cl, NH₄HCO₃, and (NH₄)₂SO₄, respectively. CaCl₂ and MgCl₂, on the other hand, showed only significant lower conjugation efficiency when increasing to 20 mM, with 28 ± 0% and 52 ± 5%, respectively. NaCl and KCl containing buffers conjugated without significant loss of efficiency, even at 20 mM (83 ± 0.8% and 82 ± 0.5%, respectively).

We showed before that PBS and phosphate buffer resulted in lower conjugation efficiency compared to HEPES, MOPS, or Trizma pH 7.6. We wanted to test and compare different ingredients of PBS: Na₂HPO₄, KH₂PO₄, NaCl in Trizma, and additionally NaH₂PO₄. At concentrations of 25 mM, NaCl Trizma pH 7.6, NaH₂PO₄, Na₂HPO₄, and KH₂PO₄ conjugated without substantial differences to 73 ± 0.5%, 84 ± 1%, 84 ± 1%, and 87 ± 3%, respectively (Figure 18, right). With concentrations of 100 mM salt, the efficiency decreased to 43 ± 1%, 30 ± 1%, 30 ± 1%, and 34 ± 0.5%, respectively. The molarity of NaCl in PBS (137 mM) most presumably has the highest impact on the lowered conjugation behavior in PBS.

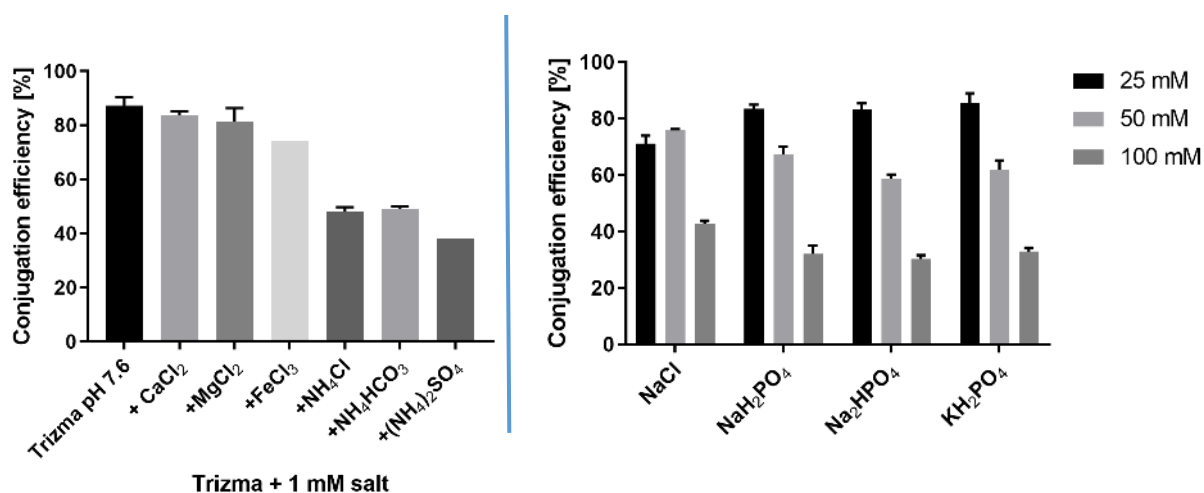


Figure 18: Left: Conjugation efficiency of linker Ac-RAKAR-NH₂ to Trastuzumab using standard conjugation conditions. In the first row, the conjugation efficiency of the reaction in Trizma pH 7.6 is shown. In the rows to the right, different salts have been added to the buffer in a concentration of 1 mM. Ammonia containing buffers conjugated less efficiently compared to Trizma pH 7.6 only. N=3. Right: conjugation efficiency of Ac-RAKAR-NH₂ to Trastuzumab using standard conjugation conditions. On the left, the conjugation efficiency of the reaction in Trizma pH 7.6 with 25, 50, and 100 mM NaCl is shown. In the rows to the right, different phosphate buffer concentrations have been tested. The higher the buffer/salt concentration, the lower the conjugation efficiency. N=3 for the NaCl tests, N=5 for the phosphate buffers.

Fourth, we investigated the influence of different mAb concentrations and the amount of linker-substrates used in the conjugation reaction with MTG. We tested different equivalents of peptidic linkers (Figure 19). While standard conditions are 80 equivalents, we detected no substantial changes in conjugation efficiency when reducing to 20 equivalents or even increasing to 160. As a final variable

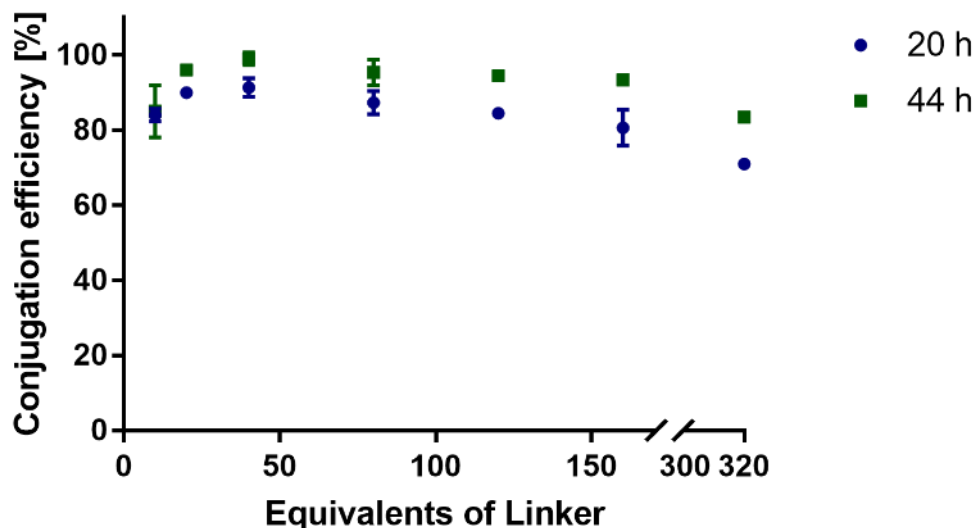


Figure 19: Conjugation efficiency of Ac-RAKAR-NH₂ to Trastuzumab on the y-axis, with different equivalents of the peptidic linker used. In blue, the 20 h conjugation reactions are shown whereas in green the same experiment was stopped and measured after 44 h. For both reactions, we clearly see that we can reduce the 80 equivalents of linker that we normally use with standard conditions while still reaching similar conjugation efficiencies.

we tested the mAb concentration. Increasing the mAb concentration from 1 mg/mL to 3 mg/mL respectively 5 mg/mL led to higher conjugation efficiency for all the tested peptides, and even quantitative conversion as can be seen in Chapter 6. The influence of mAb concentration is demonstrated in Figure 22 and 23.

4.2.3. MTG mediated backreaction

It has been reported that H₂O can act as nucleophilic substrate. We wanted to evaluate if MTG can deconjugate the glutamine-lysine isopeptidic bond on the mAb. For this purpose, we incubated the substrate Ac-RAKAR-NH₂ for 24 h after which it was separated by a PD10 column. Subsequently, fresh MTG was added (6 U/mg mAb). After 96 h at 37 °C 50% of the conjugated substrate was cleaved from Q295 (Figure 20). This same effect could be detected at room temperature, but less pronounced. At 8 °C, the original peptide-Trastuzumab ratio did not change.

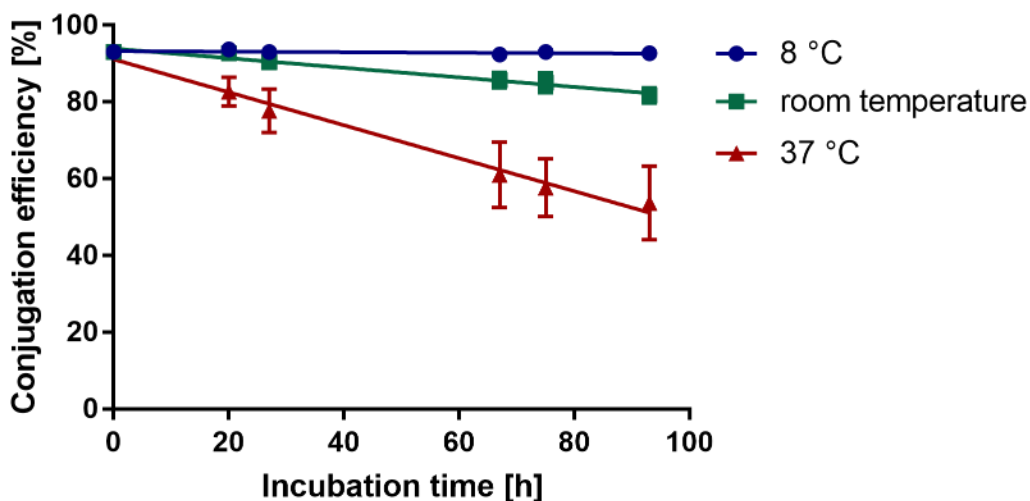


Figure 20: Conjugation efficiency of Ac-RAKAR-NH₂ towards Trastuzumab. After the conjugation, the sample was cleaned from substrate with a PD10 column, but further incubated with MTG at three different temperatures 8 °C, room temperature, and 37 °C. Detachment of up to 50% can be detected for the sample incubated at 37 °C, while at 8 °C no back reaction could be detected. The colored lines correspond to a linear regression made with Prism. N=3.

4.2.4. Equipping peptides with ϵ -azido-lysine and separation of MTG

For subsequent biorthogonal coupling of an additional chemical entity (e.g. a toxin) to the MTG functionalized mAbs, selected peptide substrates were equipped with an azido group. We chose the best conjugating peptide Ac-RAK-NH₂ (94±0.4%) as well as our lead peptide Ac-RAKAR-NH₂ (87±4%), and equipped them N-terminally with ϵ -azido-lysine K(N₃), which enables a two-step functionalization by click reaction (with toxins, dyes, or chelators with DBCO- or TCO-modification). Furthermore, we also equipped two new sequences with an azido group to enhance the substrate scope, resulting in the four functionalized peptides Ac-RAK-K(N₃)-NH₂, Ac-KHR-K(N₃)-NH₂, Ac-RSK-K(N₃)-NH₂, and Ac-RAKAR-K(N₃)-NH₂ (Figure 21). The conjugation efficiency under standard conditions yielded in 87±0.4%, 93±0.4%, 97±2%, and 80±5%, respectively (N=2). Applying the optimized protocol (5 mg/mL Trastuzumab, 6 U MTG/ mg mAb, Trizma pH 7.6, 20 h, 37 °C), we reached quantitative attachment (>95%), tested by LC-MS analysis. For the longer peptide Ac-RAKAR-K(N₃)-NH₂ we reached >95% conjugation efficiency using these conditions, however, only after 42-48 h. 100% we achieved using 12 U/mg MTG. We successfully scaled the reaction to yield 20 mg immunoconjugate. MTG was separated using Protein A purification or size exclusion chromatography (Figure A 36 and Figure A 37) for further *in vitro* and *in vivo* experiments.

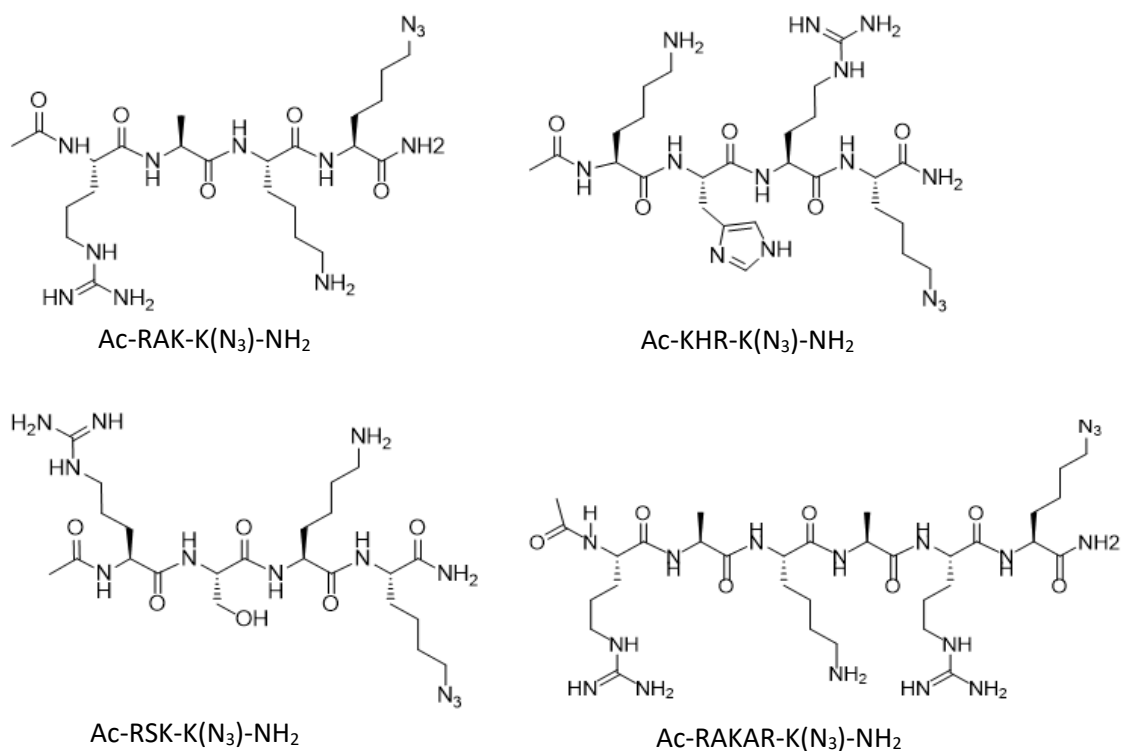


Figure 21: Chemical structures of azide functionalized linkers Ac-RAK-K(N₃)-NH₂, Ac-KHR-K(N₃)-NH₂, Ac-RSK-K(N₃)-NH₂, and Ac-RAKAR-K(N₃)-NH₂

4.2.5. Conjugating Ac-RAK-K(N₃)-NH₂ towards different antibodies and isotypes

To test the scope of the method, different mAb types, including IgG1, IgG2, and IgG4, as well as the FDA approved ADCs Kadcyla[®] and Adcetris[®] were conjugated with peptide Ac-RAK-K(N₃)-NH₂. Results are summarized in Figure 22 (1 mg/mL reactions) and Figure 23 (3 mg/mL reactions). Human IgG1 and IgG2 showed conjugation efficiencies of 80% or higher using 1 mg/mL mAb. For all the isotypes but IgG2 the 3 mg/mL reaction lead to >95% conjugation of the peptide, whereas human IgG2 conjugated to 93±3%. Nivolumab, a PD-1 targeting monoclonal IgG4 revealed a peculiarity that has previously not been observed: a second conjugation site. MS/MS analysis from the functional genomics center in Zurich revealed that besides Q295 also Q311 can be modified, yet only 5-17%, depending on the reaction conditions (Figure A 35). The observation is surprising since Q311 is conserved in other IgG1s (including Trastuzumab). Armenian Hamster IgG and rat IgG1/IgG2a/IgG2b showed on the other hand more pronounced conjugation of a second Gln, which even reaches quantitative or almost quantitative dual conjugation for Rat IgG1 and Armenian Hamster IgG. While all tested human mAbs did not show any sign of peptide modification at the light chains, Adcetris[®] showed minor modification at the 3 mg/mL mAb conditions (3±0.2%). Furthermore, rat IgG2b was modified also on the light chain, an observation that could be seen for mouse IgG2b as well. Looking more close into the mouse IgG1, IgG2a and IgG2b's, all of them showed minor peptide attachment in the Fc region of mouse mAbs.

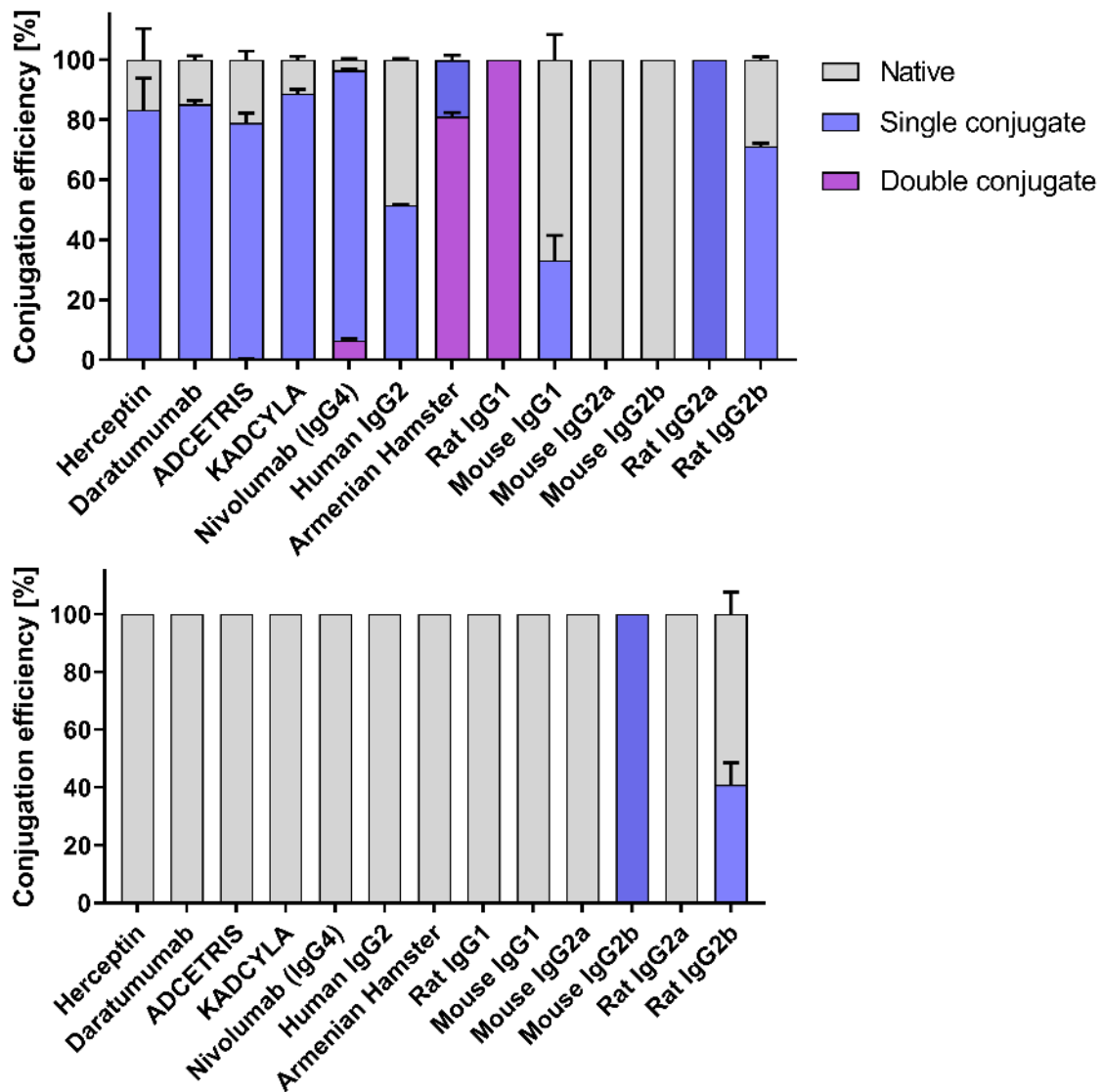


Figure 22: Conjugation efficiencies of Ac-RAK-K(N₃)-NH₂ towards different commercial mAbs, ADCs, and isotypes with MTG. Standard conditions were used, whereas the mAb concentrations was 1 mg/mL for all the reactions. In grey is shown non-conjugated species, in violet single conjugated species, and in pink double conjugated mAbs. Top: Heavy chain, Bottom: corresponding light chain. Conjugation analyses were made by LC-MS analysis. Whereas only for mouse IgG2b and rat IgG2b single chain conjugation was detected, most of the human IgG heavy chains conjugated in the range of 80%. Mouse IgG2a did not show any coupling of Ac-RAK-K(N₃)-NH₂. $N_{all}=2$, $N_{Daratumumab, ADCETRIS, KADCYLA, NIVOLUMAB}=3$

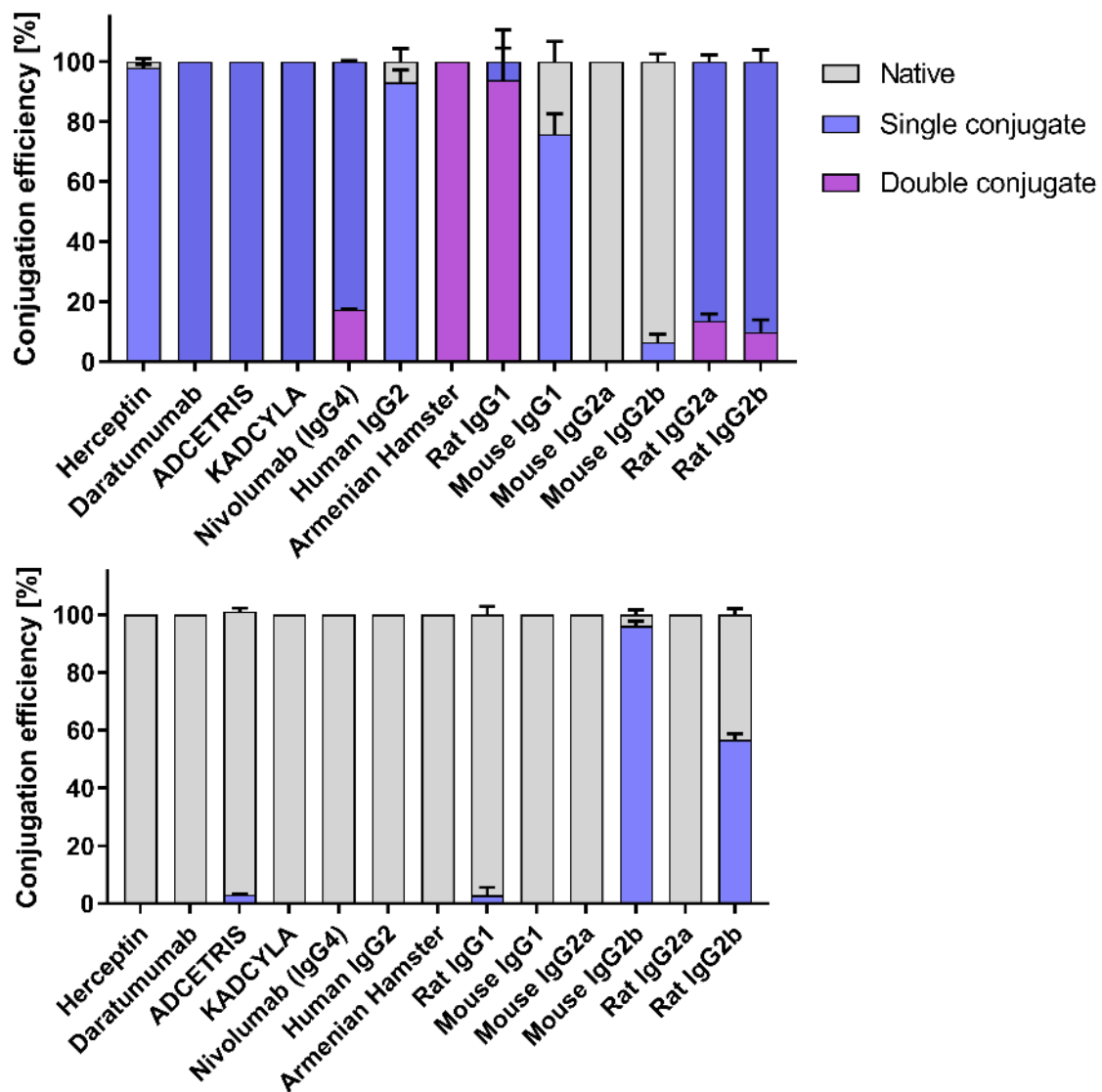


Figure 23: Conjugation efficiencies of Ac-RAK-K(N₃)-NH₂ with different commercial mAbs, ADCs, and isotypes with MTG. Standard conditions were used, whereas the mAb concentrations was 3 mg/mL for all the reactions. In grey is shown non-conjugated species, in violet single conjugated species, and in pink double conjugated mAbs. Top: Heavy chain, Bottom: corresponding light chain. Conjugation analyses were made by LC-MS analysis. Most of the human IgG heavy chains conjugated in the range of >95%, whereas the light chain was just slightly affected for ADCETRIS. Mouse IgG2a did not show any coupling of Ac-RAK-K(N₃)-NH₂. N_{all}=3, N_{Daratumumab, ADCETRIS, KADCYLA, NIVOLUMAB}=2

4.3. Discussion

Q295 is just two amino acid positions apart from Asn297, the site where IgG CH2 domains are glycosylated with oligosaccharides^[18]. Their diantennary structure can vary and mainly is composed of N-acetylglucosamine (GlcNAc), galactose, fucose, mannose, and sialic acid as building blocks^[30]. Despite the convincing results reported by Jeger *et al.* and Lhospice *et al.*, which reported modification of Q295 exclusively after deglycosylation of the mAbs at N97, we have seen the quantitative shift of one of the chCE7 HC-species when incubated with amino-PEG₃-azide (Figure 11)^[81,140]. The mass of the peak give rise to the assumption that it is the Man5 glycan (reported mass^[112]: 50574 Da, detected mass = 50567 Da). Since it is known that glycans have a significant influence on the structural integrity of the heavy chain^[141], we can speculate that HC-Man5 has a favorable conformation, that allows the modification of Q295, while other glycosylation patterns do not offer this opportunity for most substrates with primary amino group. This observation inspired us to put an emphasis on the search for potential substrates that could also be attached to HC with all types of glycosylation. In case of IgG1

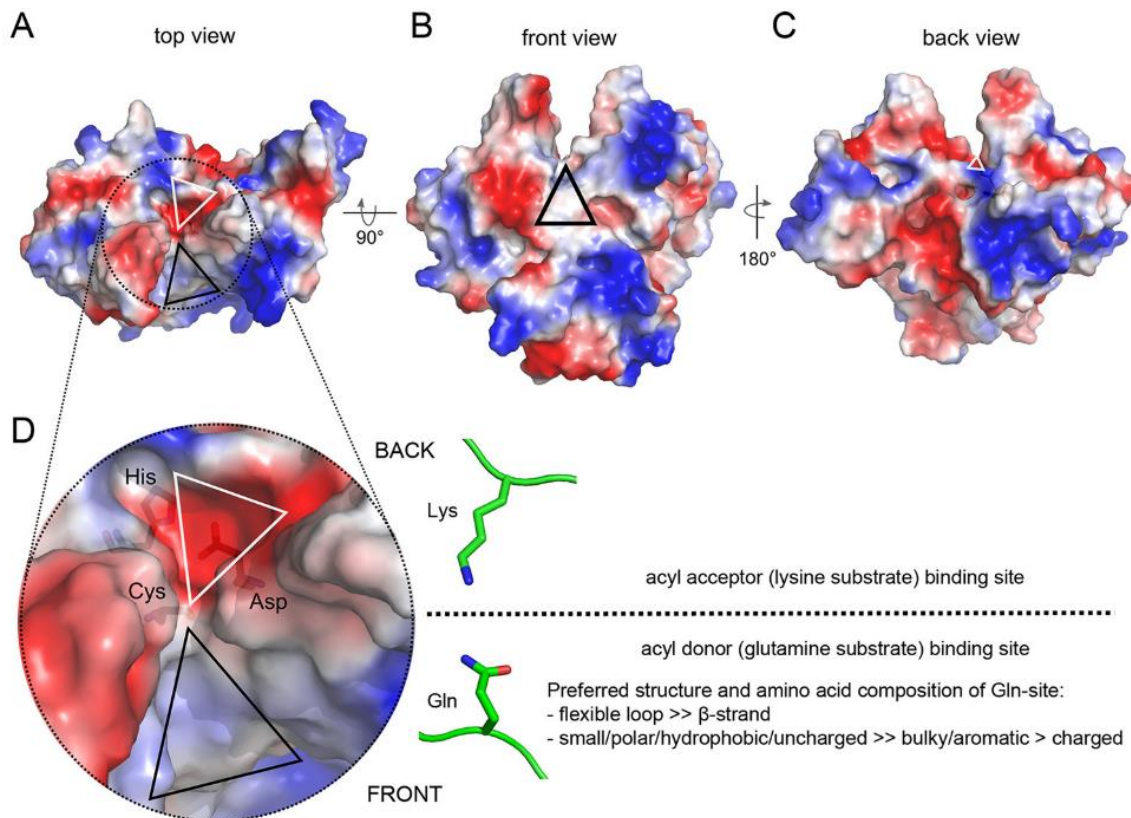


Figure 24: "A-C electrostatic surface representation of transglutaminase from *S. mobarensis* (PD entry 1IU4). The front vestibule (black triangle) carries a weak positively charged patch, which is likely to bind the acyl donor (glutamine substrate). The back vestibule (white triangle) is strongly negatively charged and is likely to accommodate the positively charged acyl acceptor (lysine substrate). D, catalytic triad residues (Cys-64, Asp-255, His-274) positions are superposed in the close-up. The front vestibule is narrowed toward the active site cysteine, suggesting that substrate glutamines in flexible loops are more easily accommodated and reach the active site cysteine for efficient modification. In addition to flexibility, small/polar/hydrophobic/uncharged residues are preferred for efficient modification, whereas bulky/aromatic and/or charged residues are likely to interfere with accommodation of the substrate glutamine in the cleft, resulting in inefficient MTG-mediated modification." Cited from Fiebig *et al.*

Trastuzumab that reveals 3 different HC-glycans species (the two main glycosylations are G0F and G1F^[142]), peptidic substrates were efficiently to Q295 conjugated. The main difference between the substrate tested by Mindt, Jeger, Lhospice, and Dennler *et al.* and our substrates is the peptidic nature. In fact, lysines are also the natural substrates of MTG. Thus, we have a closer look at active site of the MTG. Fiebig *et al.*^[143] published a crystal structure, which emphasizes on the importance of amino acid sequence and flexibility for glutamine binding. Furthermore, as can be seen in Figure 24, they display the highly negatively charged binding pocket for the acyl-accepting substrates. We assumed that after binding of MTG with Q295, the rear part of MTG's active site is accessible specifically for our peptide amine-donors, without any steric or charge interferences from the glycan. This is supported by the observation that overall positively charged peptides (+1 - +3) show on average the better performance for conjugation compared to negatively charged ones (-1 - -2), as pointed out in Figure 14. A similar observation was made by Malesevic *et al.*, who found in a fluorescent assay with tripeptides (Ac-Xaa-Lys-Yaa) that adjacent negative charges lower enzymatic activity (with Cbz-QG-OH as acyl-donor)^[114]. Gundersen *et al.* made a screening with simple acyl acceptors of different length, showing that a longer chain length is generating better substrates when conjugated with Cbz-QG-OH^[119]. However, when looking closer into those substrates, we see that this chain is keeping off a negative charge from the primary amine, which might be more influencing for MTG recognition rather than the length. Thus, we argue that positive charges help for an optimal MTG-Peptide interaction, which due to a possible conformational change additionally also can help the specific binding of Q295. These described interactions might either enhance beneficial-, or lower obstructive interactions with the glycan at N297. This is supported by the recent work with MTG with non-peptidic linkers, such as amino-PEG₃-azide^[120], that conjugate poorly without a precedent deglycosylation step. Looking closer into the sequence of our peptide library, we observe that steric demanding amino acids (aa) in the positions +1/2 -1/2 aa's from the conjugated Lys only play a minor role, at least for our short flexible peptides, as bulkier amino acids such as Tyr and His can be found among the better conjugated substrates. The length of our sequences has an impact as well, since we observe slightly better conjugation between RAK or KAR over the full length protein RAKAR (Figure 14, same for RYKYR and others). There is no clear tendency that the position of the lysine is decisive for conjugation efficiency. Since the peptides are charge-sensitive, we also tested peptide Ac-RAKAR-NH₂ without N- and C-terminal acylation and amidation, which did not show a significant difference. These protecting groups are neutral in physiological conditions; in consequence, deprotection restores a positive and a negative charge, respectively. Hence, the overall charge of the linker is not affected.

The efficient conjugation at higher temperature is not surprising, since most of the known enzymes have an optimal activity around 37 °C - 42 °C and become inactive at low temperatures. Going even

higher we risk denaturation of either MTG or our mAb substrate. Another factor that we do have to keep in mind when working with enzymes is the possibility of a back- or cross-reaction. MTG cannot only attach primary amines to glutamine, but it also accepts other nucleophiles such as H₂O to small amounts. Water is not a good substrate, as it lacks the positive charge, which would be strongly advantageous for the active site interaction with Asp255 of MTG^[108]. Furthermore, the deamidation capacity of MTG is negligible, up to seven times lower compared to other transglutaminases^{[144][109]}. Thus, we have never had an issue with glutamine hydrolysis and could reach quantitative attachment with our lysine substrate when using improved conditions. We do see a problem, however, when we incubate our mAb-linker conjugate with MTG in absence of linker (Figure 20). We hypothesize that bound peptide to Q295 results in a more open MTG binding pocket conformation, which makes the nucleophilic attack of worse substrates such as H₂O more accessible. Additionally, preliminary results (not shown) support that already covalently bound linker easily can be exchanged with a different one, an observation that could get handy in future to attach non-optimized substrates to Q295 in a secondary step.

To evaluate further parameters that influence the conjugation reaction we tested attachment of to Trastuzumab with different salt additions and with common physiological buffers. A strong negative influence had especially NH₄⁺, Mg²⁺, and Ca²⁺. The last two are ions with a high charge density and known cofactors for various enzymes^[145]. However, the MTG reaction mechanism is known to be Ca²⁺ independent^[146]. The negative impact of ammonia is especially interesting, since the transamidation process releases ammonia as side product. This leaves the question if MTG has a possible feedback inhibition mechanism, something, which has not been reported yet to our best knowledge.

For Trastuzumab (IgG1) and Nivolumab (IgG4) we confirmed Q295 (European numbering) as main conjugation site. Additionally we sent in a sample of Nivolumab to validate the second small conjugation site. A sequence alignment with Trastuzumab shows, that besides Q295, Q312 is getting recognized by MTG (Figure A 35). Surprisingly, IgG1s bear a Gln as well at this position. Even though both HC sequences are very similar, we assume that the structural change of the IgG4 CH2 region of Nivolumab seems to be enough to decide over the site-selectivity. Marculescu *et al.* has recently shown minor side conjugations with other Gln's in the HC when conjugating deglycosylated Trastuzumab^[147]. With our LC-MS analysis, we could not detect any further sites. For some mAbs, especially the rodent ones, the light chain attachments could become problematic, when they block the complement determining region of the mAb. We observed no efficient conjugation to mouse IgGs, since the conserved Q295 residue is absent from mouse Fc.

5. Computational screening for suitable MTG-substrates

Scientific Contributors:

This project was made in collaboration with the Schneider group from ETH Zurich. Dr. Jan Hiss and Jöri Wehrmüller were involved in planning/designing/analysis of the project, whereas Dr. Jan Hiss conducted the SOM analysis. Jöri Wehrmüller did designing of new sequences for the SOM validation, whereas synthesis of the peptides was done together with Damian Gautschi.

5.1. Introduction

In a classical, experimental approach we aimed at identifying suitable lysine substrates for MTG via screening of a peptide library (vide supra). As it was challenging to find critical properties a “good” peptide substrate should possess, we were keen to generate a computational tool that could provide us with new lead peptides. For this purpose we engaged the toolset from the field of *de novo* drug Science, more specifically, a visualization technique called self-organizing map (SOM)^[148,149]. A SOM is a two-dimensional toroidal data projection of compounds that are sorted into neurons in a high-dimensional space. The sorting, or distribution, of these compounds into patterns in the space is made by descriptors (algorithms), which make use of encoded pharmacophores^[150,151]. In other words, a descriptor sorts compounds relatively by similarity, which can be common properties such as charge, length, or a common functional group. SOM analysis has already been successfully applied, e.g. in the visualization of bioactive compounds for peroxisome proliferator-activated receptor subtype α antagonists (PPAR α) or for thrombin inhibitors^[150]. For our study we created such a map for the peptides that had been experimentally tested for conjugation efficiency with two different descriptors, pepCATS and ppCALI^[152]. The algorithm is using these descriptors to see similarities in-between sequences and sorting them accordingly into groups (called neurons). These neurons are all connected with each other in the computational space, being closer or far apart neighbors. Each comparison is adding another dimension in this space, resulting with neurons in a multidimensional input space. The descriptors are naïve regarding the experimental results and are only provided with the peptide sequences. Peptides, that conjugated well, are locally clustered together on the SOM, in a so called “activity island”^[153]. It is a match between sequences with similar experimental results and sequences that the algorithm considers to be similar in chemical structure. The SOM can now be used as a tool, to screen and analyze a vast library of peptides and attribute them to active and inactive peptide substrates. In our case, this is done by feeding the map with numerous possible lysine-containing peptides, and by assuming that all the sequences that fall into an “activity island” on the SOM are suitable substrates for the MTG reaction.

5.2. Results

To quickly identify suitable peptides for future experiments and applications, we subjected the *in vitro* tested peptide sequences (Figure 12) to a computational analysis. A restriction of the system was that exclusively sequences could be subjected to analysis without N- and C- terminal acylation and amidation, respectively. However, in our experimental peptide screening, we had predominantly tested N/C-terminal protected peptides. The algorithm is using descriptors to see similarities in-

between sequences, whereas the end result in our comparison are neurons arranged in a 633 dimensional input space. A two dimensional toroidal representation was made out of that multidimensional space resulting in the two dimensional SOM (Figure 25, bottom). Neurons next to each other on the SOM are also neighbors in the original input space. We set an artificial threshold of 60% conjugation efficiency to classify the peptides from the experimental screening into positive peptides (>60% efficiency) and negative peptides (<60% efficiency). After sorting, when the neurons now contain sequences which are rated as “positive”, >60% conjugation efficiency, the neuron is

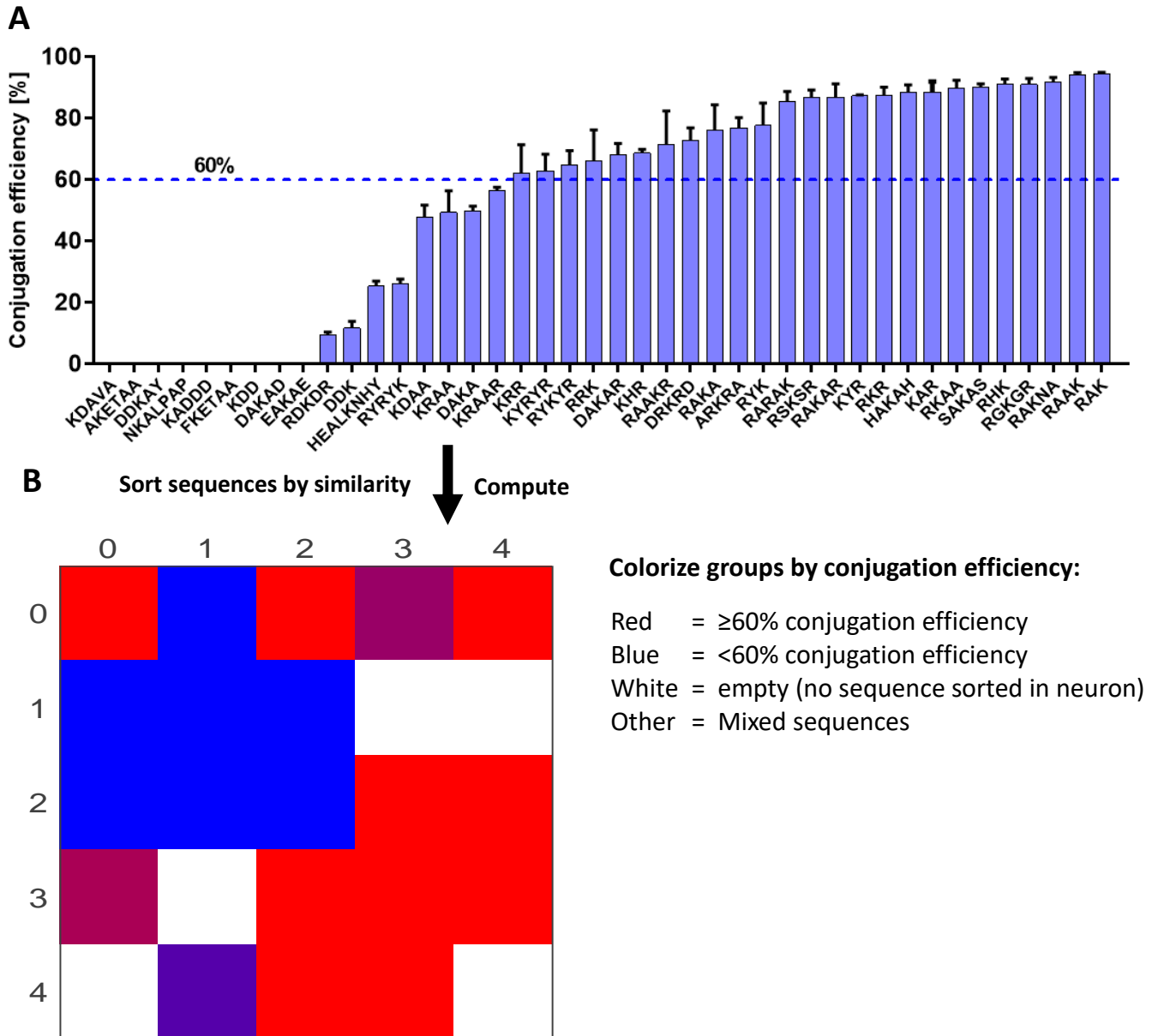
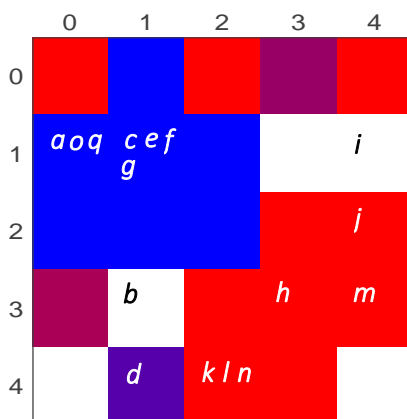


Figure 25: Top: Peptide conjugation efficiency screening towards Q295 on Trastuzumab (Plot already shown in Figure 12). On the x-axis the different tested sequences are shown, whereas the y-axis shows the conjugation efficiency in %. The range is from 0% conjugation to almost quantitative attachment towards the mAb. Standard conditions were used (20 h at 37 °C with 80 eq. linker). Bottom: 5x5 Self organizing map (SOM) with 25 neurons. The neurons are colored according to activity ranging from red (only actives) to blue (only inactive). The threshold for activity was >60% conjugation efficiency towards Trastuzumab. White neurons do not contain data points. The SOM map is toroidal. The visualization was done with SomVIS.

colored in red. Blue neurons are the ones that do contain “negative” sequences only. White neurons got no sequences assigned, whereas negative/positive mixed neurons are shown in the corresponding mixed colors.

The map was used as a tool to find novel lysine substrates for MTG. 511 random amino acid sequences (with the sole criteria to comprise one lysine) were fed to the map. The sequences were subsequently sorted to the best fitting neuron. The sorting was performed without further training on the dataset. A full list with all sequences and their according positions can be found in Table A 5. 17 sequences (a-q) were selected out of differently colored neurons and synthesized with N-terminal acylation and C-terminal amidation. The sequences differed with respect to aa’s and length compared to the peptides

SOM, generated with previous experimental data



New experimental data with sequences taken from SOM

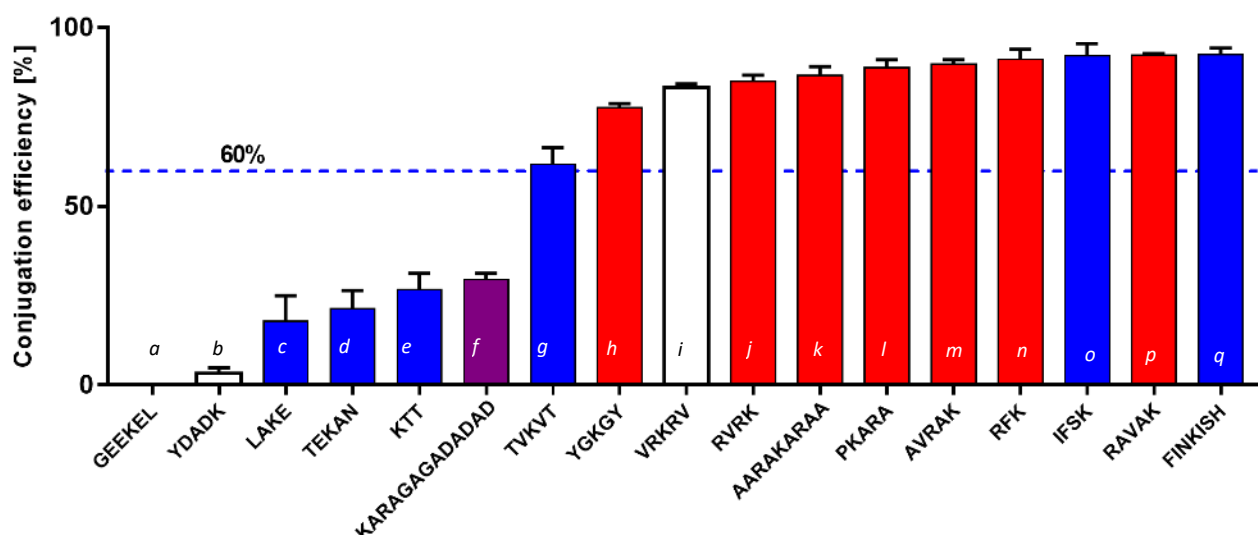


Figure 26: Top: The developed 5x5 SOM is shown (previously described). Bottom: Out of different neurons (red, blue, white, mixed) 17 sequences were taken out, synthesized, and experimentally tested on Trastuzumab with standard conditions. The x-axis shows the chosen sequences, with a letter- and color-code (a-q) to display from which neuron in the map they have been taken. The y-axis shows the conjugation efficiency in %. All the positive predicted sequences conjugate above the 60% threshold.

of the original screening. We tested them for conjugation efficiency using the same conditions as used for our screening in Figure 12: Figure 12 (80 eq. peptide, 20 h at 37°C). In Figure 26 the exact location and conjugation efficiency of each sequence can be found (and in Table A 4, Figure A 38 – A 54). All seven sequences that were predicted “positive” (taken from red neuron on the SOM), conjugated above the 60% threshold (YGKGY, RVRK, AARAKARAA, PKARA, RFK, AVRAK, RAVAK). The map did not show the same strong feedback for negative predicted sequences (GEEKEL, TEKAN, KTT, LAKE, TVKVT, IFSK, FINKISH), taken out from blue neurons of the SOM. Three out of these six negatively predicted sequences, namely Ac-TVKVT-NH₂, Ac-IFSK-NH₂ and Ac-FINKISH-NH₂, conjugated with an efficiency above 60% and thus, should be in a positive neuron. Two of these peptides contain phenylalanine and/or isoleucine and were selected out of the same group, whereas one, TVKVT, conjugated exactly around 60%. Three out of 17 sequences did not fall into a neuron that allows for a clear prediction. YDADK and VRKRV were taken from white, neutral neurons. KARAGAGADADAD was taken from a mixed neuron, containing one positive and two negative assigned peptides.

5.3. Discussion

Before discussing the SOM data in detail, three important points need to be taken into account:

- 1) A strong bias is implemented by using non-protected sequence variants for the algorithm, while the experimental results were made with variants carrying N-terminal acylation and C-terminal amidation. Since positive and negative charges of the peptides at physiological conditions are key factors for good linker conjugation, we expect that sequences with the lysine close to one of the termini are more substantially influenced.
- 2) The 511 sequences were not generated randomly by a non-biased computing system, but by the author in a semi-rational approach to include interesting and/or random sequences, as well as amino acids that have not been tested before.
- 3) The choice of the sequences to validate the predictions can contain a bias as well. As it was impossible to synthesize and test experimentally all the 511 peptide sequences, only a non-representative selection of peptides was chosen. The neurons can have more or less weight, dependent on how many and which sequences from our experimental data have been sorted into it. Thus, with only 17 sequences tested, we cannot determine how accurately each neuron actually predicts the conjugation efficiency.

To gain statistical significance of the prediction power of the SOM, the experimental set-up would need more data and randomization than herein presented. In example, an algorithm creating random sequences with one Lys and n(any other amino acid but Q/K)= 0-6 aa up- and/or downstream the Lys should be run. Subsequently, another algorithm should randomly propose a critical number of

sequences out of every neuron for experimental testing. However, in perspective with the possible bias, choosing sequences from negative and positive (blue/red) neurons in the present work revealed some information that will be further discussed.

We decided on a threshold of 60% conjugation efficiency, whereas positive sequences were colored red and negative sequences blue. The threshold was chosen based on the observation that with improved conditions (amount of MTG, mAb concentration, etc.) we could push peptides that conjugated $\geq 60\%$ under standard screening conditions to quantitative or almost quantitative coupling. We can see on the map (Figure 25) that the neurons cluster together in a red and a blue area. This demonstrates that differences between “positive” and “negative” peptides exist, and that the algorithm was able to separate them. That pattern can be seen also in both the original 9x9 pepCATs and ppCALI outputs, with a difference that they contain more empty neurons (Figure A 55). In an ideal case, the SOM would have one complete blue, and one complete red side, given that the input argument for the differentiation is true. However, our experimental screening data do not indicate such a clear argument, as we do not have clear active and inactive peptides, but a gradient ranging from 0-95% conjugation efficiency. Thus, we were not surprised the arbitrary threshold of $>60\%$ did not yield two complete distinct patterns. Interestingly, the two clusters of positive and negative neurons can be seen as well when putting the activity threshold to 75%, but as expected with more mixed regions (Figure A 56). Nevertheless, all the sequences where the SOM predicted a conjugation efficiency of $\geq 60\%$ did conjugate above. Three of the sequences that were predicted to be negative, Ac-TVKVT-NH₂, Ac-IFSK-NH₂, and Ac-FINKISH-NH₂, conjugated among the positive sequences. Peptide Ac-TVKVT-NH₂ conjugated with $62\pm 4\%$ around the set threshold of 60%. Interestingly, the other two wrongly predicted peptides Ac-IFSK-NH₂ and Ac-FINKISH-NH₂, share the same negative neuron on the map (0,1). It can be interpreted, that sequences out of this neuron most presumably are unpredictable regarding their substrate activity. Analyzing the two sequences shows that both contain phenylalanine (F) and isoleucine (I), amino acids that were scarcely available from our original sequences from which the SOM has been generated. Thus, we presume that the SOM is not strong enough for the prediction of these substrates, just by the lack of training on these amino acids. The third sequence in the very same neuron (0,1), Ac-GEEKEL-NH₂, is highly negative. We speculate, that a SOM training with F and I containing peptides could have clustered them in two separate neurons. Peptide Ac-VRKRV-NH₂ conjugated around 80% towards Herceptin, but originates from a non-assigned neutral neuron, which is neighbored by two red positive ones. Relative distance on the map to such positive “activity islands” can have an influence. In other words, sequences taken from a mixed or neutral neuron, which is close to positive neurons, can rather be expected to be positive as well. The same counts for neutral sequences that are close to negative neurons, which can be assumed to conjugate below 60% in our

case. This is an observation we made for low conjugating peptides Ac-YDADK-NH₂ and Ac-KARAGAGADADAD-NH₂, which were taken out of a neutral and a mixed group. Even though both are neighbors to a positive neuron, they share also a border with a negative one and are located in a rather undefined region. Consistently, peptide Ac-KARAGAGADADAD-NH₂, which was taken out of the mixed neuron, conjugates with 30±2% better than linker Ac-YDADK-NH₂ from the neutral neuron with 3 ± 1%. Taken into account only peptides that were either assigned to red or blue neurons, 11 out of 14 were predicted correctly, with a 100% hit rate for positive sequences. It would be interesting to see changes of the positive and negative cluster of the SOM, when we re-train our data set with the newly tested peptides. Furthermore, we should test more peptides experimentally, especially sequences and combinations with scarcely used amino acids.

6. Chemo-enzymatic functionalization of native antibodies with mono- and bifunctional peptide linkers and toxins

Scientific Contributors:

Dr. Philipp Spycher and Jöri Wehrmüller were involved in planning/designing/analyzing of linker Ac-RAKAR-K(N₃)-NH₂ and Ac-K(N₃)-CRAK-NH₂ and their subsequent experiments. Peptide NODAGA-K(N₃)-RAK-NH₂ was designed by Jöri Wehrmüller, and synthesized together with the help of Dr. Nathalie Grob. All the other work and analysis was performed by Jöri Wehrmüller.

6.1. Introduction

In chapter 4.2.4 we introduced the attachment of peptides including an ϵ -azido-lysine. In this chapter, we introduce three strategies to chemo-enzymatically decorate Trastuzumab with toxin maytansine and chelator NODAGA leading to immunoconjugates with well-defined stoichiometry (Figure 27). The third approach would enable a very sophisticated homogeneous one-step reaction. Aside an azide, the chelator NODAGA is already covalently attached in linker NODAGA-K(N₃)-RAK-NH₂. It would mean that we can site-specifically and homogeneously turn any IgG with efficient Q295 recognition into a functional theranostic biomolecule over-night. With the non-laborious attachment of a toxin in a secondary step even into an ADC.

6.2. Results

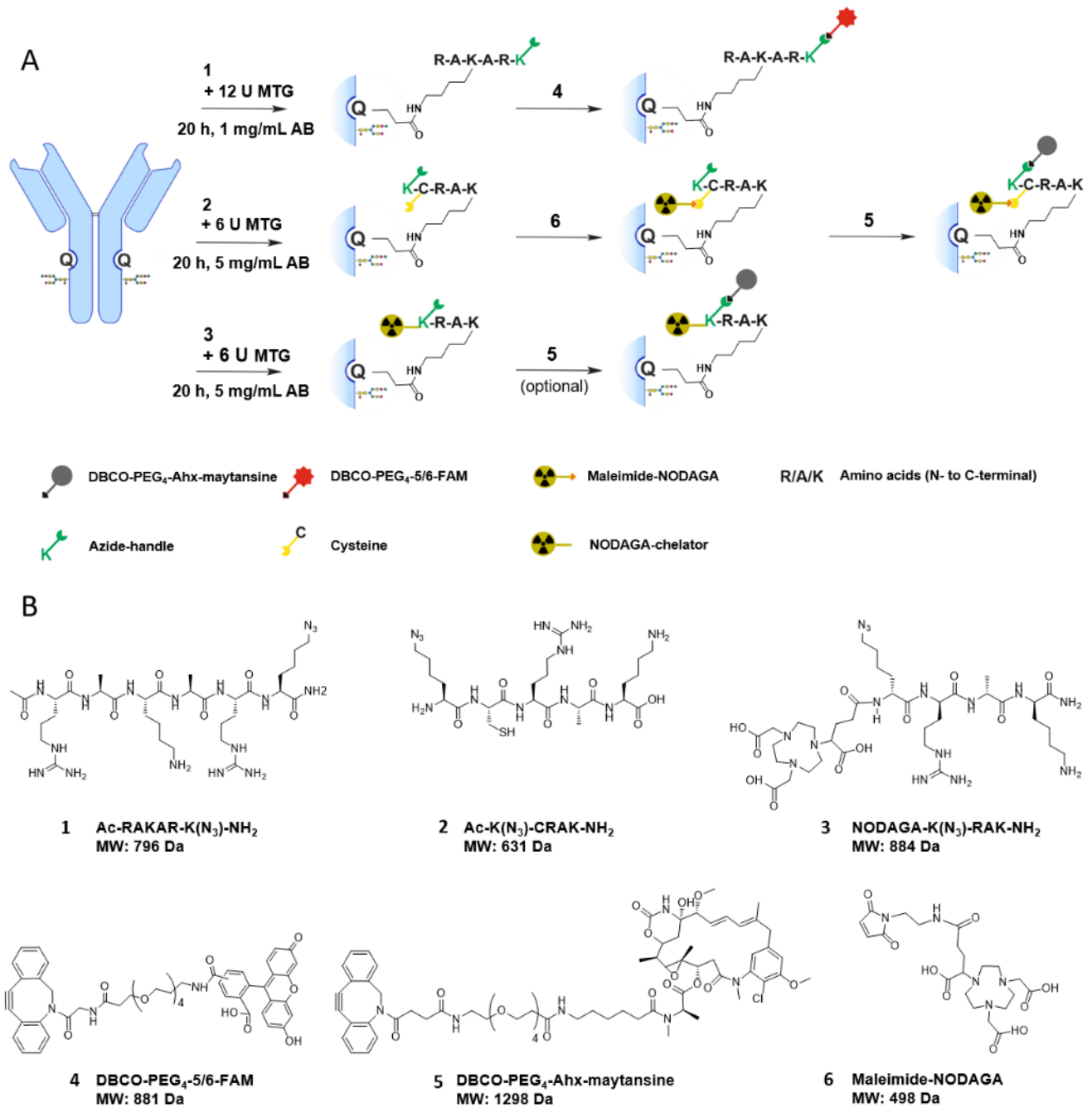


Figure 27: A) Schematic display of three different functionalization reactions with Trastuzumab. Top: Peptide Ac-RAKAR-K(N₃)-NH₂ is attached in a first step, whereas dye FAM is conjugated to the linker in a secondary step, using the click reaction. Middle: Peptide Ac-K(N₃)-CRAK-NH₂ is attached in a first step, whereas chelator Maleimide-NODAGA is conjugated to cysteine in a secondary step. In a third step, toxin maytansine is attached to the linker using click chemistry. Bottom: One step functionalization with peptide NODAGA-K(N₃)-RAK-NH₂. Optionally, a toxin can be attached using the click chemistry. B) Chemical structures of the peptide linkers and the functionalization moieties FAM (4, dye), maytansine (5, toxin), and Maleimide-NODAGA (6, chelator).

6.2.1. Conjugation of peptide Ac-RAKAR-K(N₃)-NH₂ to Trastuzumab and functionalization with the fluorescent dye DBCO-PEG₄-5/6-FAM

Ac-RAKAR-K(N₃)-NH₂ has been introduced in chapter 4.2.4. The conjugation was quantitative using 12 U MTG/mg Trastuzumab after 20 h. A PD10 column was used to remove the excess peptide substrate. For the biorthogonal coupling 10 eq. DBCO-PEG₄-5/6-FAM were added and the reaction incubated for 4 h at 37 °C. The MS spectra of the different chemo-enzymatic steps are shown in Figure 28.

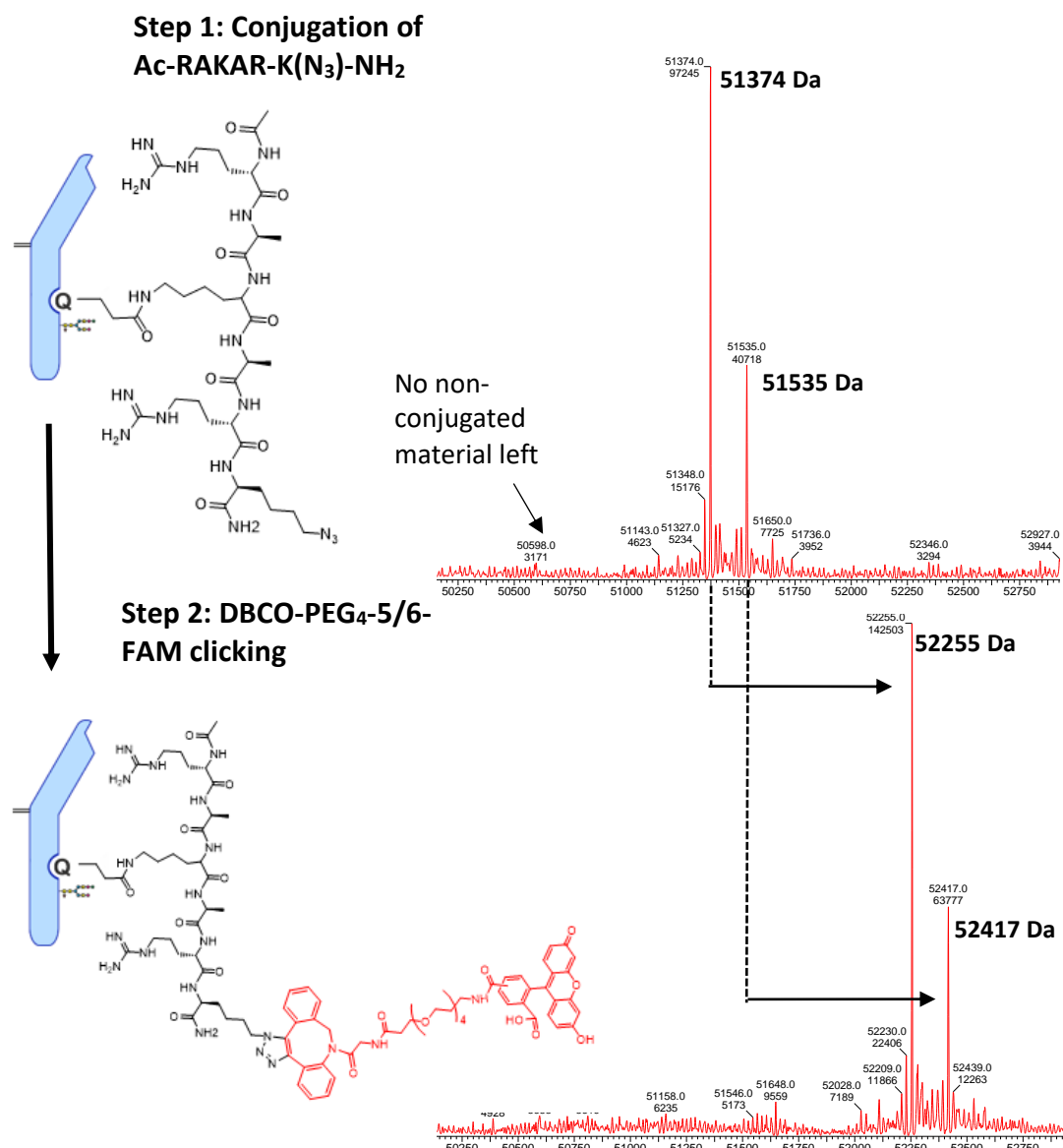


Figure 28: Heavy chain LC-MS spectra (right) of the according species Trastuzumab-Ac-RAKAR-K(N₃)-NH₂ (top), and Trastuzumab-Ac-RAKAR-K(FAM)-NH₂ (bottom). The azide on the peptide is subsequently being clicked with DBCO-PEG₄-5/6-FAM. Calculated clicked DBCO-PEG₄-5/6-FAM HC's: 52255 Da and 52417 Da; Detected conjugated HC's: 52255 Da and 52416 Da.

6.2.2. Conjugation of peptide Ac-K(N₃)-CRAK-NH₂ to Trastuzumab and dual functionalization with Maleimide-NODAGA and toxin maytansine

For dual functionalization of Trastuzumab (e.g. with a metal chelator for labeling with a radiometal and a therapeutic toxin) we used the hetero-bifunctional peptide Ac-K(N₃)-CRAK-NH₂. The sulfhydryl group of cysteine can be conjugated with maleimide and the azide group or biorthogonal reactions with alkynes. Cysteine containing substrates NH₂-K(N₃)-CRAK-OH, NH₂-RAKARC-K(N₃)-OH, and NH₂-KC-K(N₃)-OH were tested for their conjugation efficiency towards Trastuzumab. Results are shown in Table 1. Linker NH₂-K(N₃)-CRAK-OH with the highest conjugation efficiency (67±8% using standard conditions: 1 mg/mL Trastuzumab, 80 eq. peptide, 6 U MTG/ mg mAb, 20 h at 37 °C, Trizma pH 7.6) was chosen for further experiments. Coupling yields of >95% were achieved after an incubation time of approx. 44 h, with the improved protocol of 5 mg/mL Trastuzumab within the reaction mix. Excess linker and MTG were separated by Protein A purification.

Table 1: Chemical structures of cysteine containing linkers tested for conjugation efficiency to Trastuzumab with standard conditions

	MW [Da]	Conj. effic. N=3	Chemical structure
NH ₂ -RAKARC-K(N ₃)-OH	858.0	59±7%	
NH ₂ -K(N ₃)-CRAK-OH	630.8	67±8%	
NH ₂ -KC-K(N ₃)-OH	403.5	44±5%	

The commercially available metal chelator maleimide-NODAGA was chemically coupled to the cysteine of Trastuzumab-NH₂-K(N₃)-CRAK-OH using 30 eq. DTT and a subsequent reoxidation step with dhAA to avoid cleavage of the mAb's inter-chain disulfide bonds. Coupling yields of >95% were achieved. Finally, DBCO-PEG₄-Ahx-maytansine was coupled quantitatively via ε-azido-lysine (10 eq., overnight at rt, Figure 29). Excess toxin and NODAGA was separated by Amicon centrifugation (size exclusion).

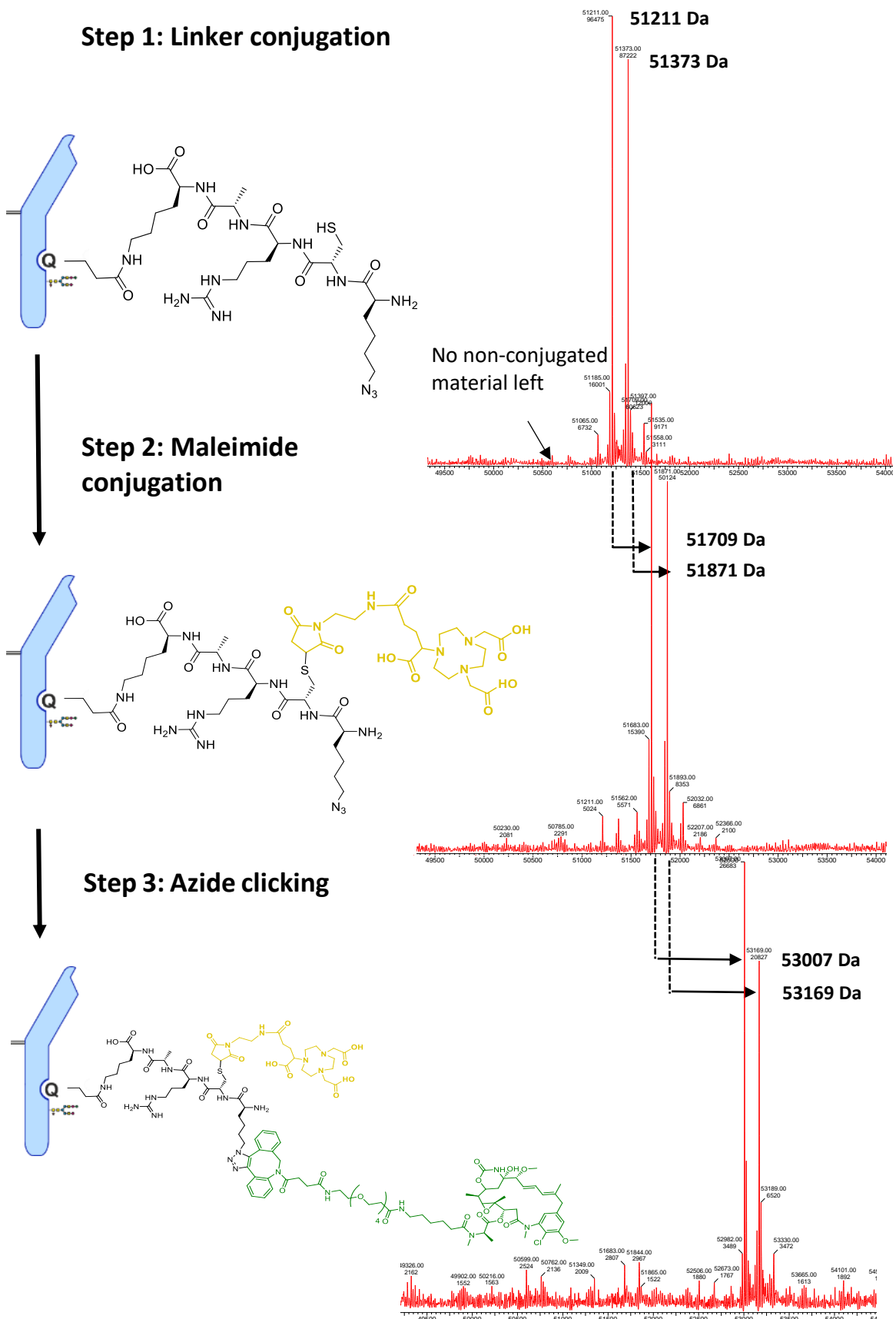


Figure 29: Heavy chain LC-MS spectra (right) of the according species Trastuzumab-NH₂-K(N₃)-CRAK-OH (top), Trastuzumab-NH₂-K(N₃)-C(NODAGA)RAK-OH (middle), and Trastuzumab-NH₂-K(maytansine)-C(NODAGA)RAK-OH (bottom). The cysteine on the peptide is subsequently being conjugated with Maleimide-NODAGA, and then clicked with toxin DBCO-PEG4-Ahx-maytansine. Calculated conjugated Maleimide-NODAGA HC's: 51709 Da and 51871 Da; Detected conjugated HC's: 51709 Da and 51871 Da. Calculated clicked toxin HC's: 53007 Da and 53169 Da. Detected conjugated HC's: 53007 Da and 53169 Da.

6.2.3. Conjugation of peptide NODAGA-K(N₃)-RAK-NH₂ to Trastuzumab and functionalization with toxin DBCO-PEG₄-Ahx-maytansine

NODAGA-K(N₃)-RAK-NH₂ was synthesized according to the procedure described in chapter 10.3.2. Quantitative conjugation of NODAGA-K(N₃)-RAK-NH₂ towards Trastuzumab was achieved at protein concentration of 3 mg/mL. Quantitative coupling of the toxin DBCO-PEG₄-Ahx-maytansine was

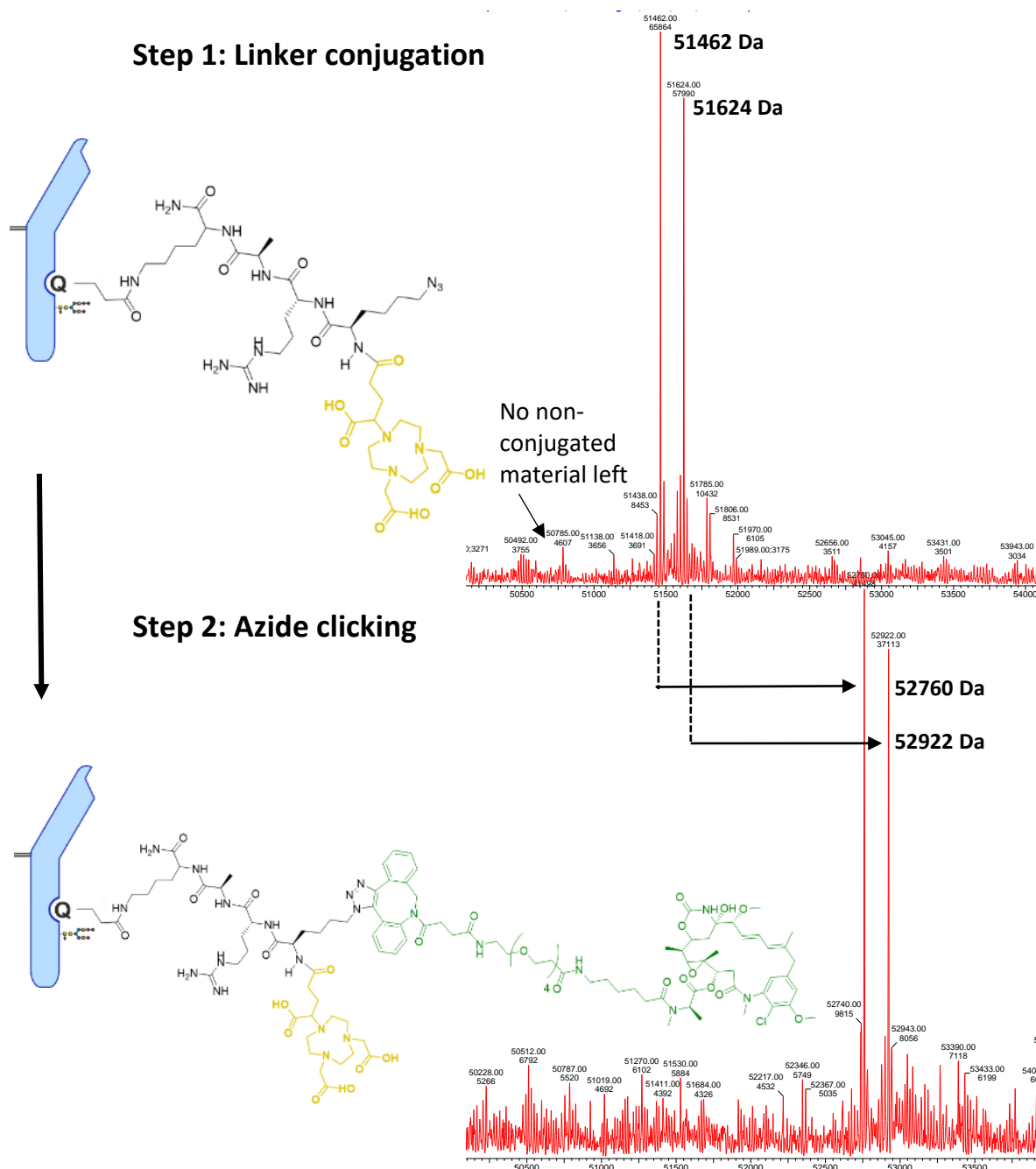


Figure 30: Heavy chain LC-MS spectra (right) of the according species Trastuzumab-NODAGA-K(N₃)-RAK-NH₂ (top), and Trastuzumab-NODAGA-K(maytansine)-RAK-NH₂ (bottom). The azide on the peptide is subsequently being clicked with DBCO-PEG₄-Ahx-maytansine. Calculated clicked DBCO-PEG₄-Ahx-DM HC's: 52760 Da and 52922 Da; Detected conjugated HC's: 52760 Da and 52922 Da.

achieved using 10 eq. overnight at room temperature after an overnight reaction at room temperature (N=2, Figure 30). The quantitative DAR 2 batches of Trastuzumab-NODAGA-K(maytansine)-RAK-NH₂ were used for further *in vitro* and *in vivo* analyses.

6.2.4. *In vitro* characterization of Trastuzumab-Ac-RAKAR-K(FAM)-NH₂, Trastuzumab-NH₂-K(maytansine)-C(NODAGA)RAK-OH, and Trastuzumab-NODAGA-K(maytansine)-RAK-NH₂

Trastuzumab-Ac-RAKAR-K(FAM)-NH₂ was used to analyze the binding capacity of chemo-enzymatic Q295-functionalized Trastuzumab towards HER2/neu expressing Skov3ip cells by flow cytometry (Figure A 57). *In vitro* evaluation of the immunoconjugates Trastuzumab-NODAGA-K(maytansine)-RAK-NH₂ and Trastuzumab-NH₂-K(maytansine)-C(NODAGA)RAK-OH was performed after radiolabeling with ¹¹¹InCl₃. Labeling efficiency reached 97±1% for Trastuzumab-NH₂-K(maytansine)-C(NODAGA)RAK-OH (N=2). Lindmo analysis determined an immunoreactive fraction of 101±6% (N=3). For the variants Trastuzumab-NODAGA-K(N₃)-RAK-NH₂ and Trastuzumab-NODAGA-K(maytansine)-RAK-NH₂, the labeling efficiency was 99±1% and 98±1%, respectively (N=2). Lindmo analysis for the species with and without toxin showed immunoreactive fractions of 110.9% and 111.1%. Selected saturation binding graphs and the Lindmo plots can be found in Figure A 58 - Figure A 60 for all the 4 tested species. The non-specific binding was below 1%.

6.3. Discussion

All the three linkers showed lower conjugation efficiencies compared to short peptides like Ac-RAK-NH₂ when applying standard conditions. For the cysteine containing linker NH₂-K(N₃)-CRAK-OH, we have to assume that we attach dimers rather than monomers, due to the formation of disulfide bonds. This assumption is corroborated by the fact that coupling of maleimide-NODAGA failed under non-reducing conditions due to lack of free sulfhydryl groups. On the other hand, for linker NODAGA-K(N₃)-RAK-NH₂, the challenge were the three additional negative charges of the chelator, which we have shown to be destructive for efficient conjugation by MTG. However, since we reached >95% conjugation efficiency, we assume that the sterical distance of these charges to the primary amine was big enough not to significantly influence the enzymatic reaction.

NODAGA-K(N₃)-RAK-NH₂ has several advantages compared to NH₂-K(N₃)-CRAK-OH. It allows an easy over-night one step functionalization with a drug-to-chelator ratio of > 1.9. Dickgiesser *et al.* recently published a MTG-mediated, one-step functionalization of Trastuzumab, using an engineered variant of MTG to conjugate linkers, including toxins covalently attached, towards Q295^[126]. As a last advantage,

this mAb-construct allows for quick dual functionalization, by attaching a second chelator, or in our case, a toxin. The click chemistry worked for all of the tested moieties in low equivalents quantitatively. Being able to use low quantities of precious and highly toxic chemotherapeutics is beneficial because they are very expensive.

Receptor binding was retained for all of our ADCs as proven by flow cytometry and Lindmo assays. The main difference between the new MTG technology and the previous MTG-mediated coupling methods is the retention of the mAb glycosylation. Since glycans are known to be important for the structural integrity of the IgG CH2 region^[28,154], it can be assumed that with the intact glycan, ADCs are more stable, tend to aggregate less, and thus might show longer blood half-lives. Furthermore, they can also play a role in the binding of FCγRI receptors, clearance, biodistribution, and immunogenicity.

7. Trastuzumab biodistribution with linker $\text{NH}_2\text{-K}(\text{N}_3)\text{-CRAK-OH}$ and comparative biodistributions of $\text{NODAGA-K}(\text{N}_3)\text{-RAK-NH}_2$ with and without toxin

All the work has been designed/performed and analyzed by Jöri Wehrmüller.

7.1. Introduction

First, we used ADC Trastuzumab-NH₂-K(maytansine)-C(NODAGA)RAK-OH to assess the *in vivo* performance with different amounts of co-injected Trastuzumab. The reason behind are reports that low levels of IgG2a in nude mice (<50 µg) correlate with rapid clearance of injected mAb into liver and spleen^[155]. Furthermore, it has been shown that co-administration of cold mAb in highly antigen expressing tumors can help overcoming the binding-site barrier, resulting in higher tumor uptake^[156]. Second, we performed a comparative biodistribution with the three immunoconjugates Trastuzumab-NODAGA-K(N₃)-RAK-NH₂, Trastuzumab-NODAGA-K(maytansine)-RAK-NH₂, and deglycosylated version of the latter, Trastuzumab_{deglyc.}-NODAGA-K(maytansine)-RAK-NH₂. We wanted to see direct impact on tumor uptake for species with and without toxins. Furthermore, we were interested to see if the glycosylation has an impact on organ uptake, especially since our older enzymatically produced ADCs were dependent on the deglycosylation step. For the xenograft models, we decided on Skov3-ip human ovarian cancer cells.

7.2. Results

7.2.1. Determination of the co-administration of native Trastuzumab on the biodistribution of ¹¹¹In labeled Trastuzumab-NH₂-K(maytansine)-C(NODAGA)RAK-OH

Before a time-dependent biodistribution study with ¹¹¹In-labeled Trastuzumab-NH₂-K(maytansine)-C(NODAGA)RAK-OH was conducted, we performed a study to determine the ideal amount of co-injected cold Trastuzumab to maximize the uptake of the immunoconjugates into the tumor xenografts and minimize the uptake in non-targeted tissue and organs. Five cohorts of mice (N=3) were subcutaneously injected with 5x10⁶ SKOV3-ip cells in the right flank. The tumors grew for two weeks before we injected all the groups with our ADC-species. The preparation of Trastuzumab-NH₂-K(maytansine)-C(NODAGA)RAK-OH was done according to chapter 6.2.2. Labeling with ¹¹¹In resulted in specific activity of >100 MBq/mg ADC. Each mouse was injected with 150 kBq, which equals to 1.4 µg ADC in total, 0.37 µmol ADC/kg mouse, or 0.056 mg ADC/kg mouse. Mice were co-injected with different amounts of native Trastuzumab (0, 1.5, 5, 15, and 30 mg/kg, - which is equivalent to 0, 10, 33.3, 100, and 200 µmol/kg). The biodistribution was determined at 48 h and 96 h p.i. (Figure 31, and Table A 6-Table A 8).

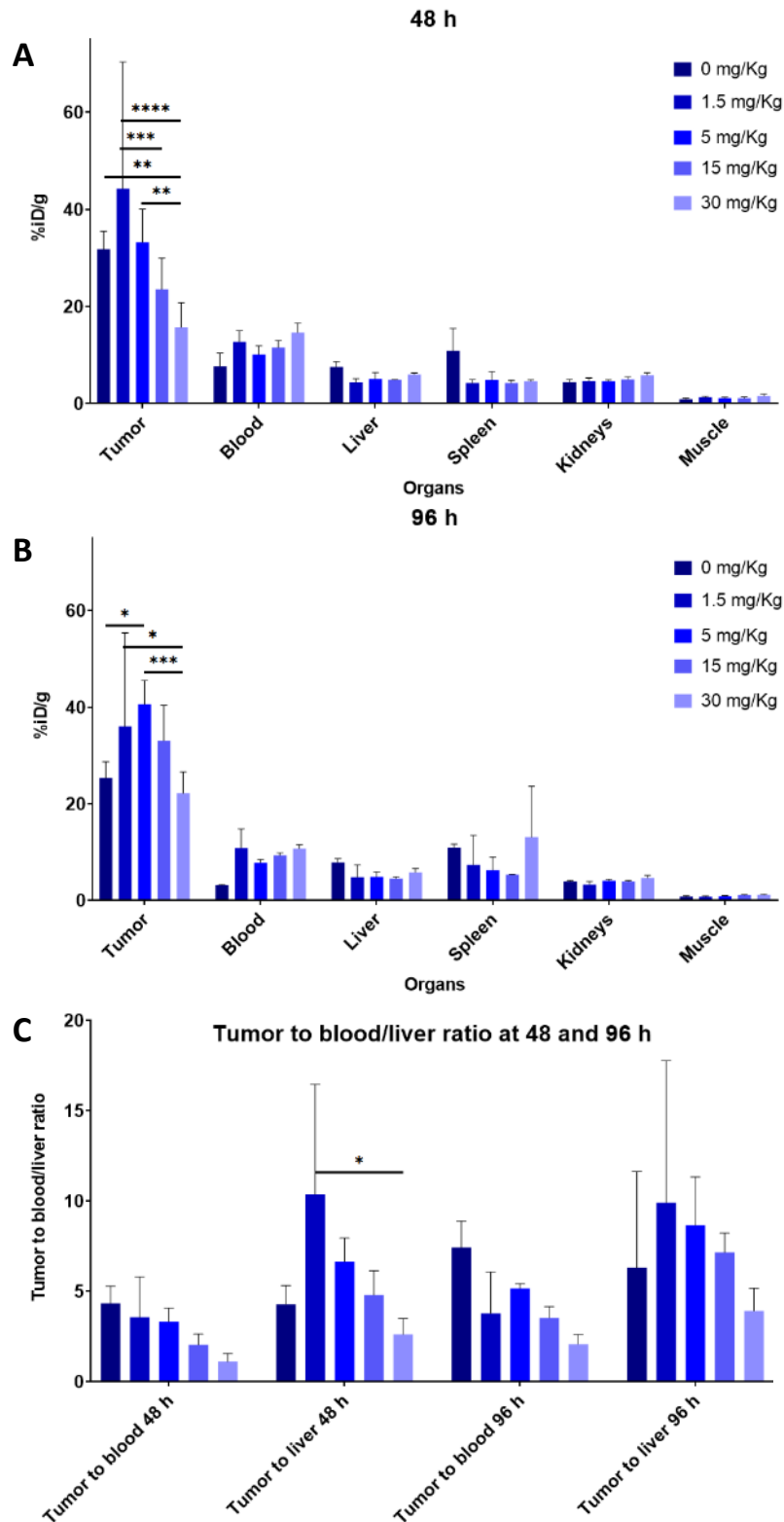


Figure 31: A/B) Biodistributions of ADC Trastuzumab-NH₂-K(maytansine)-C(NODAGA)-RAK-OH in SKOV3-ip xenografted nude SCID-mice. On the x-axis different organs are listed, whereas on the y-axes the % injected dose per gram is shown. The ADC got injected in five different groups, with additions of 0 mg native Trastuzumab / kg mouse, 1.5 mg/kg, 5 mg/kg, 15 mg/kg and 30 mg/kg. A: 48 h post-injection. B: 96 h post-injection. C: Tumor to blood/liver ratios, calculated from the ratio of each mouse. The tumor has the highest uptake compared to other organs, with around 40% for the 1.5 and 5 mg/kg group after 48 and 96 h. N=3, N_{0 mg/kg at 96 h}=2, Statistical analysis: 2-way ANOVA Bonferroni analysis in Graphpad with * = $p \leq 0.05$, ** = $p \leq 0.01$, *** = $p \leq 0.001$, **** = $p \leq 0.0001$.

After 48 h, the 1.5 mg/kg cohort showed a tumor uptake of $44 \pm 26\%$ iD/g, which is significantly higher than the uptake of the 15 mg/kg or 30 mg/kg cohort. A low uptake was observed in the 30 mg/kg group with $16 \pm 5\%$ iD/g. For the 0 mg Trastuzumab/kg group, we observed spleen and liver uptake of $11 \pm 5\%$ iD/g and $8 \pm 1\%$ iD/g, respectively. A non-significant trend to high spleen uptake ($13 \pm 11\%$ iD/g 48 h p.i.) was observed as well in the cohort with the highest amount of co-injected Trastuzumab. After 96 h, the 5 mg/kg cohort showed a tumor uptake of $41 \pm 5\%$ iD/g, more than the group with 30 mg Trastuzumab/kg ($22 \pm 4\%$ iD/g) or 0 mg/kg ($25 \pm 3\%$ iD/g). The blood shows for all cohorts less remaining ADC after 96 h compared to 48 h, which is an expected but non-significant trend.

7.2.2. Time-dependent biodistribution study with ^{111}In labeled Trastuzumab-NODAGA-K(N₃)-RAK-NH₂, Trastuzumab-NODAGA-K(maytansine)-RAK-NH₂, and Trastuzumab_{deglyc.}-NODAGA-K(maytansine)-RAK-NH₂

In this study, we analyzed the impact of the hydrophobic toxin maytansine on the overall biodistribution profile of Trastuzumab. We tested and compared Trastuzumab-NODAGA-K(N₃)-RAK-NH₂ (lacking the toxin) with Trastuzumab-NODAGA-K(maytansine)-RAK-NH₂. Additionally, we prepared a deglycosylated variant of the latter, Trastuzumab_{deglyc.}-NODAGA-K(maytansine)-RAK-NH₂. In order to observe the direct impact of the toxin on the biodistribution, we decided to use the conditions without any pre-injection of native mAb. The three species were labeled with ^{111}In following the procedure described in chapter 6.2.3. Cohorts of mice (N=4) were subcutaneously injected with 5×10^6 SKOV3-ip cells in the right flank. The tumors grew for two weeks before we injected all the groups with our ADC-species. Labeling with ^{111}In yielded specific activity of between 40 - 41 MBq/mg ADC. Each mouse was injected with 150 kBq, which corresponded to 3.7 – 3.9 μg ADC in total. This results in approx. 0.15 mg ADC/kg mouse, or 1 μmol ADC/kg mouse. For each of these cohort, the biodistribution was measured after 24 h, 48 h, 72 h, and 96 h (Figure 32, and Table A 9-Table A 11).

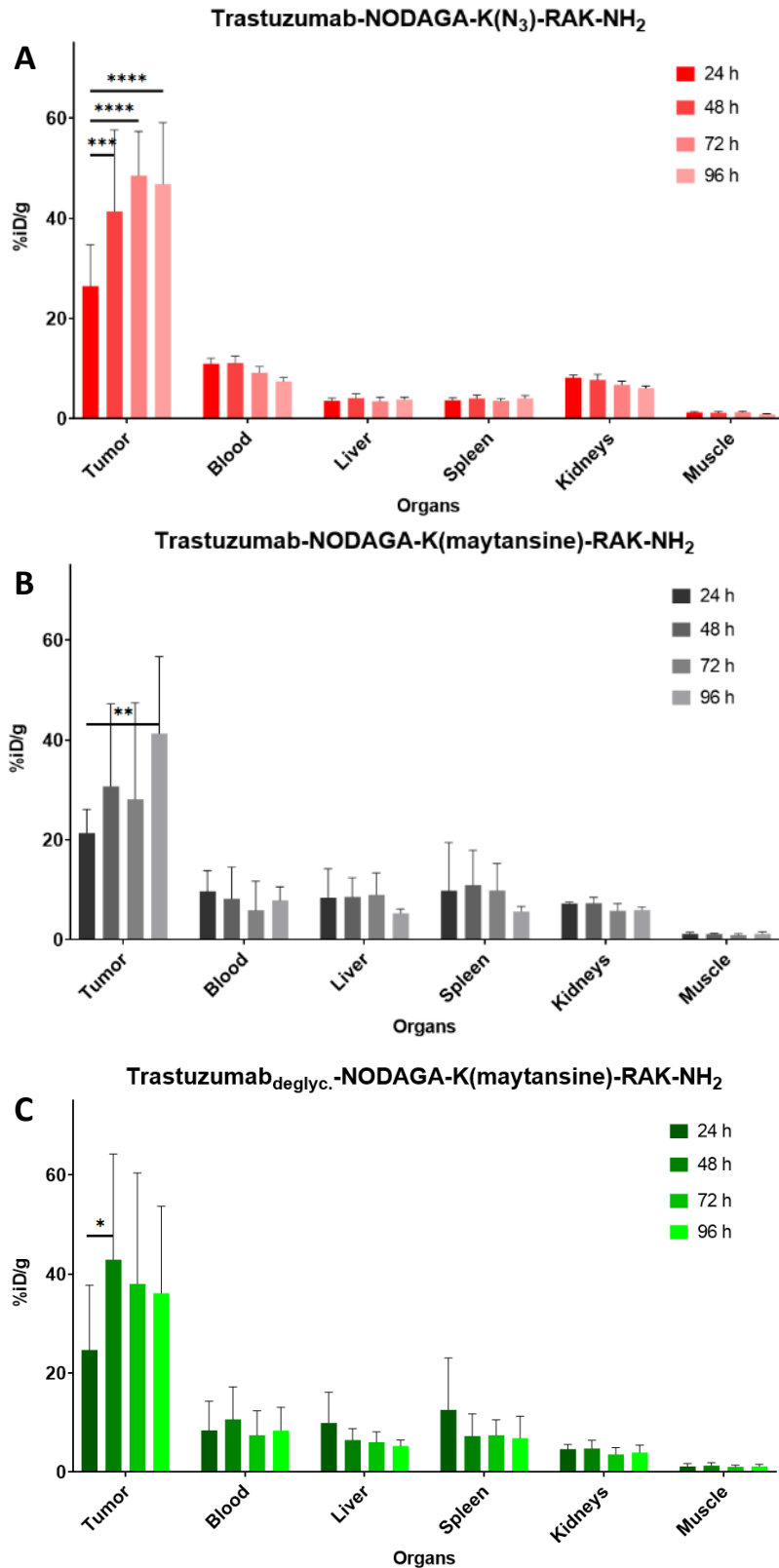


Figure 32: Biodistributions of the three In-111 labelled ADC constructs Trastuzumab-NODAGA-K(N₃)-RAK-NH₂ (A), Trastuzumab-NODAGA-K(maytansine)-RAK-NH₂ (B), and Trastuzumab_{deglyc.}-NODAGA-K(maytansine)-RAK-NH₂ (C) in SKOV3-ip xenografted nude SCID-mice. On the x-axis different organs are listed, whereas on the y-axis the %iD/g is shown. N=4. Statistical analysis: 2-way ANOVA Bonferroni analysis in Graphpad with * = $p \leq 0.05$, ** = $p \leq 0.01$, *** = $p \leq 0.001$, **** = $p \leq 0.0001$.

^{111}In labeled Trastuzumab-NODAGA-K(N₃)-RAK-NH₂, without toxin, showed a high tumor uptake after 72 h with 49±9% iD/g, which is significantly more than the one observed after 24 h with 26±8% iD/g. At all time-points, blood pool activity was high (7.5-11% iD/g). Liver, spleen, and muscle had uptake below 5% iD/g. ^{111}In labeled Trastuzumab-NODAGA-K(maytansine)-RAK-NH₂, with the toxin, showed 41±15% iD/g tumor uptake after 96 h, which is as well significantly more than the uptake after 24 h with 21±5% iD/g. In comparison to Trastuzumab-NODAGA-K(N₃)-RAK-NH₂, liver and spleen showed a non-significant trend of higher uptake at all the time-points. Other than for the kidneys and muscle, the data shows more variance for Trastuzumab-NODAGA-K(maytansine)-RAK-NH₂. A similar picture can be seen for the deglycosylated ADC Trastuzumab_{deglyc.}-NODAGA-K(maytansine)-RAK-NH₂. Here, we determined a tumor uptake of 43±21% iD/g after 48 h, which again is significantly higher than 25±13% iD/g uptake after 24 h.

Due to the high variance observed, we made a nested plot for every single mouse %iD/g for the organs tumor, spleen, and blood (Figure 33). We can see, that for both species with the toxin maytansine attached, the spleen and blood values spread over a big range, whereas the non-toxin containing mAb shows low variance in comparison. We have noticed that those mice with high spleen/liver uptake have low blood and tumor uptake (single mouse data not shown). This leads to the assumption, that in those cases the mAb was cleared rapidly from the blood pool into the liver and spleen.

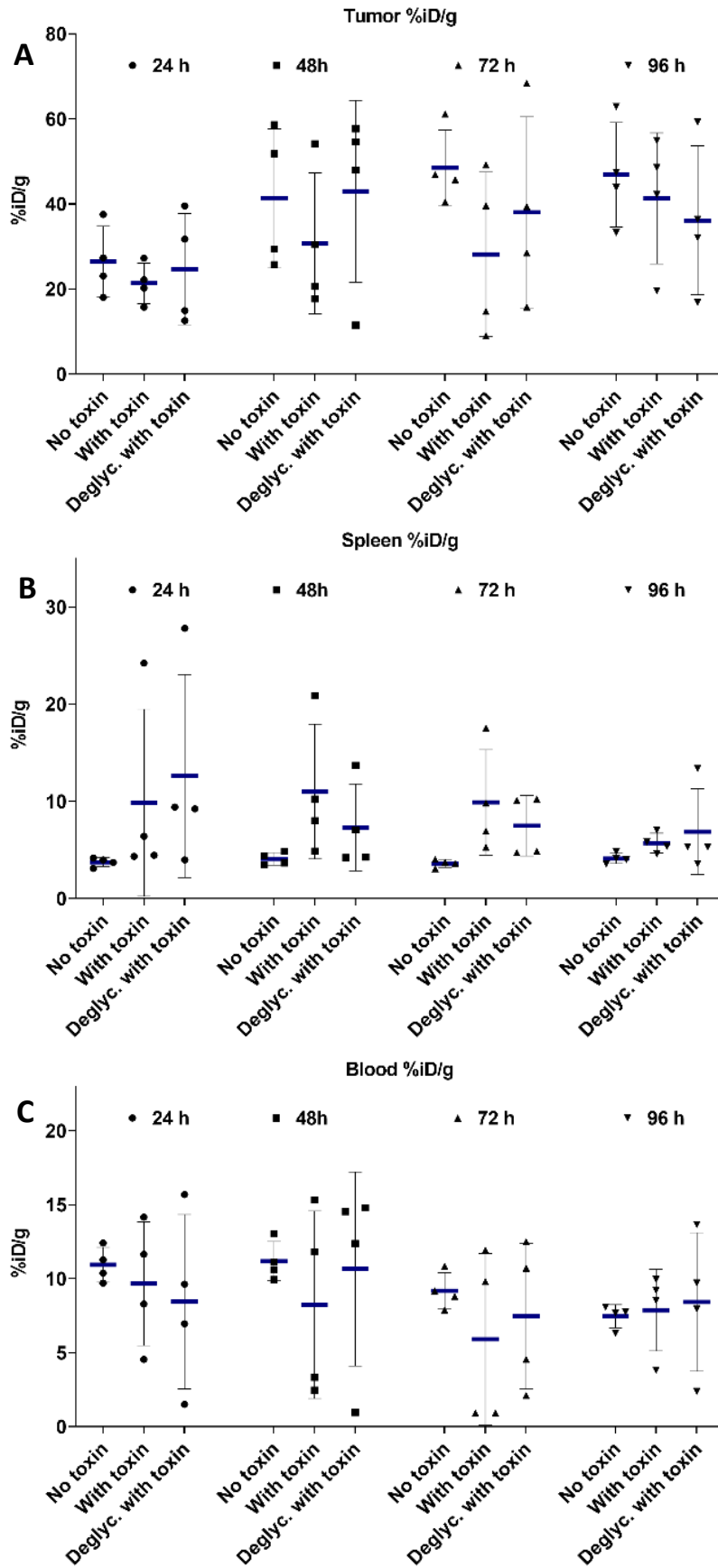


Figure 33: Nest plot of the organs tumor (A), spleen (B), and blood (C) from the biodistribution shown in Figure 32. Shown is the %iD/g of each mouse for all the three species: with and without toxin, + deglycosylated Ab with toxin. The two species with toxin show high variation for all the three organs, compared to the non-toxin species.

The high standard deviations in the biodistribution in case of ^{111}In labeled Trastuzumab-NODAGA-K(maytansine)-RAK-NH₂ and Trastuzumab_{deglyc.}-NODAGA-K(maytansine)-RAK-NH₂ were mainly because a few individual mice showed extremely low blood %iD/g, which might be the reason for the wide range of tumor uptake between 9% and 68% iD/g at 48 h and 96 h p.i.. Thus, not surprisingly, cross comparing the three immunoconjugates with each other resulted in no significant differences in tumor uptake (Figure 34, 48 h and 96 h shown). Similarly, also no difference could be detected for tumor to blood, or tumor to liver ratios (all values in Table A 12). Statistics were made with a 2-way ANOVA Bonferroni analysis in Graphpad with $p \leq 0.05$.

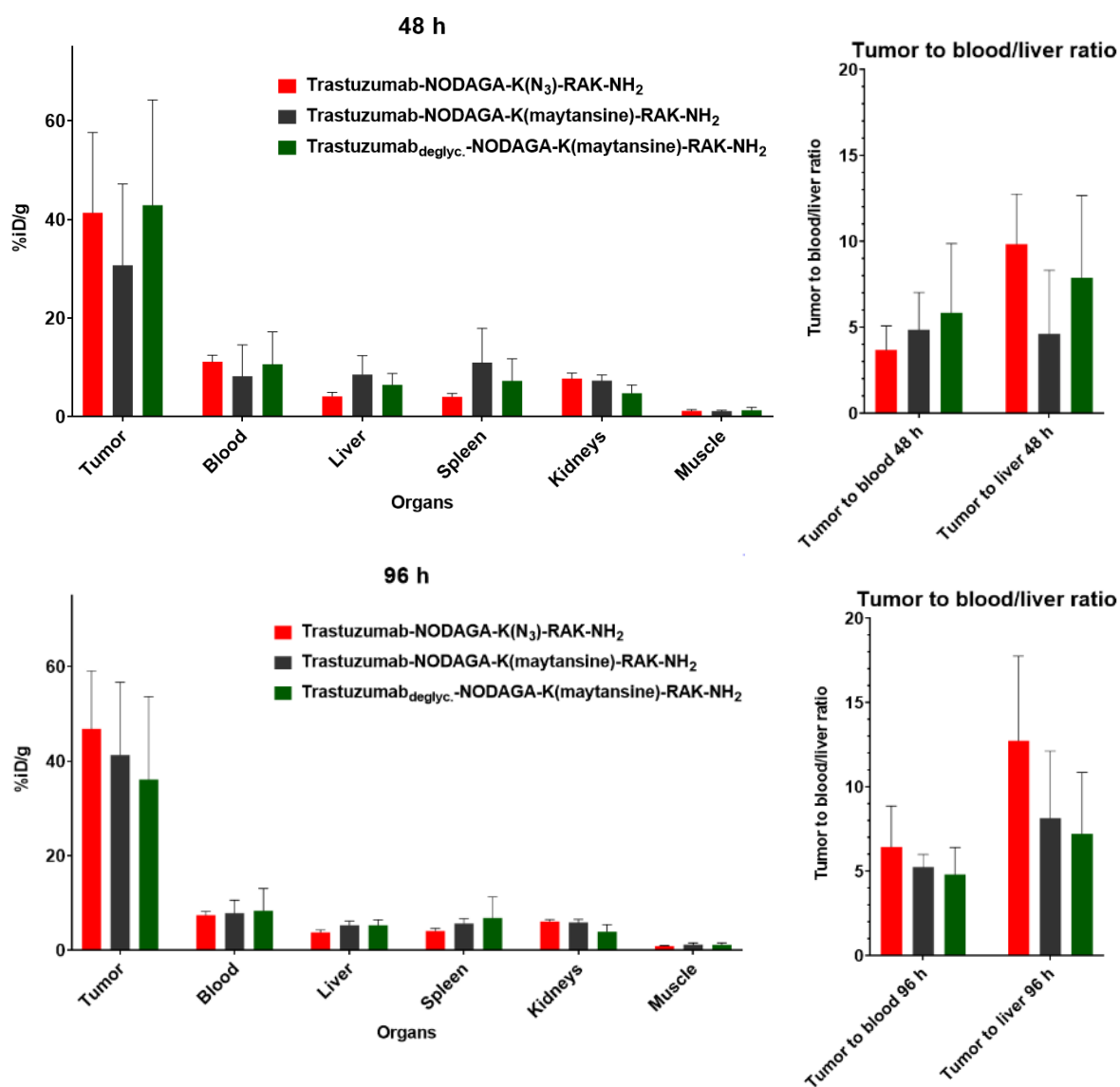


Figure 34: Left: Biodistribution of the three ADC constructs Trastuzumab-NODAGA-K(N₃)-RAK-NH₂ (in red), Trastuzumab-NODAGA-K(maytansine)-RAK-NH₂ (in black), and d-Trastuzumab-NODAGA-K(DM)-RAK-NH₂ (in green) in SKOV3-ip xenografted nude SCID-mice. On the x-axes different organs are listed, whereas on the y-axes the %iD/g is shown. Top: 48 h time point, Bottom: 96 h time point, N=4. Right: Tumor to blood/liver ratios from the corresponding biodistribution calculated on each individual mouse. Top: 48 h, Bottom: 96 h. Statistical analysis: 2-way ANOVA Bonferroni analysis in Graphpad with $p \leq 0.05$. No significant difference could be measured.

7.3. Discussion

The biodistribution with low to high amounts of co-injected Trastuzumab shows clearly the impact co-administration of native mAb has on tumor uptake. Both extremes seem to be suboptimal. For the group with the highest dose of co-administered, native Trastuzumab, low tumor uptake was observed because of partial receptor saturation on the tumors. Without co-injection of mAb, however, we do see a trend to higher spleen and liver uptake due to the fact that nude mice have low and heterogeneous IgG titer, which leads to fast clearance of any injected mAb or immunoconjugate^[155]. Another point that potentially counteracts fast tumor uptake is the lack of masking peripheral non-tumor antigens. Pre-administration has been shown to increase blood exposure of an anti-TENB2 ADC, reducing hepatic, intestinal, and splenic uptake while the tumor accretion was not affected^[157]. Also shedding of HER2/neu receptor (known in human^[158]) could be a problem with low ADC titers. Shedded HER2/neu can bind towards the ADC in the blood and thus hinder it to reach the target.

The second study was performed to determine the impact of the toxin on the pharmacokinetic profile. Other than in previous studies, where the toxin and the radiolabeling was not located at the same site on the mAb^[81], here, we coupled both, the toxin and the metal chelator to the same linker. We decided to use the peptide linker with the chelator NODAGA covalently attached at the N-terminus, NODAGA-K(N₃)-RAK-NH₂. In order to see more clearly the direct impact of the toxin on the biodistribution, we did not perform any pre-injection of native mAb. Retrospectively, this was presumably suboptimal since almost 50% of the mice injected with ¹¹¹In labeled Trastuzumab-NODAGA-K(maytansine)-RAK-NH₂ and Trastuzumab_{deglyc.}-NODAGA-K(maytansine)-RAK-NH₂ showed fast clearance of the ADC from the blood into liver and spleen. It is highly possible that a variable IgG2a titer might have led to this fast clearance. However, it does not completely explain that we only could see this effect for species with toxin. One argument could be, that due to the low IgG2 titer clearance was accelerated by highly hydrophobic toxin maytansine.

While we could not see significant differences in tumor uptake, we were surprised that deglycosylated species had high tumor uptake after 48 h. However, this effect has been explored before and might come from altered affinity of FcγR for the Fc domain^[26,159]. Vivier *et al.* found that impaired *in vitro* FcγRI binding of deglycosylated immunoconjugates correlates with significant decreases in off-target uptake, such as the liver by 3.5 fold. They even conclude that deglycosylation can be used as strategy to enhance the quality of immune-PET studies.

Projects in the future should involve another biodistribution comparing the non-toxin/toxin species with pre-injected IgG2a, to observe if it improves the overall tumor uptake and reduced the fast clearance. Conjugating the peptide in a cleavable version could also be interesting, especially to track

the toxin accumulations. Another option could be also to attach only the toxin in a cleavable version (commercially available). Furthermore, and since we are constricted to the position Q295, a direct comparison with another site-specifically modified ADC at a different position could shed light on the advantages of Q295.

8. Site-specific MTG mediated conjugation and SPECT of an EGFR-Nanobody with and without albumin binder

Scientific Contributors:

The results were accomplished in a project with the Policastro group from the Comisión Nacional de Energía Atómica in Argentina. Julia Gallino and Dailenys Espinosa joined Jöri Wehrmüller for two months at PSI, in which we gathered the following results in equal shares. Julia Gallino had her focus on the biological work, whereas Dailenys Espinosa was doing mainly the radiolabeling. Jöri Wehrmüller was planning, supervising, and partially conducting the experiments. The biodistributions were made by Jöri Wehrmüller together with Stefan Imobersteg, who took over animal care and supervised SPECT imaging. Dr. Stefan Gruber and Vera Gomez kindly synthesized for this project the two linkers referred as VG-49 and VG-56.

8.1. Introduction

The epidermal growth factor receptor (EGFR) is overexpressed in a variety of different cancers, such as lung cancer (40-80%), breast cancer (14-9%), or colon cancer (25-77%)^[160,161]. Therapy with monoclonal mAbs can be limited due to resistance cancer cells can acquire, and because of the limited EGFR(+) subpopulation^[162-166], as not all cancer cells express the antigen. Furthermore, full mAbs have been shown to give suboptimal results in patients with solid tumors, due to poor penetrability. In this project, we want to use MTG to equip an EGFR binding nanobody (VHH; 12-16 kDa) with a chelator for radioimmune therapy and diagnosis. The advantages on this small mAb fragments compared to full mAbs are that they still have full antigen-binding capacity, and retain specificity and high affinity to the target^[167,168]. Furthermore, they do not possess the FC region, thus are poorly immunogenic. Due to their small size, they can be expressed easily and cost-efficiently in bacteria, and are known to penetrate dense tissue rapidly^[169]. Their blood half-life, however, is reduced compared to mAbs, due to fast renal clearance. In this project, we want to optimize the half-life of an EGFR-targeting VHH, to improve accumulation in the cancer tissue and still obtain rapid clearance for better target-to-background contrast for imaging and therapy. The VHH is expressed together with a myc-tag, to enzymatically attach a chelator NODAGA with MTG. Two different linkers were tested. While one consists only of the chelator, a second one is additionally equipped with 4-(*p*-iodophenyl) butyric acid, an albumin binder (Figure 36). Albumin binders have been shown to bind to human and mouse serum albumin, and thus prolonging the systemic half-life of pharmaceuticals in blood^[170]. SPECT images were generated of both VHH-NODAGA variants to see the different distribution in xenografted SCID nude mice.

8.2. Results

8.2.1. VHH conjugations

The EGFR targeting VHH 7d12 was expressed in *E-coli* cells in the Policastro group (142 aa, with myc-tag and C-terminal His-tag, Sequence in Figure A 64). The two substrates VG49 and VG56 contain a primary amine, which can be recognized by MTG, as well as the chelator NODAGA. They differ, as VG56 additionally is equipped with albumin binder 4-(*p*-iodophenyl) butyric acid. Different conjugation conditions with 7d12 showed optimal conjugation efficiencies for shorter conjugation times compared to the Q295 technology. Best results were achieved after 30 min at 37 °C, with 1 mg/mL VHH in PBS with 6 U MTG/ mg VHH, and 40 eq. linker. VHH attachment reached 65±1% and 58±2% with the linkers VG49 and VG56, respectively (Figure 35, N=2). Longer incubation times reduced the yield of the VHH-conjugate.

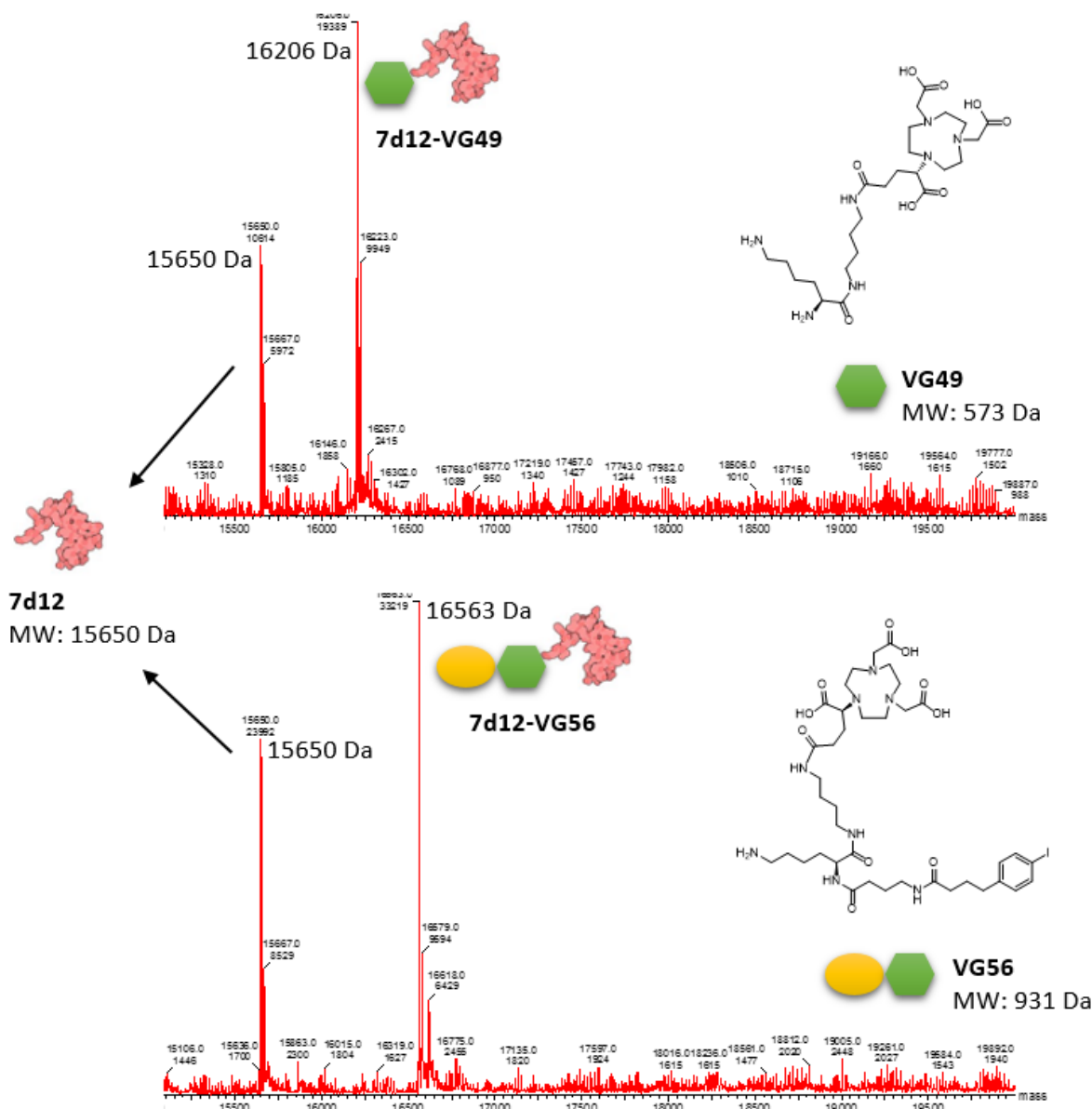


Figure 35: MS Spectra after the enzymatic MTG reaction of VHH 7d12 with linkers VG49 (top) and VG56 (bottom). The conjugation was not quantitative. In both spectra, the first peak corresponds to native 7d12, whereas the right peak is the converted product. Calculated conjugated 7d12-VG49: 16206 Da; Detected conjugated 7d12-VG9: 16206 Da. Calculated conjugated 7d12-VG56: 16564 Da; Detected conjugated 7d12-VG56: 16563 Da. The conjugation efficiency, calculated from the intensity, is 63.9% for VG49 and 60.2% for VG56.

8.2.2. MTG Separation, ¹¹¹In radiolabeling, and Lindmo assay

An efficient separation of the bacterial enzyme MTG (38 kDa) from the VHH constructs (16 kDa) is important for *in vivo* experiments and further therapy studies. Two different methods were tested. Semi-preparative size exclusion chromatography with a Superdex 75 5/150 column could not separate the two fractions with the necessary resolution. Making use of the His-tag of VHH, which binds to Ni-Resin in high affinity, could separate MTG efficiently (Figure 36).

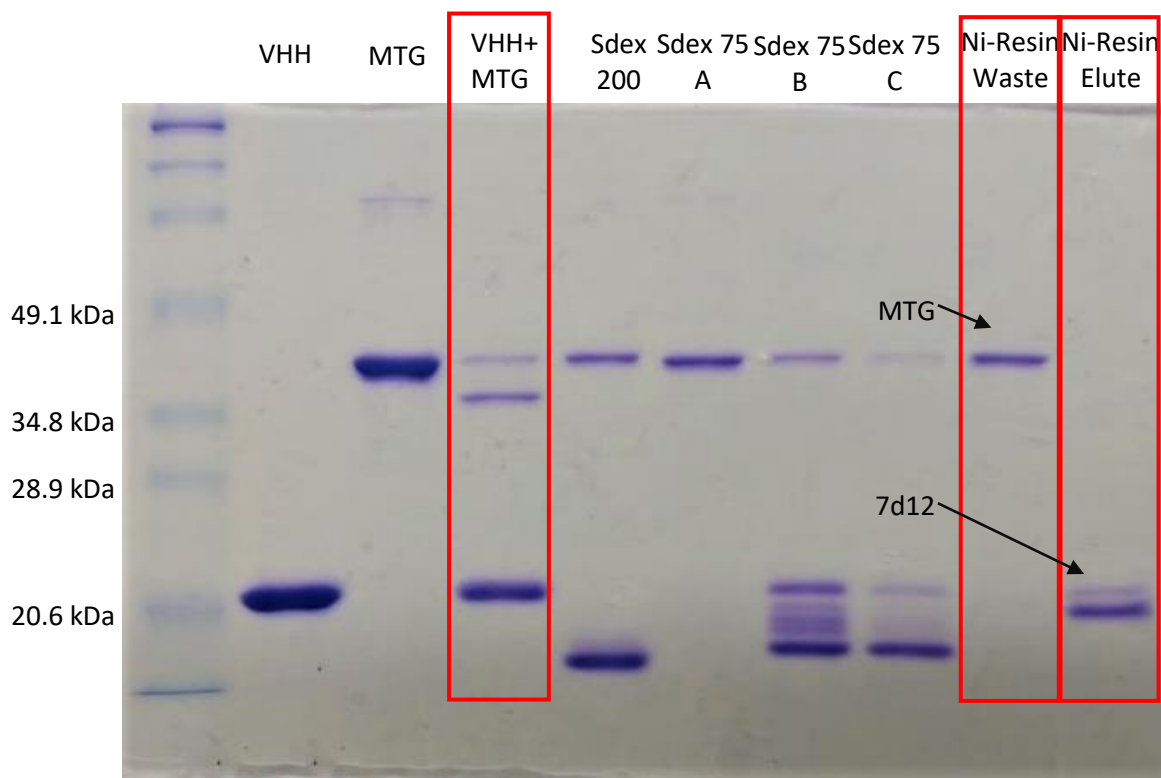


Figure 36: SDS-PAGE gel analysis of a VHH/MTG mixture (red rectangle on the left) and its separation by size exclusion and by Ni-resin. Whereas size exclusion did not give a good enough separation, Ni-resin did partition MTG from VHH 7d12 (two red rectangles on the right).

Labeling of the 7d12 nanobodies with ^{111}In resulted in efficiencies of two times 97% for VG49, and 98% as well as 96% for VG56 (different batches tested). A Lindmo binding assay was made to test for retained binding capacity with EGFR overexpressing A431 cells *in vitro*. Receptor blocking to determine the non-specific binding was made with an excess of EGFR binding mAb Cetuximab. The Lindmo assay was performed with albumin binding linker VG56 attached to 7d12. An immunoreactive fraction of 84% was achieved (Figure A 66).

8.2.3. SPECT Imaging

SPECT images of the two EGFR targeting 7d12 variants were made with A431 xenografted nude mice (representative images in Figure 37). 5×10^6 cells were injected subcutaneously into the right flank. The tumors grew for two weeks before two cohorts of mice (N=2) were injected with either one of the 7d12 variants. Labeling with ^{111}In achieved a specific activity of 1061 MBq/mg 7d12-VG49 and 865 MBq/mg 7d12-VG56. Each mouse was injected with 5 MBq. Furthermore, non-conjugated 7d12 was added to both solutions to reach an injection dose of 10 μg VHH per mouse, resulting in 0.4 mg VHH/kg mouse or 25 nmol VHH/kg mouse. Images were taken 1 h, 4 h, 24 h, and 72 h post injection. No quantification or analysis for statistical significance was made. The compound 7d12-VG56 with albumin

binder shows a trend in higher tumor uptake and longer residual time compared to the 7d12-VG49 species at all time points. But not only the tumor, also the healthy tissue distribution and especially the liver tends to have more activity accumulated for the albumin binding species. For both linkers, high renal uptake could be detected.

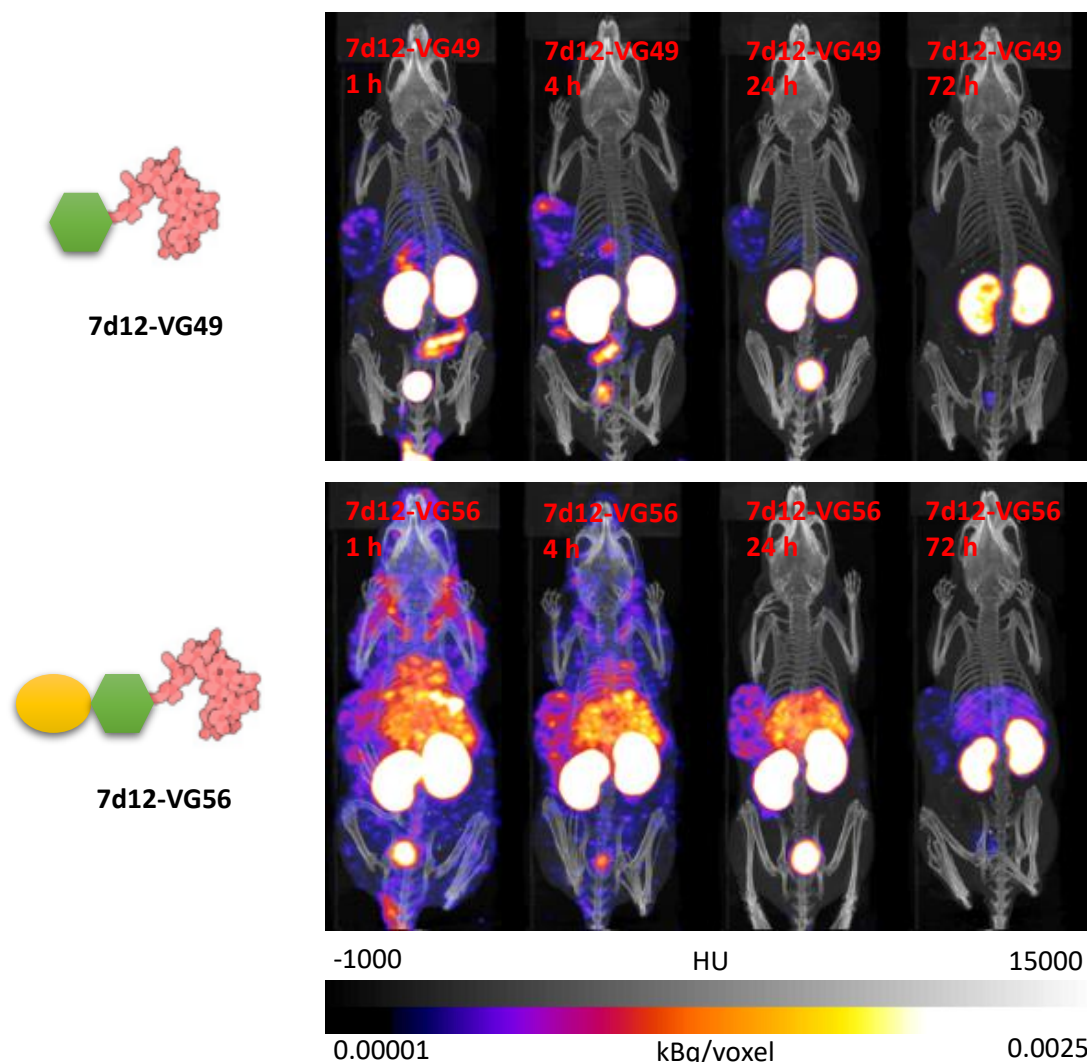


Figure 37: EGFR targeting Nanobody 7d12 got equipped with two linkers, VG49 and VG56. Both have a chelator, which was labeled with In-111. Shown are representative SPECT images at different time points of xenografted nude mice with an A431 tumor model. Linker VG56, which additionally is equipped with an albumin binder (yellow circle in the schematic structure), shows higher uptake of tumor and healthy tissue. The gradient from black (-1000) to white (15000) represents intensities in Hounsfield units of CT. The gradient from dark purple (0.00001) to yellow/white (0.0025) represents intensities in kBq/voxel of SPECT (voxel size = 0.3 mm).

8.3. Discussion

This 3-month project was very challenging in terms of time, resulting in limited availability of substrates and lack of time for follow up experiments for the herein presented results. Nevertheless, we were successful in conjugating these novel linkers VG49 and VG56 towards VHH 7d12. Enzymatic conjugation to the Gln in the myc-tag was faster compared to our experiences with Q295 on the mAb.

One reason is for sure, that the myc-tag is an optimized substrate for MTG, and has been reported to allow different acyl acceptor substrates^[123]. However, quantitative attachment was not achieved. Interestingly, the albumin binding moiety had a big impact on the biodistribution. Other than higher tumor uptake and slower blood clearance, the additional liver uptake was a surprise to us. Even though it is known that the liver has receptors for albumin, the effect of high liver uptake is not reported with other (low molecular weight) compounds bearing 4-(*p*-iodophenyl) butyric acid^[171]. Another more simple explanation for higher uptake of VHH in healthy tissue, liver, and tumor can be the longer residual half-life in blood for the compound with the albumin binder. A key experiment missing is a biodistribution assay to quantify and track the VHH in the different organs, especially to confirm the high liver uptake for the species 7d12-VG56 with albumin binder. Furthermore, ideal storage conditions and the stability of the linkers has to be analyzed.

9. Discussion and conclusion

In this thesis, we presented a novel technology to attach payloads such as toxins or chelators to antibodies. While the field has presented several methodologies to yield such antibody-drug conjugates, our method can be distinguished by its combination of site-specific and homogeneous attachment towards non-engineered mAbs. A homogeneous ADC species, compared to a mixture of ADCs with different DARs, is easier to characterize for *in vitro* and *in vivo* behavior. To achieve such a defined DAR, either enzyme engineering^[126] or the use of engineered tags^[99]/mAbs^[82] is needed among other methods, which is both not necessary for Q295 conjugation by MTG. The site-specificity is given by Q295 on mAbs, which, with some discussed exceptions, is the sole site of attachment of our payloads. Almost all new technologies make use of defined conjugation sites, whereas it has been shown that not all of them are advantageous. Engineered specific attachment sites, such as cysteines, have the advantage of being introduced to almost any site of the mAb sequence, whereas the position of Q295 is a limiting factor of our technology. The MTG conjugation requires stringent, not fully explored, conditions on the Q-positioning for the reaction to work; All the other 15 Gln's of the Trastuzumab HC show no or minor conjugation. However, up to this point we had no experiment revealing disadvantageous side effects such as aggregation, losing of binding potential or low blood half-life induced by position Q295. This is in comparison with previous work on Q295 with deglycosylated mAbs^[81,112]. Furthermore, Q295 is a conserved site within prevalently used isotypes IgG1 and IgG4 for therapies. This is important, since absence of a reactive Gln limits the MTG approach. On the other hand, as a big advantage, our enzymatic approach can produce ADCs in a quick manner directly out of native mAbs without any pre-treatment. This was normally reserved only for chemical conjugation methods, which on the downside lead to a mixture of ADC species.

The enzyme MTG is commercially available (Zedira GmbH), stable in physiological conditions and most importantly, it can be easily removed from the ADC after the reaction. In respect to these factors, MTG is not a limiting factor. However, we have shown in the results that only specific peptides, having at least one lysine, can be attached to Q295, restricted by the activity of MTG. While the other enzymatic conjugation method with sortase A has similar restrictions, chemical methods are using reactive handles, with the advantage that they can be attached to a broad scope of substrates. With the introduction of an azide on an MTG-reactive peptide, we can make use this broad scope as well and bypass the narrow substrate specificity of MTG. As an example, the click chemistry with azides and the corresponding DBCO-agent works with low equivalents (5 eq. over conjugation site), making it amendable for expensive substrates. Furthermore, this makes our technology also open for mAbs that will be used for pretargeting.

On a broader perspective, the designed peptide linkers and MTG can be a strong couple for other applications as well. Especially the use of peptides and the resulting stable isopeptidic bond can be an advantage compared to less stable linker technologies. All the experience gathered with the design of our positively charged peptides can be leveraged to other MTG applications.

10.Outlook

The herein presented technology shows that enzymatic conjugation with MTG has a lot of potential to unravel new ways of orthogonal bioconjugations. Especially interesting is the concept of designing new linkers that specifically are attached towards a single site on a protein, in our case Q295. A low initial conjugation activity was enough to find optimal conditions and linker-structure that lead to full conversion. This is a potential concept that can be adapted to any other protein, resulting in novel orthogonal bioconjugations, which is more and more important in many fields. Since there are still only a few key indicators if a Gln within a protein is recognized by MTG, a trial- and error approach has to determine if MTG conjugation can be used for each new protein. A promising example is fibronectin, where preliminary results within our group show that MTG conjugation can be used to conjugate chelators towards the protein.

While we have shown the principle of attaching a primary amine containing linker towards a glutamine on the protein, future projects should also investigate on designing glutamine linkers that show homogeneous specificity towards a single lysine on a protein. Single reactive lysines and glutamines on a protein would lead to two different orthogonal bioconjugation approaches. Dual conjugations can be used either to increase the attached payload, or to introduce different functionalities, such as chelators or toxins, at once. In comparison with dual conjugations on the same linker, attachment at different positions might reduce the aggregation potential of the mAb, since the often very hydrophobic payload can be distributed differently.

Furthermore, instead of screening for an optimal linker, enzyme engineering is another approach that can be used to reach quantitative conjugation. A sophisticated conjugation approach could involve an evolved MTG, which has an altered substrate specificity. This is especially interesting for Gln positions with small residual conjugation activity, which we have detected, e.g. for Trastuzumab. The enzyme engineering field has shown that by randomly evolving enzymes in an iterative manner, such base activities can be increased. MTG has been subjected to enzyme engineering, this hasn't been tested yet. As a result, similar as already mentioned, two orthogonal conjugations could be achieved by using the native and the engineered variant subsequently for conjugation. However, this only would work, if the engineered variant loses specificity for the native Gln. Furthermore, the initial base activity is important to develop and test a screening assay, which is sensitive enough to differentiate between activating and deactivating mutations. Such an assay could involve hydroxylamine, that forms a detectable complex at 525 nm after conjugation with Z-Gln-Gly. To reach a promising starting point if initial activity is missing, site-directed mutagenesis at MTG's active site or other at other strategic positions can be performed. Especially interesting as novel targeting substrate could be asparagine. Its

chemical structure and electron density is very close to glutamine, and differs mainly by having one carbon more in the side chain. Mutations to open up MTG's active site cleft could allow the catalytic triad to bind asparagine. A crystal structure of MTG together with bound substrate would be helpful to understand better any key positions involved. It can explain on the molecular level how the charges influence a good binding, and maybe even unravel the role of the glycan when conjugating mAbs. These insights might be used as well, to develop more challenging MTG-accepted linkers that have the functionality directly attached, similar to the one-step approach presented in this thesis.

As a last point, I would like to put emphasis on the strength of big data and computational algorithms. Our approach to predict interesting sequences was biased with our experimental results and expectations we had for some of the sequences. However, it could be interesting to write a program that creates short lysine containing peptides randomly. Validating the SOM with a critical number of completely random sequences might bring us a step forward on finding key indicators, on what makes a well-accepted MTG lysine-substrate.

11. Material and Methods

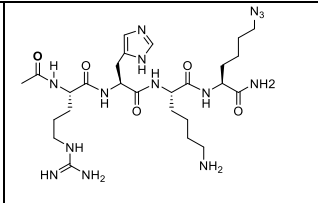
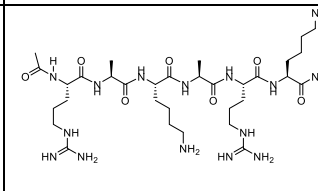
11.1. Chapter 4: MTG mediated Conjugation of primary amine containing peptides to Q295 of antibodies

11.1.1. Materials

Trastuzumab, Kadcyla[®], and Adcetris[®] were purchased from Roche (Basel, Switzerland). Nivolumab and Daratumumab have been bought from Bristol-Myers Squibb (New York, USA) and Jansen-Cilag International NV (Olen, Belgium), respectively. human IgG2; Armenian hamster IgG; rat IgG1, IgG2a, and IgG2b; and mouse IgG1, IgG2a, and IgG2b, are all InVivoMab[™] isotype controls purchased from Bio X cell (Lebanon, USA). The peptides got ordered from LifeTein (www.lifetein.com, New Jersey, USA). They show a purity of >90% (HPLC tested by supplier) and are stored at 25 mM in H₂O, at -20 °C. Azide functionalized Peptides Ac-RAK-K(N₃)-NH₂, Ac-RSK-K(N₃)-NH₂, and Ac-RHK-K(N₃)-NH₂ (Table 2) were purchased from Bachem (Bubendorf, Switzerland) and stored as already described. They have a purity of >90% (HPLC tested by supplier). MTG was purchased from Zedira (Darmstadt, Germany) and resuspended in water to a final stock concentration of 50 units/mL. Trizma base, Bis-Tris, sodium phosphate, and citrate buffer were purchased from Sigma-Aldrich (St. Louis, USA). Dulbecco's Phosphate Buffered Saline (PBS) buffer was bought from Merck (Burlington, USA). All the salts (NaCl, KCl, CaCl₂, MgCl₂, FeCl₃, NH₄Cl, NH₄HCO₃, (NH₄)₂SO₄, Na₂HPO₄, and KH₂PO₄) were purchased from Merck (Burlington, USA). The LC-MS for conjugation efficiency analysis was running with 2-propanol and acetonitrile from Honeywell Riedel-de-Haen (Charlotte, USA). The acetonitrile and water contain 0.1% formic acid, purchased from VWR (Radnor, USA).

Table 2: Chemical structures of azide functionalized linkers

Sequence	Molecular weight [Da]	Structure
Ac-RAK-K(N ₃)-NH ₂	568.7	
Ac-RSK-K(N ₃)-NH ₂	584.7	

Ac-RHK-K(N ₃)-NH ₂	634.8	
Ac-RAKAR-K(N ₃)-NH ₂	796.0	

11.1.2. Sequences of antibodies

Sequence of mouse-human chimeric anti-L1CAM chCE7; produced and kindly provided by Dr. Jürgen Grünberg and Dr. Nastassja Cereghetti-Terraneo with a light chain N-terminal myc-tag modification. The production was made as previously described by Grünberg *et al.*^[172].

Heavy chain^[140]:

QVQLQQPGAELVKPGASVKLSCKASGYTFTGYWMHWVKQRPGHGLEWIGEINPSNGRNTYNERFKSKATLTVDKS
STTAFMQLSGLTSEDSAVYFCARDYYGTSYNFDYWGGQTTLTVSSASTKGPSVFPLAPSSKSTSGGTAALGCLVK
DYFPEPVTVSWNSGALTSGVHTFPAVLQSSGLYSLSSVVTVPSSSLGTQTYICNVNHKPSNTKVDKKEPKSCDK
THTCPPCPAPELLGGPSVFLFPPKPKDTLMI SRTPEVTCVVDVSHEDPEVKFNWYVDGVEVHNAKTKPREEQYN
STYRVVSVLTVLHQDWLNGKEYKCKVSNKALPAPI EKTISKAKGQPREPQVYTLPPSRDELTKNQVSLTCLVKGF
YPSDIAVEWESNGQPENNYKTTTPVLDSDGSFFLYSKLTVDKSRWQQGNVVFSCVMHEALHNHYTQKSLSLSPGK

Sequence of commercial anti-HER2/neu mAb Trastuzumab. Purchased from Roche (Basel, Switzerland)

Heavy chain (<https://www.drugbank.ca/drugs/DB00072>):

EVQLVESGGGLVQPGGSLRLSACAASGFNIKDTYIHWVRQAPGKGLEWVARIYPTNGYTRYADSVKGRFTISADTS
KNTAYLQMNSLRAEDTAVYYCSRWGGDGFYAMDYWGQGLTVTVSSASTKGPSVFPLAPSSKSTSGGTAALGCLVK
DYFPEPVTVSWNSGALTSGVHTFPAVLQSSGLYSLSSVVTVPSSSLGTQTYICNVNHKPSNTKVDKKEPKSCDK
THTCPPCPAPELLGGPSVFLFPPKPKDTLMI SRTPEVTCVVDVSHEDPEVKFNWYVDGVEVHNAKTKPREEQYN
STYRVVSVLTVLHQDWLNGKEYKCKVSNKALPAPI EKTISKAKGQPREPQVYTLPPSREEMTKNQVSLTCLVKGF
YPSDIAVEWESNGQPENNYKTTTPVLDSDGSFFLYSKLTVDKSRWQQGNVVFSCVMHEALHNHYTQKSLSLSPGK

Sequence of anti-PD-1 mAb Nivolumab. Purchased from Bristol Myers Squibb (New York, USA)

Heavy chain (<https://www.drugbank.ca/drugs/DB09035>):

QVQLVESGGGVVQPGRSLRLDCKASGITFSNSGMHWVRQAPGKGLEWVAVIWDGSKRYADSVKGRFTISRDN
KNTLFLQMNSLRAEDTAVYYCATNDDYWGQGLTVTVSSASTKGPSVFPLAPCSRSTSESTAALGCLVKDYFPEPV
TVSWNSGALTSGVHTFPAVLQSSGLYSLSSVVTVPSSSLGTQTYTCNVNHDKPSNTKVDKRVESKYGPPCPPCPAP
EFLGGPSVFLFPPKPKDTLMI SRTPEVTCVVDVSDQEDPEVQFNWYVDGVEVHNAKTKPREEQFNSTYRVVSVLT
VLHQDWLNGKEYKCKVSNKGLPSSIEKTISKAKGQPREPQVYTLPPSQEEMTKNQVSLTCLVKGFYPSDIAVEWE
SNGQPENNYKTTTPVLDSDGSFFLYSRLTVDKSRWQEGNVVFSCVMHEALHNHYTQKSLSLSLGK

11.1.3. Antibody conjugation using microbial Transglutaminase

Method 1 (for peptide screening and condition testing):

As standard conjugation procedure, we provided 1 mg/mL mAb with 80 equivalents peptides. MAb was taken directly from the official formulation buffer from the provider, whereas the peptides were taken from a 25 mM stock solution in water. 6 U MTG/mg mAb were added to the reaction mix, out of a 50 U MTG/mL stock in water. Trizma pH 7.6 50 mM was added to reach the standard end volume of 50 μ L. The sample was incubated for 20 h at 37 °C before LC/MS analysis. This method was adapted accordingly to test different buffers, temperatures, concentrations of peptides, and additional salts (see chapter 4.2).

Method 2 (for the isotype/species screening):

3 mg/mL mAb incubation at 37 °C for 45 h led to quantitative conjugation for peptide-linkers that already perform well with method 1 (>80% conj. efficiency). Additionally, for all the reactions with > 1 mg/mL mAb, the mAb was buffer exchanged into the according reaction buffer (mainly Trizma pH 7.6 50 mM) prior to aliquotation (by PD10, Merck, Kenilworth, United States, standard protocol). For the short peptides containing 3 aa's, 20 h was for most reactions enough to reach >95% conj. efficiency, whereas the longer peptides showed quantitative attachment after 45 h, monitored by LC/MS analysis.

Method 3 (for azide-functionalized peptides):

5 mg/mL mAb was used for the azide functionalized peptides. We found 20 h to be sufficient for the short peptides RAK-K(N₃) and RHK-K(N₃) to reach >95% conjugation efficiency. Excess peptide was separated by PD10.

MAb concentrations were measured by a NanoPhotometer® P360 from Implen (Munich, Germany).

11.1.4. Protein A and size exclusion purification of conjugated antibodies

Protein A

Post-conjugation, mAbs were purified by protein A chromatography. In brief, an equal volume of PBS pH 8.5 was added to each sample prior to batch binding to Protein A Sepharose™ 4 Fast Flow beads (GE Healthcare, Chicago, USA) for 1 hour at room temperature (RT). Beads were washed with 10 column volumes (CV) prior to elution with 5 CV 0.1M Glycine pH 2.5 directly into 1 CV 2M Tris-HCl pH 7.5. Conjugated mAbs were then concentrated, and their concentrations were measured by a NanoPhotometer® P360 from Implen (Munich, Germany). Antibody concentrations steps and buffer

exchange were performed with Amicon Ultra-0.5 Centrifugal Filter Units (50 kDa cut-off, 5x repetitions, 2 min with 16k rcf, Centrifuge 5415 R, Eppendorf, Hamburg, Germany).

Size exclusion

A Superdex200 10/300 column (GE Healthcare, Chicago, USA) was equilibrated with 1x PBS prior to injection of the mAb/MTG mixture. After injection, an isocratic flow of 1 ml/min PBS (room temperature) was run for 120 min on a ÄKTAprime plus (GE Healthcare, Chicago, USA) FPLC. 5 mL samples were collected, and the mAb/ADC fractions concentrated by Amicon centrifugation as previously described.

11.1.5. SDS-PAGE electrophoresis

SDS-PAGE gels (12.5%, 1.5 mm) were prepared as following: 8.3 mL acrylamide solution 30 % (Gerbu, Heidelberg, Germany), 5.0 mL resolving gel buffer (1.5 M Trizma HCl, pH 8.8), 0.2 mL SDS 10 % (Sigma-Aldrich, St. Louis, USA), 6.4 mL H₂O, 75 µL ammonium persulfate 10 % (Thermo Scientific, Waltham, USA), and 30 µL TEMED® (Thermo Scientific, Waltham, USA) was mixed. After solidifying (30 min) a stacking gel (0.88 mL acrylamide, 1.66 mL 0.5 M Trizma HCl pH 6.8, 66 µL SDS, 33 µL ammonium persulfate, and 33 µL TEMED) was poured on top. Samples were loaded after 5 min incubation at 95 °C with pre-stained SDS loading buffer (BioRad, Hercules, United States) and the electrophoresis run for 1.5 h at 100-150 V in running buffer (25 mM Trizma, 190 mM glycine (Sigma-Aldrich, St. Louis, USA), 0.1% SDS, pH 8.3). Staining was made with Simply Blue™ (Invitrogen, Carlsbad, USA).

11.1.6. ESI-TOF LC-MS analysis of ADCs and antibodies

MAb samples (0.2 mg/mL) were incubated in 50 mM dithioerithrol (DTT, Sigma-Aldrich, St. Louis, USA) for 10 min at 37 °C to reduce the interchain disulfide bonds prior to the injection of 7.5 µL into a Waters LTC Premier ESI-TOF mass spectrometer (Waters, Milford, USA) coupled with a Waters 2795 Alliance HT HPLC (Waters, Milford, USA) for separation. An Aeris™ 3.6 µm WIDEPOR XB-C18 100x21 mm column from Phenomenex (Torrance, USA) was used with the following gradient:

Table 3: HPLC gradient for ADC and mAb analysis

Time [min]	Acetonitrile [%]	Water [%]	2-Propanole [%]	Flow [ml/min]
0	20	75	5	0.4
3	22	73	5	0.5
18	55	40	5	0.5
20	85	10	5	0.4

Analysis and deconvolution was made with the software MassLynx 4.1 and the MaxEnt 1 algorithm (Waters, Milford, USA). Differences in peak intensity of the corresponding deconvoluted masses were used to calculate the conjugation efficiency.

11.2. Chapter 5: Computational screening for suitable MTG substrates

11.2.1. Solid-phase Peptide Synthesis

Peptides for the computational project were synthesized using the 9-fluorenylmethoxycarbonyl (Fmoc) strategy on an automated peptide synthesizer (Gyros Protein Technologies, Tucson, USA). The production was scaled for a theoretical yield of 50 μmol of peptide. Rink Amide 4-methyl benzhydrylamine (MBHA) resin (0.52 mmol g^{-1} , 100-200 mesh size, AAPPTec, Louisville, KY) was used as solid support. Fmoc-protected amino acids were acquired from AAPPTec and Gyros Protein Technologies and dissolved in N,N-dimethylformamide (DMF, Sigma-Aldrich, St. Luis, USA) to a concentration of 200 mM. Amino acids were applied in a 10-fold excess in respect to the loaded resin. Deprotection of the amino acids and the resin was done with 20% pyrrolidine (v/v, Acros Organics Geel, Belgium) in DMF. A mixture between 800 mM 4-methyl morpholine (NMM, Fisher Chemical, Pittsburgh, PA) in DMF and 400 mM 1H-benzotriazolium,1-[bis(dimethylamino)methylene]-5-chloro-,3-oxide,hexafluorophosphate (HCTU, Gyros Protein Technologies, Tucson, USA) was used as coupling reagent. Washing and cleaving was made with dichloromethane (DCM, Sigma-Aldrich, St. Louis, USA) and a mixture of 88% trifluoroacetic acid (TFA, ABCR, Karlsruhe, Germany), 2% triisopropylsilane (TIPS, 98%, ABCR, Karlsruhe, Germany), 5% H_2O , and 5% phenole (Sigma-Aldrich, St. Luis, USA), respectively (v/v/v). Precipitation and repeated washing steps were made in di-isopropyl ether (Fluka, Buchs, Switzerland) and the centrifugation (Rotina 380R centrifuge, Hettich AG, Bäch, Switzerland) took place at 3320 x g for 10 min at -10°C . After drying the peptide over night, purification was done with a reversed-phase NucleodurTM C18 HTec column (150 x 21 mm, 5 μm , 110 Å, Macherey-Nagel, Düren, Germany) on a preparative high performance liquid chromatography system (Shimadzu, Kyoto, Japan) with a linear gradient going from 5-70% in 25 min with acetonitrile (Sigma-Aldrich, St. Luis, USA) in water (containing 0.1% formic acid from Sigma-Aldrich, St. Luis, USA) with a flow rate of 0.5 mL/min. Detection was done by UV spectroscopy at 210 nm. Peptide purity was analysed with a NucleodurTM C18 HTec column (150 x 3 mm, 5 μm , 110 Å, Macherey-Nagel, Düren, Germany) by an analytical reversed-phase-HPLC (Shimadzu, Kyoto, Japan). The same gradient was used as for the preparative system, but with a lower flow rate of 0.5 mL/min. Detection was made with an electro-spray mass detection with a quadrupole mass spectrometer in the range from 300 to 2000 m/z and by UV with a SPD-M20A Prominence HPLC photo diode array detector (Shimadzu, Kyoto, Japan).

11.2.2. Conjugation of peptides

17 sequences (GEEKEL, YDADK, TEKAN, KARAGAGADADAD, KTT, LAKE, TVKVT, YGKGY, VRKRV, RVRK, AARAKARAA, PKARA, RFK, AVRAK, IFSK, RAVAK, FINKISH) were chosen out of different neurons and tested for conjugation efficiency on Trastuzumab with method 1 (described in section 11.1.3). All of them are N- and C- terminally acylated and amidated, respectively.

11.2.3. Generating of the self organizing map (SOM)

The experimental data from the screening (Figure 12) was used to compute a self-organizing map (SOM). A threshold of >60% conjugation efficiency was set defining the group of “positive” peptides, whereas every peptide below 60% efficiency is rated as “negative” (42 sequences, 17 negative and 25 positive). The experimental results have been done with a mixture of N-terminal acylated and C-terminal amidated peptides, as well as with some non-protected variants (7 out of 42). The algorithm could only be fed with the non-protected version of these sequences. The SOM was trained for 10'000 iterations using Molmap. The visualization (Figure 25) was done using SomVIS^[151]. The sequences were described using the pepCATS^[152] and PPCAL^[152] descriptor as implemented in the modIAMP package^[173] with a cross correlation distance of three. The SOM is a two dimensional toroidal representation of the 633 dimensional input space. The neurons are colored accordingly to the sequences they contain. Red neurons contain peptides which conjugated above the 60% threshold. Blue ones contain “negative” sequences only. White neurons got no sequences assigned, whereas some mixed neurons are shown in the corresponding blue/red mixture. The full list of sorted peptides can be found in Table A 5.

11.3. Chapter 6: Chemo-enzymatic functionalization of native antibodies with mono- and bifunctional peptide linkers and toxins

11.3.1. Materials

Linker NH₂-K(N₃)-CRAK-OH was purchased from LifeTein (New Jersey, USA) and the purity of >90% tested by HPLC from the supplier. Clickable toxin DBCO-PEG₄-Ahx-maytansine (DM1, SET0303) was purchased from Levena Biotech (San Diego, USA), dissolved in DMSO (Sigma-Aldrich, St. Louis, USA) as

5 mM stock concentration, and stored at -20 °C. Maleimide-NODAGA was purchased from Chematech (Dijon, France), and dissolved in DMSO as 25 mM stock, stored at -20 °C.

11.3.2. Synthesis of NODAGA-K(N₃)-RAK-NH₂

Manual solid-phase peptide synthesis for peptide NODAGA-K(N₃)-RAK-NH₂ was performed on low-loading 4-methyl benzhydrylamine (MBHA) Rink amide resin (0.30–0.40 mmol/g, 100-200 mesh) in fritted reaction vessels (10 mL for scale of 0.025 mmol). Following swelling in alternating DMF and DCM, the N-terminal Fmoc protecting group was removed by treatment with 20% piperidine in DMF (3 x 3 min, ambient temperature). Fmoc-protected amino acids (2 equiv.) were coupled to the deprotected N-terminus through activation by O-(7-Azabenzotriazol-1-yl)-*N,N,N',N'*-tetramethyluronium hexafluorophosphate (HATU, 1.9 equiv) and *N,N*-diisopropylethylamine (DIPEA, 5 equiv.) in DMF (1 h, ambient temperature). Fmoc deprotection and coupling were repeated until completion of the sequence. Cleavage and global deprotection were achieved by suspension of the resin in TFA/TIPS/Phenol/H₂O (92.5/2.5/2.5/2.5, 5 h, ambient temperature). After evaporation of TFA by a stream of nitrogen, peptides were precipitated using ice-cold diethyl ether. The crude peptide was washed twice by centrifugation, decanting of the supernatant and addition of fresh ice-cold diethyl ether. The resulting crude peptide was dried, dissolved in H₂O, and purified by reversed-phase high-performance liquid chromatography using a Phenomenex Jupiter Proteo 90 Å column (4 µm, 250 x 10 mm) with a gradient of 5-20% acetonitrile in H₂O (+0.1% TFA) at a flow of 4 mL/min.

11.3.3. Antibody conjugation and LC/MS analysis

Conjugations have been done according to 11.1.311.3.3. LC/MS analysis according to 11.1.6.

11.3.4. Click reactions with DBCO-moieties

Purified mAbs with azide-functionalized linkers were incubated with DBCO-PEG₄-Ahx-maytansine (emtansine derivative, 5 equivalents) in Trizma pH 7.6 for 14-18 h at room temperature. Complete toxin attachment was monitored by LC/MS analysis. Excess toxin was removed by five repeated centrifugation steps (2 min with 16k rcf, Centrifuge 5415 R, Eppendorf, Hamburg, Germany) in Amicon® Ultra 0.5mL Filters (50 kDa cut off, Sigma-Aldrich, St. Louis, USA) with PBS pH 7.4.

11.3.5. Conjugation reactions with maleimide-NODAGA

The purified mAb-linker conjugate was buffer exchanged into Bis-Tris pH 6.0 by Amicon® centrifugation, as previously described. 30 eq. DTT was added and the mixture (2-4 mg/mL) was incubated at 37 °C for 2 h before a PD10 (Merck, Kenilworth, United States, standard protocol) separation step. The conjugate was concentrated in 30 kDa cut-off Amicons (3x, to 2-5 mg/mL), supplied with 10 eq. (L)-dehydroascorbic acid (dhaa), and incubated for 2 h at 8 °C. Another Amicon step is used to rebuffer the conjugate into Trizma pH 7.6 (to 2-4 mg/mL), before adding 20 eq. maleimide-NODAGA. This step was made at room temperature until completion of conjugation (ca. 3 h at rt), monitored by LC-MS.

11.3.6. Labeling with ¹¹¹In

Radiolabeling was achieved with ¹¹¹In in HCl 0.02 N purchased from Curium (Le Petten, Netherlands). In a typical experiment, 20 µg mAb-linker or ADC, 4 mg/mL in PBS, was mixed 1:1 v/v with ammonium acetate buffer (0.5 M, pH 5.5), and left to react at 37 °C for 60 min with a chelator to ¹¹¹In ratio of 1:300. The labeling efficiency was tested by γ-HPLC on an Agilent Technologies 1200 Series (Santa Clara, United States) with a Gabi Star gamma detector (Raytest, Straubenhardt, Germany) and a MassPREP Phenyl Guard Column (1000 Å, 20 µm, 2.1 mm X 10 mm, Waters, Milford, United States) The applied gradient is shown in table 4. For animal experiments, 10:1 molar equivalents of EDTA (Sigma-Aldrich, St. Louis, United States)/ mAb was added to the final labeled solution.

Table 4 : HPLC gradient to test the labeling efficiency of the mAb-conjugates

Time [min]	Acetonitrile [%] + 0.1% TFA	Water [%] + 0.1% TFA	Flow [ml/min]
0	20	80	1
1	20	80	1
1.1	75	25	1
3	75	25	1
3.1	20	80	1
5	20	80	1

11.3.7. Cell culture

HER-2 expressing cell line Skov3-ip was kindly provided by P. Altevogt (German Cancer Research Center, Heidelberg, Germany) and maintained in RPMI 1640 media supplemented with 2 mM L-

glutamine, 10% FCS, 100 µg/mL streptomycin, 100 µg/mL penicillin, and 0.25 µg/mL fungizone (BioConcept, Allschwil, Switzerland) in a humidified chamber at 37 °C and 5% CO₂.

11.3.8. Flow cytometry assay

Cells were centrifuged at 1000g for 10 min, washed with 1x PBS and again centrifuged. The cells were resuspended in PBS containing 1% BSA (Amresco, Solon, United States). 100 µl of cell suspension containing 10⁶ cells were prepared in the wells of a 96-well plate, which was stored on ice. 5 µg of Trastuzumab or humanized IgG1 (isotype, LifeTechnologies, Carlsbad, United States) was applied to the control wells with the cells and incubated for 15 min, resuspended and repeated, while gentle shaking on ice. 1% BSA in PBS buffer was used to wash the cells, and resuspended in 100 µL of the same buffer. 100 µl of the suspension was transferred to the other wells and 5 µg of the Trastuzumab-dye conjugate was applied and preceded as above. Simultaneously, the control wells were treated with secondary goat anti-human IgG-FITC (1:75 dilution, Santa Cruz Biotechnology, United States). Flow-cytometry was done with Guava easyCyte Flow Cytometer (Merck, Kenilworth, United States) and data were analyzed with FlowJo software (TreeStar Inc, San Francisco, United States).

11.3.9. Lindmo assay

The Lindmo^[174] assay was performed with SKOV3-ip cells. Cells were detached in PBS containing 10 mM EDTA and diluted into groups of 4, 2, 1, 0.5, and 0.25 Mio/tube with an end volume of 0.5 mL in PBS + 1% BSA (Amresco, Solon, United States). One series was additionally supplied with 15 µg Trastuzumab per tube as control for non-specific binding. Each tube was provided with 50 µL ¹¹¹In labeled mAb-linker or ADC, giving 25'000 counts on a gamma counter. Using our standard labeling condition, this corresponds to approx. 200 ng ADC/L, or 1.3 nmol ADC/L. All the cells were incubated for 30 min at 37 °C at 230 rpm, before adding 2 mL ice-cold PBS + 1 % BSA. The tubes were centrifuged at 4 °C for 5 minutes at 1500 rpm, followed by removal of the supernatant. The washing step was repeated, before measuring the cells on a gamma counter and plotting the data in Excel.

11.4. Chapter 7: Trastuzumab biodistribution with linker $\text{NH}_2\text{-K}(\text{N}_3)\text{-CRAK-OH}$ and comparative biodistributions of $\text{NODAGA-K}(\text{N}_3)\text{-RAK-NH}_2$ with and without toxin

All animal experiments were made in compliance with the Swiss laws on animal protection. The cantonal committee on animal experiments approved the experiments and permission was given by the responsible cantonal authorities (Kanton Aargau, permission number: AG-75686). 6-week-old CD1-Foxn1 nu mice (Charles River, Sulzfeld, Germany) were inoculated with 5×10^6 Skov3-ip cells (in 100 μL PBS) subcutaneously into the right flank. Tumors grew for 12-16 days. The mice were randomly grouped into 3 mice per cohort, prior to injection. Each mouse was injected via the tail vein with 150 kBq ^{111}In labeled ADC (100 μL in PBS), which was 1.4 μg ADC in total, or 0.056 mg ADC/kg mouse, for the Trastuzumab- $\text{NH}_2\text{-K}(\text{maytansine})\text{-C}(\text{NODAGA})\text{RAK-OH}$ species. Additionally, this ADC sample was co-injected with different amounts of native Trastuzumab (no peptide attached, no chelator or drug attached), going from 0 mg addition, to 1.5 mg Ab/kg Mouse, 5 mg/kg, 15 mg/kg, and 30 mg/kg for different cohorts. The mice were kept with water and food *ad libitum*. For each of this subgroup, mice were sacrificed after 48 h and 96 h and the % injected radioactivity per gram organ (tumor, blood, liver, spleen, kidney, muscle, bone, heart, lung, pancreas, stomach, intestines) was measured on a Packard Cobra II Auto-Gamma counter (GMI, Ramsey, United States). For the second biodistribution, the randomized cohorts consisted of 4 animals per group. 150 kBq ^{111}In labeled ADC (100 μL in PBS) was injected via the tail vein. This corresponds to 3.8 μg , 3.7 μg , and 3.9 μg Trastuzumab- $\text{NODAGA-K}(\text{N}_3)\text{-RAK-NH}_2$, Trastuzumab- $\text{NODAGA-K}(\text{maytansine})\text{-RAK-NH}_2$, and d-Trastuzumab- $\text{NODAGA-K}(\text{maytansine})\text{-RAK-NH}_2$, respectively. For each of this group, mice were sacrificed after 24 h, 48 h, 72 h, and 96 h and the % injected radioactivity per gram organ (tumor, blood, liver, spleen, kidney, muscle, bone, heart, lung, pancreas, stomach, intestines) was measured on a Packard Cobra II Auto-Gamma counter. GraphPad Prism was used to perform statistical analysis (2-way ANOVA Bonferroni with $p \leq 0.05$).

11.4.1. Statistical analysis

All the statistics have been performed in Graphpad. An ANOVA 2-way analysis was made, with a Bonferroni's multiple comparisons test with an alpha or adjusted p-value of $* = p \leq 0.05$, $** = p \leq 0.01$, $*** = p \leq 0.001$, $**** = p \leq 0.0001$. For the analysis of tumor to blood/liver ratios, ratios of each single mouse were calculated first before comparing with each other.

11.5. *Chapter 8: Site-specific MTG mediated conjugation and SPECT of an EGFR-Nanobody with and without albumin binder*

11.5.1. *Enzymatic conjugation of 7d12 with VG49 and VG56*

1 mg/mL 7d12 in PBS was incubated for 30 min at 37 °C with 6 U MTG/mg 7d12 and 40 eq. Linker VG49 or VG56. All the reactions were blocked by 20 min incubation with 1 mM BTG-blocker (Zedira, Darmstadt, Germany) before separation of MTG. 7d12 concentrations were measured by a NanoPhotometer® P360 from Implen (Munich, Germany).

11.5.2. *Separation of 7d12-conjugate from MTG*

Separation of MTG was made by His-tag purification, as size exclusion with a Superdex 75 5/150 (GE Healthcare, Chicago, United States) did not separate the enzyme from the nanobody well enough. In brief (for 100 µg 7d12-conjugate): 30 µL Ni-NTA beads (Qiagen, Hilden, Germany) were washed with 70 µL 1x PBS (4x) in an Eppendorf tube. To separate beads from solvent, the tube was centrifuged for 1 min at 1000 rcf (Centrifuge 5415 R, Eppendorf, Hamburg, Germany), whereas the supernatant was pipetted off. After washing, our sample was added and incubated for 25 min at 8 °C. With further centrifugation steps, the sample was washed twice with 120 µL wash buffer (50 mM NaH₂PO₄, 300 mM NaCl, 20 mM imidazole (Sigma-Aldrich, St. Louis, United States)). Subsequently, the sample was incubated for 10 min at RT with 50 µL elution buffer (50 mM NaH₂PO₄, 300 mM NaCl, 250 mM imidazole). The supernatant with the eluted 7d12-Conjugate was then dialyzed in PBS with Slide-A-Lyzer™ MINI Dialysis Device, 10K MWCO, 0.1 mL tubes (ThermoFisher Scientific, Waltham, United States). Dialysis was made in two steps, first for 30 min in 200 mL PBS, and in a second step over-night in another 200 mL. To concentrate 7d12 in solution, Amicon tubes 10 kDa cut-off were used as previously described.

11.5.3. *ESI-TOF LC-MS analysis of 7d12-conjugates*

7.5 µL 7d12 samples (0.02 mg/mL) were injected into a Waters LTC Premier ESI-TOF mass spectrometer (Waters, Milford, USA) coupled with a Waters 2795 Alliance HT HPLC (Waters, Milford, USA) for separation. An Aeris™ 3.6 µm WIDEPORÉ XB-C18 100x21 mm column from Phenomenex (Torrance, USA) was used with the following gradient:

Table 5: HPLC gradient for 7d12 analysis

Time [min]	Acetonitrile [%]	Water [%]	2-Propanole [%]	Flow [ml/min]
0	10	90	0	0.4
2	10	90	0	0.4
8	70	30	0	0.4
10	100	0	0	0.4

Analysis and deconvolution was made with the software MassLynx 4.1 and the MaxEnt 1 algorithm (Waters, Milford, USA). Differences in peak intensity of the corresponding deconvoluted masses were used to calculate the conjugation efficiency.

11.5.4. Labeling with ^{111}In of 7d12-VG49 and 7d12-VG59

Radiolabeling was achieved with ^{111}In in HCl 0.02 N purchased from Curium (Le Petten, Netherlands). In a typical experiment, 15 μg 7d12-VG49/56, 0.5-1.5 mg/mL in PBS, was mixed 3:2 v/v with ammonium acetate buffer (0.5 M, pH 5.5), and was left to react at 37 °C for 60 min with a chelator to ^{111}In ratio of approx. 1:100. The labeling efficiency was tested by γ -HPLC on an Agilent Technologies 1200 Series (Santa Clara, United States) with a Gabi Star gamma detector (Raytest, Straubenhardt, Germany) and a Reprosil C18 column (200 Å, 3 μm , Dr. Maisch, Ammerbuch, Germany). The applied gradient is shown in table 6. For animal experiments, 10:1 molar equivalents of EDTA (Sigma-Aldrich, St. Louis, United States)/ 7d12 were added to the final labeled solution.

Table 6: HPLC gradient used to test labeling efficiencies of 7d12-conjugates

Time [min]	Acetonitrile [%] + 0.1% TFA	Water [%] + 0.1% TFA	Flow [ml/min]
0	5	95	1
10	80	20	1
10.1	95	5	1
12	95	5	1

11.5.5. Cell culture

EGFR expressing cell line A431 were purchased by the American Type Culture Collection (ATCC, Manassas, United States) and maintained in DMEM media supplemented with 2 mM L-glutamine, 10% FCS, 100 µg/mL streptomycin, 100 µg/mL penicillin, and 0.25 µg/mL fungizone (BioConcept, Allschwil, Switzerland) in a humidified chamber at 37 °C and 5% CO₂.

11.5.6. Lindmo assay

The Lindmo assays were performed as previously described in Chapter 11.3.9, with A431 cells and Cetuximab instead of Trastuzumab as blocking mAb.

11.5.7. SPECT imaging

All animal experiments were made in compliance with the Swiss laws on animal protection. The cantonal committee on animal experiments approved the experiments and permission was given by the responsible cantonal authorities (Kanton Aargau, permission number: AG-75686). 6-week-old CD1-Foxn1 nu mice (Charles River, Sulzfeld, Germany) were inoculated with 5×10^6 A431 cells (in 100 µl PBS) subcutaneously into the right flank. Tumors grew for 12-16 days. The mice were randomly grouped into 2 mice per cohort, prior to injection. Each mouse was injected via the tail vein with 5 MBq ¹¹¹In labeled 7d12-VG49 or 7d12-VG56 (100 µL in PBS). The labeling solution of both 7d12-species contained additionally non-conjugated 7d12, to reach an injection amount of 10 µg per mouse, resulting in 0.4 mg 7d12/kg mouse. The mice were kept with water and food *ad libitum* and images were taken 1 h, 4 h, 24 h, and 72 h post injection with a multi-pinhole NanoSPECT/CT^{plus} (Bioscan Inc., France, and Mediso, Hungary). An initial CT scan was acquired of 7.5 min (tube voltage 55 kV, tube current 145 µA) for all the time points. For 1 h, 4 h, and 24 h p.i., the SPECT time was 45 min, with a frame duration of 60 sec. For 72 h p.i, SPECT time was 1.5 h with a frame duration of 120 sec. During scanning, mice were kept under anesthesia with an isoflurane (1.5-2.5%) and oxygen mixture, and a constant airflow of 37 °C was applied. HiSPECT and VivoQuant Software was used to reconstruct and analyze the images. A Gauss-reconstruction filter was applied (full width at half max, 1 mm) and an adjusting scaling was made to visualize the organs (0.0001-0.0025 kBq/voxel, with a voxel size of 0.3 mm with the used apparatus ap008).

12. References

- [1] R. L. Siegel, K. D. Miller, A. Jemal, *CA. Cancer J. Clin.* **2020**, *70*, 7–30.
- [2] D. E. Milenic, E. D. Brady, M. W. Brechbiel, *Nat. Rev. Drug Discov.* **2004**, *3*, 488–498.
- [3] K. Strebhardt, A. Ullrich, *Nat. Rev. Cancer* **2008**, *8*, 473–480.
- [4] J. D. Scott, Andrew M; Allison, James P.; Wolchok, *Cancer Immun.* **2012**, *12*, 1–8.
- [5] Z. An, *Protein Cell* **2010**, *1*, 319–330.
- [6] H. Kaplon, M. Muralidharan, Z. Schneider, J. M. Reichert, *MAbs* **2020**, *12*, DOI 10.1080/19420862.2019.1703531.
- [7] G. Vidarsson, G. Dekkers, T. Rispens, *Front. Immunol.* **2014**, *5*, 1–17.
- [8] P. J. Carter, G. A. Lazar, *Nat. Rev. Drug Discov.* **2018**, *17*, 197–223.
- [9] A. R. Duncan, J. M. Woof, L. J. Partridge, D. R. Burton, G. Winter, *16. Johnson, K. A. A Rev. Biophys. biophys. Chem* **1980**, *86*, 125.
- [10] R. A. Clynes, T. L. Towers, L. G. Presta, J. V. Ravetch, *Nat. Med.* **2000**, *6*, 443–446.
- [11] P. Carter, **2001**, *1*, 118–129.
- [12] J. R. Desjarlais, G. A. Lazar, E. A. Zhukovsky, S. Y. Chu, *Drug Discov. Today* **2007**, *12*, 898–910.
- [13] L. M. Weiner, *Nat. Rev. Cancer* **2007**, *7*.
- [14] C. Rader, *Curr. Opin. Biotechnol.* **2020**, *65*, 9–16.
- [15] A. Thakur, M. Huang, L. G. Lum, *Blood Rev.* **2018**, *32*, 339–347.
- [16] M. Yasunaga, *Semin. Cancer Biol.* **2020**, *64*, 1–12.
- [17] D. Reusch, M. L. Tejada, *Glycobiology* **2015**, *25*, 1325–1334.
- [18] R. Jefferis, *Nat. Rev. Drug Discov.* **2009**, *8*, 226–234.
- [19] X. R. Jiang, A. Song, S. Bergelson, T. Arroll, B. Parekh, K. May, S. Chung, R. Strouse, A. Mire-Sluis, M. Schenerman, *Nat. Rev. Drug Discov.* **2011**, *10*, 101–110.
- [20] A. Okazaki, E. Shoji-Hosaka, K. Nakamura, M. Wakitani, K. Uchida, S. Kakita, K. Tsumoto, I. Kumagai, K. Shitara, *J. Mol. Biol.* **2004**, *336*, 1239–1249.
- [21] T. Shinkawa, K. Nakamura, N. Yamane, E. Shoji-Hosaka, Y. Kanda, M. Sakurada, K. Uchida, H. Anazawa, M. Satoh, M. Yamasaki, N. Hanai, K. Shitara, *J. Biol. Chem.* **2003**, *278*, 3466–3473.

- [22] X. Chen, D. Liu, G. C. Flynn, *Glycobiology* **2009**, *19*, 240–249.
- [23] T. A. Millward, M. Heitzmann, K. Bill, U. Längle, P. Schumacher, K. Forrer, *Biologicals* **2008**, *36*, 41–47.
- [24] Y. Kanda, T. Yamada, K. Mori, A. Okazaki, M. Inoue, K. Kitajima-Miyama, R. Kuni-Kamochi, R. Nakano, K. Yano, S. Kakita, K. Shitara, M. Satoh, *Glycobiology* **2007**, *17*, 104–118.
- [25] M. M. Newkirk, J. Novick, M. M. Stevenson, M. J. Fournier, P. Apostolakis, *Clin. Exp. Immunol.* **1996**, *106*, 259–264.
- [26] D. Vivier, S. K. Sharma, P. Adumeau, C. Rodriguez, K. Fung, B. M. Zeglis, *J. Nucl. Med.* **2019**, *60*, 1174–1182.
- [27] K. Zheng, C. Bantog, R. Bayer, *MAbs* **2011**, *3*, DOI 10.4161/mabs.3.6.17922.
- [28] P. M. Buck, S. Kumar, S. K. Singh, *MAbs* **2013**, *5*, 904–916.
- [29] D. Hristodorov, R. Fischer, H. Joerissen, B. Müller-Tiemann, H. Apeler, L. Linden, *Mol. Biotechnol.* **2013**, *53*, 326–335.
- [30] P. J. Carter, *Nat. Rev. Immunol.* **2006**, *6*, 343–357.
- [31] D. Schrama, R. A. Reisfeld, J. C. Becker, *Nat. Rev. Drug Discov.* **2006**, *5*, 147–159.
- [32] R. V. J. Chari, M. L. Miller, W. C. Widdison, *Angew. Chemie - Int. Ed.* **2014**, *53*, 3796–3827.
- [33] C. M. Walko, H. J. West, *JAMA Oncol.* **2019**, *5*, 1648.
- [34] P. Zhao, Y. Zhang, W. Li, C. Jeanty, G. Xiang, Y. Dong, *Acta Pharm. Sin. B* **2020**, *10*, 1589–1600.
- [35] N. Joubert, C. Denevault-Sabourin, F. Bryden, M. C. Viaud-Massuard, *Eur. J. Med. Chem.* **2017**, *142*, 393–415.
- [36] A. G. Poison, J. Calemme-Fenaux, P. Chan, W. Chang, E. Christensen, S. Clark, F. J. De Sauvage, D. Eaton, K. Elkins, J. Michael Elliott, G. Frantz, R. N. Fujii, A. Gray, K. Harden, G. S. Ingle, N. M. Kljavin, H. Koeppen, C. Nelson, S. Prabhu, H. Raab, S. Ross, J. P. Stephan, S. J. Scales, S. D. Spencer, R. Vandlen, B. Wranik, S. F. Yu, B. Zheng, A. Ebens, *Cancer Res.* **2009**, *69*, 2358–2364.
- [37] R. Gébleux, M. Stringhini, R. Casanova, A. Soltermann, D. Neri, *Int. J. Cancer* **2017**, *140*, 1670–1679.
- [38] P. D. Senter, E. L. Sievers, *Nat. Biotechnol.* **2012**, *30*, 631–637.
- [39] A. Younes, A. K. Gopal, S. E. Smith, S. M. Ansell, J. D. Rosenblatt, K. J. Savage, R. Ramchandren, N. L. Bartlett, B. D. Cheson, S. De Vos, A. Forero-Torres, C. H. Moskowitz, J. M. Connors, A.

- Engert, E. K. Larsen, D. A. Kennedy, E. L. Sievers, R. Chen, *J. Clin. Oncol.* **2012**, *30*, 2183–2189.
- [40] B. Pro, R. Advani, P. Brice, N. L. Bartlett, J. D. Rosenblatt, T. Illidge, J. Matous, R. Ramchandren, M. Fanale, J. M. Connors, Y. Yang, E. L. Sievers, D. A. Kennedy, A. Shustov, *J. Clin. Oncol.* **2012**, *30*, 2190–2196.
- [41] R. M. Sharkey, D. M. Goldenberg, **2009**, *60*, 1407–1420.
- [42] S. Verma, D. Miles, L. Gianni, I. E. Krop, M. Welslau, J. Baselga, M. Pegram, D. Y. Oh, V. Diéras, E. Guardino, L. Fang, M. W. Lu, S. Olsen, K. Blackwell, *N. Engl. J. Med.* **2012**, *367*, 1783–1791.
- [43] J. M. Lambert, R. V. J. Chari, *J. Med. Chem.* **2014**, *57*, 6949–6964.
- [44] D. Vivier, S. K. Sharma, B. M. Zeglis, *J. Label. Comp Radiopharm.* **2018**, *61*, 672–692.
- [45] F. Kraeber-Bodéré, C. Bodet-Milin, C. Rousseau, T. Eugène, A. Pallardy, E. Frampas, T. Carlier, L. Ferrer, J. Gaschet, F. Davodeau, J. F. Gestin, A. Faivre-Chauvet, J. Barbet, M. Chérel, *Semin. Oncol.* **2014**, *41*, 613–622.
- [46] S. J. Denardo, L. A. Kroger, G. L. Denardo, *Curr. Opin. Immunol.* **1999**, *11*, 563–569.
- [47] A. J. Davies, *Oncogene* **2007**, *26*, 3614–3628.
- [48] A. L. Lakes, D. D. An, S. S. Gauny, C. Ansoberlo, B. H. Liang, J. A. Rees, K. D. Mcknight, H. Karsunky, R. J. Abergel, **2020**, DOI 10.1021/acs.molpharmaceut.0c00703.
- [49] S. S. Rinne, C. D. Leitao, B. Mitran, T. Z. Bass, K. G. Andersson, V. Tolmachev, S. Ståhl, J. Löfblom, A. Orlova, *Sci. Rep.* **2019**, *9*, 1–11.
- [50] O. O. Peltek, A. R. Muslimov, M. V. Zyuzin, A. S. Timin, *J. Nanobiotechnology* **2019**, *17*, 1–34.
- [51] J. Puttemans, Y. Dekempeneer, J. L. Eersels, H. Hanssens, P. Debie, M. Keyaerts, A. D. Windhorst, F. Van Der Aa, Q. Lecocq, K. Breckpot, A. Morgenstern, F. Bruchertseifer, T. Lahoutte, N. Devoogdt, M. D’Huyvetter, *Cancers (Basel)*. **2020**, *12*, DOI 10.3390/cancers12041017.
- [52] A. M. Wu, P. D. Senter, *Nat. Biotechnol.* **2005**, *23*, 1137–1146.
- [53] A. Beck, L. Goetsch, C. Dumontet, N. Corvaia, *Nat. Publ. Gr.* **2017**, *16*, 315–337.
- [54] E. Wagner-Rousset, M. C. Janin-Bussat, O. Colas, M. Excoffier, D. Ayoub, J. F. Haeuw, I. Rilatt, M. Perez, N. Corvaia, A. Beck, *MAbs* **2014**, *6*, 173–184.
- [55] M. Lopus, E. Oroudjev, L. Wilson, S. Wilhelm, W. Widdison, R. Chari, M. A. Jordan, *Mol. Cancer Ther.* **2010**, *9*, 2689–2699.
- [56] R. V. Kolakowski, T. D. Young, P. W. Howard, S. C. Jeffrey, P. D. Senter, *Tetrahedron Lett.* **2015**,

56, 4512–4515.

- [57] B. Shor, H. P. Gerber, P. Sapra, *Mol. Immunol.* **2015**, *67*, 107–116.
- [58] T. J. Lindell, F. Weinberg, P. W. Morris, R. G. Roeder, W. J. Rutter, *Science (80-.)*. **1970**, *170*, 447–449.
- [59] S. Coats, M. Williams, B. Kebble, R. Dixit, L. Tseng, N. S. Yao, D. A. Tice, J. C. Soria, *Clin. Cancer Res.* **2019**, *25*, 5441–5448.
- [60] G. Casi, D. Neri, *J. Med. Chem.* **2015**, *58*, 8751–8761.
- [61] R. K. Jain, *Cancer Res.* **1990**, *50*.
- [62] K. Fujimori, D. G. Covell, J. E. Fletcher, J. N. Weinstein, *J. Nucl. Med.* **1990**, *31*, 1191–1198.
- [63] M. Juweid, R. Neumann, C. Paik, M. J. Perez-pacete, J. Sato, W. van Osdol, J. N. Weinstein, *Cancer Res.* **1992**, *52*, 5144–5153.
- [64] A. W. Tolcher, *Ann. Oncol. Off. J. Eur. Soc. Med. Oncol.* **2016**, *27*, 2168–2172.
- [65] I. B. Fuchs, S. Landt, H. Bueler, U. Kuehl, S. Coupland, A. Kleine-Tebbe, W. Lichtenegger, G. Schaller, *Breast Cancer Res. Treat.* **2003**, *82*, 23–28.
- [66] P. K. Mahalingaiah, R. Ciurlionis, K. R. Durbin, R. L. Yeager, B. K. Philip, B. Bawa, S. R. Mantena, B. P. Enright, M. J. Liguori, T. R. Van Vleet, *Pharmacol. Ther.* **2019**, *200*, 110–125.
- [67] M. R. Junttila, W. Mao, X. Wang, B. E. Wang, T. Pham, J. Flygare, S. F. Yu, S. Yee, D. Goldenberg, C. Fields, J. Eastham-Anderson, M. Singh, R. Vij, J. A. Hongo, R. Firestein, M. Schutten, K. Flagella, P. Polakis, A. G. Polson, *Sci. Transl. Med.* **2015**, *7*, 1–12.
- [68] L. Liu, *Protein Cell* **2018**, *9*, 15–32.
- [69] J. Poisson, S. Lemoine, C. Boulanger, F. Durand, R. Moreau, D. Valla, P. E. Rautou, *J. Hepatol.* **2017**, *66*, 212–227.
- [70] M. J. Birrer, K. N. Moore, I. Betella, R. C. Bates, *J. Natl. Cancer Inst.* **2019**, *111*, 538–549.
- [71] H. Donaghy, *MAbs* **2016**, *8*, 659–671.
- [72] P. M. Drake, D. Rabuka, *BioDrugs* **2017**, *31*, 521–531.
- [73] H. Zhao, S. Gulesserian, S. K. Ganesan, J. Ou, K. Morrison, Z. Zeng, V. Robles, J. Snyder, L. Do, H. Aviña, S. Karki, D. R. Stover, F. Doñate, *Mol. Cancer Ther.* **2017**, *16*, 1877–1886.
- [74] Z. Liu, T. Ma, H. Liu, Z. Jin, X. Sun, H. Zhao, J. Shi, B. Jia, F. Li, F. Wang, *Mol. Pharm.* **2014**, *11*, 800–807.

- [75] B. E. C. G. de Goeij, J. M. Lambert, *Curr. Opin. Immunol.* **2016**, *40*, 14–23.
- [76] I. E. Krop, M. Beeram, S. Modi, S. F. Jones, S. N. Holden, W. Yu, S. Girish, J. Tibbitts, J. H. Yi, M. X. Sliwkowski, F. Jacobson, S. G. Lutzker, H. A. Burris, *J. Clin. Oncol.* **2010**, *28*, 2698–2704.
- [77] R. Dere, J. H. Yi, C. Lei, O. M. Saad, C. Huang, Y. Li, J. Baudys, S. Kaur, *Bioanalysis* **2013**, *5*, 1025–1040.
- [78] X. Yang, Z. Pan, M. R. Choudhury, Z. Yuan, A. Anifowose, B. Yu, W. Wang, B. Wang, *Med. Res. Rev.* **2020**, 2682–2713.
- [79] P. Strop, S. Liu, M. Dorywalska, K. Delaria, R. G. Dushin, T. Tran, W. Ho, S. Farias, M. G. Casas, Y. Abdiche, D. Zhou, R. Chandrasekaran, C. Samain, C. Loo, A. Rossi, M. Rickert, S. Krimm, T. Wong, S. M. Chin, J. Yu, J. Dilley, J. Chaparro-riggers, G. F. Filzen, C. J. O. Donnell, F. Wang, J. S. Myers, J. Pons, D. L. Shelton, A. Rajpal, *Chem. Biol.* **2013**, *20*, 161–167.
- [80] P. Agarwal, C. R. Bertozzi, *Bioconjug. Chem.* **2015**, *26*, 176–192.
- [81] F. Lhospice, D. Brégeon, C. Belmant, P. Dennler, A. Chiotellis, E. Fischer, L. Gauthier, A. Boëdec, H. Rispaud, S. Savard-Chambard, A. Represa, N. Schneider, C. Paturel, M. Sapet, C. Delcambre, S. Ingoure, N. Viaud, C. Bonnafous, R. Schibli, F. Romagné, *Mol. Pharm.* **2015**, *12*, 1863–1871.
- [82] J. R. Junutula, H. Raab, S. Clark, S. Bhakta, D. D. Leipold, S. Weir, Y. Chen, M. Simpson, S. P. Tsai, M. S. Dennis, Y. Lu, Y. G. Meng, C. Ng, J. Yang, C. C. Lee, E. Duenas, J. Gorrell, V. Katta, A. Kim, K. Mcdorman, K. Flagella, R. Venook, S. Ross, S. D. Spencer, W. L. Wong, H. B. Lowman, R. Vandlen, M. X. Sliwkowski, R. H. Scheller, P. Polakis, W. Mallet, **2008**, *26*, 925–932.
- [83] K. Tsuchikama, *Z. An, Protein Cell* **2018**, *9*, 33–46.
- [84] P. Dennler, E. Fischer, R. Schibli, *Antibodies* **2015**, *4*, 197–224.
- [85] L. Wang, G. Amphlett, W. A. Blättler, J. M. Lambert, W. Zhang, *Protein Sci.* **2005**, *14*, 2436–2446.
- [86] M. M. C. Sun, K. S. Beam, C. G. Cerveny, K. J. Hamblett, R. S. Blackmore, M. Y. Torgov, F. G. M. Handley, N. C. Ihle, P. D. Senter, S. C. Alley, *Bioconjug. Chem.* **2005**, *16*, 1282–1290.
- [87] S. C. Alley, D. R. Benjamin, S. C. Jeffrey, N. M. Okeley, D. L. Meyer, R. J. Sanderson, P. D. Senter, *Bioconjug. Chem.* **2008**, *19*, 759–765.
- [88] J. P. M. Nunes, V. Vassileva, E. Robinson, M. Morais, M. E. B. Smith, R. B. Pedley, S. Caddick, J. R. Baker, V. Chudasama, *RSC Adv.* **2017**, *7*, 24828–24832.
- [89] L. Wangt, Z. Zhang, A. Brock, P. G. Schultz, *Proc. Natl. Acad. Sci. U. S. A.* **2003**, *100*, 56–61.
- [90] J. Y. Axup, K. M. Bajjuri, M. Ritland, B. M. Hutchins, C. H. Kim, S. A. Kazane, R. Halder, J. S.

- Forsyth, A. F. Santidrian, K. Stafin, Y. Lu, H. Tran, A. J. Seller, S. L. Biroc, A. Szydlak, J. K. Pinkstaff, F. Tian, S. C. Sinha, B. Felding-Habermann, V. V. Smider, P. G. Schultz, *Proc. Natl. Acad. Sci. U. S. A.* **2012**, *109*, 16101–16106.
- [91] E. S. Zimmerman, T. H. Heibeck, A. Gill, X. Li, C. J. Murray, M. R. Madlansacay, C. Tran, N. T. Uter, G. Yin, P. J. Rivers, A. Y. Yam, W. D. Wang, A. R. Steiner, S. U. Bajad, K. Penta, W. Yang, T. J. Hallam, C. D. Thanos, A. K. Sato, *Bioconjug. Chem.* **2014**, *25*, 351–361.
- [92] L. Johansson, C. Chen, J. O. Thorell, A. Fredriksson, S. Stone-Elander, G. Gafvelin, E. S. J. Arner, *Nat. Methods* **2004**, *1*, 61–66.
- [93] T. Hofer, J. D. Thomas, T. R. Burke, C. Rader, *Proc. Natl. Acad. Sci. U. S. A.* **2008**, *105*, 12451–12456.
- [94] J. Z. Hui, A. Al Zaki, Z. Cheng, V. Popik, H. Zhang, E. T. Luning Prak, A. Tsourkas, *Small* **2014**, *10*, 3354–3363.
- [95] B. H. Chung, Y. Jung, J. M. Lee, J. W. Kim, J. Yoon, H. Cho, *Anal. Chem.* **2009**, *81*, 936–942.
- [96] G. Dormán, G. D. Prestwich, *Trends Biotechnol.* **2000**, *18*, 64–77.
- [97] M. D. Witte, J. J. Cragolini, S. K. Dougan, N. C. Yoder, M. W. Popp, H. L. Ploegh, *Proc. Natl. Acad. Sci. U. S. A.* **2012**, *109*, 11993–11998.
- [98] M. W. L. Popp, J. M. Antos, H. L. Ploegh, *Curr. Protoc. Protein Sci.* **2009**, DOI 10.1002/0471140864.ps1503s56.
- [99] R. R. Beerli, T. Hell, A. S. Merkel, U. Grawunder, *PLoS One* **2015**, *10*, 1–17.
- [100] Q. Zhou, J. E. Stefano, C. Manning, J. Kyazike, B. Chen, D. A. Gianolio, A. Park, M. Busch, J. Bird, X. Zheng, H. Simonds-Mannes, J. Kim, R. C. Gregory, R. J. Miller, W. H. Brondyk, P. K. Dhal, C. Q. Pan, *Bioconjug. Chem.* **2014**, *25*, 510–520.
- [101] R. Van Geel, M. A. Wijdeven, R. Heesbeen, J. M. M. Verkade, A. A. Wasiel, S. S. Van Berkel, F. L. Van Delft, *Bioconjug. Chem.* **2015**, *26*, 2233–2242.
- [102] I. S. Carrico, B. L. Carlson, C. R. Bertozzi, *Nat. Chem. Biol.* **2007**, *3*, 321–322.
- [103] P. M. Drake, A. E. Albers, J. Baker, S. Banas, R. M. Barfield, A. S. Bhat, G. W. De Hart, A. W. Garofalo, P. Holder, L. C. Jones, R. Kudirka, J. McFarland, W. Zmolek, D. Rabuka, *Bioconjug. Chem.* **2014**, *25*, 1331–1341.
- [104] V. Siegmund, B. Piater, B. Zakeri, T. Eichhorn, F. Fischer, C. Deutsch, S. Becker, L. Toleikis, B. Hock, U. A. K. Betz, H. Kolmar, *Sci. Rep.* **2016**, *6*, 1–9.

- [105] H. Ando, M. Adachi, K. Umeda, A. Matsuura, M. Nonaka, R. Uchio, H. Tanaka, M. Motoki, *Agric. Biol. Chem.* **1989**, *53*, 2613–2617.
- [106] L. Lorand, R. M. Graham, *Nat. Rev. Mol. Cell Biol.* **2003**, *4*, 140–156.
- [107] H. Sato, E. Hayashi, N. Yamada, M. Yatagai, Y. Takahara, *Bioconjug. Chem.* **2001**, *12*, 701–710.
- [108] T. Kashiwagi, K. ichi Yokoyama, K. Ishikawa, K. Ono, D. Ejima, H. Matsui, E. ichiro Suzuki, *J. Biol. Chem.* **2002**, *277*, 44252–44260.
- [109] A. Heil, J. Ohsam, C. Büchold, R. Pasternack, K. Yokoyama, Y. Kumazawa, M. Hils, *J. Cereal Sci.* **2016**, *70*, 47–56.
- [110] N. M. Rachel, J. N. Pelletier, *Biomolecules* **2013**, *3*, 870–888.
- [111] S. K. Chan, T. S. Lim, *Appl. Microbiol. Biotechnol.* **2019**, *103*, 2973–2984.
- [112] S. Jeger, *Thesis* **2009**.
- [113] T. Ohtsuka, M. Ota, N. Nio, M. Motoki, *Biosci. Biotechnol. Biochem.* **2000**, *64*, 2608–2613.
- [114] M. Malešević, A. Migge, T. C. Hertel, M. Pietzsch, *ChemBioChem* **2015**, *16*, 1169–1174.
- [115] Y. Sugimura, K. Yokoyama, N. Nio, M. Maki, K. Hitomi, *Arch. Biochem. Biophys.* **2008**, *477*, 379–383.
- [116] A. Fontana, B. Spolaore, A. Mero, F. M. Veronese, *Adv. Drug Deliv. Rev.* **2008**, *60*, 13–28.
- [117] B. Spolaore, S. Raboni, A. Ramos Molina, A. Satwekar, N. Damiano, A. Fontana, *Biochemistry* **2012**, *51*, 8679–8689.
- [118] X. Zhao, A. C. Shaw, J. Wang, C. C. Chang, J. Deng, J. Su, *J. Biomol. Screen.* **2010**, *15*, 206–212.
- [119] M. T. Gundersen, J. W. Keillor, J. N. Pelletier, *Appl. Microbiol. Biotechnol.* **2014**, *98*, 219–230.
- [120] P. Dennler, A. Chiotellis, E. Fischer, D. Brégeon, C. Belmant, L. Gauthier, F. Lhospice, F. Romagne, R. Schibli, *Bioconjug. Chem.* **2014**, *25*, 569–578.
- [121] S. Jeger, K. Zimmermann, A. Blanc, J. Grünberg, M. Honer, P. Hunziker, H. Struthers, R. Schibli, *Angew. Chemie - Int. Ed.* **2010**, *49*, 9995–9997.
- [122] F. Lhospice, D. Brégeon, C. Belmant, P. Dennler, A. Chiotellis, E. Fischer, L. Gauthier, A. Bozec, H. Rispaud, S. Savard-Chambard, A. Represa, N. Schneider, C. Paturel, M. Sapet, C. Delcambre, S. Ingoure, N. Viaud, C. Bonnafous, R. Schibli, F. Romagnon, *Mol. Pharm.* **2015**, *12*, 1863–1871.
- [123] P. Dennler, L. K. Bailey, P. R. Spycher, R. Schibli, E. Fischer, *ChemBioChem* **2015**, *16*, 861–867.

- [124] V. Siegmund, S. Schmelz, S. Dickgiesser, J. Beck, A. Ebenig, H. Fittler, H. Frauendorf, B. Piater, U. A. K. Betz, O. Avrutina, A. Scrima, H. L. Fuchsbauer, H. Kolmar, *Angew. Chemie - Int. Ed.* **2015**, *54*, 13420–13424.
- [125] J. L. Spidel, B. Vaessen, E. F. Albone, X. Cheng, A. Verdi, J. B. Kline, **2017**, DOI 10.1021/acs.bioconjchem.7b00439.
- [126] S. Dickgiesser, M. Rieker, D. Mueller-Pompalla, C. Schröter, J. Tonillo, S. Warszawski, S. Raab-Westphal, S. Kühn, T. Knehans, D. Könnig, J. Dotterweich, U. A. K. Betz, J. Anderl, S. Hecht, N. Rasche, *Bioconj. Chem.* **2020**, acs.bioconjchem.0c00061.
- [127] A. Maruani, D. A. Richards, V. Chudasama, *Org. Biomol. Chem.* **2016**, *14*, 6165–6178.
- [128] J. M. Antos, G. L. Chew, C. P. Guimaraes, N. C. Yoder, G. M. Grotenbreg, M. W. L. Popp, H. L. Ploegh, *J. Am. Chem. Soc.* **2009**, *131*, 10800–10801.
- [129] R. Jiang, L. Wang, J. Weingart, X. L. Sun, *ChemBioChem* **2014**, *15*, 42–46.
- [130] M. Mühlberg, M. G. Hoesl, C. Kuehne, J. Dervede, N. Budisa, C. P. R. Hackenberger, *Beilstein J. Org. Chem.* **2015**, *11*, 784–791.
- [131] M. Simon, U. Zangemeister-Wittke, A. Plückthun, *Bioconj. Chem.* **2012**, *23*, 279–286.
- [132] S. Puthenveetil, S. Musto, F. Loganzo, L. N. Tumeay, C. J. O'Donnell, E. Graziani, *Bioconj. Chem.* **2016**, *27*, 1030–1039.
- [133] V. Ratner, E. Kahana, M. Eichler, E. Haas, *Bioconj. Chem.* **2002**, *13*, 1163–1170.
- [134] P. Moody, V. Chudasama, R. I. Nathani, A. Maruani, S. Martin, M. E. B. Smith, S. Caddick, *Chem. Commun.* **2014**, *50*, 4898–4900.
- [135] R. I. Nathani, P. Moody, V. Chudasama, M. E. B. Smith, R. J. Fitzmaurice, S. Caddick, *Chem. Sci.* **2013**, *4*, 3455–3458.
- [136] M. D. Lee, W. Y. Tong, T. Nebl, L. A. Pearce, T. M. Pham, A. Golbaz-Hagh, S. Puttick, S. Rose, T. E. Adams, C. C. Williams, *Bioconj. Chem.* **2019**, *30*, 2539–2543.
- [137] A. M. Butz, *Physiol. Behav.* **2017**, *176*, 139–148.
- [138] R. Cohen, D. J. Vugts, G. W. M. Visser, M. Stigter-Van Walsum, M. Bolijn, M. Spiga, P. Lazzari, E. Shankar, M. Sani, M. Zanda, G. A. M. S. Van Dongen, *Cancer Res.* **2014**, *74*, 5700–5710.
- [139] E. W. Price, B. M. Zeglis, J. F. Cawthray, C. F. Ramogida, N. Ramos, J. S. Lewis, M. J. Adam, C. Orvig, *J. Am. Chem. Soc.* **2013**, *135*, 12707–12721.
- [140] S. Jeger, K. Zimmermann, A. Blanc, J. Grønberg, M. Honer, P. Hunziker, H. Struthers, R. Schibli,

Angew. Chemie - Int. Ed. **2010**, *49*, 9995–9997.

- [141] F. Higel, A. Seidl, F. Sörgel, W. Friess, *Eur. J. Pharm. Biopharm.* **2016**, *100*, 94–100.
- [142] J. Stadlmann, M. Pabst, D. Kolarich, R. Kunert, F. Altmann, *Proteomics* **2008**, *8*, 2858–2871.
- [143] D. Fiebig, S. Schmelz, S. Zindel, V. Ehret, J. Beck, A. Ebenig, M. Ehret, S. Fröls, F. Pfeifer, H. Kolmar, H. L. Fuchsbauer, A. Scrima, *J. Biol. Chem.* **2016**, *291*, 20417–20426.
- [144] T. Ohtsuka, Y. Umezawa, N. Nio, K. Kubota, *J. Food Sci.* **2001**, *66*, 25–29.
- [145] D. S. Avila, R. L. Puntel, M. Aschner, *Interrelations between Essential Metal Ions and Human Diseases*, **2013**.
- [146] U. Tagami, N. Shimba, M. Nakamura, K. I. Yokoyama, E. I. Suzuki, T. Hirokawa, *Protein Eng. Des. Sel.* **2009**, *22*, 747–752.
- [147] C. Marculescu, A. Lakshminarayanan, J. Gault, J. C. Knight, L. K. Folkes, T. Spink, C. V. Robinson, K. Vallis, B. G. Davis, B. Cornelissen, *Chem. Commun.* **2019**, *55*, 11342–11345.
- [148] T. Kohonen, *Biol. Cybern.* **1982**, *43*, 59–69.
- [149] J. Zupan, J. Gasteiger, **1999**.
- [150] G. Schneider, P. Schneider, *Expert Opin. Drug Discov.* **2017**, *12*, 271–277.
- [151] G. Schneider, M. Hartenfeller, M. Reutlinger, Y. Tanrikulu, E. Proschak, P. Schneider, *Trends Biotechnol.* **2009**, *27*, 18–26.
- [152] C. P. Koch, A. M. Perna, M. Pillong, N. K. Todoroff, P. Wrede, G. Folkers, J. A. Hiss, G. Schneider, *PLoS Comput. Biol.* **2013**, *9*, 1–9.
- [153] G. Schneider, P. Schneider, *Navigation in Chemical Space: Ligand-Based Design of Focused Compound Libraries*, **2005**.
- [154] R. Wada, M. Matsui, N. Kawasaki, *MAbs* **2019**, *11*, 350–372.
- [155] N. Reddy, G. L. Ong, T. M. Behr, R. M. Sharkey, D. M. Goldenberg, M. J. Mattes, *Cancer Immunol. Immunother.* **1998**, *46*, 25–33.
- [156] A. P. Singh, L. Guo, A. Verma, G. G. L. Wong, G. M. Thurber, D. K. Shah, *AAPS J.* **2020**, *22*, 1–13.
- [157] C. A. Boswell, E. E. Mundo, C. Zhang, S. L. Stainton, S. F. Yu, J. A. Lacap, W. Mao, K. R. Kozak, A. Fourie, P. Polakis, L. A. Khawli, K. Lin, *J. Nucl. Med.* **2012**, *53*, 1454–1461.
- [158] C. Tsé, A. S. Gauchez, W. Jacot, P. J. Lamy, *Cancer Treat. Rev.* **2012**, *38*, 133–142.
- [159] D. Vivier, K. Fung, C. Rodriguez, P. Adumeau, G. A. Ulaner, J. S. Lewis, S. K. Sharma, B. M. Zeglis,

Theranostics **2020**, *10*, 1746–1757.

- [160] J. D. Twomey, N. N. Brahme, B. Zhang, *Drug Resist. Updat.* **2017**, *30*, 48–62.
- [161] K. Liffers, K. Lamszus, A. Schulte, *Stem Cells Int.* **2015**, *2015*, DOI 10.1155/2015/427518.
- [162] M. Ranson, S. Wardell, *J. Clin. Pharm. Ther.* **2004**, *29*, 95–103.
- [163] F. Cappuzzo, T. Ciuleanu, L. Stelmakh, S. Cicenias, A. Szczésna, E. Juhász, E. Esteban, O. Molinier, W. Brugger, I. Melezínek, G. Klingelschmitt, B. Klughammer, G. Giaccone, *Lancet Oncol.* **2010**, *11*, 521–529.
- [164] J. C. Soria, E. Felip, M. Cobo, S. Lu, K. Syrigos, K. H. Lee, E. Göker, V. Georgoulas, W. Li, D. Isla, S. Z. Guclu, A. Morabito, Y. J. Min, A. Ardizzoni, S. M. Gadgeel, B. Wang, V. K. Chand, G. D. Goss, *Lancet Oncol.* **2015**, *16*, 897–907.
- [165] M. Fukuoka, Y. L. Wu, S. Thongprasert, P. Sunpaweravong, S. S. Leong, V. Sriuranpong, T. Y. Chao, K. Nakagawa, D. T. Chu, N. Saijo, E. L. Duffield, Y. Rukazenkov, G. Speake, H. Jiang, A. A. Armour, K. F. To, J. C. H. Yang, T. S. K. Mok, *J. Clin. Oncol.* **2011**, *29*, 2866–2874.
- [166] D. A. E. Cross, S. E. Ashton, S. Ghiorghiu, C. Eberlein, C. A. Nebhan, P. J. Spitzler, J. P. Orme, M. R. V. Finlay, R. A. Ward, M. J. Mellor, G. Hughes, A. Rahi, V. N. Jacobs, M. R. Brewer, E. Ichihara, J. Sun, H. Jin, P. Ballard, K. Al-Kadhimi, R. Rowlinson, T. Klinowska, G. H. P. Richmond, M. Cantarini, D. W. Kim, M. R. Ranson, W. Pao, *Cancer Discov.* **2014**, *4*, 1046–1061.
- [167] S. Muyldermans, M. Lauwereys, *J. Mol. Recognit.* **1999**, *12*, 131–140.
- [168] V. Cortez-Retamozo, N. Backmann, P. D. Senter, U. Wernery, P. De Baetselier, S. Muyldermans, H. Revets, *Cancer Res.* **2004**, *64*, 2853–2857.
- [169] S. Steeland, R. E. Vandenbroucke, C. Libert, *Drug Discov. Today* **2016**, *21*, 1076–1113.
- [170] C. E. Dumelin, S. Trüssel, F. Buller, E. Trachsel, F. Bootz, Y. Zhang, L. Mannocci, S. C. Beck, M. Drumea-Mirancea, M. W. Seeliger, C. Baltés, T. Müggler, F. Kranz, M. Rudin, S. Melkko, J. Scheuermann, D. Neri, *Angew. Chemie - Int. Ed.* **2008**, *47*, 3196–3201.
- [171] M. Benešová, C. A. Umbricht, R. Schibli, C. Müller, *Mol. Pharm.* **2018**, *15*, 934–946.
- [172] J. Grünberg, K. Knogler, R. Waibel, I. Novak-Hofer, *Biotechniques* **2003**, *34*, 968–972.
- [173] A. T. Müller, G. Gabernet, J. A. Hiss, G. Schneider, *Bioinformatics* **2017**, *33*, 2753–2755.
- [174] T. Lindmo, E. Boven, F. Cuttitta, J. Fedorko, P. A. Bunn, *J. Immunol. Methods* **1984**, *72*, 77–89.

13. Annex

13.1. Chapter 4: MTG mediated Conjugation of primary amine containing peptides to Q295

13.1.1. LC-MS conjugation analysis of synthesized peptides

Table A 1: LC-MS conjugation efficiency results of the listed peptides with Trastuzumab. Standard conjugation conditions were used. Top are the most efficient peptides listed whereas at the bottom the least sufficient ones are shown.

Sequence (N-terminal acetylated and C-terminal amidated)	Mass [Da]	Conjugation efficiency [%]					Average [%]	Standard error [%]	
RAK	414.5	94.1	94.9	94.2		94.4	0.4		
RAAK	485.6	93.3	94.9	93.7		94.0	0.7		
RAKNA	599.7	92.1	93	90.3		91.8	1.1		
RGKGR	613.7	94	91.5	88.9	92	90	89.3	91.0	1.8
RHK	480.6	91.5	92.4	89			91.0	1.4	
SAKAS	503.4	89	90.8	90.6			90.1	0.8	
RKAA	485.6	92.7	88.5	88.2			89.8	2.1	
KAR	414.5	87.6	92.2	85.5			88.4	2.8	
HAKAH	603.7	87.7	91.1	86.5			88.4	1.9	
RKR	499.6	84.7	88	89.7			87.5	2.1	
KYR	506.6	87.5	87.3	86.7			87.2	0.3	
RAKAR	641.8	90.4	85.6	78.9	88.1	90.8	87	86.8	4.0
RSKSR	673.8	89.4	86.1	84.7			86.7	2.0	
RARAK	641.8	88.6	82	85.3			85.3	2.7	
RYK	506.6	76.5	85.3	70.8			77.5	6.0	
ARKRA	641.8	82.2	76.4	73.9	74.6	73.8	79.3	76.7	3.1
RAKA	485.6	85.4	69.9	72.8			76.0	6.7	
DRKRD	729.8	74.2	75.8	67.9			72.6	3.4	
RAAKR	641.8	80.3	59.3	74.6			71.4	8.9	
KHR	480.6	69.8	68.5	67.3			68.5	1.0	
DAKAR	600.7	70.4	69.7	63.4			67.8	3.1	
RRK	499.6	72.3	54.6	71.5			66.1	8.2	
RYKYR	826	70.1	62	62.3			64.8	3.7	
KYRYR	826	68.9	60.7	58.7			62.8	4.4	
KRR	499.6	51	67.5	67.1			61.9	7.7	

KRAAR	641.8	55.3	57.4	56.5	56.4	0.9
DAKA	444.5	51.5	48.8	49.1	49.8	1.2
KRAA	485.6	55.9	49.9	41.7	49.2	5.8
KDAA	444.5	47.1	51.9	44.1	47.7	3.2
RRYRK	826	27.8	25.2	25	26.0	1.3
HEALKNHY (no N/C- protection)	1011.1	24.1	26.4		25.3	1.2
DDK	417.4	13.4	12.1	9	11.5	1.8
RDKDR	729.8	10.2	8.2	9.5	9.3	0.8
EAKAE	587.6	0	0	0	0.0	0.0
DAKAD	559.6	0	0	0	0.0	0.0
KDD	417.4	0	0	0	0.0	0.0
FKETAA (no N/C- protection)	665.7	0	0		0.0	0.0
KADDD (no N/C- protection)	562.5	0	0		0.0	0.0
NKALPAP (no N/C- protection)	709.8	0	0		0.0	0.0
DDKAY (no N/C- protection)	610.6	0	0		0.0	0.0
AKETAA (no N/C- protection)	589.7	0	0		0.0	0.0
KDAVA (no N/C- protection)	502.6	0	0		0.0	0.0

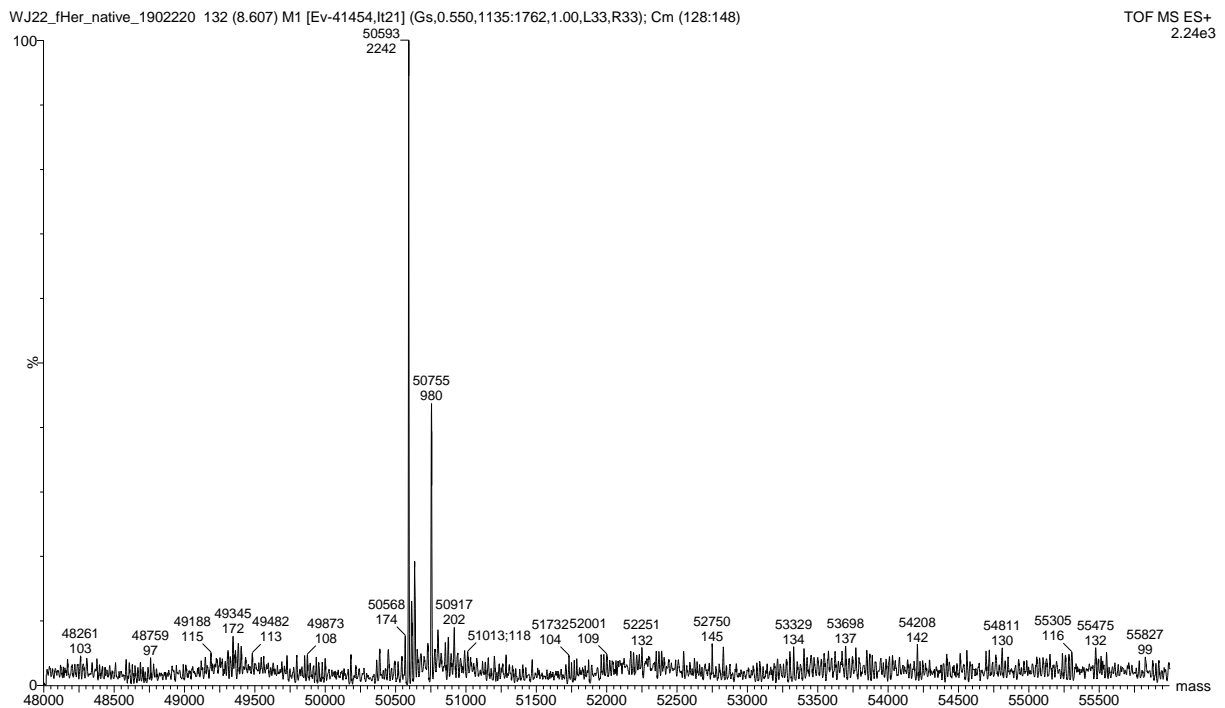


Figure A 1: Deconvoluted mass spectra of the native Trastuzumab heavy chain. The two peaks at 50593 Da and 50755 Da correspond to two different glycosylations.

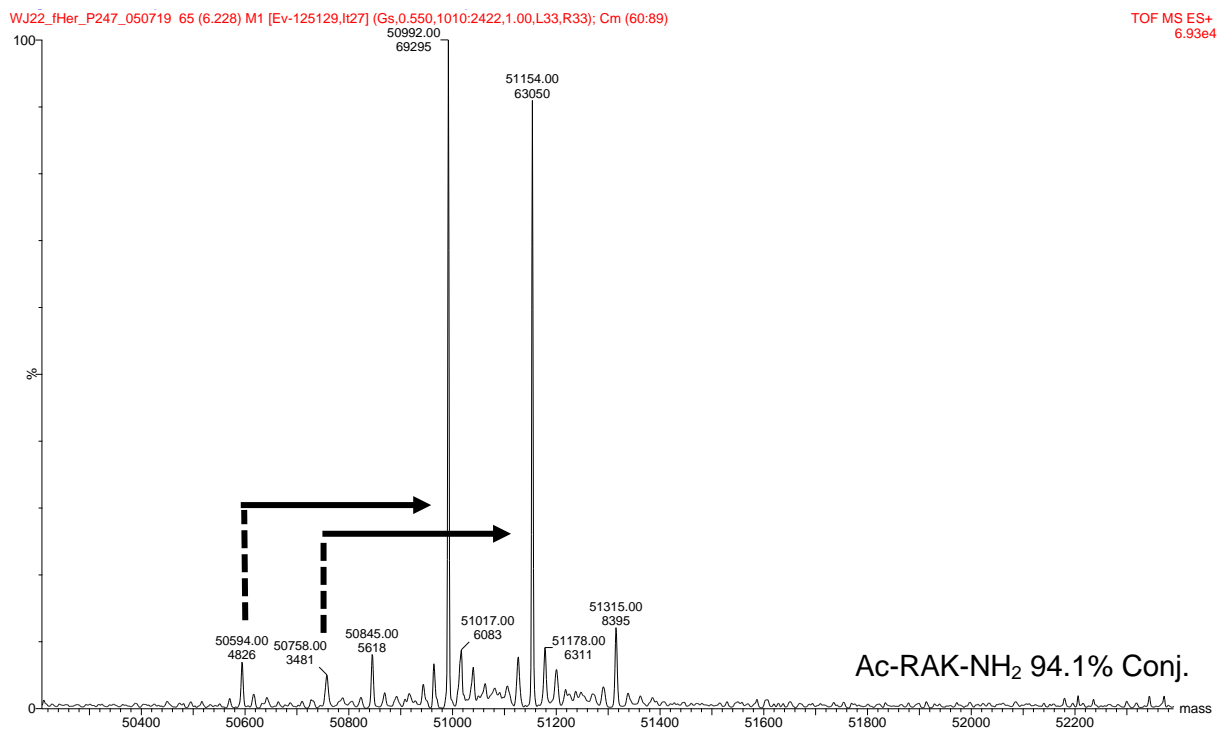


Figure A 2: Selected deconvoluted mass spectrum of mAb heavy chains after conjugation of peptide Ac-RAK-NH₂ (MW: 414.5 Da) with Trastuzumab using method 1. The two peaks at 50594 Da and 50758 Da correspond to two different glycosylations of native Trastuzumab. Calculated conjugated HC's: 50992 Da and 51156 Da; Detected conjugated HC's: 50992 Da and 51154 Da. The conjugation efficiency, calculated from the intensity, is 94.1%.

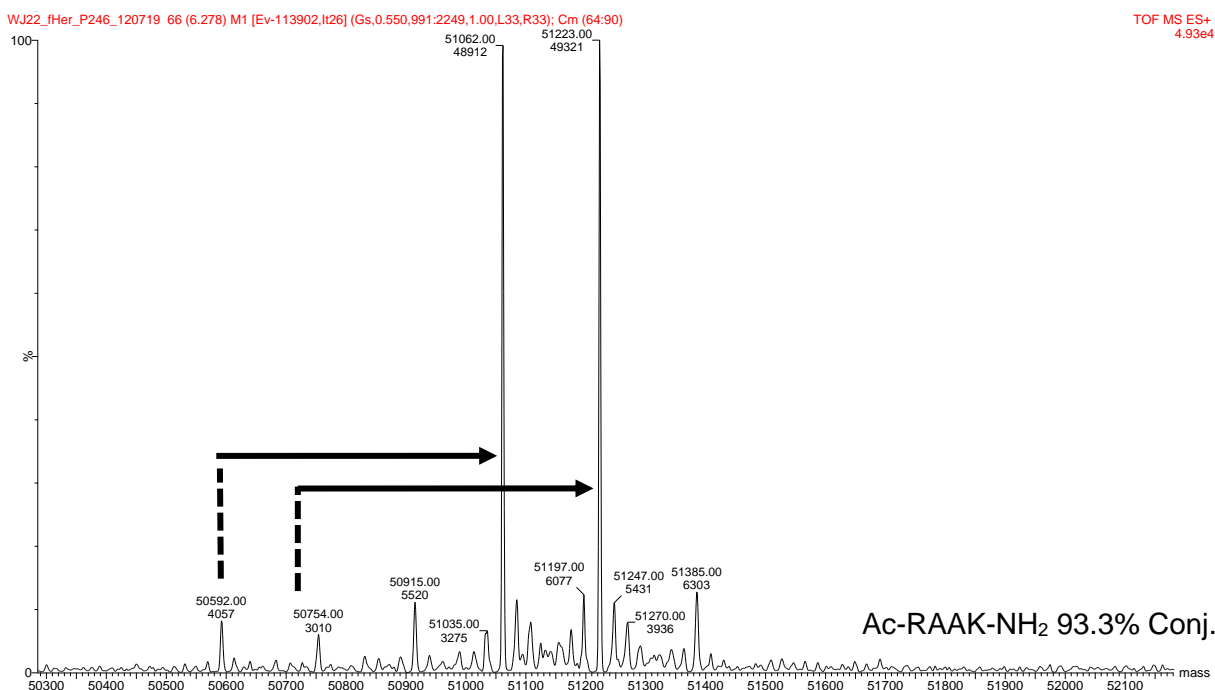


Figure A 3: Selected deconvoluted mass spectrum of mAb heavy chains after conjugation of peptide Ac-RAAK-NH₂ (MW: 485.6 Da) with Trastuzumab using method 1. The two peaks at 50592 Da and 50754 Da correspond to two different glycosylations of native Trastuzumab. Calculated conjugated HC's: 51061 Da and 51223 Da; Detected conjugated HC's: 51062 Da and 51223 Da. The conjugation efficiency, calculated from the intensity, is 93.3%.

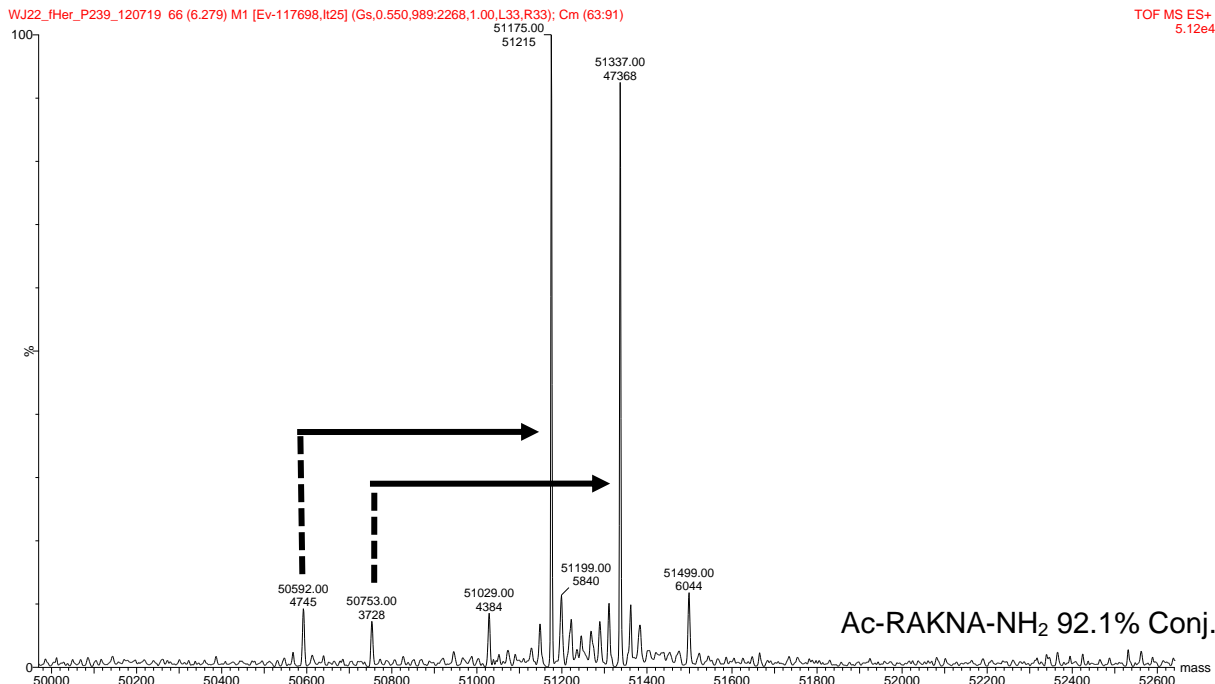


Figure A 4: Selected deconvoluted mass spectrum of mAb heavy chains after conjugation of peptide Ac-RAKNA-NH₂ (MW: 599.7 Da) with Trastuzumab using method 1. The two peaks at 50592 Da and 50753 Da correspond to two different glycosylations of native Trastuzumab. Calculated conjugated HC's: 51175 Da and 51336 Da; Detected conjugated HC's: 51175 Da and 51337 Da. The conjugation efficiency, calculated from the intensity, is 92.1%.

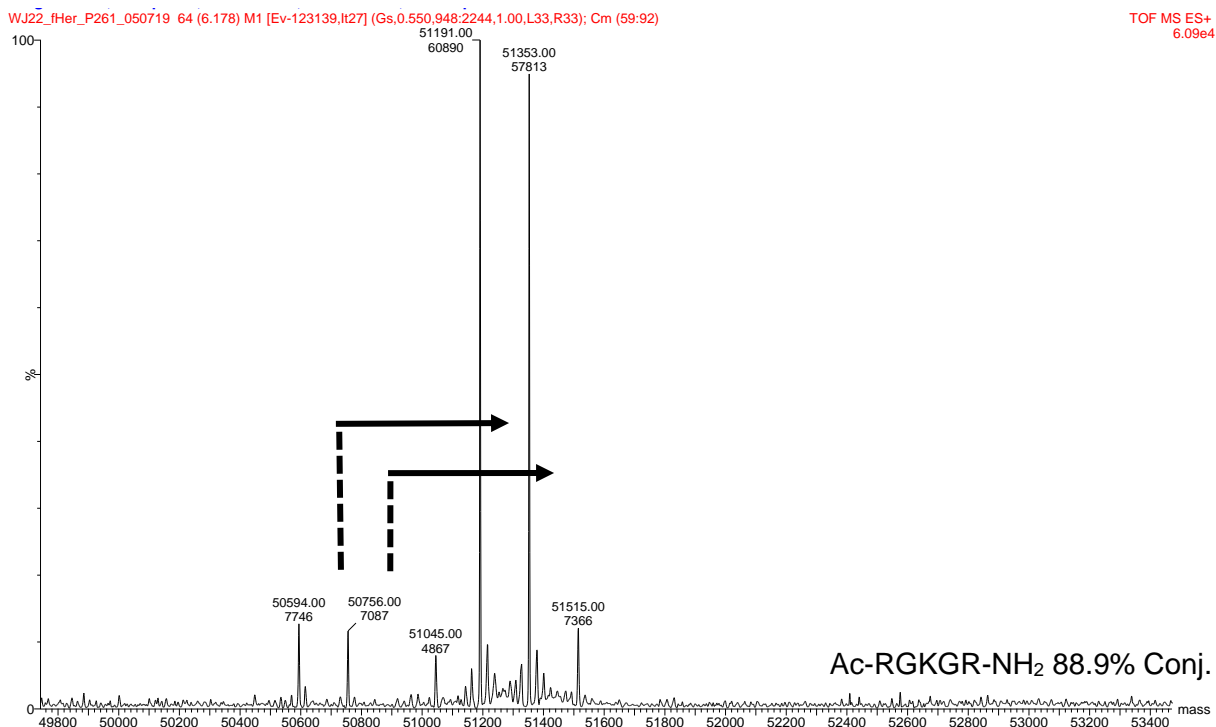


Figure A 5: Selected deconvoluted mass spectrum of mAb heavy chains after conjugation of peptide Ac-RGKGR-NH₂ (MW: 613.7 Da) with Trastuzumab using method 1. The two peaks at 50594 Da and 50756 Da correspond to two different glycosylations of native Trastuzumab. Calculated conjugated HC's: 51191 Da and 51353 Da; Detected conjugated HC's: 51191 Da and 51353 Da. The conjugation efficiency, calculated from the intensity, is 88.9%.

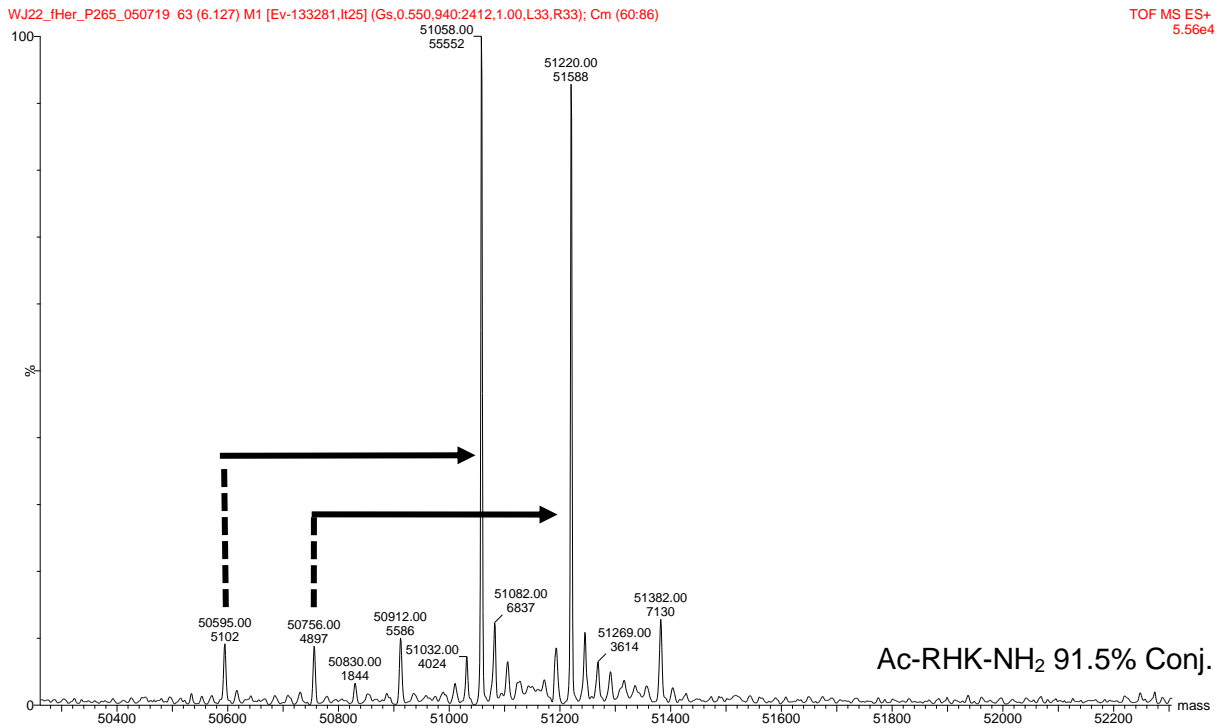


Figure A 6: Selected deconvoluted mass spectrum of mAb heavy chains after conjugation of peptide Ac-RHK-NH₂ (MW: 480.6 Da) with Trastuzumab using method 1. The two peaks at 50595 Da and 50756 Da correspond to two different glycosylations of native Trastuzumab. Calculated conjugated HC's: 51191 Da and 51353 Da; Detected conjugated HC's: 51058 Da and 51220 Da. The conjugation efficiency, calculated from the intensity, is 91.5%.

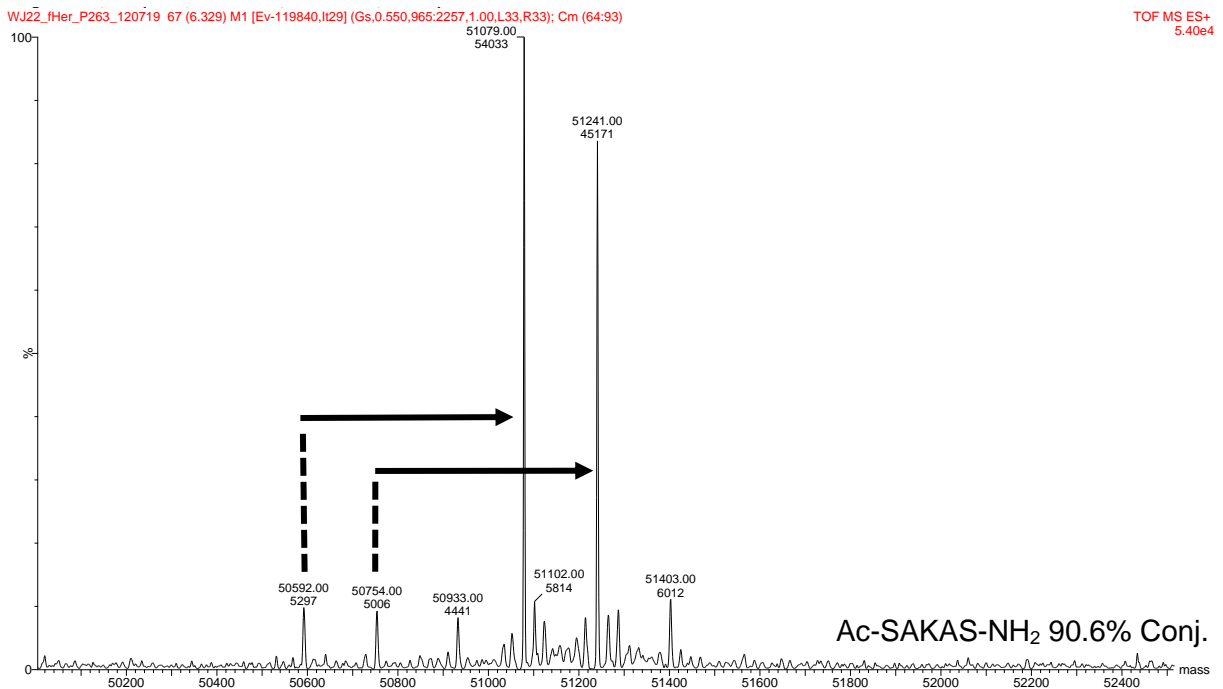


Figure A 7: Selected deconvoluted mass spectrum of mAb heavy chains after conjugation of peptide Ac-SAKAS-NH₂ (MW: 503.4 Da) with Trastuzumab using method 1. The two peaks at 50592 Da and 50754 Da correspond to two different glycosylations

of native Trastuzumab. Calculated conjugated HC's: 51078 Da and 51240 Da; Detected conjugated HC's: 51079 Da and 51241 Da. The conjugation efficiency, calculated from the intensity, is 90.6%.

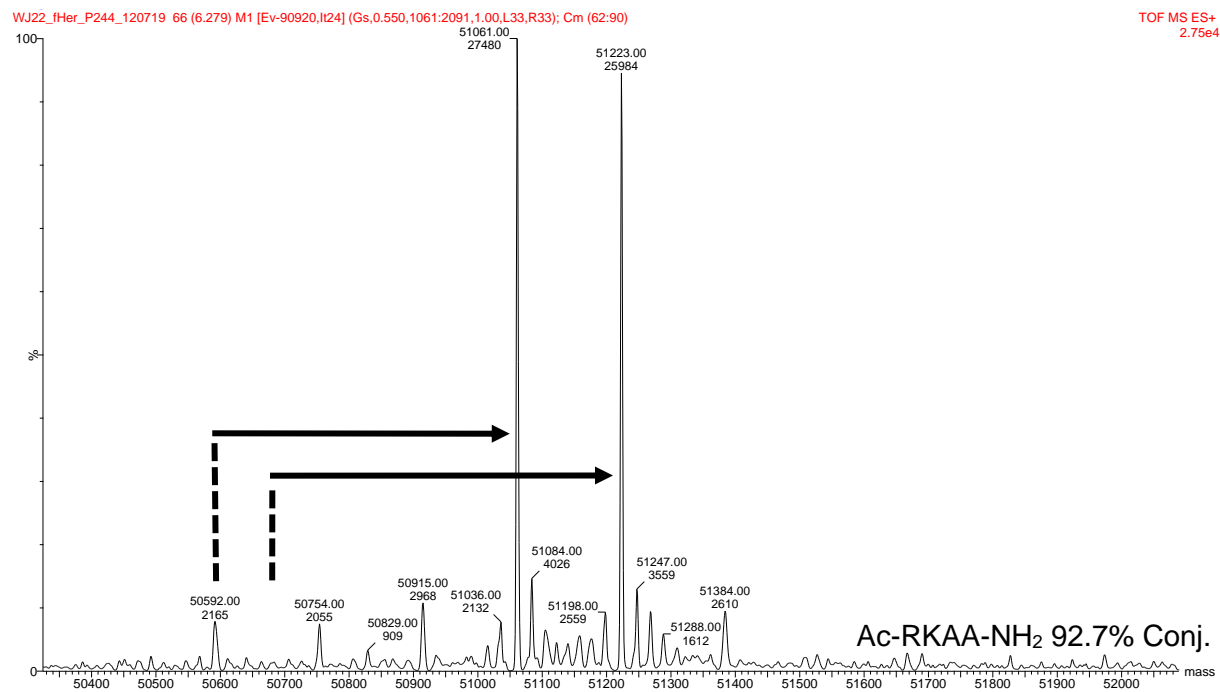


Figure A 8: Selected deconvoluted mass spectrum of mAb heavy chains after conjugation of peptide Ac-RKAA-NH₂ (MW: 485.6 Da) with Trastuzumab using method 1. The two peaks at 50592 Da and 50754 Da correspond to two different glycosylations of native Trastuzumab. Calculated conjugated HC's: 51061 Da and 51223 Da; Detected conjugated HC's: 51061 Da and 51223 Da. The conjugation efficiency, calculated from the intensity, is 92.7%.

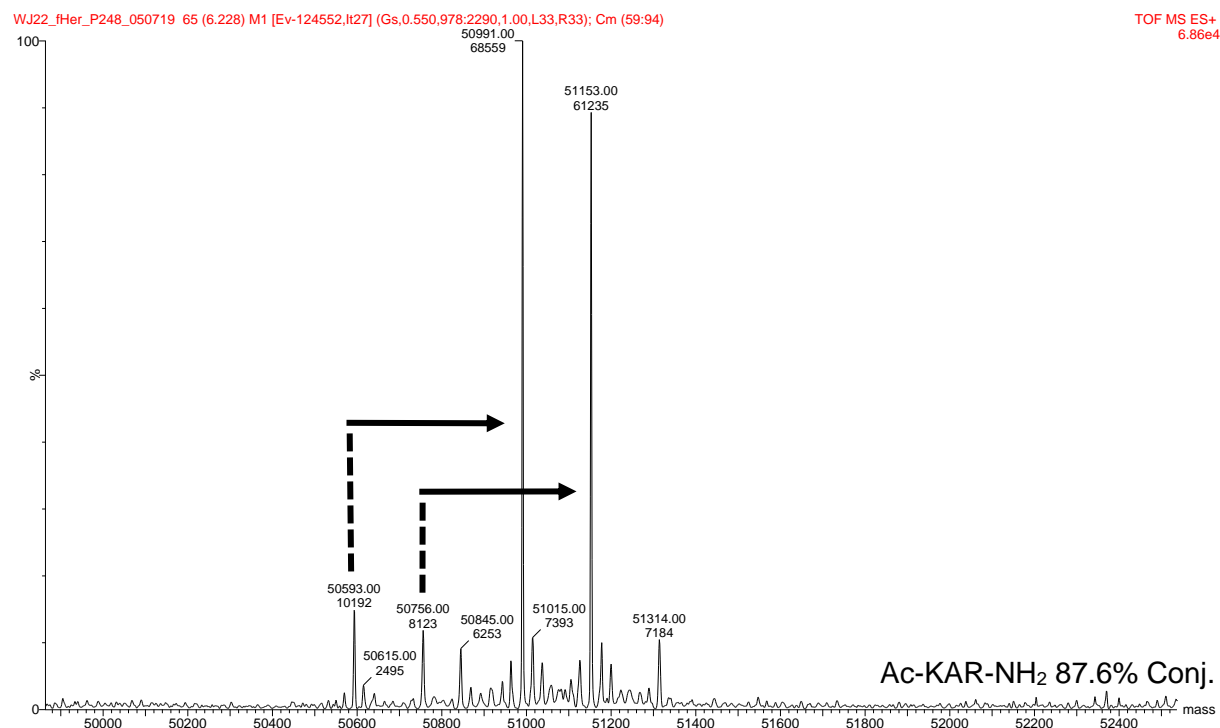


Figure A 9: Selected deconvoluted mass spectrum of mAb heavy chains after conjugation of peptide Ac-KAR-NH₂ (MW: 414.5 Da) with Trastuzumab using method 1. The two peaks at 50593 Da and 50756 Da correspond to two different glycosylations of native Trastuzumab. Calculated conjugated HC's: 50991 Da and 51154 Da; Detected conjugated HC's: 50991 Da and 51153 Da. The conjugation efficiency, calculated from the intensity, is 87.6%.

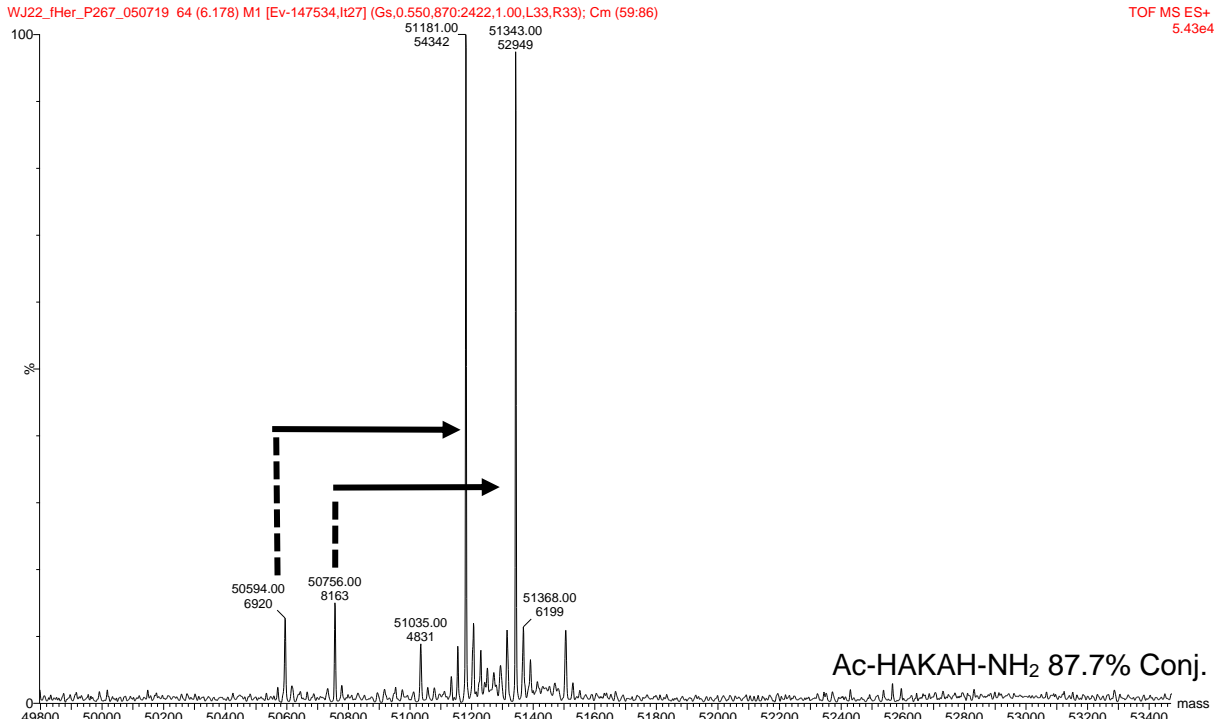


Figure A 10: Selected deconvoluted mass spectrum of mAb heavy chains after conjugation of peptide Ac-HAKAH-NH₂ (MW: 603.7 Da) with Trastuzumab using method 1. The two peaks at 50594 Da and 50756 Da correspond to two different glycosylations of native Trastuzumab. Calculated conjugated HC's: 51181 Da and 51343 Da; Detected conjugated HC's: 51181 Da and 51343 Da. The conjugation efficiency, calculated from the intensity, is 87.7%.

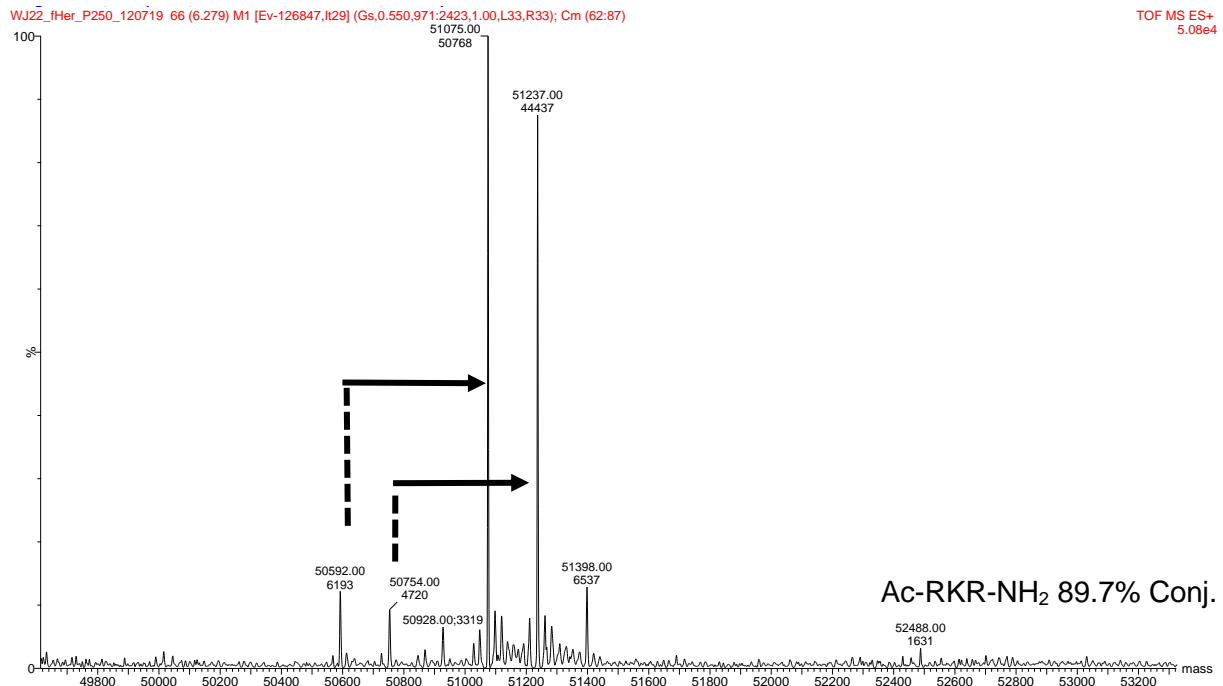


Figure A 11: Selected deconvoluted mass spectrum of mAb heavy chains after conjugation of peptide Ac-RKR-NH₂ (MW: 499.6 Da) with Trastuzumab using method 1. The two peaks at 50592 Da and 50754 Da correspond to two different glycosylations of native Trastuzumab. Calculated conjugated HC's: 51075 Da and 51237 Da; Detected conjugated HC's: 51075 Da and 51237 Da. The conjugation efficiency, calculated from the intensity, is 89.7%.

WJ22_fHer_P259_120719 66 (6.278) M1 [Ev-116773.lt29] (Gs,0.550,938:2170,1.00,L33,R33); Cm (64:91)

TOF MS ES+
5.37e4

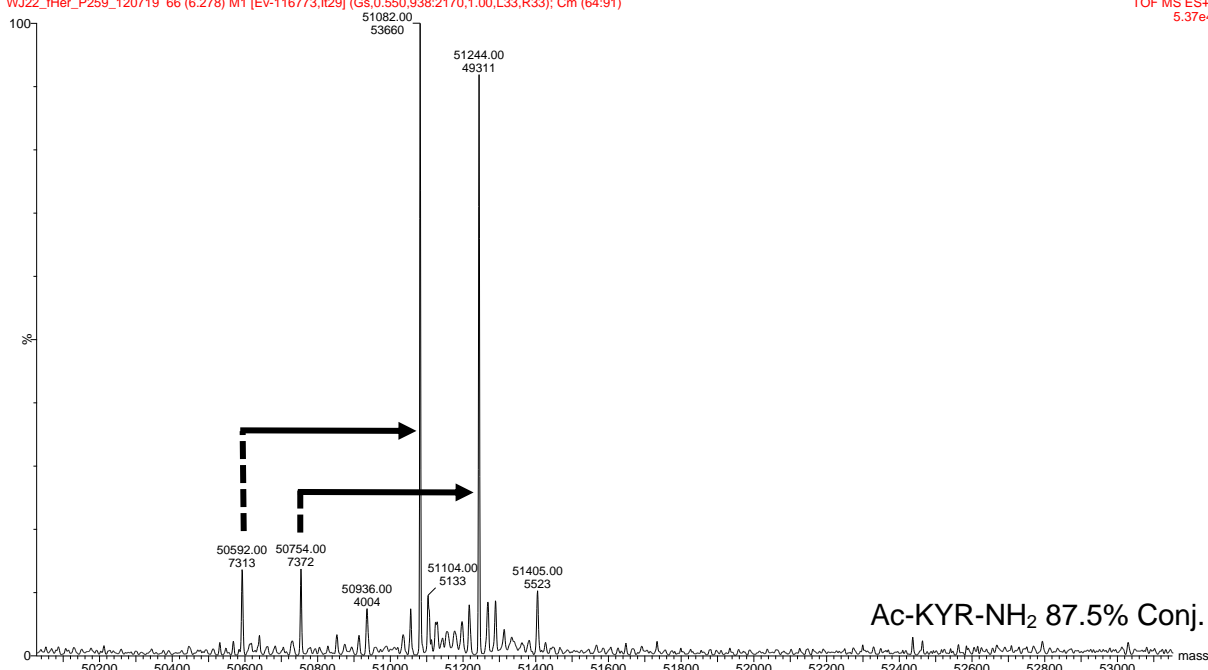


Figure A 12: Selected deconvoluted mass spectrum of mAb heavy chains after conjugation of peptide Ac-KYR-NH₂ (MW: 506.6 Da) with Trastuzumab using method 1. The two peaks at 50592 Da and 50754 Da correspond to two different glycosylations of native Trastuzumab. Calculated conjugated HC's: 51082 Da and 51244 Da; Detected conjugated HC's: 51082 Da and 51244 Da. The conjugation efficiency, calculated from the intensity, is 87.5%.

WJ22_fHer_P23_050719 64 (6.178) M1 [Ev-90160.lt24] (Gs,0.550,1074:2198,1.00,L33,R33); Cm (62:80)

TOF MS ES+
2.89e4

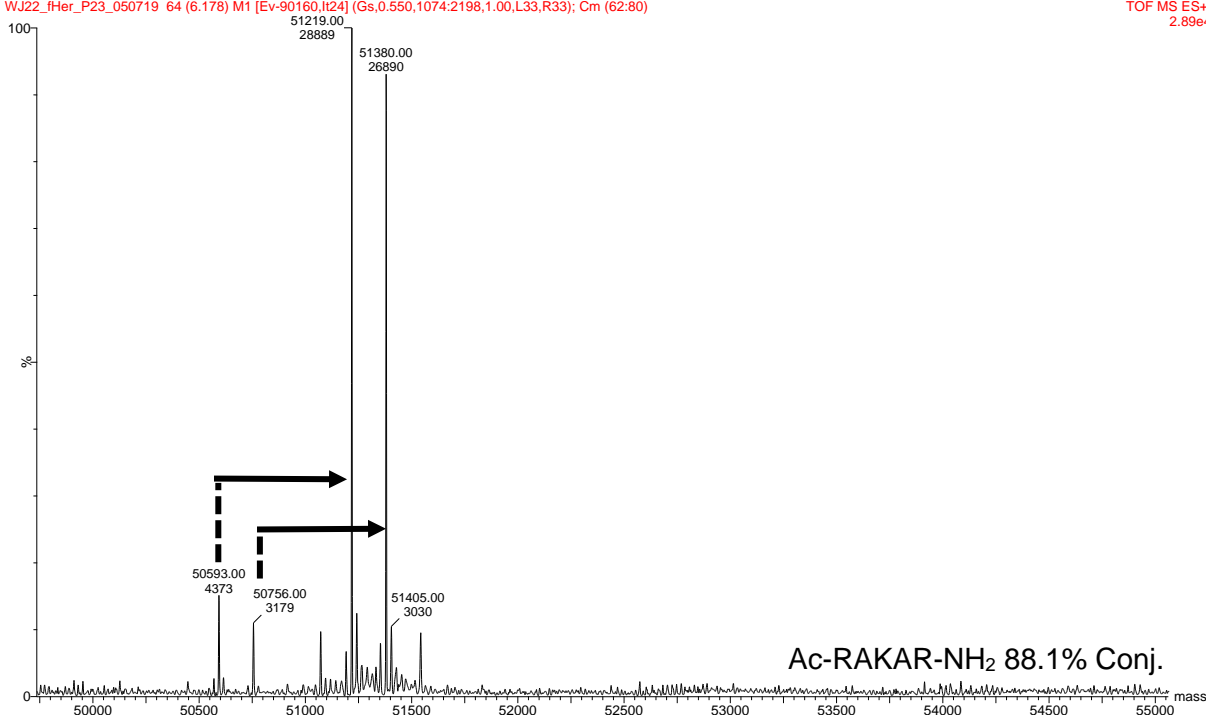


Figure A 13: Selected deconvoluted mass spectrum of mAb heavy chains after conjugation of peptide Ac-RAKAR-NH₂ (MW: 641.8 Da) with Trastuzumab using method 1. The two peaks at 50593 Da and 50756 Da correspond to two different glycosylations of native Trastuzumab. Calculated conjugated HC's: 51218 Da and 51381 Da; Detected conjugated HC's: 51219 Da and 51380 Da. The conjugation efficiency, calculated from the intensity, is 88.1%.

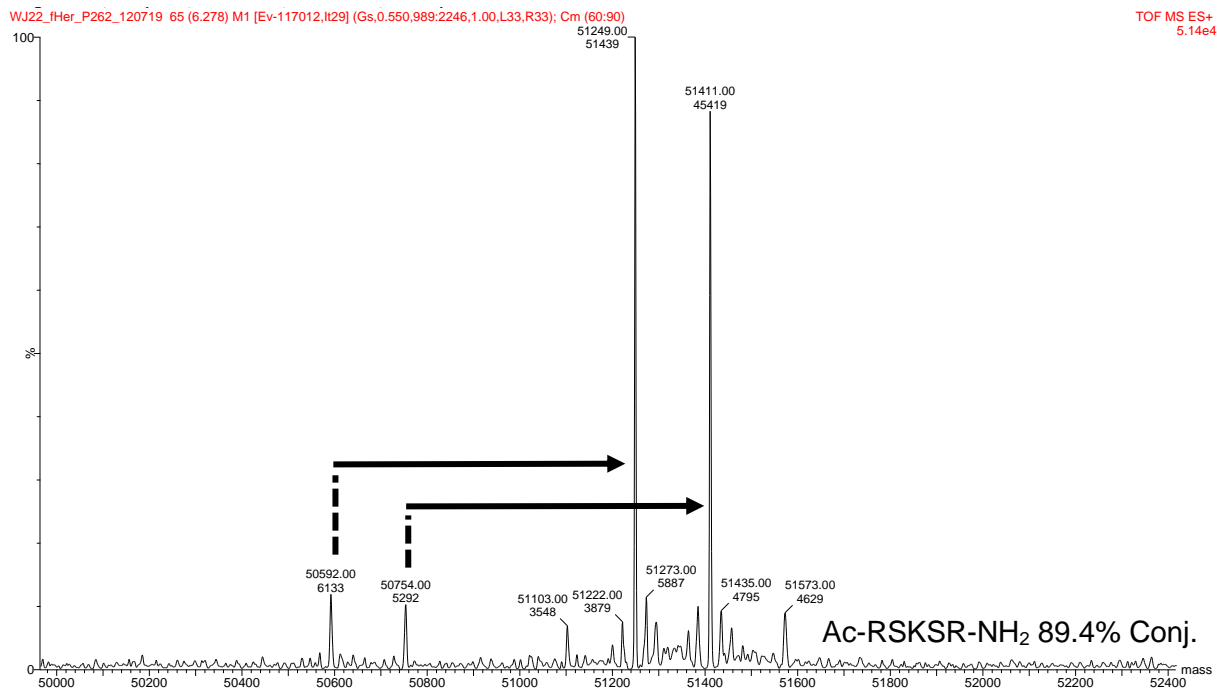


Figure A 14: Selected deconvoluted mass spectrum of mAb heavy chains after conjugation of peptide Ac-RSKSR-NH₂ (MW: 673.8 Da) with Trastuzumab using method 1. The two peaks at 50592 Da and 50754 Da correspond to two different glycosylations of native Trastuzumab. Calculated conjugated HC's: 51249 Da and 51411 Da; Detected conjugated HC's: 51249 Da and 51411 Da. The conjugation efficiency, calculated from the intensity, is 89.4%.

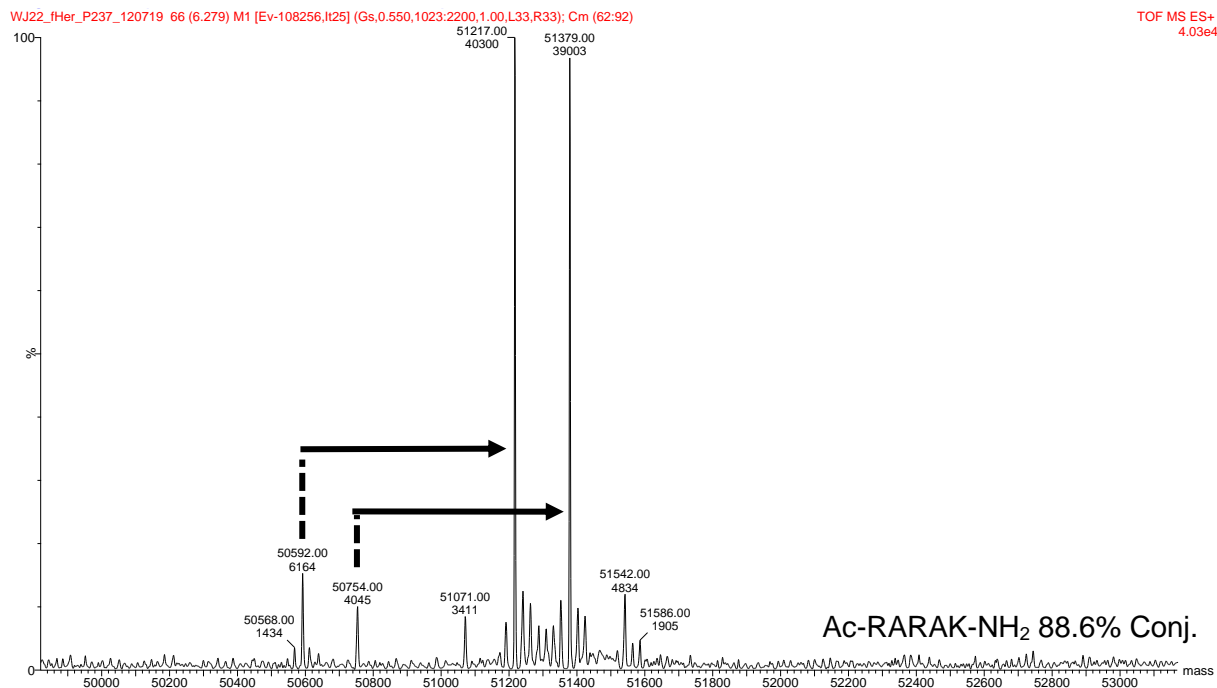


Figure A 15: Selected deconvoluted mass spectrum of mAb heavy chains after conjugation of peptide Ac-RARAK-NH₂ (MW: 641.8 Da) with Trastuzumab using method 1. The two peaks at 50592 Da and 50754 Da correspond to two different glycosylations of native Trastuzumab. Calculated conjugated HC's: 51217 Da and 51379 Da; Detected conjugated HC's: 51217 Da and 51379 Da. The conjugation efficiency, calculated from the intensity, is 88.6%.

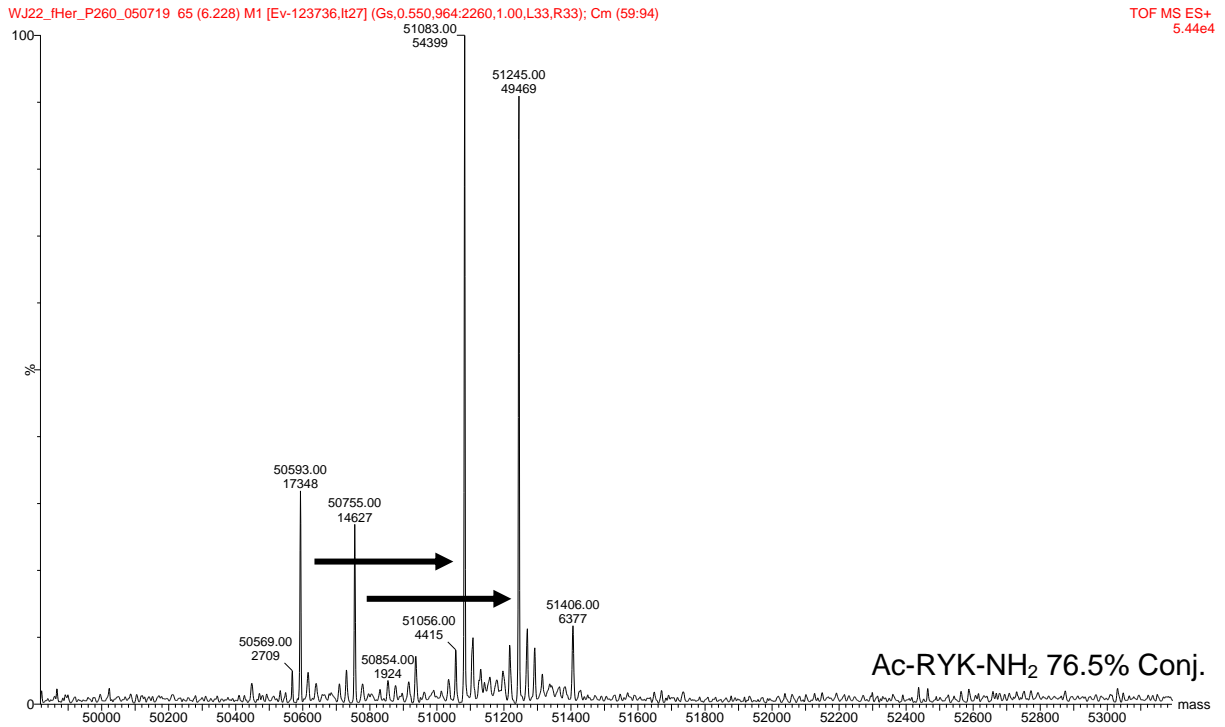


Figure A 16: Selected deconvoluted mass spectrum of mAb heavy chains after conjugation of peptide Ac-RYK-NH₂ (MW: 506.6 Da) with Trastuzumab using method 1. The two peaks at 50593 Da and 50755 Da correspond to two different glycosylations of native Trastuzumab. Calculated conjugated HC's: 51083 Da and 51245 Da; Detected conjugated HC's: 51083 Da and 51245 Da. The conjugation efficiency, calculated from the intensity, is 76.5%.

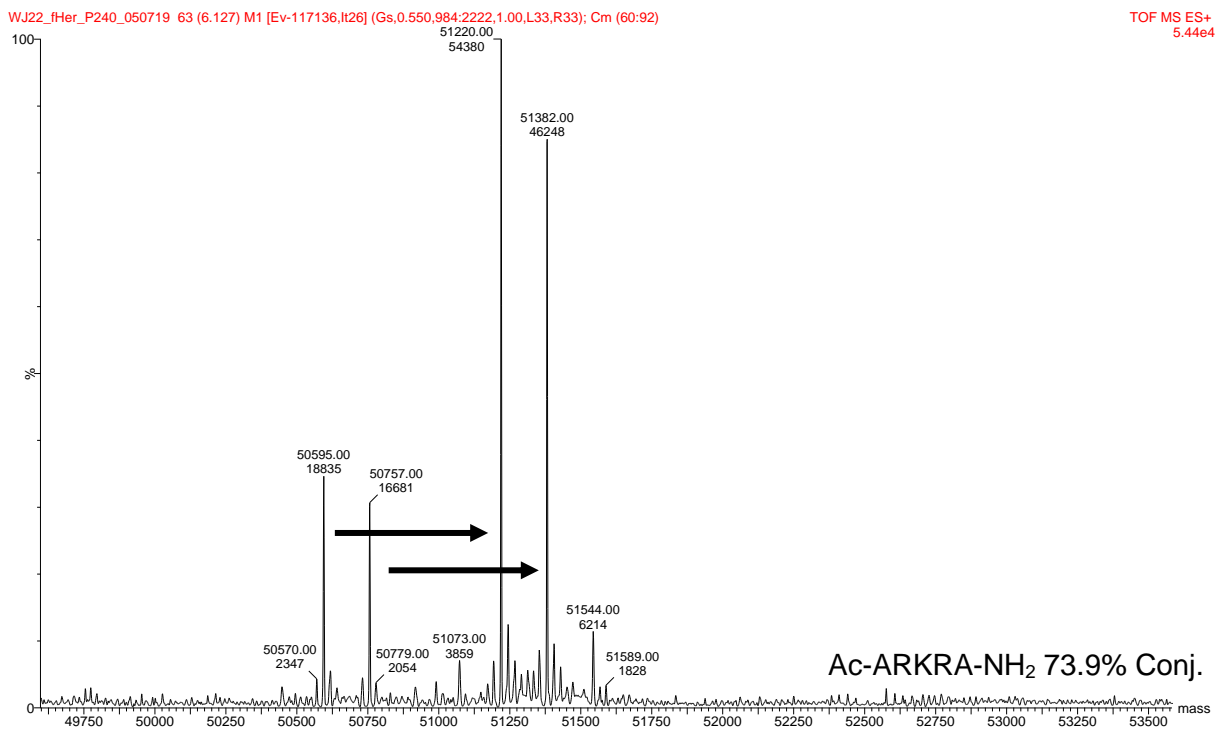


Figure A 17: Selected deconvoluted mass spectrum of mAb heavy chains after conjugation of peptide Ac-ARKRA-NH₂ (MW: 641.8 Da) with Trastuzumab using method 1. The two peaks at 50595 Da and 50757 Da correspond to two different glycosylations of native Trastuzumab. Calculated conjugated HC's: 51220 Da and 51382 Da; Detected conjugated HC's: 51220 Da and 51382 Da. The conjugation efficiency, calculated from the intensity, is 73.9%.

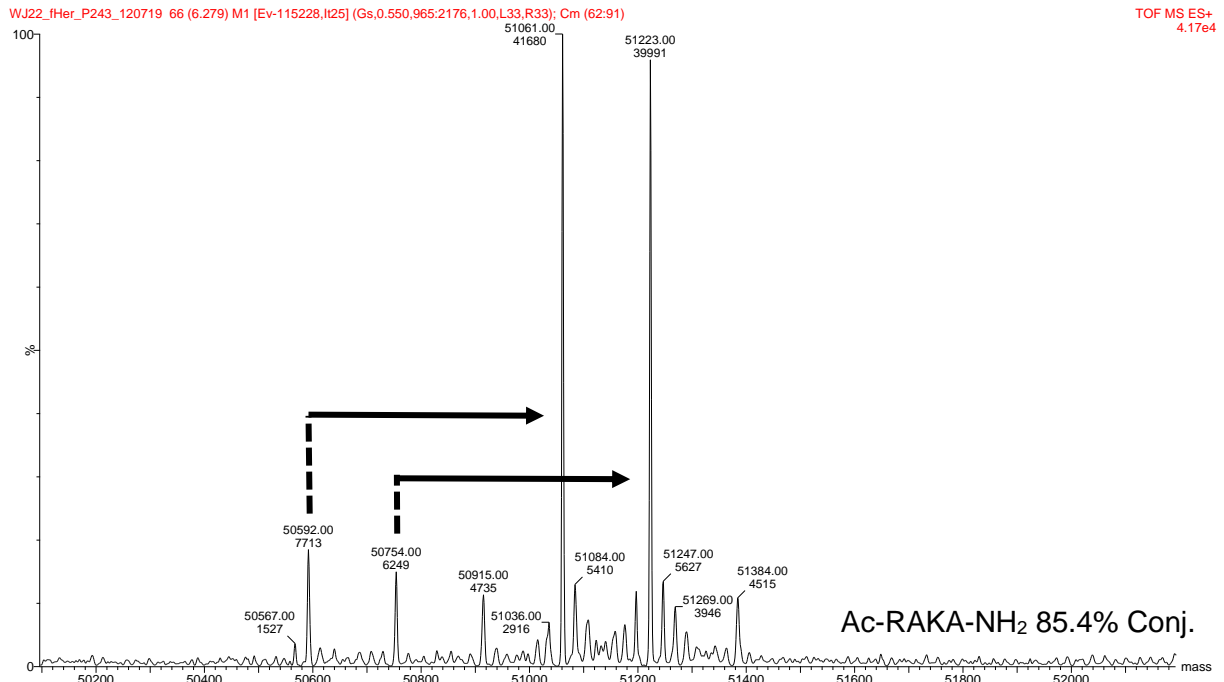


Figure A 18: Selected deconvoluted mass spectrum of mAb heavy chains after conjugation of peptide Ac-RAKA-NH₂ (MW: 485.6 Da) with Trastuzumab using method 1. The two peaks at 50592 Da and 50754 Da correspond to two different glycosylations of native Trastuzumab. Calculated conjugated HC's: 51061 Da and 51223 Da; Detected conjugated HC's: 51061 Da and 51223 Da. The conjugation efficiency, calculated from the intensity, is 85.4%.

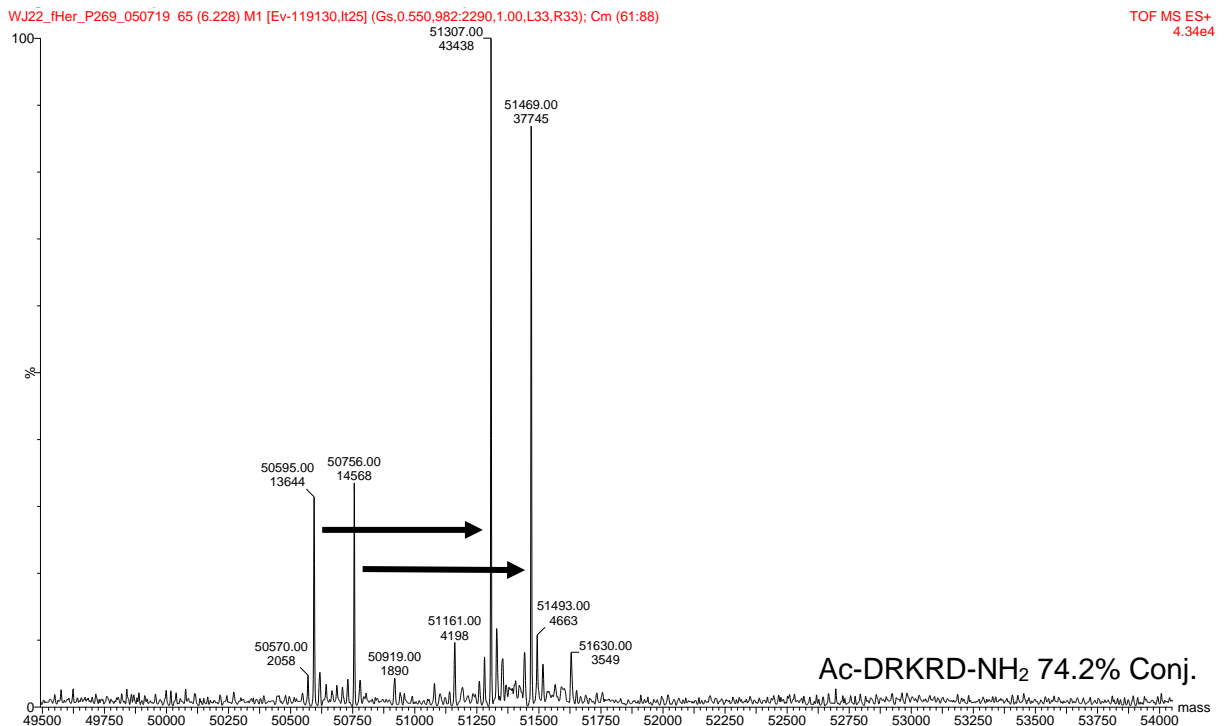


Figure A 19: Selected deconvoluted mass spectrum of mAb heavy chains after conjugation of peptide Ac-DRKRD-NH₂ (MW: 729.8 Da) with Trastuzumab using method 1. The two peaks at 50595 Da and 50756 Da correspond to two different glycosylations of native Trastuzumab. Calculated conjugated HC's: 51308 Da and 51469 Da; Detected conjugated HC's: 51307 Da and 51469 Da. The conjugation efficiency, calculated from the intensity, is 74.2%.

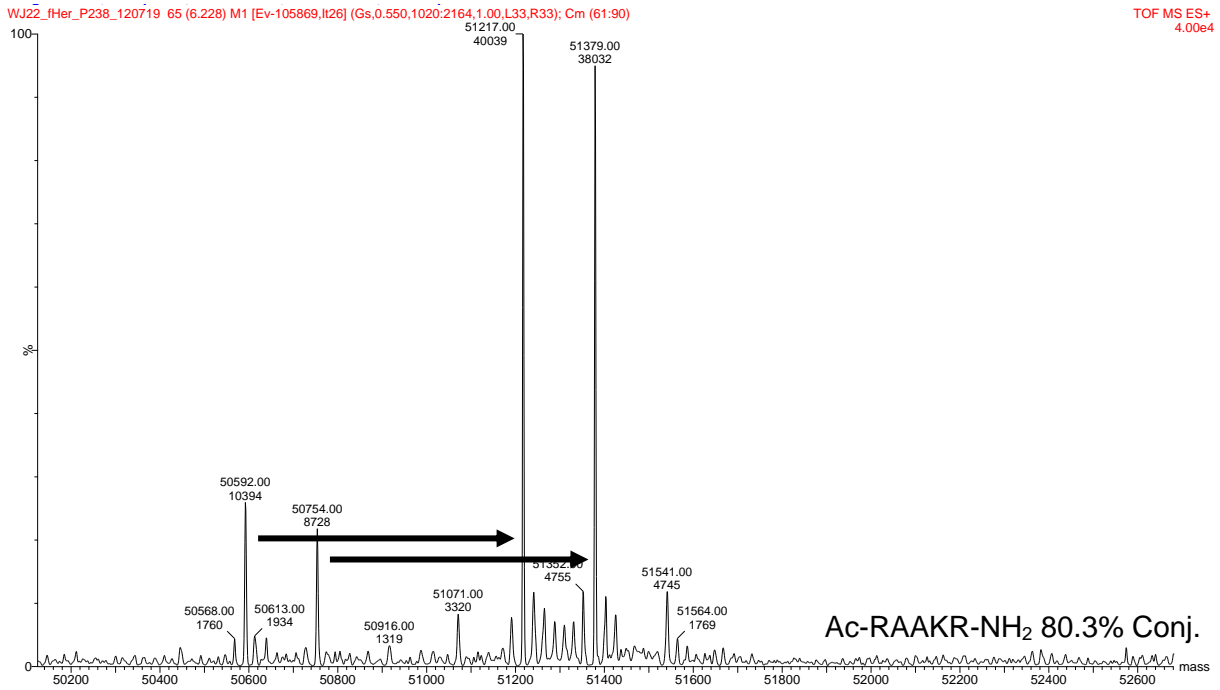


Figure A 20: Selected deconvoluted mass spectrum of mAb heavy chains after conjugation of peptide Ac-RAAKR-NH₂ (MW: 641.8 Da) with Trastuzumab using method 1. The two peaks at 50592 Da and 50754 Da correspond to two different glycosylations of native Trastuzumab. Calculated conjugated HC's: 51217 Da and 51379 Da; Detected conjugated HC's: 51217 Da and 51379 Da. The conjugation efficiency, calculated from the intensity, is 80.3%.

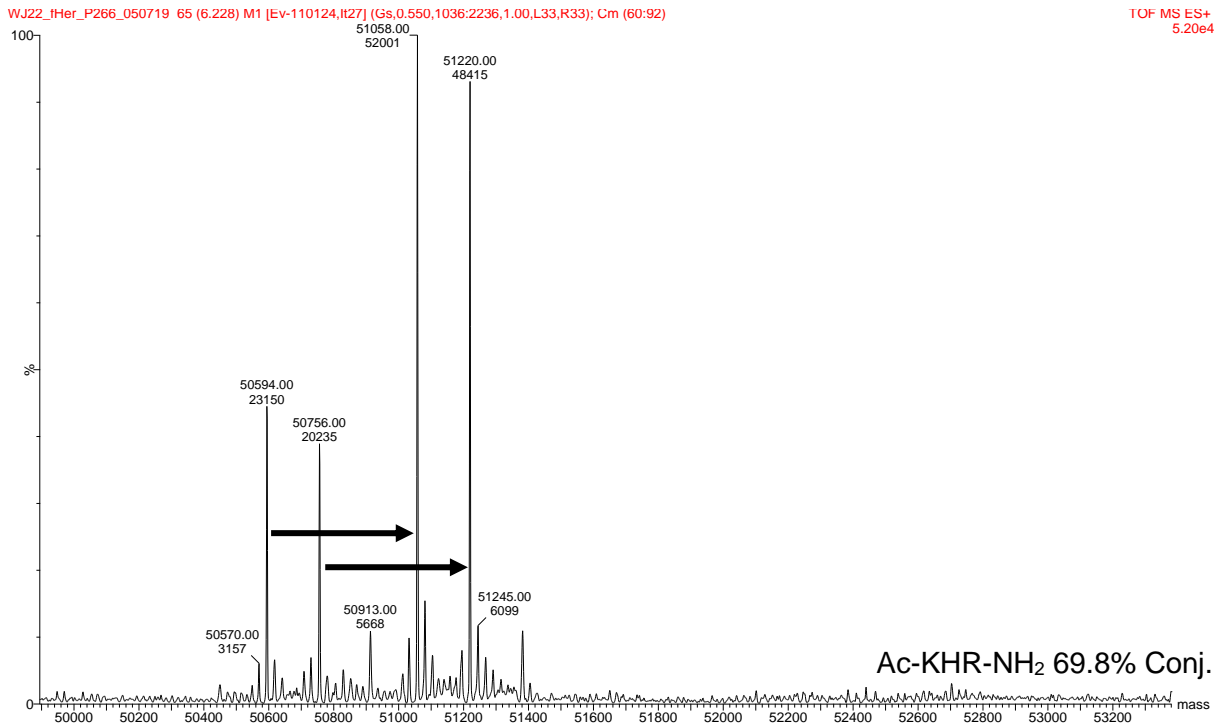


Figure A 21: Selected deconvoluted mass spectrum of mAb heavy chains after conjugation of peptide Ac-KHR-NH₂ (MW: 480.6 Da) with Trastuzumab using method 1. The two peaks at 50594 Da and 50756 Da correspond to two different glycosylations of native Trastuzumab. Calculated conjugated HC's: 51058 Da and 51220 Da; Detected conjugated HC's: 51058 Da and 51220 Da. The conjugation efficiency, calculated from the intensity, is 69.8%.

WJ22_fHer_P241_120719 67 (6.329) M1 [Ev-112439,I126] (Gs,0.550,971:2170,1.00,L33,R33); Cm (64:90)

TOF MS ES+
3.84e4

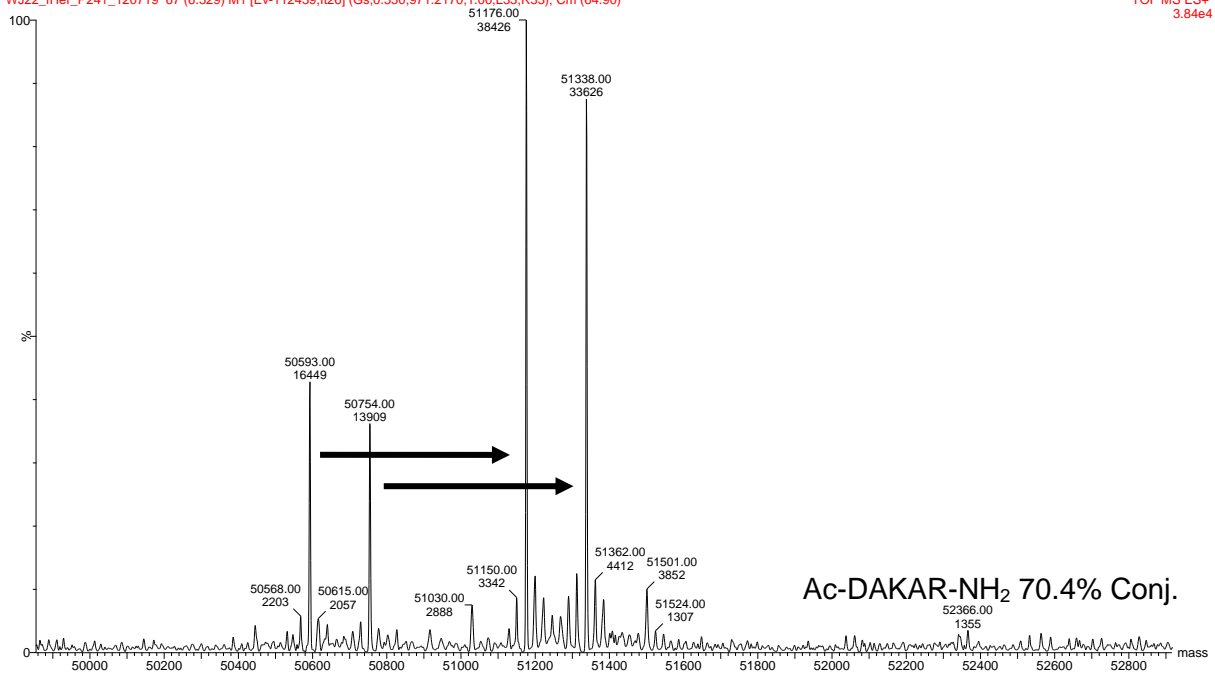


Figure A 22: Selected deconvoluted mass spectrum of mAb heavy chains after conjugation of peptide Ac-DAKAR-NH₂ (MW: 600.7 Da) with Trastuzumab using method 1. The two peaks at 50593 Da and 50754 Da correspond to two different glycosylations of native Trastuzumab. Calculated conjugated HC's: 51177 Da and 51338 Da; Detected conjugated HC's: 51176 Da and 51338 Da. The conjugation efficiency, calculated from the intensity, is 70.4%.

WJ22_fHer_P253_120719 66 (6.279) M1 [Ev-111476,I127] (Gs,0.550,1006:2151,1.00,L33,R33); Cm (61:98)

TOF MS ES+
3.92e4

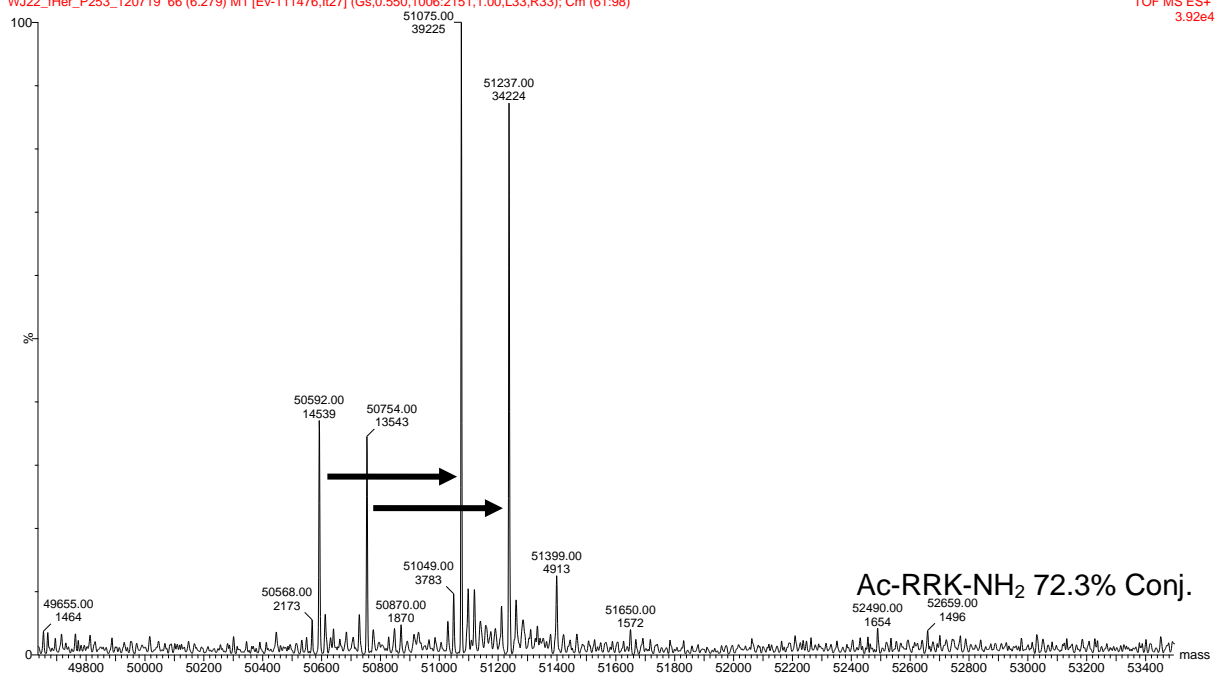


Figure A 23: Selected deconvoluted mass spectrum of mAb heavy chains after conjugation of peptide Ac-RRK-NH₂ (MW: 499.6 Da) with Trastuzumab using method 1. The two peaks at 50592 Da and 50754 Da correspond to two different glycosylations of native Trastuzumab. Calculated conjugated HC's: 51075 Da and 51237 Da; Detected conjugated HC's: 51075 Da and 51237 Da. The conjugation efficiency, calculated from the intensity, is 72.3%.

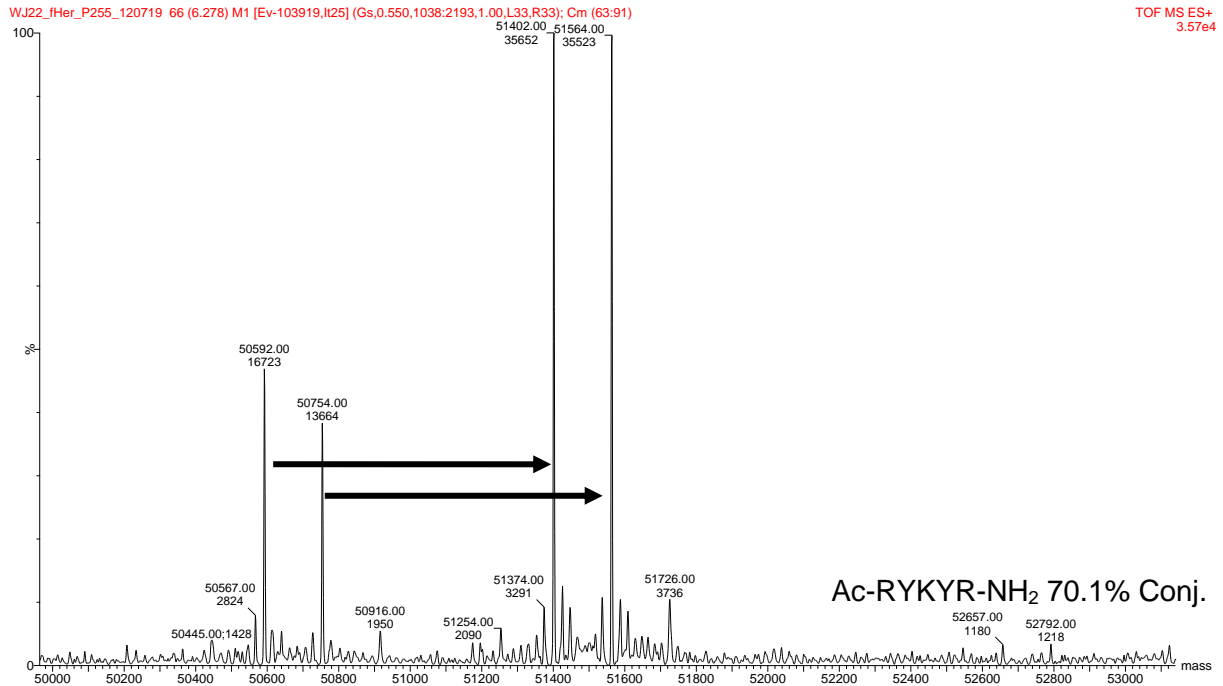


Figure A 24: Selected deconvoluted mass spectrum of mAb heavy chains after conjugation of peptide Ac-RYKYR-NH₂ (MW: 826.0 Da) with Trastuzumab using method 1. The two peaks at 50592 Da and 50754 Da correspond to two different glycosylations of native Trastuzumab. Calculated conjugated HC's: 51401 Da and 51563 Da; Detected conjugated HC's: 51402 Da and 51564 Da. The conjugation efficiency, calculated from the intensity, is 70.1%.

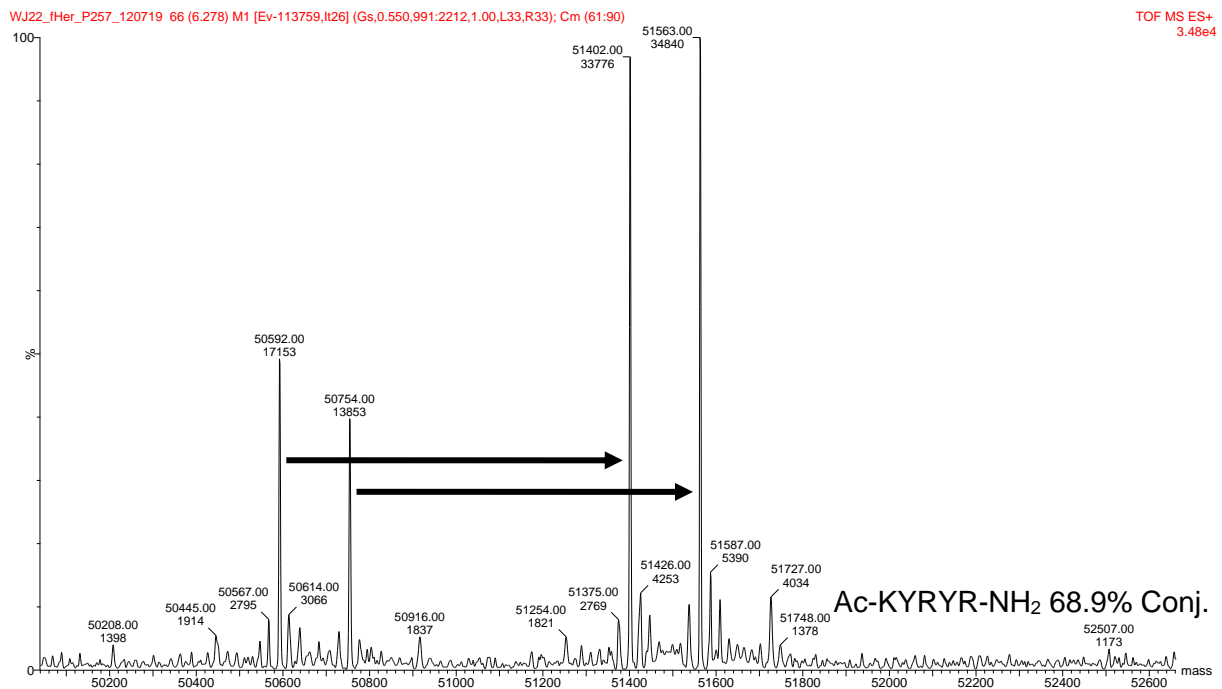


Figure A 25: Selected deconvoluted mass spectrum of mAb heavy chains after conjugation of peptide Ac-KYRYR-NH₂ (MW: 826.0 Da) with Trastuzumab using method 1. The two peaks at 50592 Da and 50754 Da correspond to two different glycosylations of native Trastuzumab. Calculated conjugated HC's: 51401 Da and 51563 Da; Detected conjugated HC's: 51402 Da and 51563 Da. The conjugation efficiency, calculated from the intensity, is 68.9%.

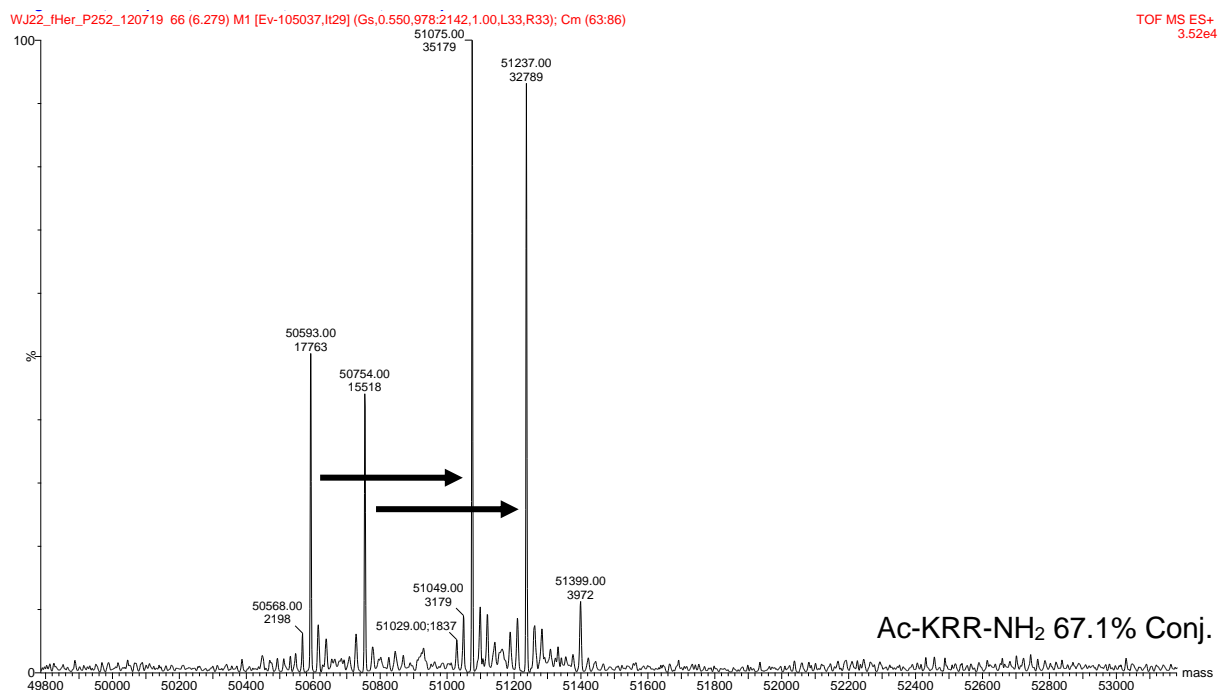


Figure A 26: Selected deconvoluted mass spectrum of mAb heavy chains after conjugation of peptide Ac-KRR-NH₂ (MW: 499.6 Da) with Trastuzumab using method 1. The two peaks at 50593 Da and 50754 Da correspond to two different glycosylations of native Trastuzumab. Calculated conjugated HC's: 51076 Da and 51237 Da; Detected conjugated HC's: 51075 Da and 51237 Da. The conjugation efficiency, calculated from the intensity, is 67.1%.

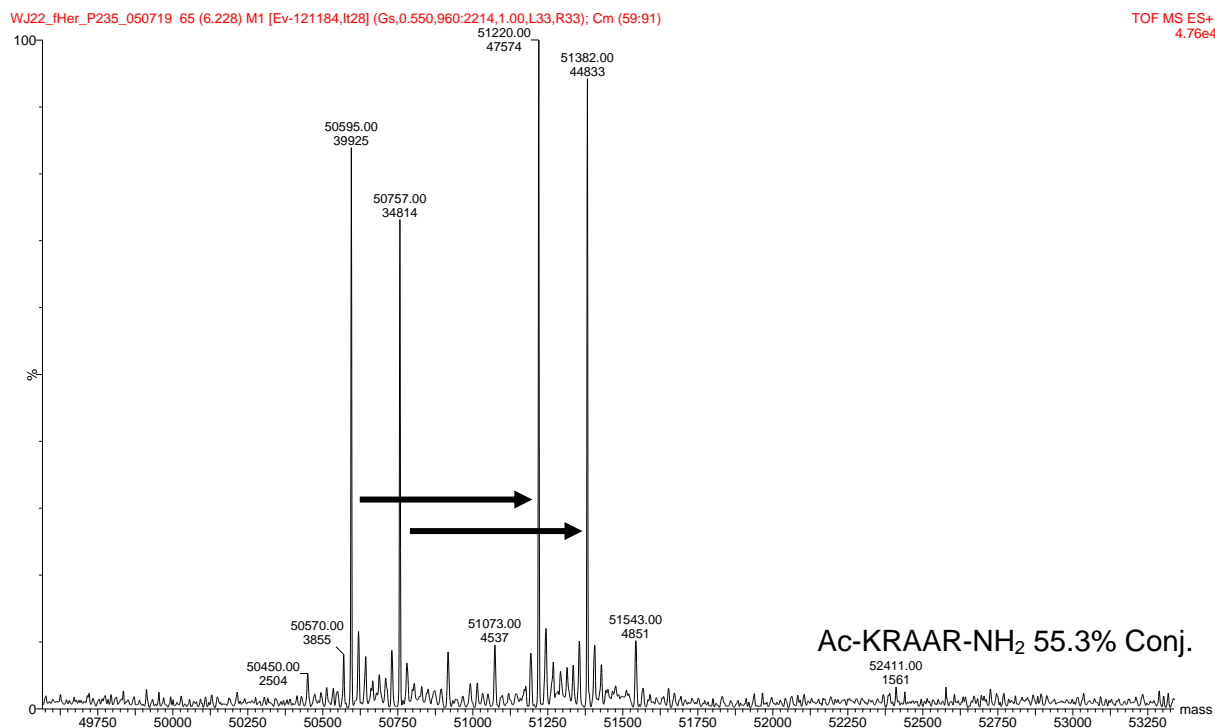


Figure A 27: Selected deconvoluted mass spectrum of mAb heavy chains after conjugation of peptide Ac-KRAAR-NH₂ (MW: 641.8 Da) with Trastuzumab using method 1. The two peaks at 50595 Da and 50757 Da correspond to two different glycosylations of native Trastuzumab. Calculated conjugated HC's: 51220 Da and 51382 Da; Detected conjugated HC's: 51220 Da and 51382 Da. The conjugation efficiency, calculated from the intensity, is 55.3%.

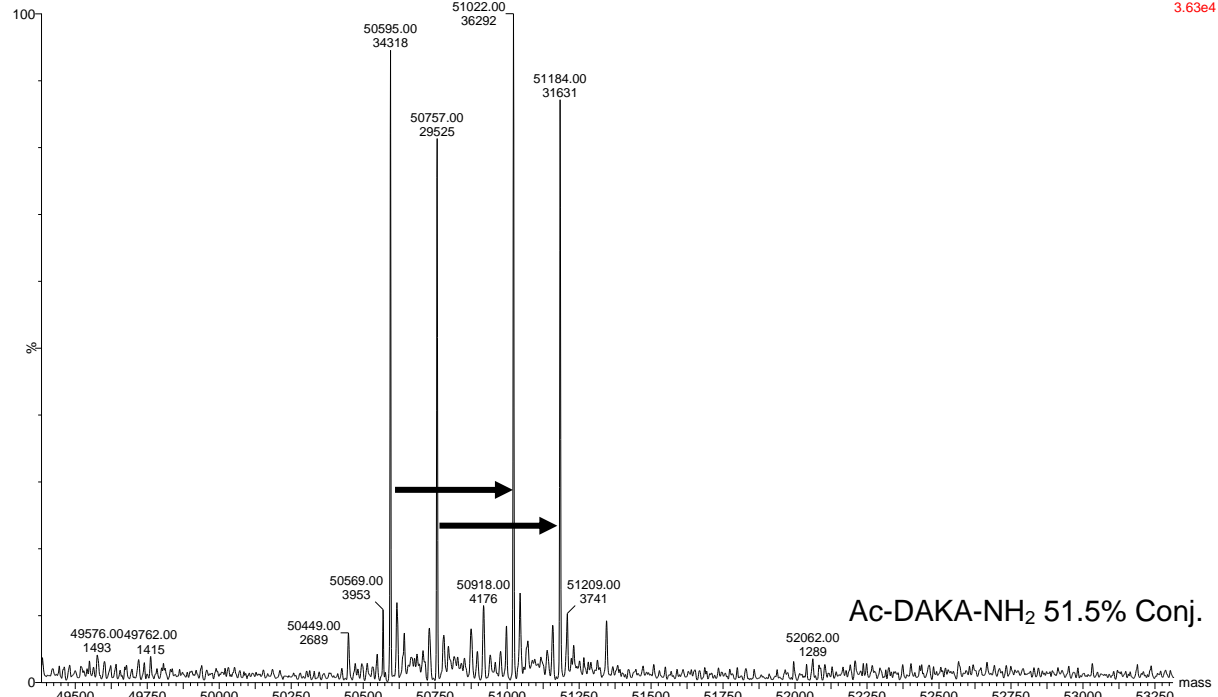


Figure A 28: Selected deconvoluted mass spectrum of mAb heavy chains after conjugation of peptide Ac-DAKA-NH₂ (MW: 444.5 Da) with Trastuzumab using method 1. The two peaks at 50595 Da and 50757 Da correspond to two different glycosylations of native Trastuzumab. Calculated conjugated HC's: 51023 Da and 51185 Da; Detected conjugated HC's: 51022 Da and 51184 Da. The conjugation efficiency, calculated from the intensity, is 51.5%.

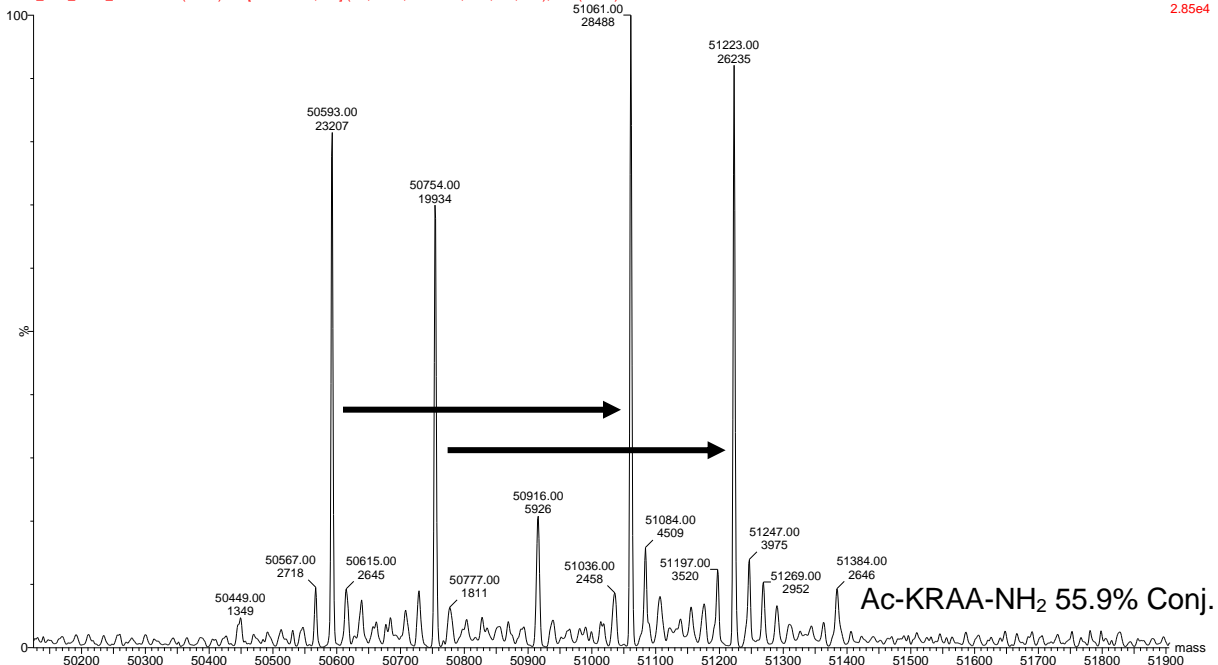


Figure A 29: Selected deconvoluted mass spectrum of mAb heavy chains after conjugation of peptide Ac-KRAA-NH₂ (MW: 485.6 Da) with Trastuzumab using method 1. The two peaks at 50593 Da and 50754 Da correspond to two different glycosylations of native Trastuzumab. Calculated conjugated HC's: 51062 Da and 51223 Da; Detected conjugated HC's: 51061 Da and 51223 Da. The conjugation efficiency, calculated from the intensity, is 55.9%.

WJ22_fHer_P950_050719 66 (6.278) M1 [Ev-105166,It24] (Gs,0.550,992:2180,1.00,L33,R33); Cm (61:87)

TOF MS ES+
2.07e4

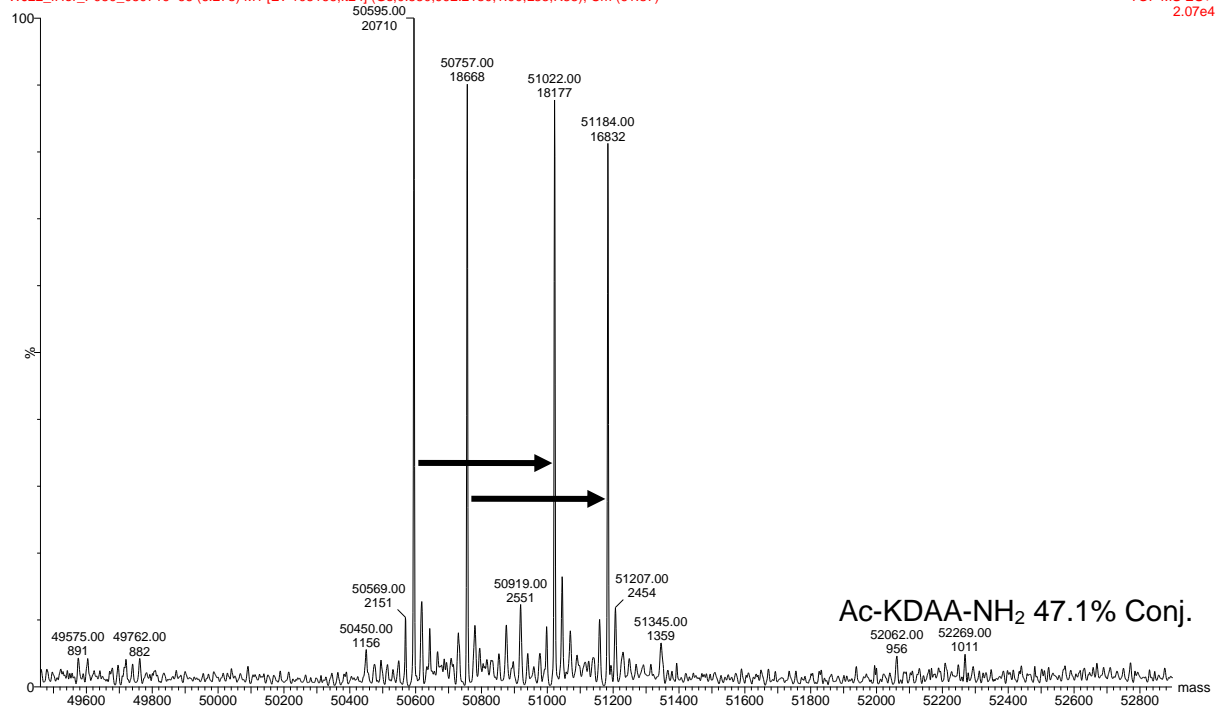


Figure A 30: Selected deconvoluted mass spectrum of mAb heavy chains after conjugation of peptide Ac-KDAA-NH₂ (MW: 444.5 Da) with Trastuzumab using method 1. The two peaks at 50595 Da and 50757 Da correspond to two different glycosylations of native Trastuzumab. Calculated conjugated HC's: 51023 Da and 51185 Da; Detected conjugated HC's: 51022 Da and 51184 Da. The conjugation efficiency, calculated from the intensity, is 47.1%.

WJ22_fHer_P258_120719 67 (6.330) M1 [Ev-95969,It24] (Gs,0.550,1006:2068,1.00,L33,R33); Cm (63:87)

TOF MS ES+
3.19e4

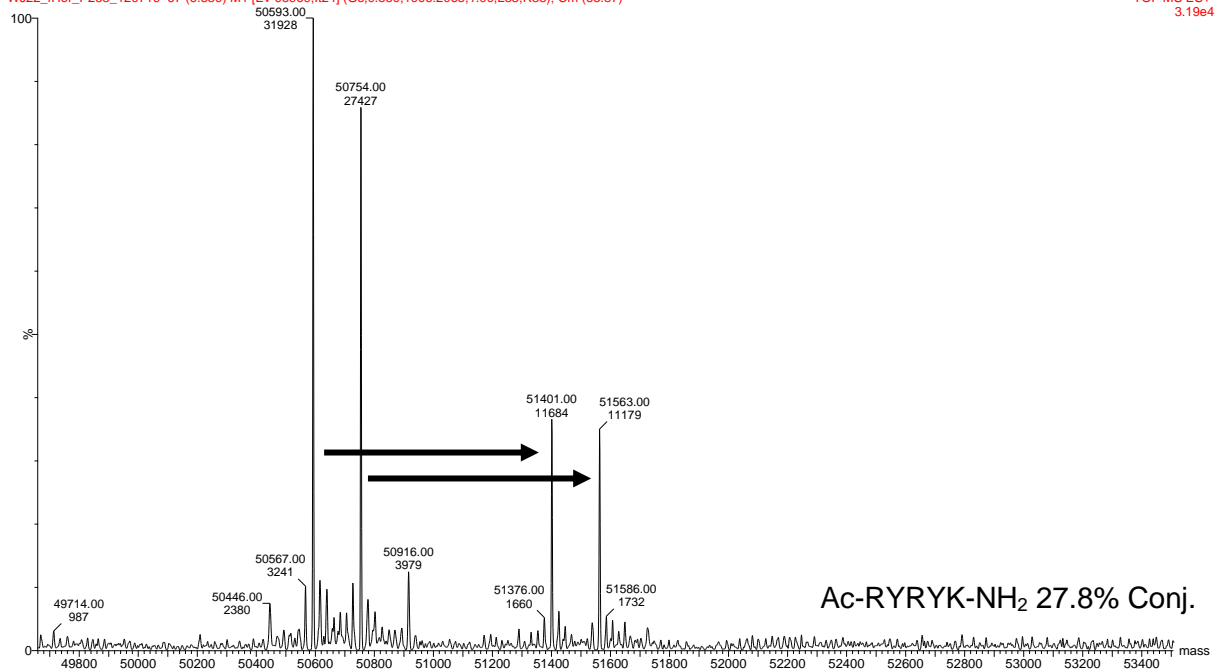


Figure A 31: Selected deconvoluted mass spectrum of mAb heavy chains after conjugation of peptide Ac-RYRYK-NH₂ (MW: 826.0 Da) with Trastuzumab using method 1. The two peaks at 50593 Da and 50754 Da correspond to two different glycosylations of native Trastuzumab. Calculated conjugated HC's: 51402 Da and 51563 Da; Detected conjugated HC's: 51401 Da and 51563 Da. The conjugation efficiency, calculated from the intensity, is 27.8%.

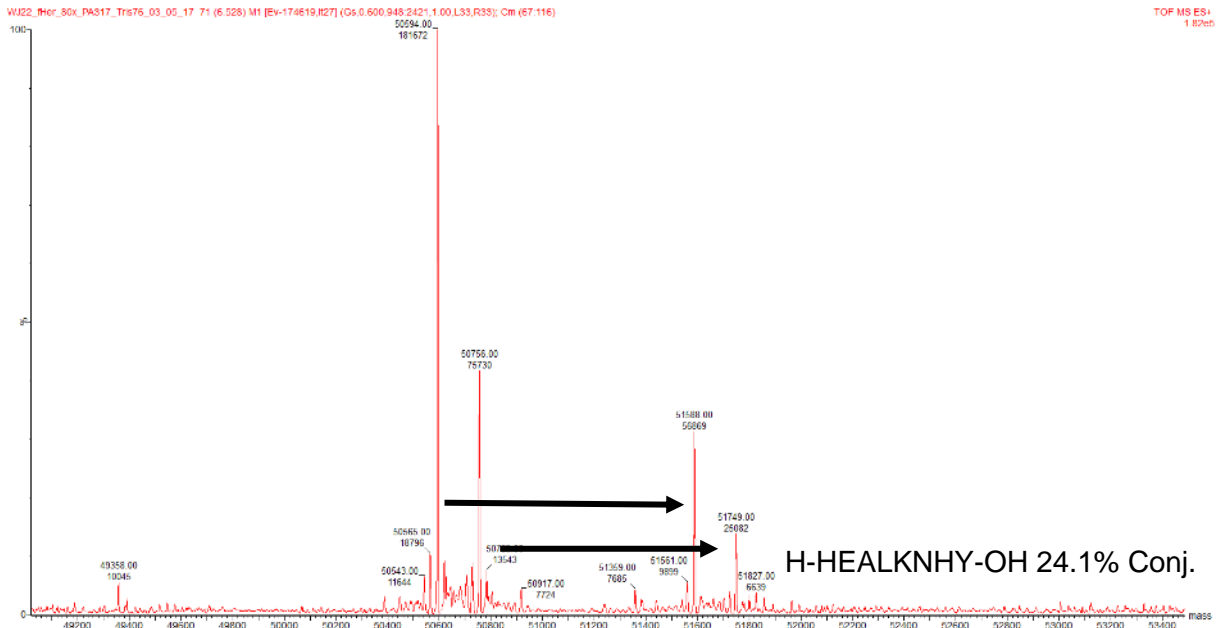


Figure A 32: Selected deconvoluted mass spectrum of mAb heavy chains after conjugation of peptide H-HEALKNHY-OH (MW: 1011.1 Da) with Trastuzumab using method 1. The two peaks at 50594 Da and 50756 Da correspond to two different glycosylations of native Trastuzumab. Calculated conjugated HC's: 51588 Da and 51750 Da; Detected conjugated HC's: 51588 Da and 51749 Da. The conjugation efficiency, calculated from the intensity, is 24.1%.

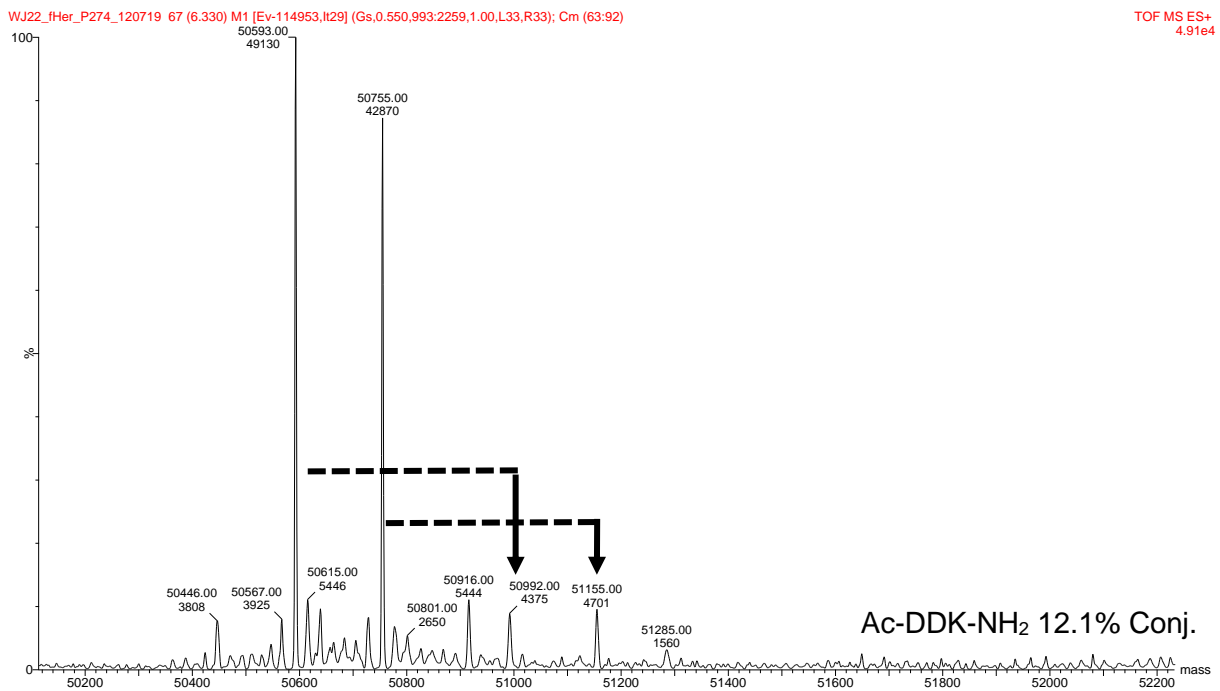


Figure A 33: Selected deconvoluted mass spectrum of mAb heavy chains after conjugation of peptide Ac-DDK-NH₂ (MW: 417.4 Da) with Trastuzumab using method 1. The two peaks at 50593 Da and 50755 Da correspond to two different glycosylations of native Trastuzumab. Calculated conjugated HC's: 50993 Da and 51155 Da; Detected conjugated HC's: 50992 Da and 51155 Da. The conjugation efficiency, calculated from the intensity, is 12.1%.

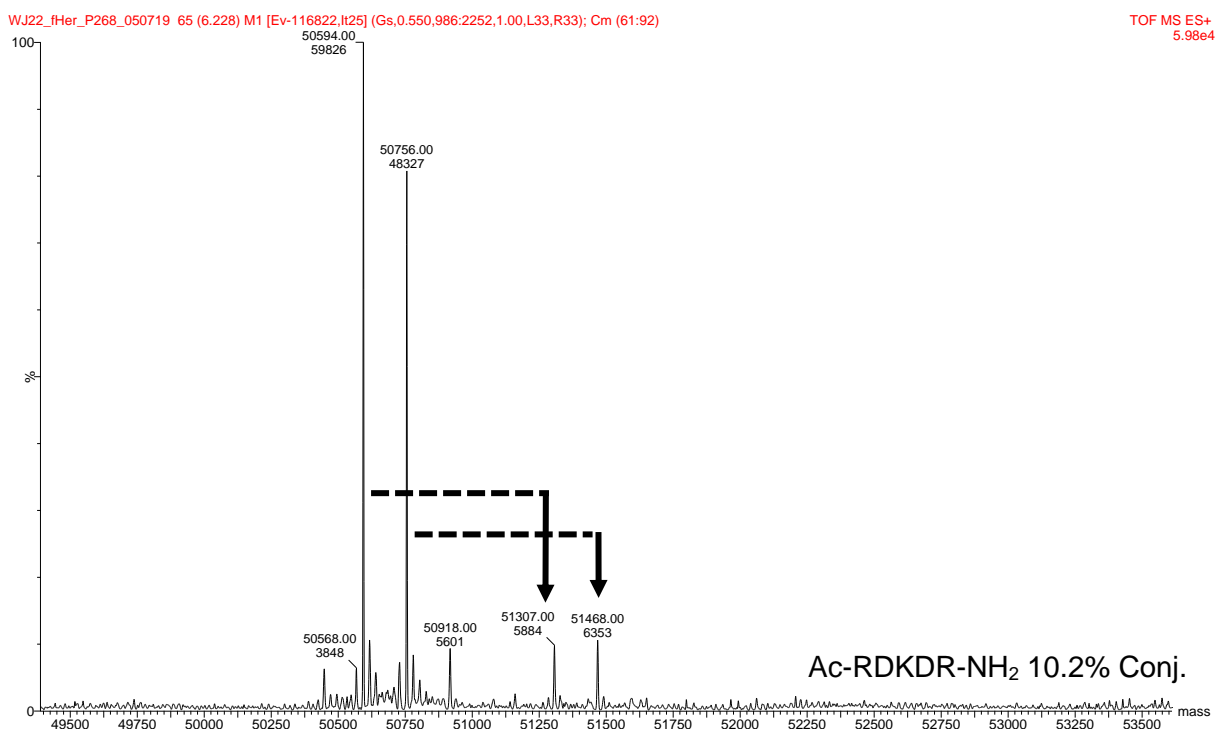


Figure A 34: Selected deconvoluted mass spectrum of mAb heavy chains after conjugation of peptide Ac-RDKDR-NH₂ (MW: 729.8 Da) with Trastuzumab using method 1. The two peaks at 50594 Da and 50756 Da correspond to two different glycosylations of native Trastuzumab. Calculated conjugated HC's: 51307 Da and 51469 Da; Detected conjugated HC's: 51307 Da and 51468 Da. The conjugation efficiency, calculated from the intensity, is 10.2%.

13.1.2. Summarized conjugation efficiencies for non- N- and C-terminal acylated and amidated peptide linkers

Table A 2: Conjugation efficiencies of different peptides (protected vs. non-protected) to Trastuzumab using standard conditions. Especially the last five peptides, synthesized for the computational project, show different efficiencies of up to 30%. N=4, N_{RAKAR}=6, N_{VRKR}=3

Sequence	N-terminal Acetylated C-terminal Amidated	N-terminal Acetylated No c-terminal protection	No protection
RAKAR	87±4%	-	89±2%
RAK-K(N ₃)	88±1%	-	91±1
YDADK	3±1%	0%	-
AVRAK	90±1%	71±3%	-
VRKR	83±1%	77±1%	-
YGKGY	77±1%	43±2%	-
KARAGAGADADAD	25±1%	45±5%	-

13.1.3. Influence on the conjugation efficiency of antibody formulation buffers

Table A 3: Conjugation efficiency of Trastuzumab, Daratumumab, and Nivolumab with RAKAR using standard conditions. In the first row, the mAbs were directly taken out of their formulation buffer. In the right row, the mAbs were first rebuffed into Trizma pH 7.6. Only small differences were found for Trastuzumab and Daratumumab. Nivolumab tends to conjugate better when taken out directly from formulation buffer. $n_{\text{Trastuzumab formulated}} = 7$, $n_{\text{Daratumumab/Nivolumab formulated}} = 4$, $n_{\text{Trastuzumab/Daratumumab in Trizma}} = 6$.

	mAb in formulation buffer	Buffer exchanged mAb into Trizma pH 7.6
Trastuzumab	87 ± 3%	90 ± 4%
Daratumumab	90 ± 4%	82 ± 3%
Nivolumab	108 ± 2%	83 ± 1%

13.1.4. Sequence alignment between Trastuzumab and Nivolumab

A Nivolumab sample has been conjugated with Peptide Ac-RAK-NH₂, deglycosylated, and sent to the functional genomics center of Zurich to confirm all the three sites of attachment seen with our sample. The sequence coverage of heavy chain from IgG4 was 91.74%. The site Q288(EE₂₈₈QFNSTRYR) was confirmed by numerous MS/MS spectra. Based on PSM, it should be the major site. In addition, the Q304(VVSVLTVLH₃₀₄QDWLNGK) was also modified by one Ac-RAK-NH₂ peptide. Furthermore, there was a very low proportion of modified Q observed at position 431 (WQEGNVFSCSVMHEALHNHYT₄₃₁QK). The major conjugation site Q288 corresponds to Q295 on Trastuzumab, as a sequent alignment in Figure A 35 shows (top row: Trastuzumab, bottom row: Nivolumab). Marked in red are the observed positions that have our linker attached.

Score	Expect	Method	Identities	Positives	Gaps
733 bits(1892)	0.0	Compositional matrix adjust.	383/450(85%)	401/450(89%)	10/450(2%)
Query	1	EVQLVESGGGLVQPGGSLRLS	CAASGFNIKDTYIHWVRQAPGK	GLEWVARIYPTNGYTRY	60
Sbjct	1	+VQLVESGGG+VQPG SLRL C	ASG ++ +HWVRQAPGKLEWVA	I+ Y	60
Query	61	ADSVKGRFTISADTSKNTAYLQ	MNSLRAEDTAVYYCSRWGGDGFY	AMDYWGQGLVTVSS	120
Sbjct	61	ADSVKGRFTIS D SKNT +LQ	MNSLRAEDTAVYYC+ DYWGQGLVTVSS		113
Query	121	ASTKGPSVFPLAPSSKSTSGGT	AALGCLVKDYFPEPVTVSWNSG	ALTSQVHTFPAVLQSS	180
Sbjct	114	ASTKGPSVFPLAPCSRSTSE	STAALGCLVKDYFPEPVTVSWNSG	ALTSQVHTFPAVLQSS	173
Query	181	GLYSLSSVVTVPSSSLGTQTY	ICNVNHKPSNTKVDKKEPKSCDK	THTCPPCPAPELGG	240
Sbjct	174	GLYSLSSVVTVPSSSLGT+TY	CNV+HKPSNTKVDK+VE K CP	APE LGG	230


```

Query 241 PSVFLFPPKPKDTLMISRTPEVTCVVVDVSHEDPEVKFNWYVDGVEVHNAKTKPREEQYN 300
          PSVFLFPPKPKDTLMISRTPEVTCVVVDVSEDEPEV+FNWYVDGVEVHNAKTKPREEQ+N
Sbjct 231 PSVFLFPPKPKDTLMISRTPEVTCVVVDVSEDEPEVQFNWYVDGVEVHNAKTKPREEQFN 290

Query 301 STYRVVSVLTVLHQDWLNGKEYKCKVSNKALPAPIEKTISKAKGQPREPQVYTLPPSREE 360
          STYRVVSVLTVLHQDWLNGKEYKCKVSNK LP+ IEKTISKAKGQPREPQVYTLPPS+EE
Sbjct 291 STYRVVSVLTVLHQDWLNGKEYKCKVSNKGLPSSIEKTISKAKGQPREPQVYTLPPSQEE 350

Query 361 MTKNQVSLTCLVKGFYPSDIAVEWESNGQPENNYKTTPVLDSDGSFFLYSKLTVDKSRW 420
          MTKNQVSLTCLVKGFYPSDIAVEWESNGQPENNYKTTPVLDSDGSFFLYS+LTVDKSRW
Sbjct 351 MTKNQVSLTCLVKGFYPSDIAVEWESNGQPENNYKTTPVLDSDGSFFLYSRLTVDKSRW 410

Query 421 QQGNVFSCSVMEALHNHYTQKSLSLSPGK 450
          Q+GNVFSCSVMEALHNHYTQKSLSL GK
Sbjct 411 QEGNVFSCSVMEALHNHYTQKSLSLGLGK 440

```

Figure A 35: Shown is a sequent alignment between the HC of Trastuzumab (top row) and Nivolumab (bottom row). The middle row shows possible differences between the two HC's. Marked in red are the three positions Q288 (Q295, European numbering), Q304 (Q311), and Q431 (Q438) which have been detected from the functional genomics center Zurich.

13.1.5. MTG separation from the antibody reaction mix, Protein A and size exclusion

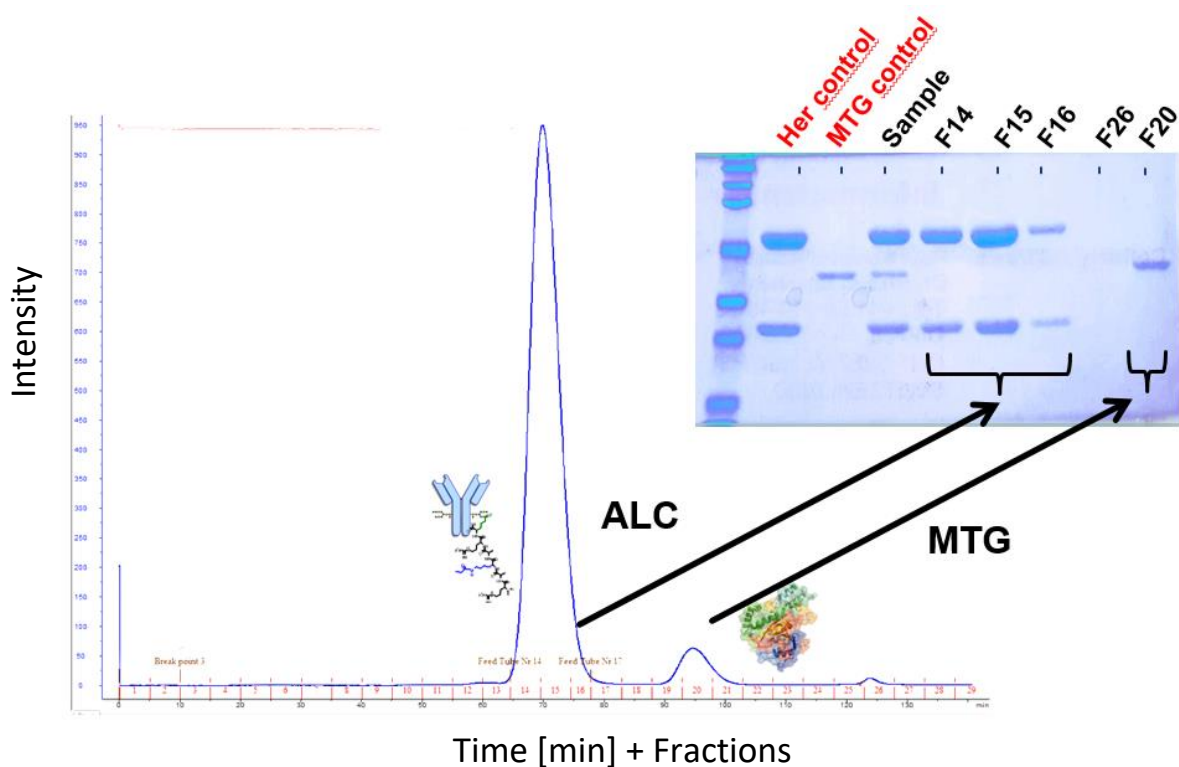


Figure A 36: Shown is the spectra of an FPLC purification based on size exclusion of a Trastuzumab reaction sample with the enzyme MTG. A SDS-Page gel confirms successful separation between our mAb-linker conjugate from MTG.

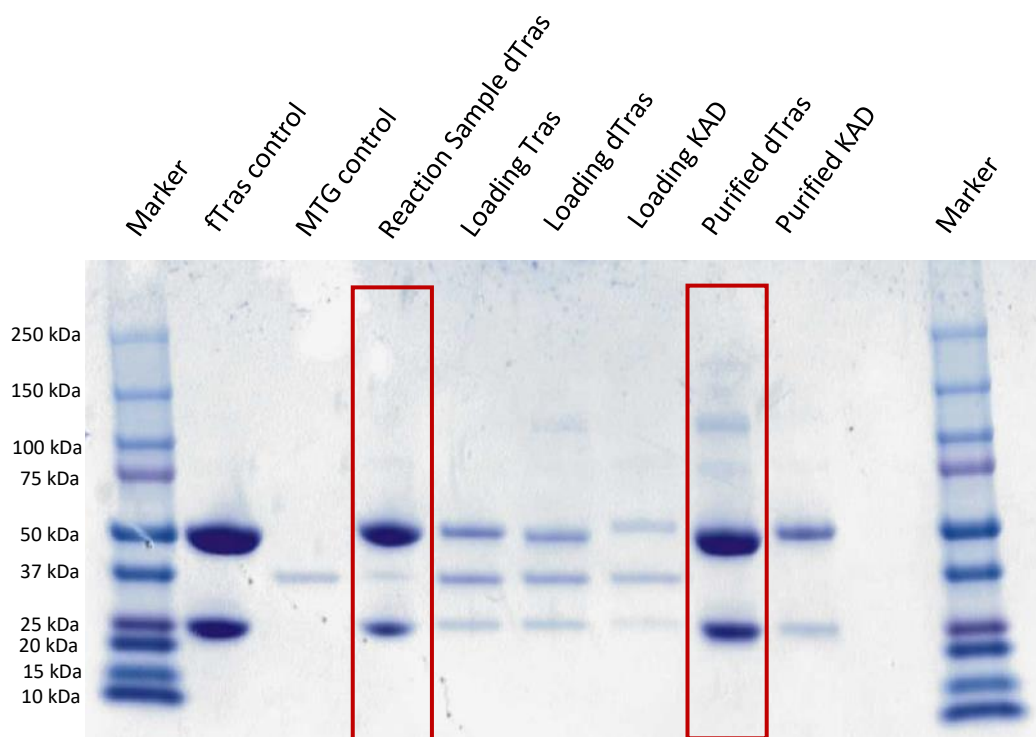


Figure A 37: Shown is a SDS-PAGE gel with antibody/MTG samples at different stages during a protein A purification.

13.2. Chapter 5: Computational screening for suitable MTG-substrates

13.2.1. LC-MS conjugation analysis of synthesized peptides

Table A 4: Conjugation efficiencies of the synthesized peptides with Trastuzumab. Standard conjugation conditions were used. Additionally the mass and the positive/negative prediction on the SOM are listed.

Sequence (N-terminal acetylated and C-terminal amidated)	Mass [Da]	Pos/Neg on SOM (60% Threshold)	Conj. Efficiency [%]			Average [%]	Standard error [%]
FINKISH	899.1	neg	92.6	94.2	90.7	92.5	1.4
RAVAK	584.7	pos	92.1	92	92.9	92.3	0.4
IFSK	534.7	neg	92	95.6	88.8	92.1	2.8
RFK	490.6	pos	88.1	91.5	93.7	91.1	2.3
AVRAK	584.7	pos	91.1	88.6	89.6	89.8	1.0
PKARA	582.7	pos	87.2	91.3	88	88.8	1.8
AARAKARAA	926.1	pos	84.2	88.9	87.1	86.7	1.9
RVRK	598.8	pos	84	87	84.2	85.1	1.4
VRKRV	697.9	n/d	84.3	82.2	83.3	83.3	0.9
YGKGY	627.7	pos	77.5	76.6	78.9	77.7	0.9
TVKVT	587.7	neg	62	67.8	60.4	61.7	4.0
KARAGAGADADAD	1229.3	mixed	31.6	28.3	28.6	29.5	1.5
KTT	389.5	neg	30.6	28.9	27.1	26.7	4.0
TEKAN	602.6	neg	21.8	27.1	14.7	21.2	5.1
LAKE	500.6	neg	25.7	22.1	11.1	18.0	6.0
YDADK	651.7	n/d	4.3	4	1.6	3.3	1.2
GEEKEL	744.8	neg	0	0	0	0.0	0.0

only fHer to test if the +213 Da peak disappears

WJ22_fHer_native_1902220 132 (8.607) M1 [Ev-41454,1121] (Gs,0.550,1135:1762,1.00,L33,R33); Cm (128:148)

TOF MS ES+
2.24e3

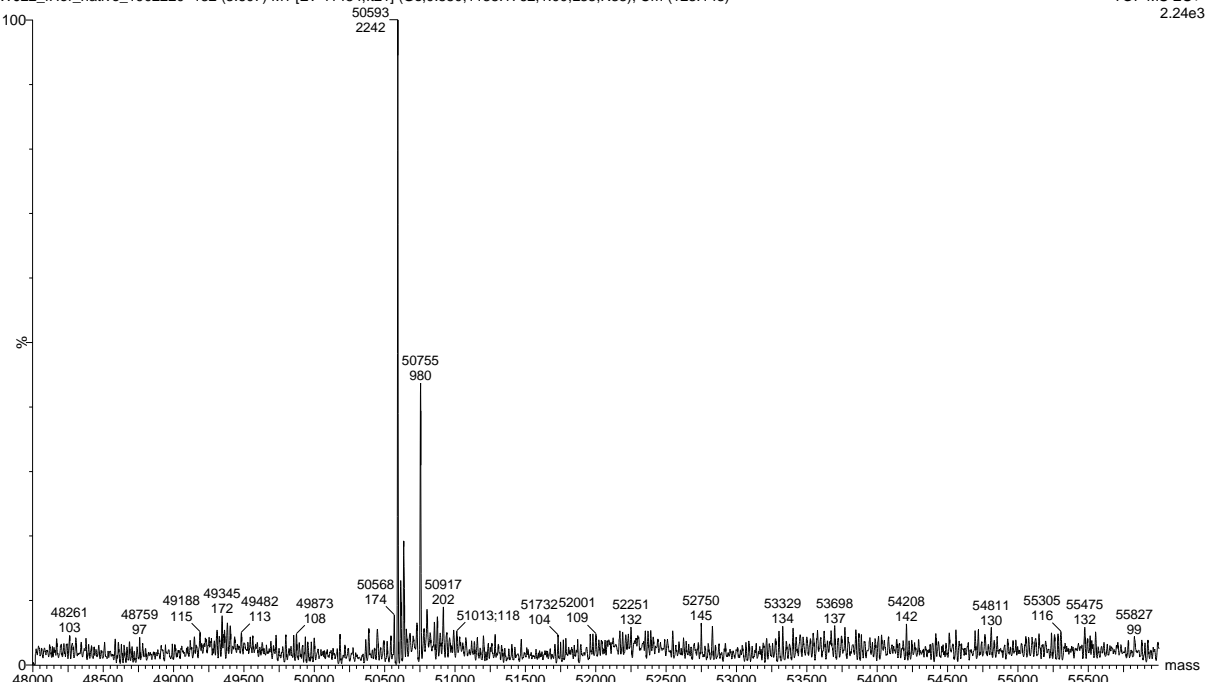


Figure A 38: Deconvoluted mass spectra of the native Trastuzumab heavy chain. The two peaks at 50593 Da and 50755 Da correspond to two different glycosylations.

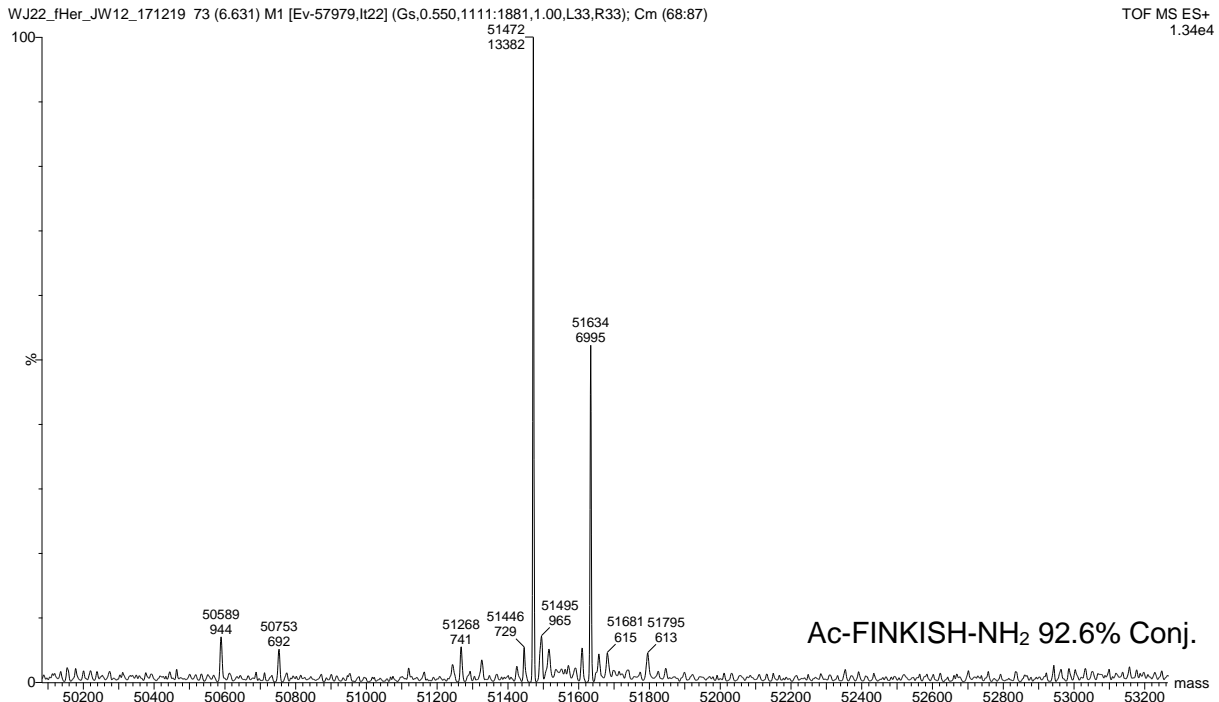


Figure A 39: Selected deconvoluted mass spectrum of mAb heavy chains after conjugation of peptide Ac-FINKISH-NH₂ (MW: 899.1 Da) with Trastuzumab using method 1. The two peaks at 50589 Da and 50753 Da correspond to two different glycosylations of native Trastuzumab. Calculated conjugated HC's: 51061 Da and 51223 Da; Detected conjugated HC's: 51472 Da and 51634 Da. The conjugation efficiency, calculated from the intensity, is 92.6%.

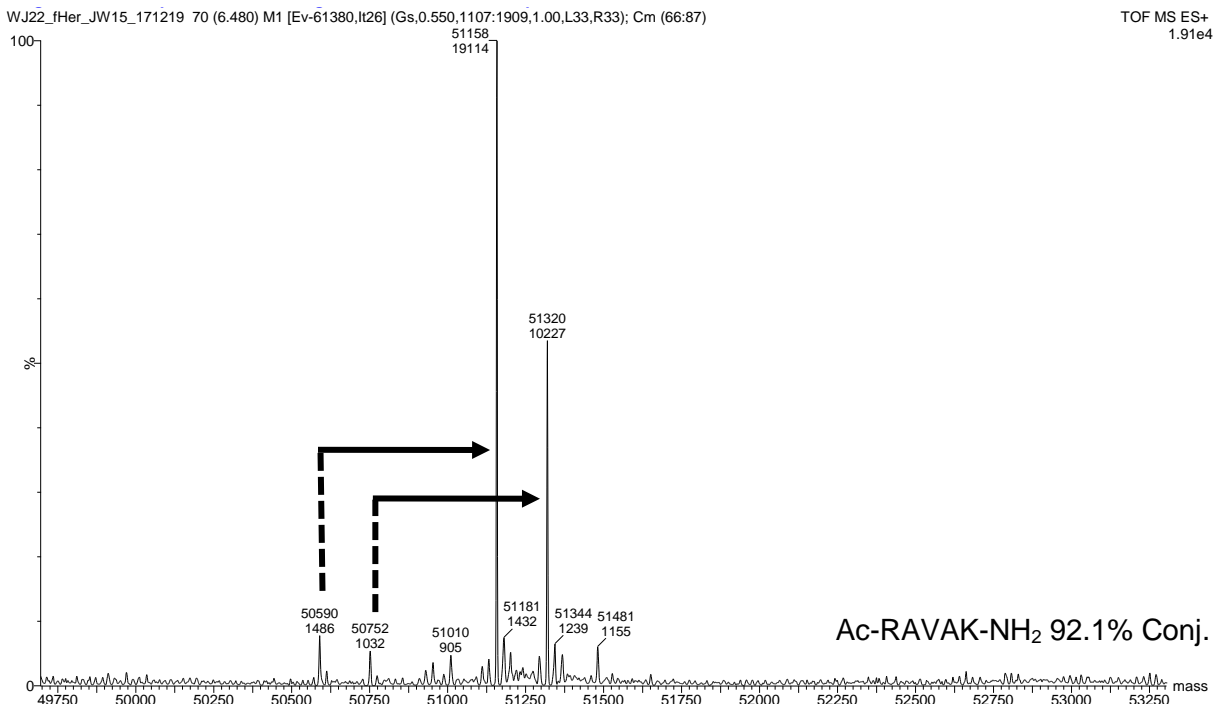


Figure A 40: Selected deconvoluted mass spectrum of mAb heavy chains after conjugation of peptide Ac-RAVAK-NH₂ (MW: 584.7 Da) with Trastuzumab using method 1. The two peaks at 50590 Da and 50752 Da correspond to two different glycosylations of native Trastuzumab. Calculated conjugated HC's: 51158 Da and 51320 Da; Detected conjugated HC's: 51158 Da and 51320 Da. The conjugation efficiency, calculated from the intensity, is 92.1%.

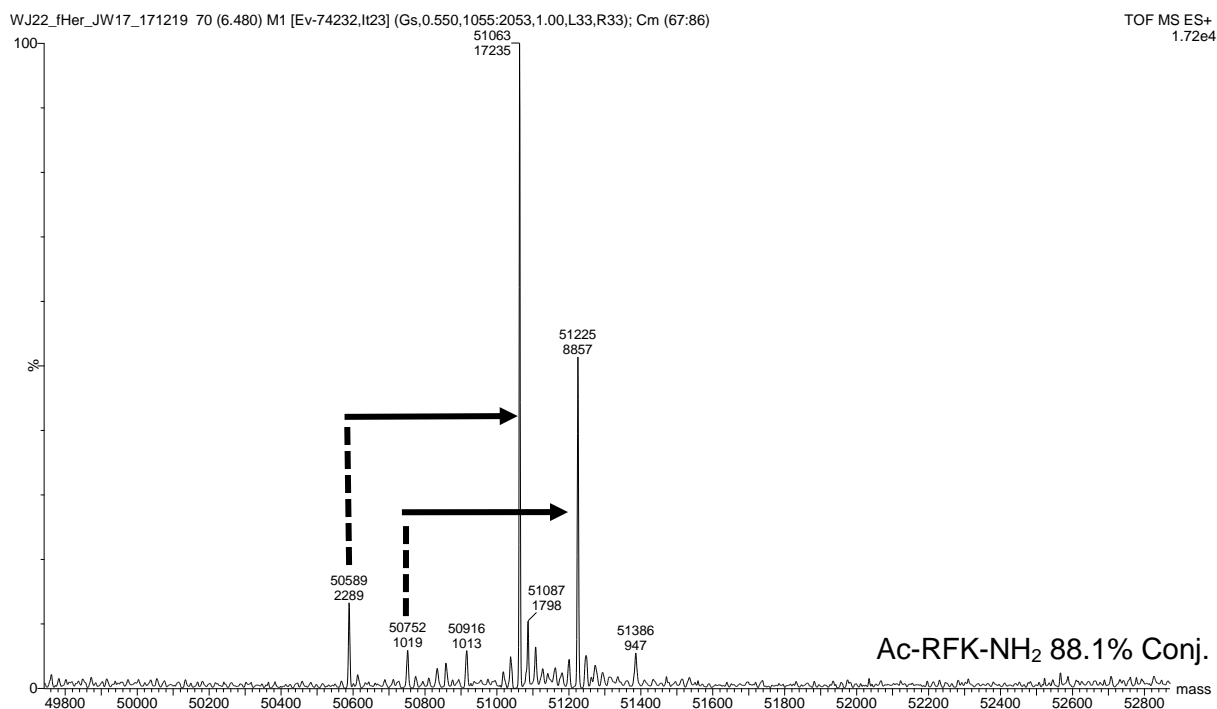


Figure A 41: Selected deconvoluted mass spectrum of mAb heavy chains after conjugation of peptide Ac-IFSK-NH₂ (MW: 534.7 Da) with Trastuzumab using method 1. The two peaks at 50589 Da and 50753 Da correspond to two different glycosylations of native Trastuzumab. Calculated conjugated HC's: 51107 Da and 51271 Da; Detected conjugated HC's: 51107 Da and 51269 Da. The conjugation efficiency, calculated from the intensity, is 91.9%.

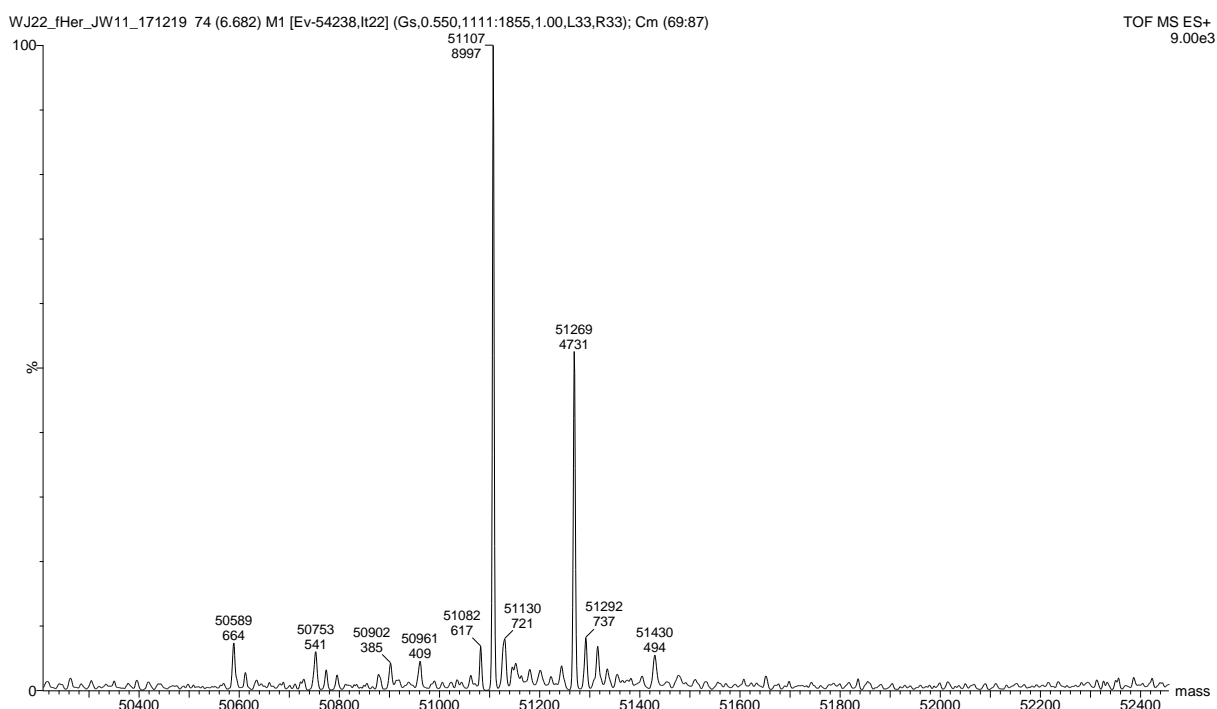


Figure A 42: Selected deconvoluted mass spectrum of mAb heavy chains after conjugation of peptide Ac-RFK-NH₂ (MW: 490.6 Da) with Trastuzumab using method 1. The two peaks at 50589 Da and 50752 Da correspond to two different glycosylations of native Trastuzumab. Calculated conjugated HC's: 51063 Da and 51226 Da; Detected conjugated HC's: 51063 Da and 51225 Da. The conjugation efficiency, calculated from the intensity, is 88.1%.

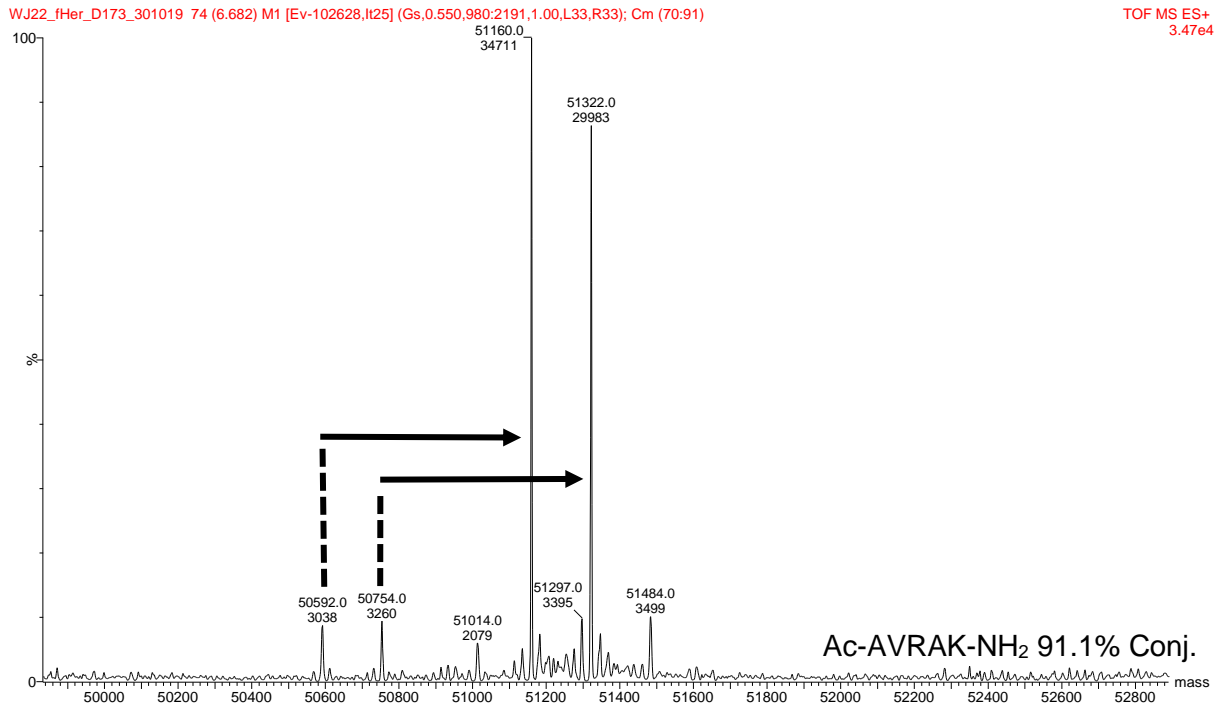


Figure A 43: Selected deconvoluted mass spectrum of mAb heavy chains after conjugation of peptide Ac-AVRAK-NH₂ (MW: 585.0 Da) with Trastuzumab using method 1. The two peaks at 50592 Da and 50754 Da correspond to two different glycosylations of native Trastuzumab. Calculated conjugated HC's: 51160 Da and 51322 Da; Detected conjugated HC's: 51160 Da and 51322 Da. The conjugation efficiency, calculated from the intensity, is 91.1%.

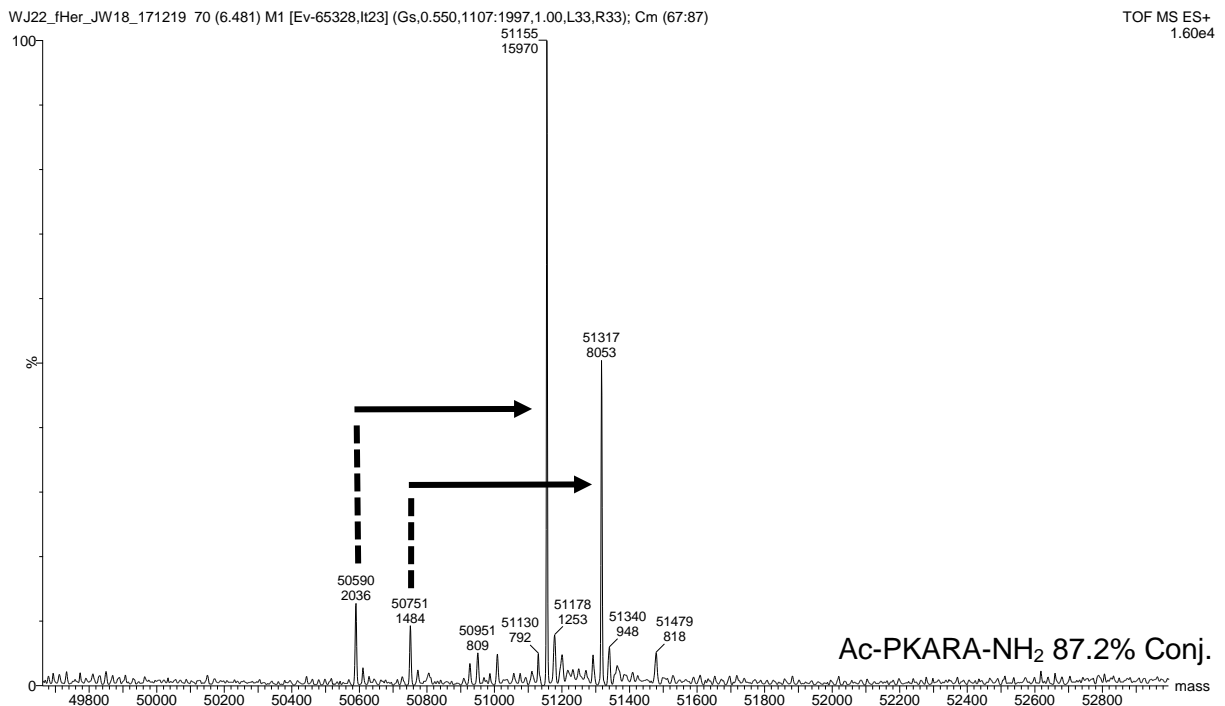


Figure A 44: Selected deconvoluted mass spectrum of mAb heavy chains after conjugation of peptide Ac-PKARA-NH₂ (MW: 582.7 Da) with Trastuzumab using method 1. The two peaks at 50590 Da and 50751 Da correspond to two different glycosylations of native Trastuzumab. Calculated conjugated HC's: 51156 Da and 51317 Da; Detected conjugated HC's: 51155 Da and 51317 Da. The conjugation efficiency, calculated from the intensity, is 87.2%.

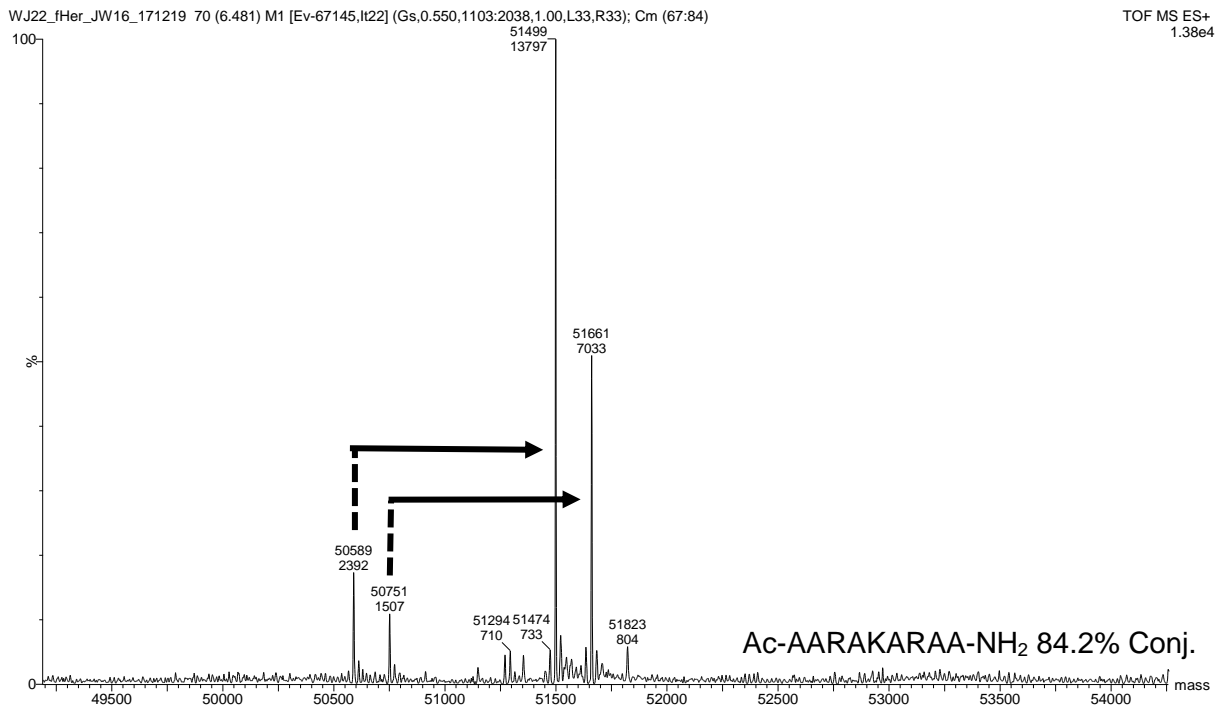


Figure A 45: Selected deconvoluted mass spectrum of mAb heavy chains after conjugation of peptide Ac-AARAKARAA-NH₂ (MW: 926.1 Da) with Trastuzumab using method 1. The two peaks at 50589 Da and 50751 Da correspond to two different glycosylations of native Trastuzumab. Calculated conjugated HC's: 51498 Da and 51660 Da; Detected conjugated HC's: 51499 Da and 51661 Da. The conjugation efficiency, calculated from the intensity, is 84.2%.

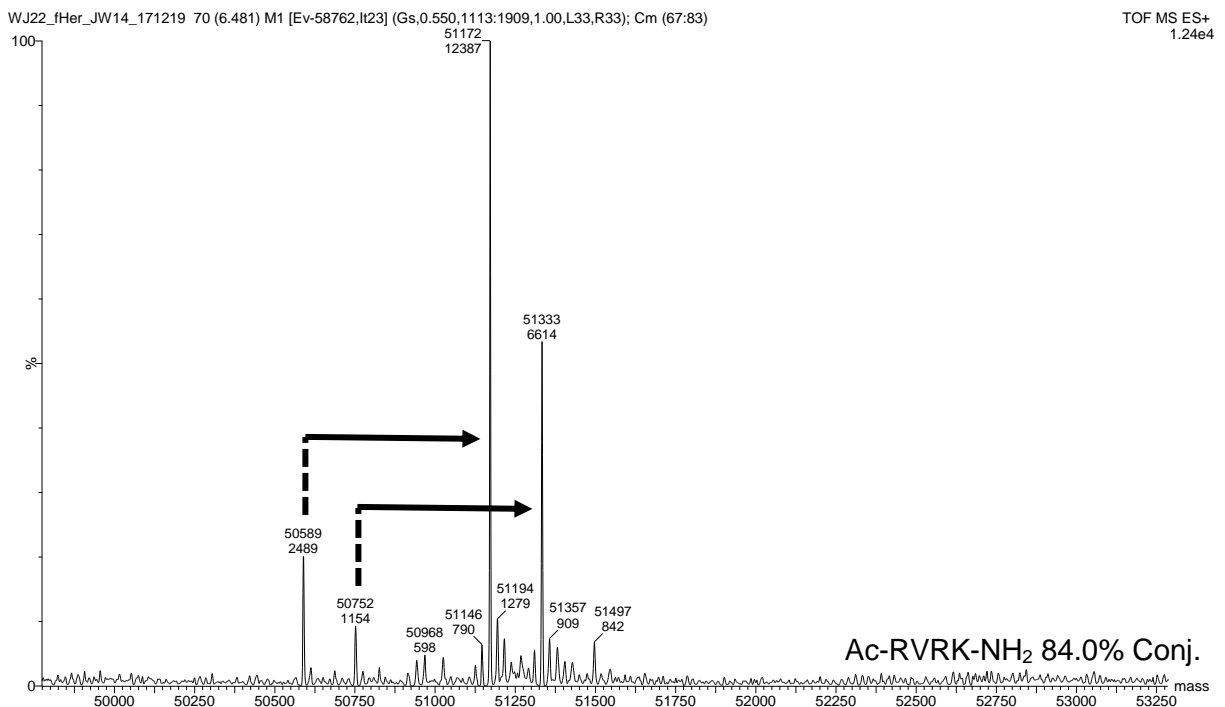


Figure A 46: Selected deconvoluted mass spectrum of mAb heavy chains after conjugation of peptide Ac-RVRK-NH₂ (MW: 598.8 Da) with Trastuzumab using method 1. The two peaks at 50589 Da and 50752 Da correspond to two different glycosylations

of native Trastuzumab. Calculated conjugated HC's: 51172 Da and 51334 Da; Detected conjugated HC's: 51172 Da and 51333 Da. The conjugation efficiency, calculated from the intensity, is 84.0%.

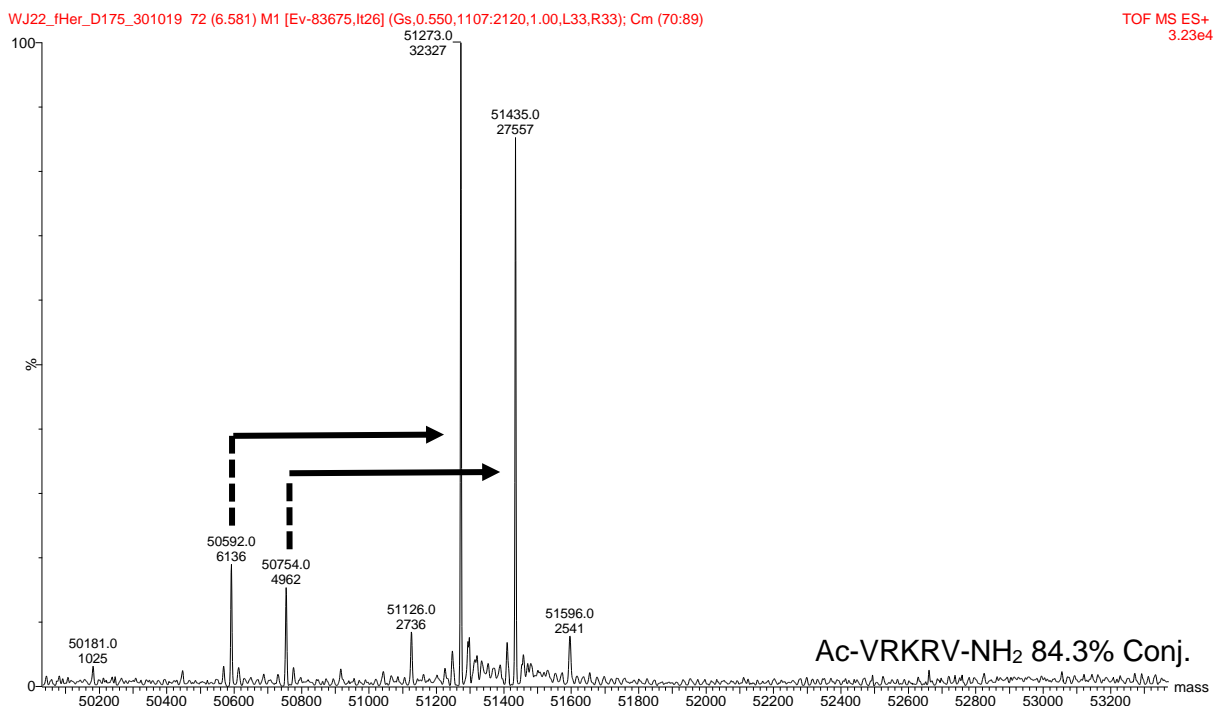


Figure A 47: Selected deconvoluted mass spectrum of mAb heavy chains after conjugation of peptide Ac-VRKRV-NH₂ (MW: 698.0 Da) with Trastuzumab using method 1. The two peaks at 50592 Da and 50754 Da correspond to two different glycosylations of native Trastuzumab. Calculated conjugated HC's: 51273 Da and 51435 Da; Detected conjugated HC's: 51273 Da and 51435 Da. The conjugation efficiency, calculated from the intensity, is 84.3%.

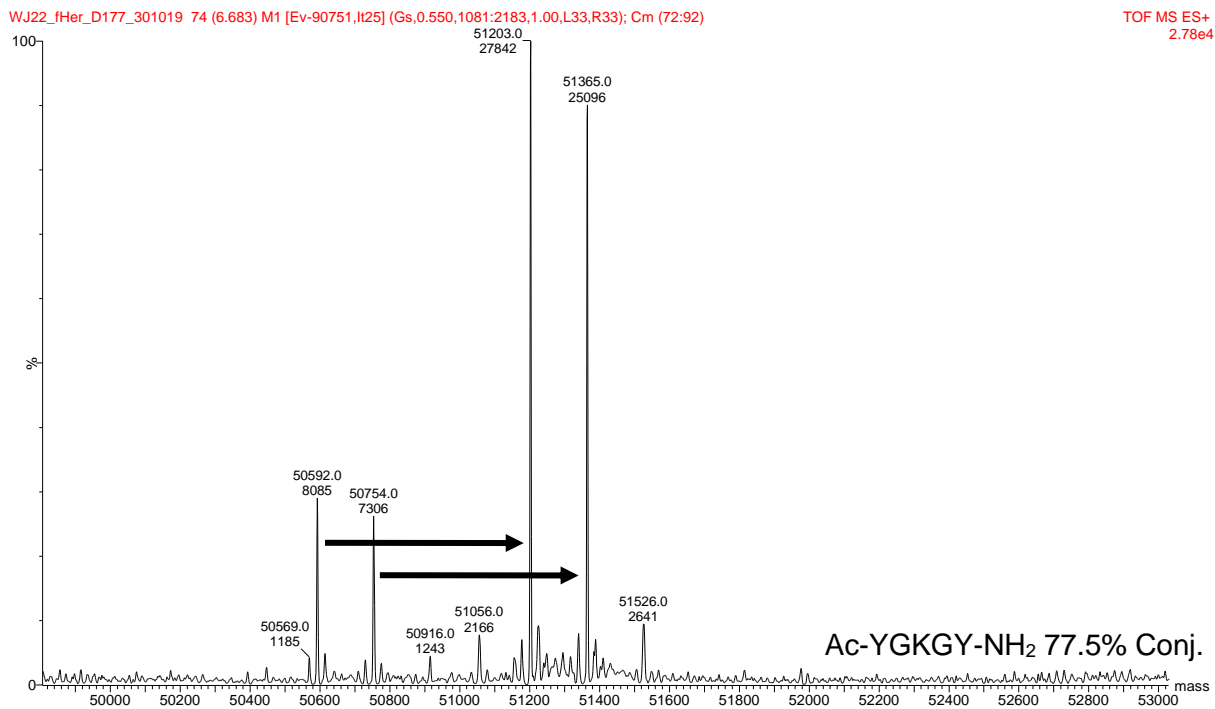


Figure A 48: Selected deconvoluted mass spectrum of mAb heavy chains after conjugation of peptide Ac-YGKGY-NH₂ (MW: 628.0 Da) with Trastuzumab using method 1. The two peaks at 50592 Da and 50754 Da correspond to two different glycosylations of native Trastuzumab. Calculated conjugated HC's: 51203 Da and 51365 Da; Detected conjugated HC's: 51203 Da and 51365 Da. The conjugation efficiency, calculated from the intensity, is 77.5%.

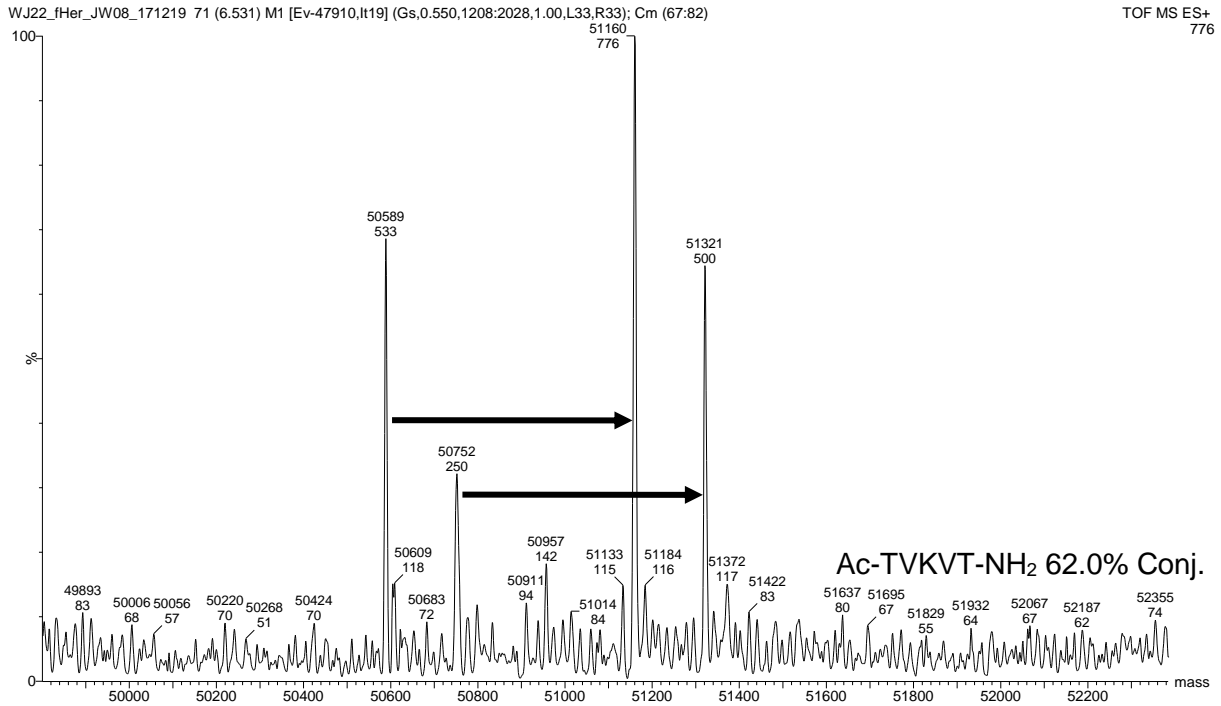


Figure A 49: Selected deconvoluted mass spectrum of mAb heavy chains after conjugation of peptide Ac-TVKVT-NH₂ (MW: 587.7 Da) with Trastuzumab using method 1. The two peaks at 50589 Da and 50752 Da correspond to two different glycosylations of native Trastuzumab. Calculated conjugated HC's: 51160 Da and 51323 Da; Detected conjugated HC's: 51160 Da and 51321 Da. The conjugation efficiency, calculated from the intensity, is 62.0%.

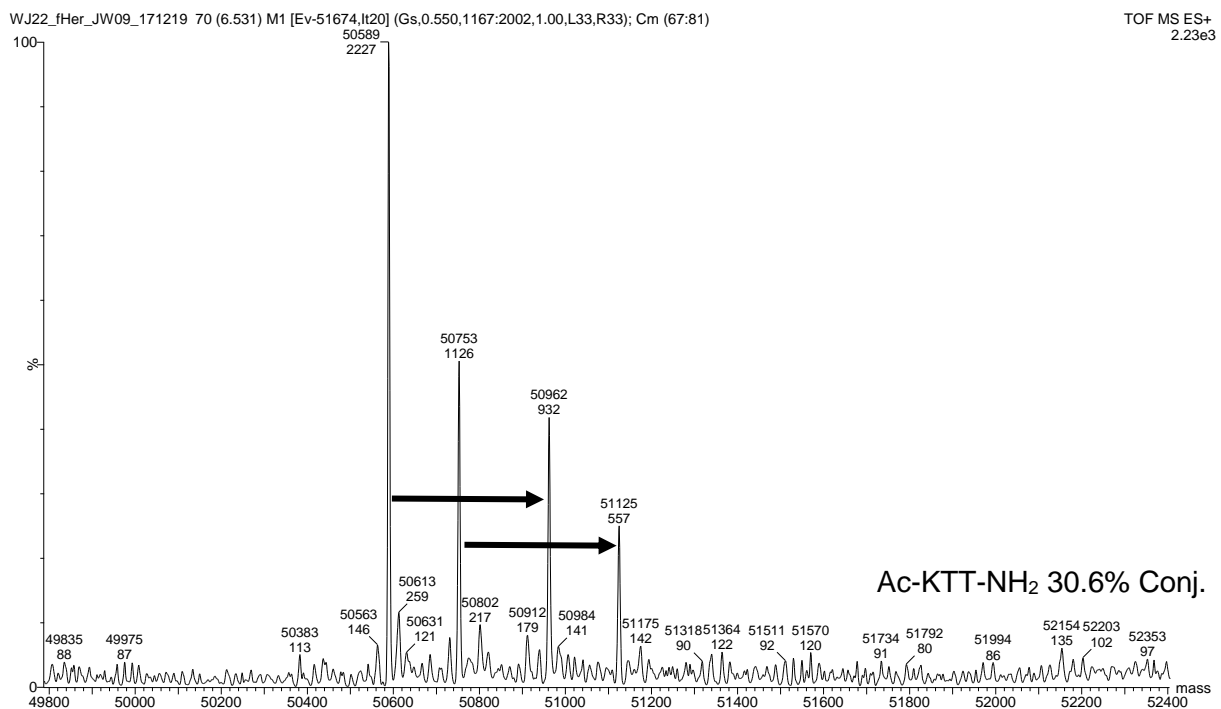


Figure A 50: Selected deconvoluted mass spectrum of mAb heavy chains after conjugation of peptide Ac-KTT-NH₂ (MW: 389.5 Da) with Trastuzumab using method 1. The two peaks at 50589 Da and 50753 Da correspond to two different glycosylations of native Trastuzumab. Calculated conjugated HC's: 50962 Da and 51126 Da; Detected conjugated HC's: 50962 Da and 51125 Da. The conjugation efficiency, calculated from the intensity, is 30.6%.

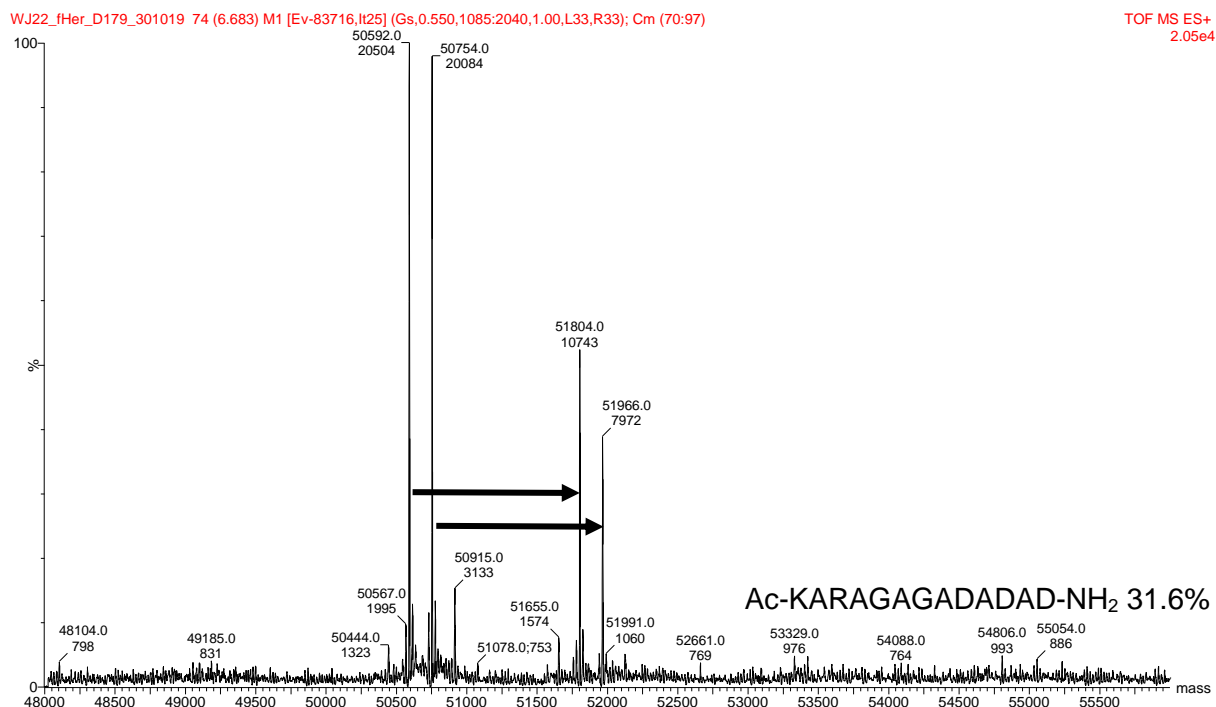


Figure A 51: Selected deconvoluted mass spectrum of mAb heavy chains after conjugation of peptide Ac-KARAGAGADADAD-NH₂ (MW: 1230.0 Da) with Trastuzumab using method 1. The two peaks at 50592 Da and 50754 Da correspond to two different glycosylations of native Trastuzumab. Calculated conjugated HC's: 51805 Da and 51967 Da; Detected conjugated HC's: 51804 Da and 51966 Da. The conjugation efficiency, calculated from the intensity, is 31.6%.

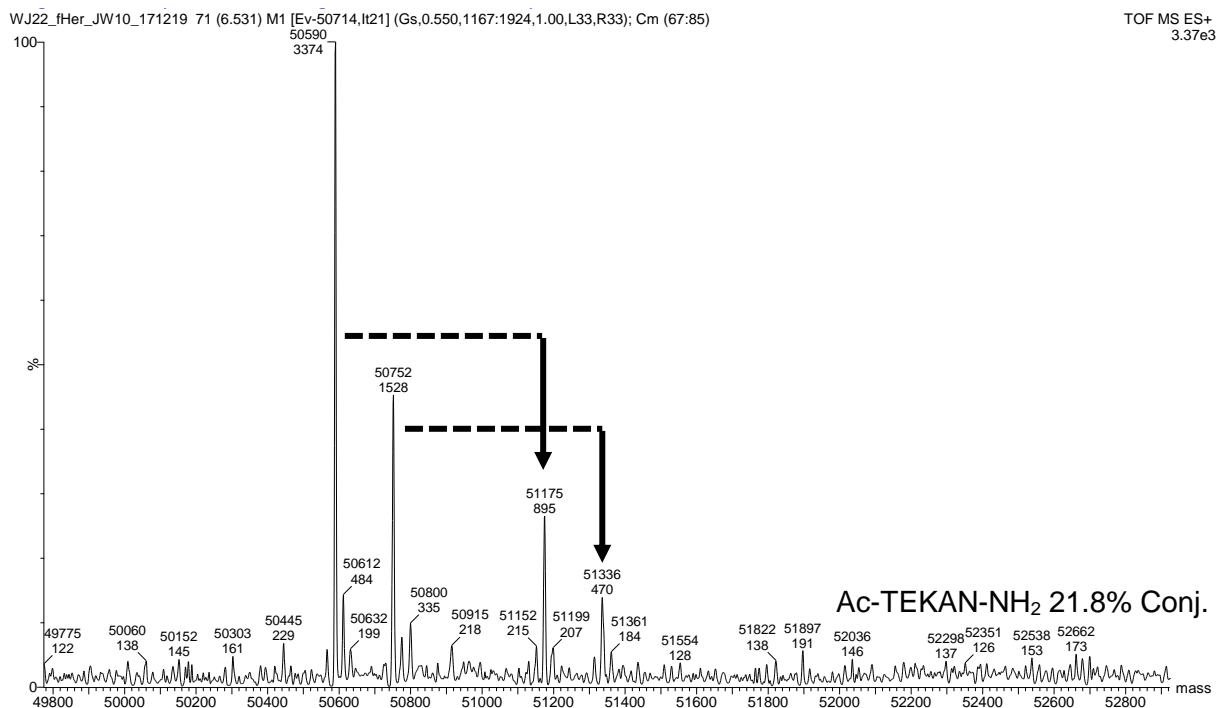


Figure A 52: Selected deconvoluted mass spectrum of mAb heavy chains after conjugation of peptide Ac-TEKAN-NH₂ (MW: 602.6 Da) with Trastuzumab using method 1. The two peaks at 50590 Da and 50752 Da correspond to two different glycosylations of native Trastuzumab. Calculated conjugated HC's: 51176 Da and 51338 Da; detected conjugated HC's: 51175 Da and 51336 Da. The conjugation efficiency, calculated from the intensity, is 21.8%.

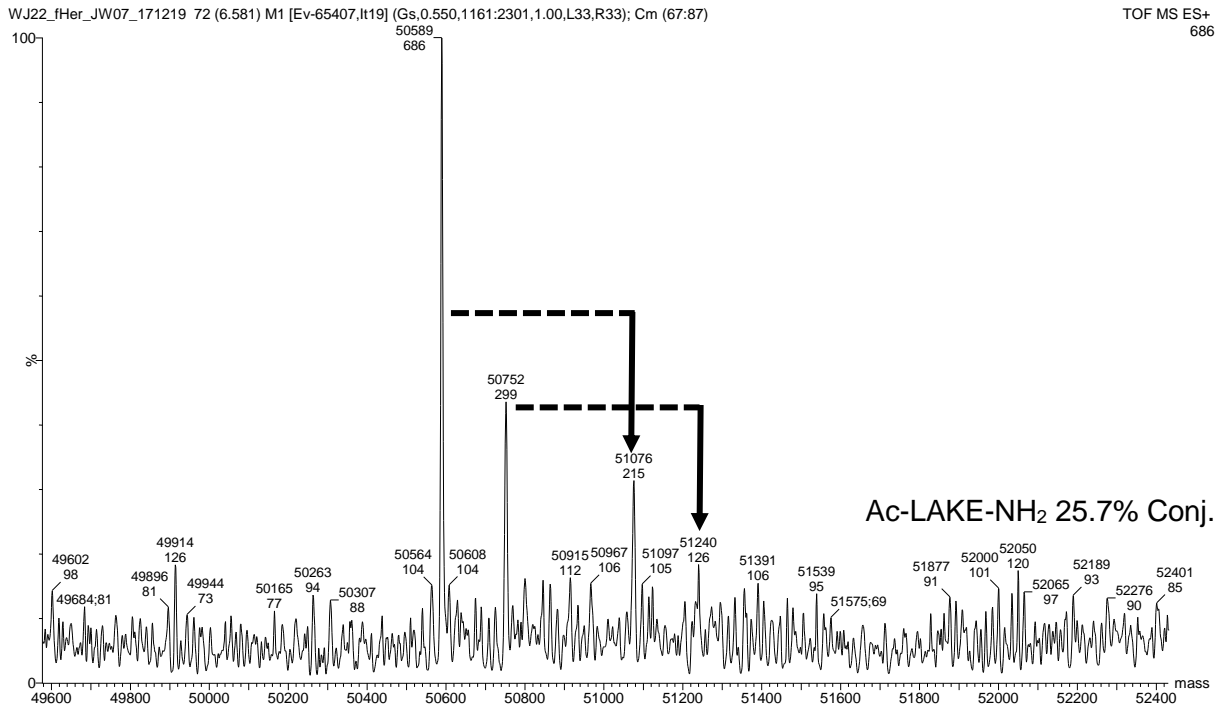


Figure A 53: Selected deconvoluted mass spectrum of mAb heavy chains after conjugation of peptide Ac-LAKE-NH₂ (MW: 500.6 Da) with Trastuzumab using method 1. The two peaks at 50589 Da and 50752 Da correspond to two different glycosylations of native Trastuzumab. Calculated conjugated HC's: 51073 Da and 51236 Da; Detected conjugated HC's: 51076 Da and 51240 Da. The conjugation efficiency, calculated from the intensity, is 25.7%.

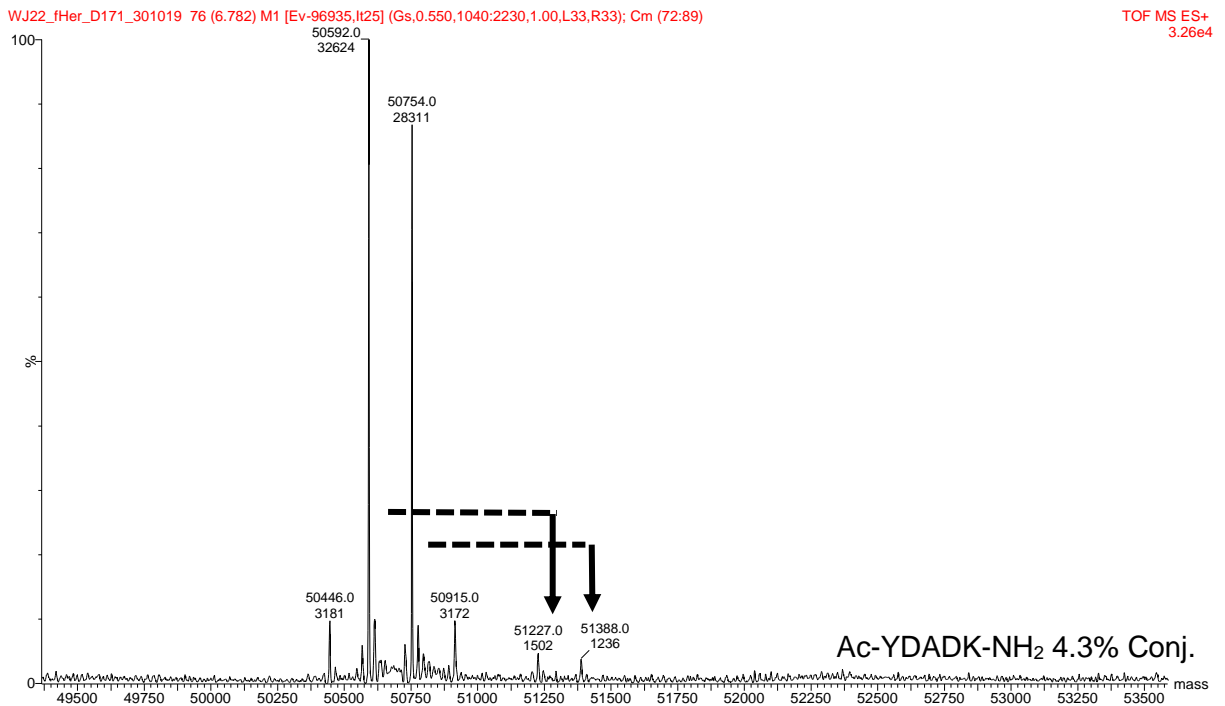


Figure A 54: Selected deconvoluted mass spectrum of mAb heavy chains after conjugation of peptide Ac-YDADK-NH₂ (MW: 652.0 Da) with Trastuzumab using method 1. The two peaks at 50592 Da and 50754 Da correspond to two different glycosylations of native Trastuzumab. Calculated conjugated HC's: 51227 Da and 51389 Da; Detected conjugated HC's: 51227 Da and 51388 Da. The conjugation efficiency, calculated from the intensity, is 4.3%.

13.2.2. 9x9 SOMs and SOM with 75% Threshold

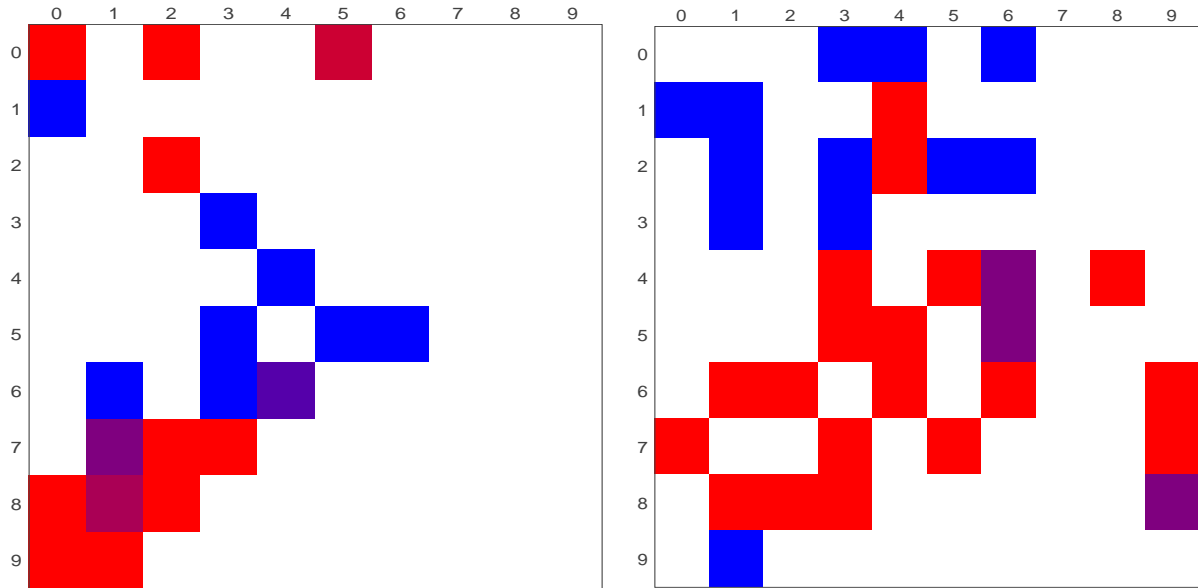


Figure A 55: 9x9 Self organizing map with 81 neurons (SOM). The input data is the peptide screening shown in chapter 5.2. The neurons are colored according to activity ranging from red (only actives) to blue (only inactives). The threshold for activity was >60% conjugation efficiency towards Trastuzumab. White neurons do not contain data points. The SOM map is toroidal. Visualization was done with SomVIS. Left: Descriptor pepCATS, with a cross-correlation distance of 3. 63 Dimensions. Right: ppCALI, with a cross-correlation distance of 3. 570 Dimensions.

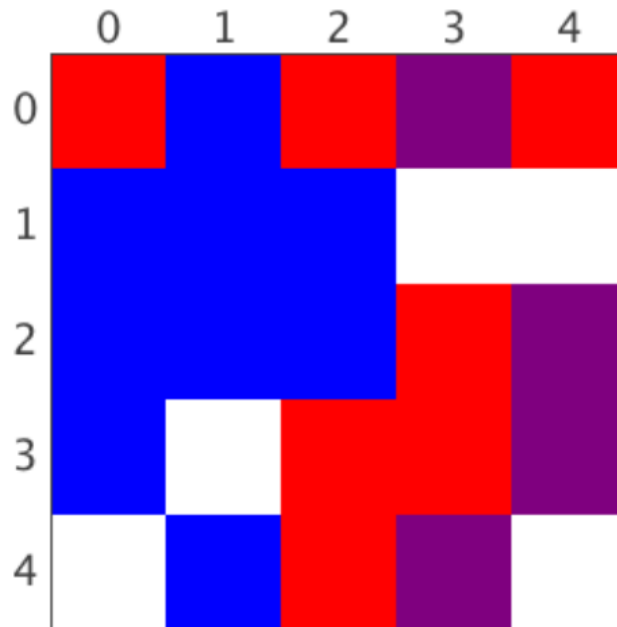


Figure A 56: 5x5 Self organizing map with 25 neurons (SOM). The neurons are colored according to activity ranging from red (only actives) to blue (only inactives). The threshold for activity was >75% conjugation efficiency towards Trastuzumab. White neurons do not contain data points. The SOM map is toroidal. Compared to the the SOM with a threshold of >60% (Figure 25), less active red neurons are visible (The same peptides were used to train as described in 5.2). The visualisation was done with SomVIS.

13.2.3. SOM with all sequences shown

Table A 5: Sequences from our screening together with the complete list of random fed sequences in their according neuron. The coordinates are 0-4 from left to right and 0-4 from top to bottom. The peptides with the additions 0 and 1 come from our experimental screening and were used to generate the SOM, whereas 0 are negative peptides, and 1 are positive (above 60% Conjugation efficiency) peptides.

HAKAH_1 HAKAHR SAKAS_1 TAKA LAKA CAKA SAKS	EAKAE_0 RADAKAEEE DEEKCEE LEKA REEK EEK EKNE ENK	RAKNA_1 RRAKANN AKNAANA ANAAKNA KNAAN NAAKN KNA NAK	KRAAR_0 RAAKR_1 KRAA_0 RAAK_1 RKAA_1	ARKRA_1
NKALPAP_0, HEALKNHY_0 RANDALF, RAKNDALF RANDALF, RKANDALF RANDKALF, PAVIKAN PAVIANK, FSSKALL RANDAKLF, PKAVIANK FLIPKNAR, HARNGAK PAVIANK, FLANKE KPAVIAN, ARGENTINAK IDEALK, ELNAKAN, PAVKIAN DAIKLENYS, KAPTAIN CRITICALK, PAKVIAN EANNKNNAE, DAILENYSK KAP, FLKAN, MKANIA, KFLAN NAANK, NKP, AVIKAN KAPTWN, KALIF MANIAK, MAKNIA FINKISH, FKLAN YANNKI, YANNIK, MANIKA SYNAGK, PANIKS, FIKNISH YKANNI, INKELN, VIKAN PNKAN, YANKNI, FINISHK KFINISH, DAIPK, NYYKA FINKEN, PKANA, KAIP PANIK, TIKIIP, YAKNNI FRINKEN, LIFKIN, PEKAN ALK, PNKNP, YKLLL, KFFP KINISH, LIAK, LIPIK, KANIS TANK, GEEKEL, VVLVKVLVV PAVK, LWKWL, LKWVL NANK, EPKVS, IFSK MNKNM, NVVK, PIAK HINK, LGAK, PINK, PKP FPK, PISK, NKNE, NMKNM KFNF, NKW, LKW, KSNF WWFK, FFFK, NNKN IPIK, KLL, KVVV, NNKNN NKNN, LIK, LKL, KANN, NNK KNS, KPN, KNNN, PKN, WKNN	AKETAA_0 FKETAA_0 TAKE KATAN TTAKATT TEKAN LAKE MAKE TVKVT TIKIT KAT KTT	KDAA_0 KDAVA_0 KMA	TKAAR, NKSAARK EDEAARAK, TKAAP VARKA, TAKAAP NSKAAR, SLAAKAR KAAP, SLARDARK NSAAKR, RANKDALF KRANDALF, KARTAIN NAAKAAN, TKAAN PKAAP, RATAK KNASCAR PRATAK PAAKP APKPA RANAWAK RAAAAAAKAAAAAR MKMAA FSKSAN NKAAN VKGA RAFTK NVKGA AAK AVIATIK VKSA SSAK KAC RCAK MEKA AKW YYAAK KAW AKF AAAAAAAKAAAA KAI GAK	NSAKARK, KARH, RANDKAR PKARR, KARL, SHKRAN NASCKAR, VKAR, SARK HANRGAK, KARWL HANGARK, RKCP, HKHR NKAR, KART, KLRH, AKR FLIPKIR, CERKAIN, FRKRF NARK, DKLR, DARK, VKVR SSRK, VRKR, KWCP, PARK TTRK, CVKVR, KFRM FRISPEK, KFRF, SECRETK RINKSH, EKMR, KVRV PRKAN, VVRK, SKR, SKR EVKR, RIJKIIR, MIJKIIR RHHHHHHH, VIFKFIV NERK, IKR, YAIKS, RTVKV RHHTKT, VKR, THKHN SSGK, KMRM, NKR, PPRK RVVK, RVVK, MHKHM VKMC, KRLL, RISK, CRITK HRK, SKH, FMKMF, RKME GVKVG, KISS, ESKF, RTTK HVKV, KRL, RINK STK, EVVK, FCK, WKR, TVK ERK, PWCK, VGTK, FFK RKW, VVK, VVKVVV KRF, KRM, VCK, RKV CWKW, KWW, MKH, VVK KVV, KVV, HKH, KMNM HKS, WWWWWIK, HKM PKW, EKS, WKW, KII, TKT TKT, WWW, KVN
RDKDR_0 DRDK RRDKDRR	KADDD_0 KDD_0 KDD DDK_0 DNDKDND	DDKAY_0 YDKDY KAY KYY KYY KMY	RKSR_1, RRSK DKSR, SSKS SKSS, SKS SSKSS, ISKSI KSSS, GGSKSGG NSKSNN, IKSS, KSS, RKS VKS, KSN, GSK	KRR_1 RRKRR RKR_1 RRRK RMRKRRR RVRK PKR
RYRYK_0 RYKYR_1 KYRYR_1 CYKYR YYRK FYKY GYKYG YKY YYKYY YRK YYYKYY	YDADK, YDADK, DYAYK DKVR, DKMR, EDEKA DEREKERED, DRECK DMKR, DEREK, DERNK MDKR, ENDEK, MENKY RKMD, RKLD, NKMD DVKV, YLKLY, DKVV NKLD, DVVK, HWDK MFKFM, DKW, KTY ISIK, DTK, ENEK, ENEKENE KENE, VEK, KDM, KDE MKY, YKE, EKY, MMMK KEM, DKN, IKI, EKE, KMN	KCKRAK_1	RGKGR_1 GRGK GRGK KGRG GGRGKGRGG RAKGGG GRRK RGGK KGNR KRG YKGY GRKNG KGNR KGI	RRK_1 RAK_1 RHK_1 RHK RYK_1 RPK RCK RVK RFK RGK RWK REK RNK

SDRAKARDS, KARY ELPRIKIR, SMARTK HARNK, KLRY DARTK, RIKAN SYRK, KYVAG EMREK, FRFK YCVRK, KYNAG NYKKYIN, YAKW RVKVT, LYKYL YKR, RIKN, AKY, YKV	DAKAR_1, DAKA, DAKA_0 DAKAD_0, ARAGAKADADAD ARAKAGADADAD KARAGAGADADAD ARAGAGAKDADAD ARAGAKGADADAD AKRAGAGADADAD ARAKGAGADADAD ARAGAGADADADK ADAKTA, GAGAKDADAD PAKAP, NSDAK, NAKAN NAKAN, ANAKANA MKANA, AKA, DLKL, KAM	RAKAR_1 RARAK_1 RAKA_1 ARAK DARAKARAD KARARARAR AARAKARAA ENDERARAKARAR MKARA PKARA AVRAK RAVAK	KHR_1 KYR_1 KAR_1 KFR KDR KCR KWR KVR KNR KER	RRAKARR RVKVR RVKVR RRFKFRR NGRAK RHKIP RIKL RMKMN MRMK RIKI WRK RKN
--	--	--	--	---

13.3. Chapter 6: Chemo-enzymatic functionalization of native antibodies with mono- and bifunctional peptide linkers and toxins

13.3.1. Flow cytometry assay with Trastuzumab-Ac-RAKAR-K(FAM)-NH₂

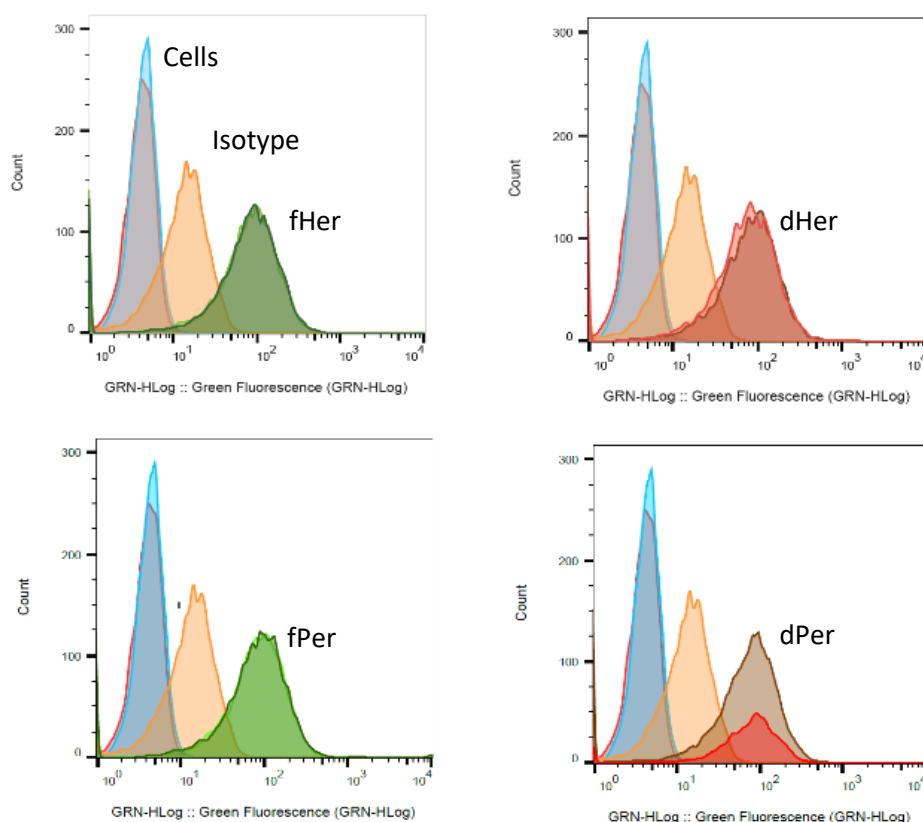


Figure A 57: FC binding results with the green fluorescence on the x-axis and counts on the y-axis. The cells without having any fluorescence dye attached are shown in blue. The isotype control is shown in orange. Top: Trastuzumab-Ac-RAKAR-K(FAM)-NH₂ binding is similar with the native (left, fHer) and deglycosylated (right, dHer) species. Bottom: Perjeta binding is similar with the native (left) and deglycosylated (right) species.

13.3.2. Lindmo assays

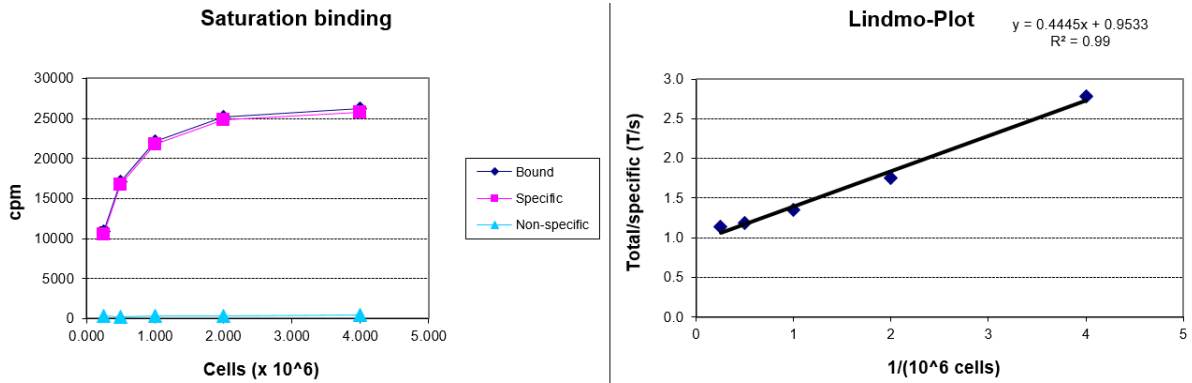


Figure A 58: Selected Lindmo assay: Left: Saturation binding plot of Trastuzumab-NH₂-K(maytansine)-C(NODAGA)-RAK-OH binding to Skov3ip cells. The x-axis shows the number of cells, the y-axis shows the counts per minute from ¹¹¹In. Right: Plotted are the total added cpm / specific bound cpm on the y-axis and the 1/ number of cells on the x-axis. The black line is the linear regression. The immunoreactive fraction can be calculated with $IF=1/\text{intercept} \times 100$ and was 105.8%.

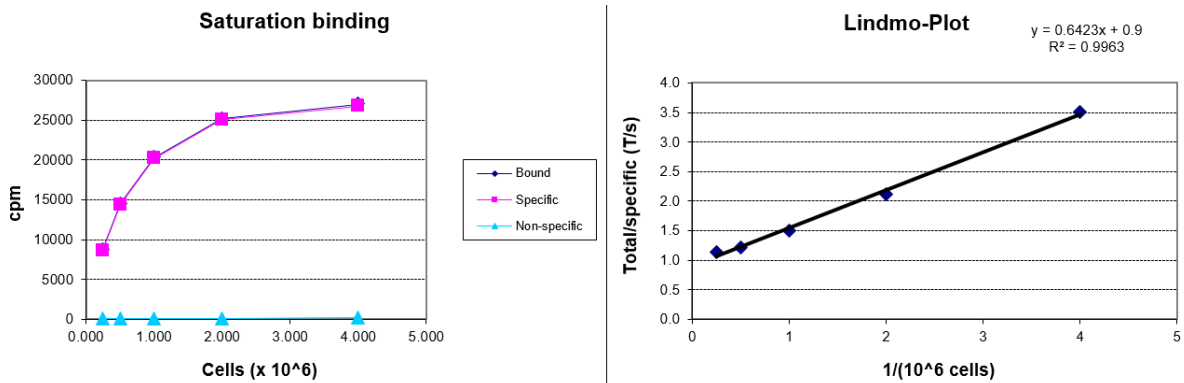


Figure A 59: Left: Saturation binding plot of Trastuzumab-NODAGA-K(N₃)-RAK-NH₂ binding to Skov3ip cells. The x-axis shows the number of cells, the y-axis shows the counts per minute from ¹¹¹In. Right: Plotted are the total added cpm / specific bound cpm on the y-axis and the 1/ number of cells on the x-axis. The black line is the linear regression. The immunoreactive fraction can be calculated with $IF=1/\text{intercept} \times 100$ and was 111.1%.

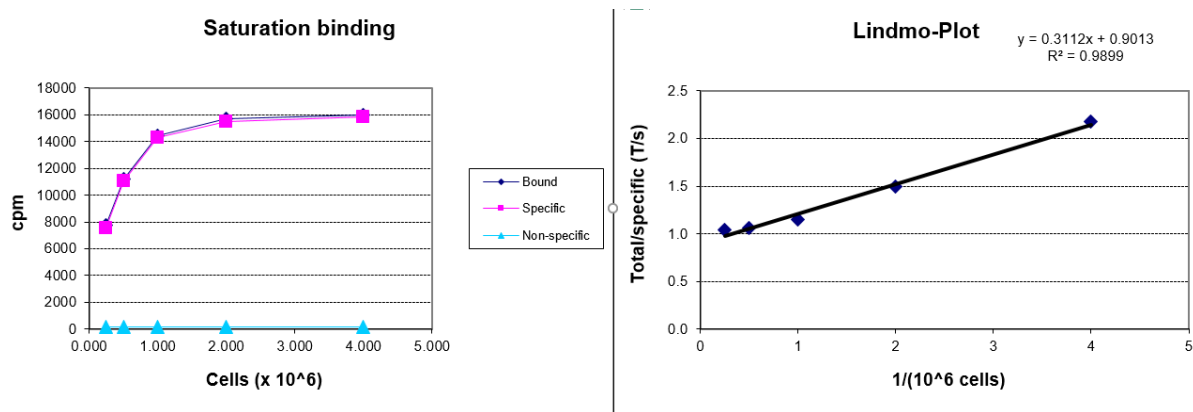


Figure A 60: Left: Saturation binding plot of Trastuzumab-NODAGA-K(maytansine)-RAK-NH₂ binding to Skov3ip cells. The x-axis shows the number of cells, the y-axis shows the counts per minute from ¹¹¹In. Right: Plotted are the total added cpm / specific bound cpm on the y-axis and the 1/ number of cells on the x-axis. The black line is the linear regression. The immunoreactive fraction can be calculated with $IF=1/\text{intercept} \cdot 100$ and was 110.9%.

13.3.3. DBCO-PEG₄-Ahx-maytansine clicking efficiencies using 2.5-10 eq. vs. Trastuzumab with Ac-RAK-K(N₃)-NH₂ conjugated

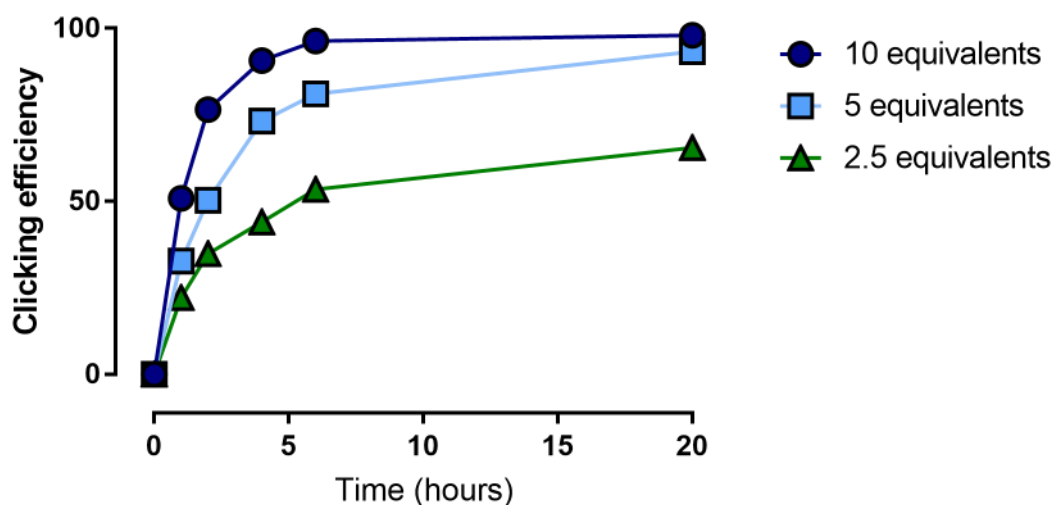


Figure A 61: Coupling yields of toxin DBCO-PEG₄-Ahx-maytansine with Trastuzumab-Ac-RAK-K(N₃)-NH₂ using three different conditions over time (2.5-, 5-, and 10 equivalents, reaction in Trizma pH 7.6 50 mM). Quantitative coupling was reached after 5 hours at room temperature with 10 equivalents of toxin per azide-group on the mAb. N=1

13.3.4. High resolution MS (MALDI) of NODAGA-K(N₃)-RAK-NH₂

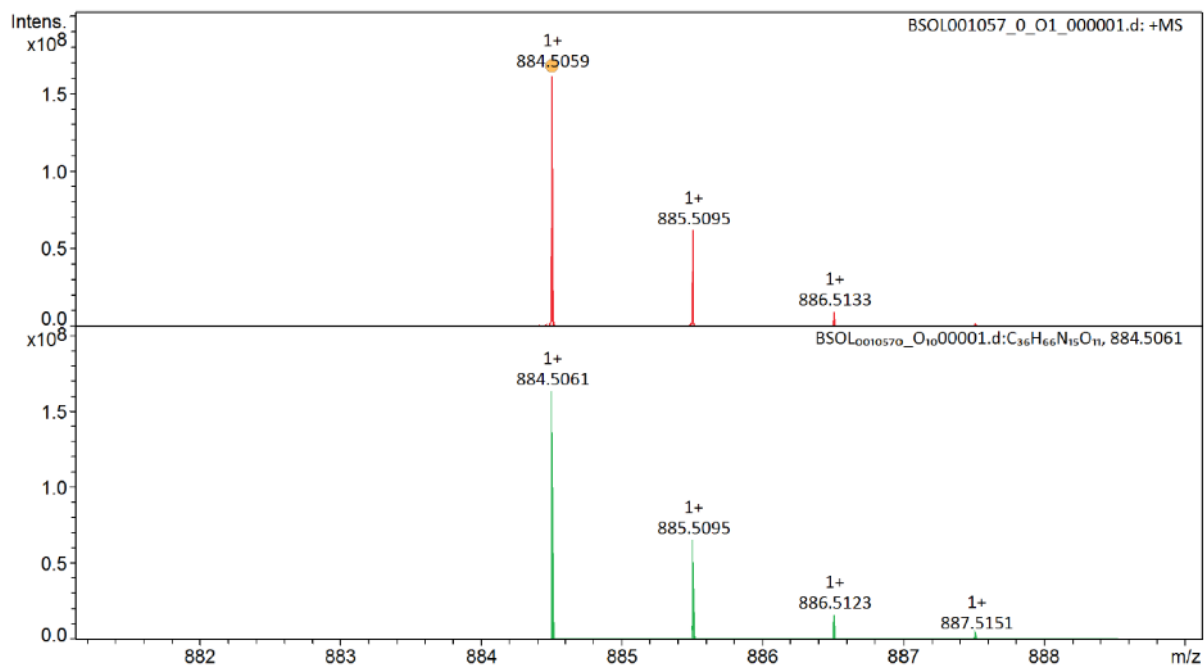


Figure A 62: High resolution MALDI/ESI MS confirms the mass of NODAGA-K(N₃)-RAK-NH₂ of 884.5 Da. The sample was submitted to and measured by the Molecular and Biomolecular Analysis Service (MoBiAS) ETHZ.

13.4. Chapter 7: Trastuzumab biodistribution with linker NH₂-K(N₃)-CRAK-OH and comparative biodistributions of NODAGA-K(N₃)-RAK-NH₂ with and without toxin

13.4.1. Biodistribution data of ¹¹¹In labeled Trastuzumab-NH₂-K(maytansine)-CRAK-OH

Table A 6: Biodistribution values after 48 h of compound Trastuzumab-NH₂-K(maytansine)-CRAK-OH with different co-injected amounts of native Trastuzumab. N=3

	48 h post-injection of ¹¹¹ In labeled Trastuzumab-NH ₂ -K(maytansine)-C(NODAGA)RAK-OH									
	0 mg/Kg		1.5 mg/Kg		5 mg/Kg		15 mg/Kg		30 mg/Kg	
Tumor	31.8	± 3.7	44.3	± 26.1	33.3	± 6.8	23.5	± 6.5	15.8	± 5.0
Liver	7.6	± 1.1	4.3	± 0.8	5.1	± 1.3	4.9	± 0.1	6.0	± 0.3
Spleen	10.9	± 4.6	4.3	± 0.7	4.9	± 1.8	4.3	± 0.6	4.6	± 0.3
Blood	7.7	± 2.7	12.8	± 2.2	10.1	± 1.7	11.6	± 1.5	14.7	± 1.9
Kidneys	4.4	± 0.6	4.7	± 0.6	4.7	± 0.2	5.0	± 0.5	5.9	± 0.5
Pancreas	1.7	± 0.1	1.6	± 0.3	2.2	± 1.0	1.6	± 0.2	2.0	± 0.1
Stomach	2.1	± 0.3	1.6	± 0.2	1.6	± 0.3	1.7	± 0.3	2.0	± 0.2
Intestines	2.6	± 0.8	1.6	± 0.2	1.8	± 0.4	1.7	± 0.2	2.2	± 0.2
Lung	4.5	± 1.0	6.0	± 0.9	5.0	± 0.8	5.8	± 0.9	8.1	± 0.9
Muscle	0.9	± 0.2	1.3	± 0.2	1.2	± 0.1	1.1	± 0.2	1.6	± 0.3
Bone	2.4	± 0.5	1.6	± 0.3	1.8	± 0.4	1.5	± 0.5	1.6	± 0.6
Heart	3.4	± 0.9	4.7	± 0.7	3.3	± 0.5	3.8	± 0.2	4.5	± 0.5

Table A 7: Biodistribution values after 96 h of compound Trastuzumab-NH₂-K(maytansine)-CRAK-OH with different co-injected amounts of native Trastuzumab. N=3, N_{0 mg/Kg}=2

	96 h post-injection of ¹¹¹ In labeled Trastuzumab-NH ₂ -K(maytansine)-C(NODAGA)RAK-OH									
	0 mg/Kg		1.5 mg/Kg		5 mg/Kg		15 mg/Kg		30 mg/Kg	
Tumor	25.4	± 3.4	36.1	± 19.4	40.7	± 4.9	33.2	± 7.3	22.2	± 4.4
Liver	7.9	± 0.8	4.8	± 2.5	4.9	± 1.0	4.6	± 0.3	5.8	± 0.8
Spleen	11.0	± 0.7	7.4	± 6.1	6.3	± 2.7	5.4	± 0.1	13.1	± 10.5
Blood	3.2	± 0.1	10.9	± 3.9	7.8	± 0.6	9.3	± 0.6	10.8	± 0.8
Kidneys	4.0	± 0.2	3.3	± 0.7	4.1	± 0.4	4.0	± 0.2	4.7	± 0.5
Pancreas	1.3	± 0.6	1.0	± 0.3	1.3	± 0.1	1.5	± 0.1	1.8	± 0.1
Stomach	1.5	± 0.7	1.3	± 0.2	1.3	± 0.3	1.5	± 0.3	1.4	± 0.2
Intestines	2.4	± 1.0	1.8	± 0.7	1.7	± 0.5	1.7	± 0.1	1.8	± 0.2
Lung	2.4	± 0.4	3.3	± 1.8	4.4	± 0.5	4.7	± 0.7	5.1	± 0.7
Muscle	0.8	± 0.2	0.8	± 0.2	0.9	± 0.1	1.1	± 0.1	1.1	± 0.2
Bone	2.2	± 0.5	1.6	± 0.3	1.4	± 0.4	1.8	± 0.1	1.9	± 0.1
Heart	1.8	± 0.3	2.4	± 1.2	2.8	± 0.1	2.9	± 0.4	4.0	± 0.3

Table A 8: Tumor to blood/liver ratios of the biodistribution with species Trastuzumab-NH₂-K(maytansine)-CRAK-OH. Calculated from the corresponding ratio of each mouse. N=3

	Tumor to blood ratio				Tumor to liver ratio				
	48 h		96 h		48 h		96 h		
0 mg/kg	4.3 ±	0.8	7.4 ±	1.2	0 mg/kg	4.3 ±	0.9	6.3 ±	4.4
1.5 mg/kg	3.6 ±	1.8	3.8 ±	1.9	1.5 mg/kg	10.4 ±	5.0	9.9 ±	6.4
5 mg/kg	3.3 ±	0.6	5.2 ±	0.2	5 mg/kg	6.7 ±	1.1	8.7 ±	2.2
15 mg/kg	2.0 ±	0.5	3.5 ±	0.5	15 mg/kg	4.8 ±	1.1	7.2 ±	0.9
30 mg/kg	1.1 ±	0.4	2.1 ±	0.4	30 mg/kg	2.6 ±	0.7	3.9 ±	1.0

13.4.2. Biodistribution data of ^{111}In labeled Trastuzumab-NODAGA-K(N_3)-RAK-NH₂, Trastuzumab-NODAGA-K(maytansine)-RAK-NH₂, and Trastuzumab_{deglyc.}-NODAGA-K(maytansine)-RAK-NH₂

Table A 9: Biodistribution values of compound Trastuzumab-NODAGA-K(N_3)-RAK-NH₂ at time points 24 h, 48 h, 72 h, and 96 h. N=4

^{111}In labeled Trastuzumab-NODAGA-K(N_3)-RAK-NH ₂								
	24 h		48 h		72 h		96 h	
Tumor	26.5 ±	8.3	41.4 ±	16.3	48.6 ±	8.9	46.9 ±	12.3
Liver	3.6 ±	0.5	4.2 ±	0.8	3.5 ±	0.8	3.8 ±	0.5
Spleen	3.7 ±	0.5	4.1 ±	0.6	3.6 ±	0.4	4.1 ±	0.5
Blood	10.9 ±	1.2	11.2 ±	1.3	9.2 ±	1.2	7.5 ±	0.8
Kidneys	8.2 ±	0.5	7.8 ±	1.1	6.8 ±	0.7	6.1 ±	0.4
Pancreas	2.0 ±	0.1	1.8 ±	0.5	1.7 ±	0.2	1.7 ±	0.1
Stomach	1.8 ±	0.3	1.7 ±	0.5	1.6 ±	0.3	1.5 ±	0.2
Intestines	2.0 ±	0.2	2.0 ±	0.5	1.4 ±	0.3	1.2 ±	0.1
Lung	5.8 ±	0.7	5.7 ±	1.1	5.1 ±	0.4	4.3 ±	0.1
Muscle	1.3 ±	0.1	1.2 ±	0.2	1.3 ±	0.2	0.9 ±	0.1
Bone	2.3 ±	0.0	2.4 ±	0.6	2.5 ±	0.3	2.3 ±	0.3
Heart	3.3 ±	0.4	3.5 ±	0.6	3.0 ±	0.5	2.4 ±	0.3

Table A 10: Biodistribution values of compound Trastuzumab-NODAGA-K(maytansine)-RAK-NH₂ at time points 24 h, 48 h, 72 h, and 96 h. N=4

^{111}In labeled Trastuzumab-NODAGA-K(maytansine)-RAK-NH ₂								
	24 h		48 h		72 h		96 h	
Tumor	21.4 ±	4.8	30.7 ±	16.5	28.2 ±	19.3	41.3 ±	15.4
Liver	8.4 ±	5.8	8.6 ±	3.8	9.0 ±	4.4	5.3 ±	0.9
Spleen	9.9 ±	9.6	11.0 ±	6.9	9.9 ±	5.4	5.7 ±	1.0
Blood	9.7 ±	4.2	8.2 ±	6.3	5.9 ±	5.8	7.9 ±	2.8
Kidneys	7.3 ±	0.3	7.4 ±	1.1	5.8 ±	1.4	5.9 ±	0.7
Pancreas	1.8 ±	0.2	1.8 ±	0.4	1.6 ±	0.4	1.8 ±	0.2
Stomach	2.1 ±	0.4	2.0 ±	0.3	1.7 ±	0.3	1.7 ±	0.3
Intestines	2.9 ±	1.2	2.8 ±	0.8	2.2 ±	0.3	1.4 ±	0.3
Lung	5.6 ±	1.7	4.8 ±	2.3	3.7 ±	2.4	4.7 ±	1.3
Muscle	1.2 ±	0.3	1.2 ±	0.2	0.9 ±	0.3	1.2 ±	0.4
Bone	3.3 ±	1.8	3.5 ±	1.3	3.2 ±	0.7	2.3 ±	0.4
Heart	3.8 ±	0.8	3.3 ±	1.1	2.7 ±	0.9	2.9 ±	1.1

Table A 11: Biodistribution values of compound Trastuzumab_{deglyc.}-NODAGA-K(maytansine)-RAK-NH₂ at time points 24 h, 48 h, 72 h, and 96 h. N=4

¹¹¹ In labeled Trastuzumab _{deglyc.} -NODAGA-K(maytansine)-RAK-NH ₂								
	24 h	48 h		72 h		96 h		
Tumor	24.7 ±	13.1	42.9 ±	21.4	38.0 ±	22.4	36.1 ±	17.6
Liver	10.0 ±	6.2	6.5 ±	2.3	6.1 ±	2.1	5.3 ±	1.2
Spleen	12.6 ±	10.4	7.3 ±	4.5	7.5 ±	3.1	6.9 ±	4.4
Blood	8.4 ±	5.9	10.7 ±	6.6	7.5 ±	4.9	8.4 ±	4.7
Kidneys	4.6 ±	0.9	4.8 ±	1.7	3.6 ±	1.4	4.0 ±	1.5
Pancreas	1.6 ±	0.2	1.8 ±	0.2	1.4 ±	0.2	1.6 ±	0.3
Stomach	2.4 ±	0.5	2.0 ±	0.1	1.7 ±	0.3	1.7 ±	0.4
Intestines	3.3 ±	1.7	2.3 ±	0.8	2.0 ±	0.1	1.6 ±	0.4
Lung	4.7 ±	2.9	6.3 ±	2.9	4.9 ±	2.8	5.0 ±	2.3
Muscle	1.2 ±	0.6	1.3 ±	0.6	1.1 ±	0.3	1.2 ±	0.4
Bone	3.7 ±	2.0	2.4 ±	0.9	2.5 ±	0.4	2.2 ±	0.4
Heart	4.4 ±	1.2	4.0 ±	1.3	2.7 ±	1.1	2.8 ±	0.8

Table A 12: Tumor to blood/liver ratio of the biodistribution. Calculated from the corresponding ratio of each mouse. N=4

	Tumor to blood ratio			
	24 h	48 h	72 h	96 h
Trastuzumab-NODAGA-K(N ₃)-RAK-NH ₂	2.4 ± 0.7	3.7 ± 1.2	5.3 ± 0.2	6.4 ± 2.1
Trastuzumab-NODAGA-K(maytansine)-RAK-NH ₂	2.5 ± 0.7	4.9 ± 1.9	8.4 ± 4.9	5.3 ± 0.7
Trastuzumab _{deglyc.} -NODAGA-K(maytansine)-RAK-NH ₂	4.2 ± 2.6	5.9 ± 3.5	5.7 ± 1.4	4.8 ± 1.4

	Tumor to liver ratio			
	24 h	48 h	72 h	96 h
Trastuzumab-NODAGA-K(N ₃)-RAK-NH ₂	7.5 ± 2.6	9.9 ± 2.5	13.9 ± 1.2	12.7 ± 4.4
Trastuzumab-NODAGA-K(maytansine)-RAK-NH ₂	3.6 ± 2.0	4.6 ± 3.2	4.6 ± 3.6	8.2 ± 3.5
Trastuzumab _{deglyc.} -NODAGA-K(maytansine)-RAK-NH ₂	3.5 ± 2.3	7.9 ± 4.2	7.8 ± 5.9	7.2 ± 3.1

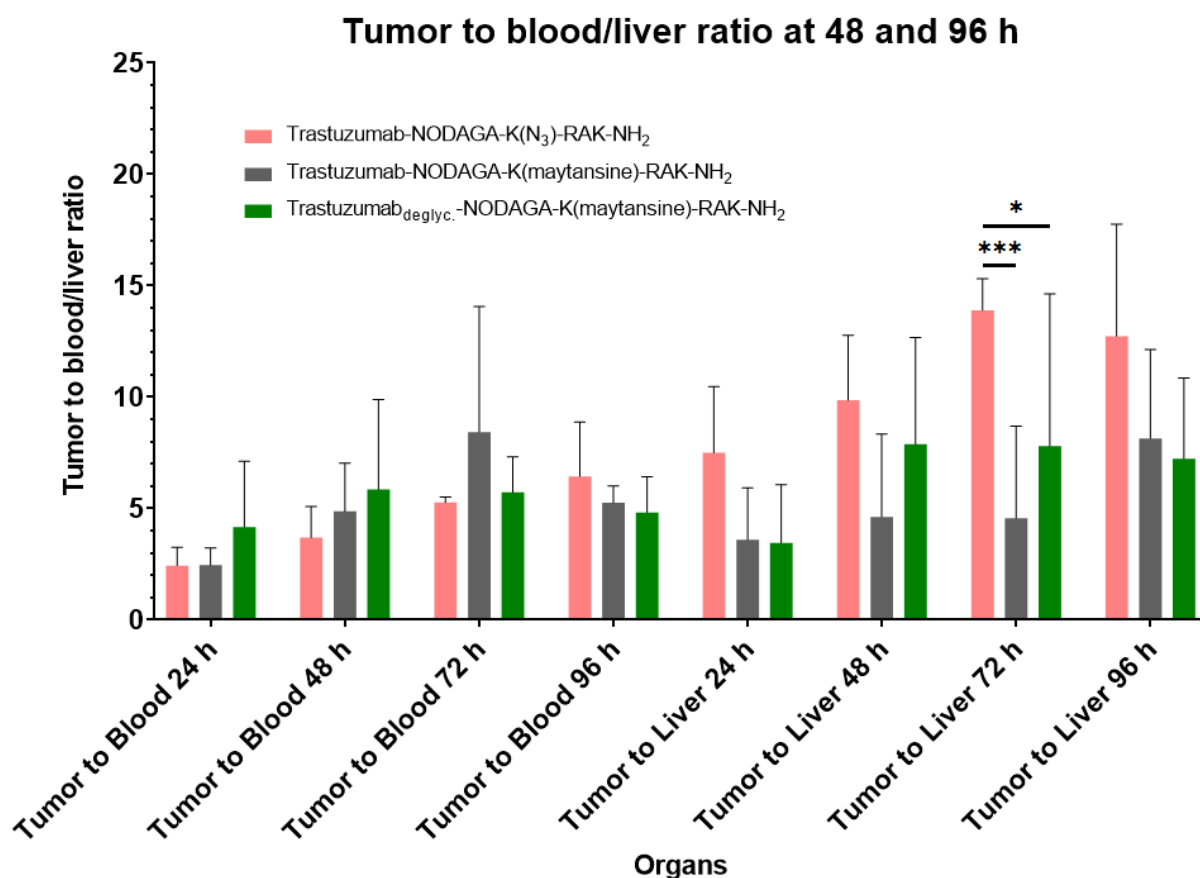


Figure A 63: Organ uptake ratio between tumor and blood/liver of the three In-111 labelled ADC constructs Trastuzumab-NODAGA-K(N₃)-RAK-NH₂ (red), Trastuzumab-NODAGA-K(maytansine)-RAK-NH₂ (blue), and Trastuzumab_{deglyc.}-NODAGA-K(DM)-RAK-NH₂ (green) at time points 24/48/72 and 96 h. N=4, Statistical analysis: 2-way Anova Bonferroni analysis in Graphpad with $p \leq 0.05$.

13.5. Chapter 8: Site-specific MTG mediated conjugation and SPECT of an EGFR-Nanobody

13.5.1. Sequence of 7d12 with myc- and His-tag

QVKLEESGGGSVQTGGSLRLTCAASGRTRS**SYGMG**WFRQAPGKEREFVS**GISWRGDSTGYADSVKGR**RFTISRDN
 KNTVDLQMNSLKPEDTAIYYCAA**AAGSAWYGTLYEYDY**WGQGTQVTVSSLEEQLISEEDLHHHHHH

Complementarity-determining region 1,2 and 3

Framework regions 1,2,3 and 4

Figure A 64: Amino acid sequence of nanobody 7d12. In yellow shade, the complementary-determining region is displayed.

13.5.2. Labeling of 7d12-VG49 and 7d12-VG56 with ^{111}In , and Lindmo with 7d12-VG56

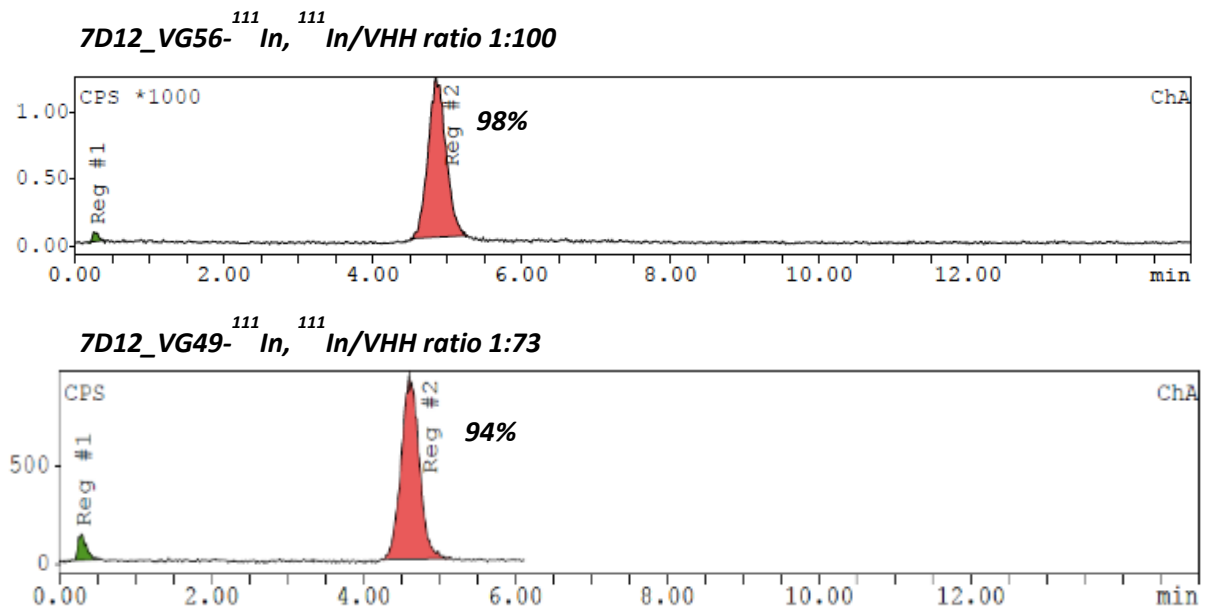


Figure A 65: Selected HPLC spectra of ^{111}In labeled 7d12-VG56 (top) and 7d12-VG49 (bottom). The efficiency was 98% and 94%, respectively. The small green peak at the beginning is free non-labeled ^{111}In .

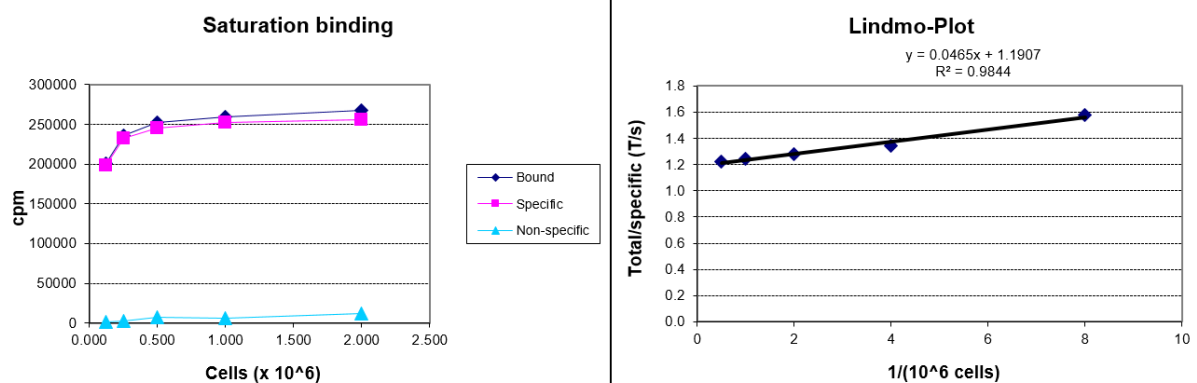


Figure A 66: Lindmo assay results of VHH 7d12-VG56 with A431 cells. The immunoreactive fraction was 84%. Non-specific binding was determined by blocking with an excess of mAb Cetuximab. The linear regression has an R^2 of 0.9844. Analysis was made in Excel. $N=3$ for each group of cells.

14. CURRICULUM VITAE

Jöri
Wehrmüller

Curriculum
Vitae

Dialogweg 6
8050 Zurich, Switzerland
+41 (0) 78 670 1700
joeriwe@hotmail.com
Born in Lucerne, Switzerland, November 14, 1988



I am an empathetic team player with a creative and innovative mind. I am self-motivated, pragmatic, and bring strong analytical skills

Education


- 11/2016-11/2020 **PhD student**, *ETH/PSI*, Zurich/Villigen, Defence in November.
- 09/2014-09/2016 **MSc. Biological Chemistry**, *ETH/Caltech*, Zurich/Pasadena.
- 10/2011-09/2014 **BSc. Biology, Chemical Direction**, *ETH*, Zurich.
- 09/2010-09/2011 **Assessment year**, *Kantonsschule Reussbühl MSE*, Reussbuehl.
Top grade
- 08/2009-07/2010 **Berufsmatura**, *Berufs- und Weiterbildung Kanton Luzern*, Lucerne.
Technical direction

Work and Lab Experience

- 11/2016-11/2020 **PhD student**, *Schibli Group*, Paul Scherrer Institute/ETH Zurich.
Managing stand alone project that lead to the successful development of a new enzymatic technology to produce site-specific Antibody-Drug-Conjugates. I gained experiences in:
- Diverse biochemical/enzymatic assays (including HPLC/MS, work with radioactive Tracers, and chemical/ chemo-enzymatic bioconjugations)
 - In vitro assays with human cancer cells and in vivo assays with mice
 - Peptide Synthesis
 - Project management
 - Troubleshooting
 - Communication Skills/Team Work/Supervision of Students
 - Collaborations with Academia and Industry including GMP-like work
 - Giving oral Presentations in- and outside of the Group
- 10/2016-12/2019 **Teaching**, *D-CHAB*, ETH Zurich.
Assistant in practical Chemistry courses in groups of up to 20 students, with positive feedback of the students and the examiner (approx. 200 hours)

- 2014-2016 **Master's and Semester Thesis**, *Arnold/Hilvert/Schertler Group*, California Institute of Technology / ETH Zurich.
Three projects (3/3/6 months) with focus on enzyme engineering and programming, among them working for 6-months in the United States on the Synthesis of Tryptophan Analogues
- 2014 **Multiple 3-week Practical lab projects**, *ETH Zurich*.
Focus on X-Ray Crystallography, NMR Spectroscopy, and Protein Folding
- 2009-2014 **Truck Driver**, *Franz Arnold GmbH*, Hochdorf.
Transporting milk from the farmers in the regions Lucerne/Berne/Aargau to the dairy product companies. At weekends and during holidays
- 07/2008-05/2009 **Military Service**, *Swiss Military*, Spiez/Burgdorf.
Training as a truck driver and in Nuclear/Biological/Chemical defense for one year
- 08/2005-06/2008 **Vocational Education as Chemical Laboratory Assistant**, *Emmi Milch AG*, Dagmersellen.
Training in diverse analytical skills with a focus on dairy products, in a highly regulated environment. The final exam was passed with distinction

Patents and Publications

- Patents **WO/2019/057772 and WO/2020/188061**.
Invented during my PhD thesis, resulting in Start up Araris (www.ararisbiotech.com)
- US20180057806**.
Invented during my Master's thesis, licenced from Start up Aralez Bio (www.aralezbio.com)
- Publications Co-author on two publications, one first-author in preparation 

ICT

- Basic Perl, R, CorelDRAW, C++
- Intermediate L^AT_EX, Chemdraw, GraphPad Prism, GIMP, Pymol
- Advanced Microsoft Office, OpenOffice

Languages

- German Mother tongue
- English Fluent (written and oral)
- French Solid knowledge (oral)
- 2009 **Language Stay**, Montpellier, Two months training in French.
- 2010 **Language Stay**, San Francisco, Two months training in English.

Interests and Extracurricular Activity

- Former member/president in the career commission of the Pharmacy Student Association (PSA) at ETH
- Integration Mentoring for Refugees at Red Cross Switzerland
- Experience in the Scout Movement for more than 10 years, 5 years in leading position
- Trekking / Lindy Hop Dancing / Football / Cooking / Computer gaming